Structural and biochemical characterization of c-di-AMP synthesizing enzymes

Dissertation

for the award of the degree

“Doctor rerum naturalium” (Dr. rer. nat.)

of the Georg-August-Universität Göttingen

within the doctoral program “Biomolecules: Structure-Function-Dynamics”

of the Georg-August University School of Science (GAUSS)

submitted by

Jana Laura Heidemann

from Ankum

Göttingen, 2020

Members of the Thesis Advisory Committee

Prof. Dr. Ralf Ficner (Reviewer 1)
Georg-August-University Göttingen
Institute for Microbiology and Genetics
Department for Molecular Structural Biology

Prof. Dr. Kai Tittmann (Reviewer 2)
Georg-August-University Göttingen
Schwann-Schleiden-research center
Department of Molecular Enzymology

Prof. Dr. Fabian Commichau
Brandenburg University of Technology
Department of Synthetic Microbiology

Members of the Examination Board

Prof. Dr. Rolf Daniel
Georg-August-University Göttingen
Institute for Microbiology and Genetics
Department of Genomic and Applied Microbiology

Dr. Till Ischebeck
Georg-August-University Göttingen
Albrecht-von-Haller-Institute for Plant Sciences
Department of Plant Biochemistry

Prof. Dr. Carsten Lüder
University Medical Centre Göttingen
Department of Medical Microbiology

Date of oral examination: 28th Mai, 2020

Hereby I declare that I prepared the doctoral thesis in hand titled "Structural and biochemical characterization of c-di-AMP synthesizing enzymes" independently and with no sources and aids other than quoted. The thesis has not been submitted elsewhere.

Jana Laura Heidemann, April 2020

Table of Contents

Chapter 1: Introduction

1.1 Bacterial nucleotide-based second messengers

Signal transduction is an important mechanism in bacteria in order to adapt to environmental changes. Key components are nucleotide-based second messengers that are synthesized upon signal sensing. Bacteria possess a plethora of signal transduction systems, many comprising signal receptors associated with the cell membrane in order to sense extracellular signals (Goudreau and Stock 1998).

In the late 1950s during intensive studies of the hormone epinephrine (also known as adrenaline) the first nucleotide-based second messenger cyclic AMP (cAMP) was discovered which leads to hormone-induced changes in the metabolism of mammalian cells. Directly afterwards, cAMP was identified in bacterial cells, linked to catabolic repression (Makman and Sutherland 1964; Ullmann and Monod 1968; Brückner and Titgemeyer 2002). Shortly after the allomone guanosine-(penta)-tetraphosphate ((p)ppGpp) was discovered in *E.coli* to appear in response to nutrition limitation (Cashel and Gallant 1969). These discoveries set the foundation of a simple model which is considered as todays central dogma of signal transduction in cells (Sutherland and Rall 1957; Rall and Sutherland 1958). Thirty years after cAMP was discovered the existence of the first cyclic dinucleotide bis-(3',5')-cyclic di-guanosine monophosphate (cyclic di-GMP/c-di-GMP) was reported (Ross et al. 1987). Due to the high research interest on c-di-GMP it became one of the most comprehensively studied secondary nucleotides. It is a ubiquitous bacterial second messenger which is in general involved in different physiological functions including cell differentiation, flagella motility, biofilm formation, virulence and other processes (Jenal 2004; Cotter and Stibitz 2007; Hengge 2009; Romling et al. 2013).

Over the past few years a wealth of different nucleotide-based secondary metabolites was described comprising linear and cyclic nucleotides as well as cyclic di- and tri- nucleotides (Pesavento and Hengge 2009; Severin and Waters 2019; Whiteley et al. 2019). A biological relevance of the bacterial second messenger bis-(3'-5')-cyclic dimeric adenosine monophosphate (cyclic di-AMP/c-di-AMP) was initially discovered in 2008 during structural analyses of the DNA integrity scanning protein DisA from *Thermotoga maritima*. Thenceforward, DisA was described as the first diadenylate cyclase (DAC) synthesizing c-di-AMP. Subsequently c-di-AMP was shown to be produced by a variety of different proteins (Witte et al. 2008; Commichau et al. 2019).

1.2 C-di-AMP a nucleotide-based second messenger

Since the discovery of c-di-AMP the research interest on its synthesis and function has increased rapidly (Corrigan R. M. and Gründling 2013; Commichau et al. 2015a; Commichau et al. 2019). The community around secondary metabolites ascertained quickly the enormous potential of this small molecule among other known second messengers, not least due to its uniqueness of being essential. Like c-di-GMP, c-di-AMP is carrying two nucleotide moieties (adenine moiety) that are linked by 3'-5' phosphodiester bond forming a ribose-phosphate ring (Romling et al. 2013; He et al. 2020).
Several studies referred to c-di-AMP as the only known essential signaling nucleotide (under standard conditions) due to its important role in potassium homeostasis and osmotic adaptation, yet an extensive excess is harmful to the cell (Woodward et al. 2010; Luo Y and Helmann 2012; Mehne et al. 2013; Gundlach et al. 2015a; Commichau et al. 2017; Gundlach et al. 2017a; Gundlach et al. 2017b; Commichau et al. 2019). However, it is not only an important component in osmoregulation, it is also involved in a plethora of different physiological functions (Corrigan Rebecca M and Gründling 2013; Commichau et al. 2019). Furthermore, c-di-AMP is known to be the first secondary metabolite to regulate a biological process on two distinct levels, namely protein expression and protein activity (Nelson et al. 2013; Gundlach et al. 2017b; Gundlach et al. 2019). Over the years the presence of c-di-AMP in pathogenic bacteria expressing a diadenylate cyclase was reported in several studies, however, its existence in human cells could not be verified so far. The importance of c-di-AMP for the bacterial survival opened new perspectives in antibiotic research since there is an urgent need of new substances to control bacterial infections (Song et al. 2005; Woodward et al. 2010; Corrigan et al. 2011; Bai et al. 2012).
c-di-AMP is synthesized out of two ATP molecules by the diadenylate cyclases, releasing two pyrophosphates as a side product (PPi). Its degradation into the linear phosphoadenylyl adenosine nucleotide (5'pApA) which can be further hydrolyzed to AMP is facilitated by specific phosphodiesterases (Rao et al. 2010; Manikandan et al. 2014; Huynh and Woodward 2016; Commichau et al. 2019).

1.3 Diadenylate cyclases and c-di-AMP synthesis

DACs were detected in a wide range of different bacterial species. So far five different classes of DACs have been identified (DisA, CdaA, CdaS, CdaM, and CdaZ) many in Gram-positive bacteria belonging to the phyla of Firmicutes and Actinobacteria but also in Gram-negative bacteria and archaea (Romling 2008; Corrigan Rebecca M and Gründling 2013; Blötz et al. 2017; Commichau et al. 2019). These different classes of DACs share the highly conserved

diadenylate cyclase domain (DAC domain) accompanied by different types of regulatory domains (Fig. 1) (Witte et al. 2008; Corrigan Rebecca M and Gründling 2013; Commichau et al. 2015b; Rosenberg et al. 2015).

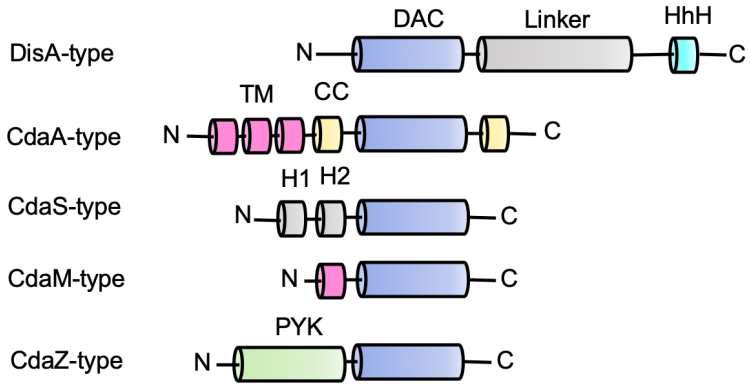

Figure 1: Diadenylate cyclase domain (DAC domain) organization of the different classes. The different domains are characterized by a colour code. The highly conserved DAC domain is represented in blue. HhH, helix-hinge-helix domain; TM, transmembrane domain; cc, coiled-coil domain; H1 and H2, inhibitory helix 1 and 2; PYK, pyruvate kinase-like domain (modified from Commichau et al. 2019).

In contrast to many pathogenic bacteria (*Listeria monocytogenes, Staphylococcus aureus*, *Staphylococcus pneumonia*) that possess only a sole class of DACs, some bacteria are equipped with for example three different classes like bacteria of the order Bacillales. *Bacillus subtilis* for instance is known to carry the DAC prototype DisA, a DNA-damage sensing protein (Oppenheimer-Shaanan et al. 2011). In response to DNA lesions the synthesis of c-di-AMP is reduced leading to a delay in sporulation while an elevated intracellular c-di-AMP level stimulates spore formation (Bejerano-Sagie et al. 2006; Oppenheimer-Shaanan et al. 2011). The second DAC type, c-di-AMP synthase S (CdaS), was reported to be exclusively needed for the successful germation of spores in the order Bacillales, yet its function and regulation is still not well understood (Corrigan Rebecca M and Gründling 2013; Mehne et al. 2013; Mehne et al. 2014). The third DAC domain protein in *B. subtilis* is the most abundant and conserved class of DACs represented by CdaA (Romling 2008; Luo Y and Helmann 2012). Interestingly the deletion of all three DACs is lethal for the survival of *B. subtilis* emphasizing the essentiality of c-di-AMP (Luo Y and Helmann 2012; Bai et al. 2013; Mehne et al. 2013; Witte et al. 2013). Thus far, DisA is the only DACs which was crystallized with its product c-di-AMP enabling a better understanding of the DAC reaction mechanism. DisA is a homo octamer composed of two “head-to-head” tetrameric DAC domain rings and an N-terminal part described as the DNA binding domain (HhH domain). The catalytic site is positioned between the interface of the tetrameric rings, where two DAC domain monomers are facing each other in order to form one reaction center (Fig. 2 A & B) (Witte et al. 2008). Each DAC dimer was described to form one c-di-AMP molecule and two pyrophosphates out of two ATP molecules in a metal-ion dependent manner (Mg^{2+}or Mn^{2+}).

By sequence alignment three highly conserved amino acid motifs were identified in the nucleotide binding pocket. Structural and biochemical analyses demonstrate the involvement of these amino acids in nucleotide binding and catalysis (for DisA: $D^{75}GA$, $T^{107}RHR$, S^{127}) (Witte et al. 2008). Crystallization of DisA in complex with an ATP analogue enabled the characterization of its pre-reaction state and the description of a detailed reaction mechanism (Müller et al. 2015).

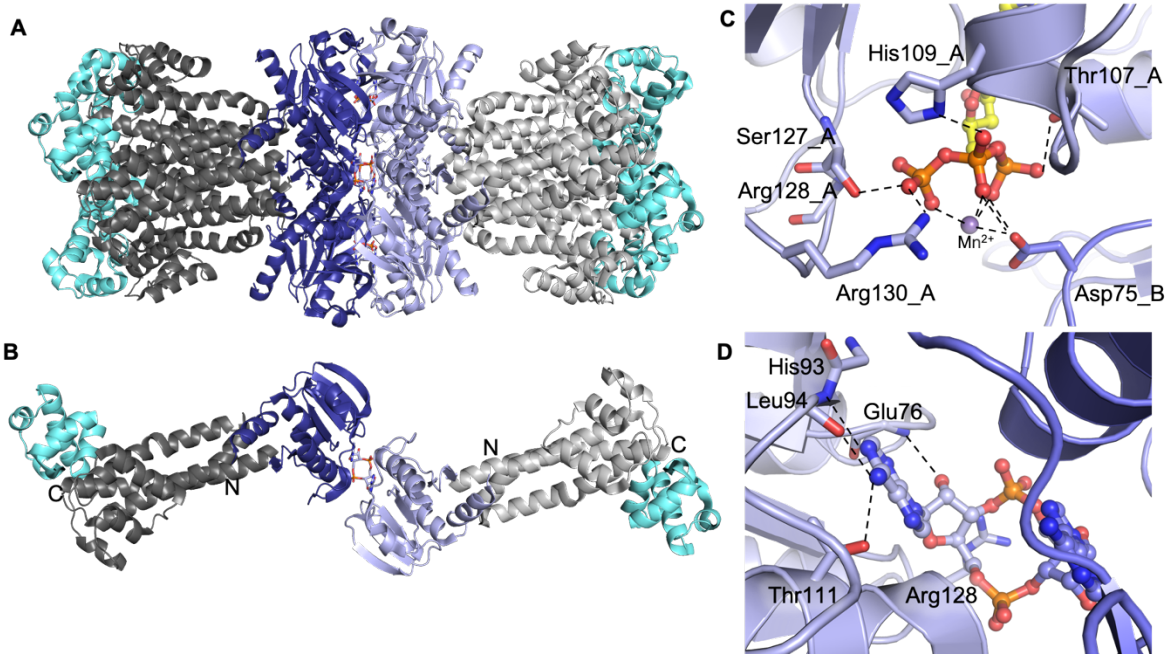

Figure 2: Crystal structure of DisA and active site. (A) Overall octameric DisA (PDB code: 3C21) structure with a central DAC domain (molecule A light and molecule B dark blue) and the C-terminal DNA binding HhH domain (cyan) depicted as a cartoon model. Both functional domains of the protein are linked by a helical spine linker (dark and light grey). **(B)** DisA cartoon model of the two protomers forming the central, functional DAC unit with a bound c-di-AMP. The colour code as described in A (PDB code: 4YVZ). **(C)** Pre-reaction state with bound ATP analogue 3'-deoxyATP and a Mn^{2+} ion. The ATP is displayed in ball and stick mode (carbon in yellow, phosphates in orange, oxygens in red, and nitrogen in blue). Shown are amino acids that are involved in metal ion and phosphate coordination. The two DAC domains that are facing each other are coloured in light and dark blue. **(D)** Post-catalytic state with c-di-AMP bound. C-di-AMP is depicted in ball and sticks (carbon in light blue and dark blue, phosphates in orange, oxygens in red, and nitrogen in blue). All amino acids involved in purine base coordination are shown as sticks.

The N1 nitrogen of the nucleotide adenine is forming a hydrogen bond with the amide of the leucine main chain at position 94 while the N6 amine is hydrogen bonded by the leucine main chain carbonyl and the threonine 111 side chain (Fig. 2C). The three phosphates of the ATP analogue (3'deoxyATP) are bent around a catalytic metal ion. While the β- and γ-phosphate are additionally coordinated by the Arg^{108}, His^{109}, Ser^{127} and Arg^{130} through hydrogen bonds, the α-phosphate interacts with Thr^{107} and Asp^{75} of the opposite monomer (Fig. 2D). An interaction of the γ-phosphate with the amino acids Ser^{127}, Arg^{128} and Arg^{130} result in its polarization

which is described as the preparation of the first reaction step (Müller et al. 2015). The reaction mechanism was reported as a two-step synthesis with two transition state complexes (Fig. 3). The polarized γ-phosphate facilitates the nucleophilic attack of the ribose 3'OH on the α-phosphate on the neighboring ATP molecule resulting in the release of the first pyrophosphate and the formation of a linearized intermediate (pppApA). The second step is described as an additional nucleophilic attack of the second ribose 3'OH and α-phosphate which is facilitated by a complex formation of the deprotonated pppApA with the catalytic metal ion (Mg^{2+} or Mn^{2+}). This process results in the cyclization of two ATP molecules and therefore the formation of c-di-AMP (Manikandan et al. 2014). A similar mechanism was also reported for the enzyme cyclic GMP-AMP synthase (cGAS) (Ablasser et al. 2013; Kranzusch 2019).

In comparison to ATP, c-di-AMP is less coordinated. In the pre-catalytic state, the phosphates mainly contribute to the coordination of the nucleotide while the post-catalytic state shows less interaction points in order to facilitate product release (Fig. 3) (Müller et al. 2015). The guanidine group of arginine 108 which is positioned in one of the conserved amino acid patches binds the ribose via stacking. In addition, the ribose 3' hydroxyl is forming a hydrogen bond with the amide nitrogen of glycine 76 located in the first conserved amino acid motif (DGA) and the aspartic acid 75 is positioned in the vicinity of the phosphate moiety. The adenine moiety of c-di-AMP is coordinated as described for the ATP analogue binding (Witte et al. 2008; Müller et al. 2015).

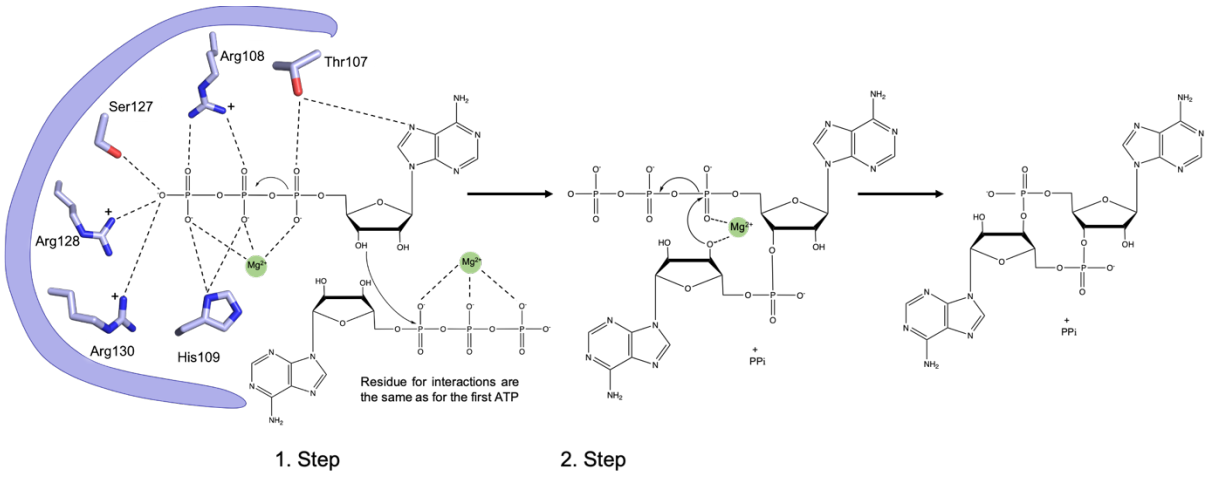

Figure 3: The two-step mechanism of c-di-AMP synthesis. c-di-AMP is synthesized out of two ATP molecules in a metal ion-dependent manner. The first synthesis step describes the nucleophilic attack by the 3'OH group of one ATP on the α-phosphate of the opposite ATP molecule which results in the intermediate I pppApA and the release of PPi. This follows a second synthesis steps, which involves the intermediate II (pppApA in complex with Mn^{2+}). A similar nucleophilic attack results in formation of c-di-AMP and the release of PPi. Important residues are depicted in stick mode (carbon in light blue, oxygens in red, and nitrogen in blue) generated with pymol (modified from Opoku-Temeng C. et al. 2016) (Manikandan et al. 2014, Schrödinger L.L.C. 2010).

1.4 The most abundant and conserved diadenylate cyclase

Many bacteria that are known to synthesize c-di-AMP possess either the DAC class DisA or CdaA, whereas the latter is described as the most prevailing DAC domain containing protein among different bacterial species (Corrigan et al. 2013; Commichau et al. 2019). In most Firmicutes the gene of CdaA is embedded in a well-known and highly conserved gene cluster which encodes besides *cdaA,* the regulatory protein CdaR as well as the glucosamine mutase GlmM (Mehne et al. 2013; Rismondo et al. 2016; Zhu et al. 2016).

CdaA is a membrane bound protein harboring an N-terminal transmembrane domain consisting of three α-helices followed by a linker (coiled-coil) connecting the membrane domain and the cyclase domain (Fig. 1) (Gundlach et al. 2015a; Rismondo et al. 2016).

In 2015 the first crystal structure of a truncated *L. monocytogenes* CdaA monomer in complex with an ATP molecule and a bound Mg^{2+} ion was solved. Protein purification was established with a truncated variant due to the transmembrane domain which hampers the solubility success. Henceforth, Δ100CdaA referrers to the truncated CdaA variant missing the first 100 amino acids, composed of the linker (coiled-coil) and the preceding membrane domain. Biochemical characterization of the full length CdaA and also its truncated variants indicated as described for DisA a metal ion dependency. In comparison to DisA which shows cyclase activity in presence of Mg^{2+} or Mn^{2+} ions CdaA exhibits *in vitro* activity either in presence of the divalent metal ions Mn^{2+} or Co^{2+} (Witte et al. 2008; Manikandan et al. 2014; Müller et al. 2015; Rosenberg et al. 2015).

In agreement with DisA, also the cyclase domain in CdaA shows an overall globular fold. The core of the DAC domain is formed by a slightly twisted β-sheet made of seven parallel and antiparallel β-strands (β1-β7) which is surrounded by five α-helices (Fig. 4A) (Rosenberg et al. 2015).

The previous structural and biochemical analysis of DisA suggested a two-step catalytic mechanism (Manikandan et al. 2014; Müller et al. 2015). In order to form c-di-AMP two ATP molecules are required to be positioned in close vicinity which is ensured by two DAC domains facing each other (Witte et al. 2008). In line with the solved DisA structure and biochemical data a model of a CdaA pair in a face-to-face orientation forming a homodimer was suggested (Fig. 4C) (Witte et al. 2008; Rosenberg et al. 2015).

The nucleotide binding pocket is defined by α-helix 4, the β-strands 1 and 5 as well as several loops connecting α1 and β1, α3 and β3, α4 and β4, and β5 and β6. Structural-based sequence alignment unveiled three conserved amino acid patches also seen in DisA. The first conserved motif consists of a D^{171}GA sequence. In the CdaA dimer model the aspartic acid is positioned close to the ATP α-phosphate and the ribose. The adenine moiety in CdaA is coordinated similar as described for DisA (CdaA: Thr^{202}, Leu^{188}; DisA: Thr^{111}, Leu^{94}) (Rosenberg et al. 2015). Amino acid motif two (GTR203HR) possesses an arginine 203 which stacks against the ribose

with its guanidine group. The third and last amino patch embodies the conserved serine 222 followed by two glutamic acids 223 and 224 which take over the function of the two arginine 128 and 130 in DisA to coordinate the catalytic metal ion and the β- and γ-phosphate. Additionally, the histidine 204 in CdaA contributes to the coordination of the phosphates as it was reported for the ATP analogue in DisA (Fig. 4B). In summary, the amino acid arrangement in the nucleotide binding center is similar to that in DisA from *T. maritima*. Also, sequence alignment of DACs from different organisms suggest the presence of these described amino acids that importantly contribute to ATP and c-di-AMP binding. Taken together these findings emphasize a similar synthesis mechanism between different classes of DACs which explains the high conservation.

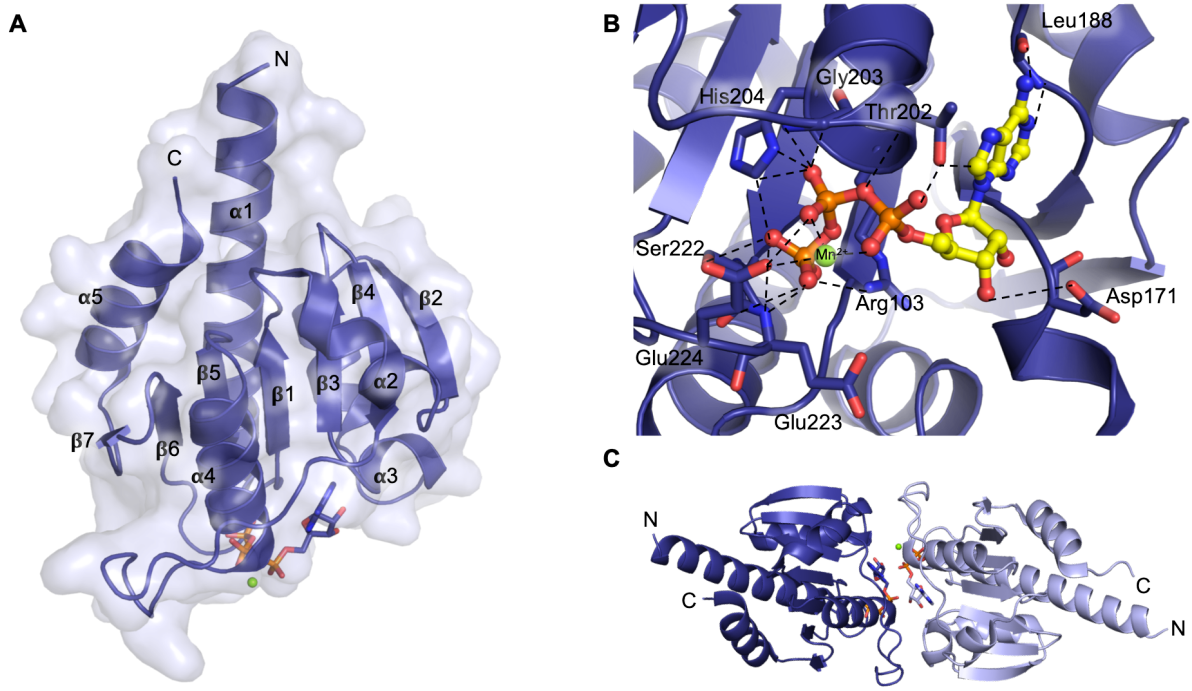

Figure 4: Crystal structure of CdaA. (A) Overall structure of the truncated Δ100CdaA. CdaA shows an overall globular fold with a slightly twisted β-sheet which is surrounded by five α–helices. The protein structure is depicted in cartoon mode in dark blue and the surface is represented in light blue. **(B)** Nucleotide binding site in CdaA. The bound ATP is depicted in ball and sticks mode (carbon in yellow, phosphates in orange, oxygens in red, and nitrogen in blue). The Mg^{2+} is represented as green sphere. All amino acids are shown that contribute to ATP binding. The dashed lines represent binding interactions of up to 3.2 Å. **(C)** The CdaA dimer model was generated by superposition of the DisA dimer. The two DAC domain monomers are coloured dark and light blue. In the interface two bound ATPs are oriented antiparallel to each other.

1.5 Regulation of c-di-AMP synthesis in CdaA

The intracellular c-di-AMP level needs to be tightly controlled. Even though its synthesis is crucial for some bacteria to grow, an excessive accumulation is equally harmful (Mehne et al. 2013; Gundlach et al. 2015a). Since the gene encoding CdaA is embedded upstream of CdaR and GlmM in a conserved gene cluster a direct interaction and functional relation between these proteins was suggested and proven in several studies (Corrigan et al. 2011; Luo Y and Helmann 2012; Witte et al. 2013).

CdaR is described as a CdaA regulator containing four similar YbbR domains of unknown function as well as an N-terminal transmembrane domain (Barb et al. 2010). An *in silico* membrane topology prediction suggested the location of CdaR outside the cell (Corrigan Rebecca M and Gründling 2013). Furthermore, it has been shown that CdaR is able to interact with itself via the YbbR domain but also with the full-length CdaA and has an influence on the intracellular c-di-AMP level (Luo Y and Helmann 2012; Gundlach et al. 2015a). On the one hand CdaR was described to negatively affect the CdaA activity (*L. monocytogenes, S. aureus and Lactococcus lacti*) (Gundlach et al. 2015a; Bowman et al. 2016; Rismondo et al. 2016) yet on the other hand it shows a stimulating effect (*B. subtilis*) (Mehne et al. 2013). So far, a conclusive role of CdaR and whether it acts as a signaling receptor is unknown. Even structural data of the CdaR YbbR domain I and IV did not suggest a putative function (Barb et al. 2010; Corrigan Rebecca M and Gründling 2013).

The second protein suggested to be involved in CdaA regulation is the cytosolic phosphoglucosamine mutase GlmM which is required for cell wall synthesis. GlmM catalyzes glucosamine-6-phosphate into glucosamine-1-phospahate, an early intermediate of the peptidoglycan biosynthesis (Mengin-Lecreulx and Van Heijenoort 1996; Barreteau et al. 2008). Previously a physical interaction between CdaA and GlmM was reported which was in comparison to the strong CdaA-CdaR interaction described as weak but significant (Mehne et al. 2013; Gundlach et al. 2015a). An osmoresistance study in *L. lactis* unveiled a suppressor mutant strain carrying a mutation in the GlmM protein resulting in a decrease of the intracellular c-di-AMP concentration. This proves a functional relevance of the GlmM-CdaA interaction and describes GlmM as a negative effector of CdaA (Zhu et al. 2016).

The intracellular c-di-AMP level is not only regulated through the regulation of its synthesizing enzyme CdaA but also through other mechanisms like degradation or secretion (Commichau et al. 2015b). Specific phosphodiesterases (PDE) are known to degrade c-di-AMP via hydrolysis similar to the two-step mechanism described for c-di-AMP synthesis (Manikandan et al. 2014). Four classes of PDEs have been identified (Commichau et al. 2019). *L. monocytogenes* and *B. subtilis* possess the two main PDEs, the GdpP-type (in *lmo*PdeA) and PgpH-type. Orthologs of the GdpP-type PDE have been identified in a plethora of different Firmicutes (Rao et al. 2011). A deletion or depletion was described to result in an increased c-di-AMP

level accountable for increased resistance to β-lactam antibiotics (Corrigan et al. 2011; Luo Y and Helmann 2012; Witte et al. 2013).
The GdpP-type PDE belongs to the DHH/DHHA1 domain family and carries two transmembrane domains followed by a Per-Arnt-Sim (PAS) domain and a highly modified GGDEF domain preceding the catalytic DHH/DHHA1 domain degrading c-di-AMP in a metal ion dependent manner (Rao et al. 2010). GGDEF domains were previously reported as the functional domain of diguanylate cyclases catalyzing the reaction of two GTP molecules to c-di-GMP (Hengge 2009). In the described phosphodiesterase this domain is missing the conserved GGDEF motif and is lacking cyclase activity. Instead it exhibits ATPase activity with an undefined physiological role (Rao et al. 2010). A binding of b-type heme to the regulatory PAS domain has been demonstrated to have an inhibitory effect on the GGDEF and DHH/DHHA1 domains, respectively (Rao et al. 2011). In addition, the alamone ppGpp which is known to be elevated during the stringent response has been described to competitively inhibit the DHH/DHHA1 activity linking the c-di-AMP and ppGpp signaling pathways (Rao et al. 2010).
The second type of PDEs present in *L. monocytogenes* and *B. subtilis* are the PgpH-type specifically degrading c-di-AMP. These enzymes consist of an extracellular seven-transmembrane helix-HDED domain (7TMR-HDED), followed by seven transmembrane helices and an HD domain. An additional transmembrane helix is located at the N-terminus preceding the 7TMR-HDED domain. The HD domain is described as the catalytic domain hydrolyzing c-di-AMP and is also reported to be inhibited by ppGpp (Huynh et al. 2015). A third way to regulate the intracellular c-di-AMP concentration is its export via secretion systems like multidrug efflux pumps (MDRs) (Woodward et al. 2010). While some bacteria tried to evade the hosts immune response due to secretion of the signaling molecule, they evolved mechanisms to hydrolyze external c-di-AMP (Andrade et al. 2016). Instead, the human pathogen *L. monocytogenes* for example actively secretes c-di-AMP which trigger the mammalian host Type I interferon response as a result of STING activation (Crimmins et al. 2008; Woodward et al. 2010; Archer et al. 2014; Dey et al. 2015). In addition, c-di-AMP binds to the oxidoreductase RACON a cytosolic sensor of cyclic dinucleotides and inhibits its activity which results in an enhanced cell-to-cell spread of the bacteria (McFarland et al. 2017; McFarland et al. 2018).

1.6 The complex network of c-di-AMP

The huge research interest over the last ten years on the small molecule c-di-AMP unveiled insights into its complex signaling network and a variety of different binding partners.
The first described c-di-AMP binding protein is the transcription factor DarR of the TetR family from *Mycobacterium smegmatis* (Zhang et al. 2013). DarR represses its own gene expression and that of three further proteins by binding to a palindromic sequence in their promotor

region which is stimulated by binding of c-di-AMP to DarR (Zhang et al. 2013; Commichau et al. 2015b). Due to its important role in osmoregulation further c-di-AMP targets were identified that are involved in potassium ion transport. c-di-AMP was reported to regulate a biological process on the level of protein expression and at the same time on protein activity (Corrigan Rebecca M and Gründling 2013; Nelson et al. 2013; Gundlach et al. 2017b; Gundlach et al. 2019). The *B. subtilis* high affinity potassium ion uptake system KtrAB (in *L. monocytogenes* KdpABC (probably does not contribute to K^+ uptake) and *S. aureus* KdpFABC) and KimA were described to be inhibited upon binding of c-di-AMP to the protein but also to the corresponding mRNA which leads to a repression of protein expression (Corrigan et al. 2013; Nelson et al. 2013; Gundlach et al. 2017b; Gundlach et al. 2019). So far a c-di-AMP-dependent riboswitch to control protein expression was not detected in *L. monocytogenes* rising the question whether c-di-AMP controls protein expression in these bacteria (Gibhardt et al. 2019). In addition, the low affinity transporter system KtrCD and the KdpD sensor kinase which controls the expression of the Kdp potassium transporter, get inhibited upon c-di-AMP binding (Moscoso et al. 2016).

Potassium ions are the most abundant cations in living cells. Not only because of its importance in ribosome functionality but also for maintenance of the intracellular pH (Epstein 2003). However, an intracellular ion excess can be harmful to the cell and therefore it needs to be tightly regulated (Chandrangsu et al. 2017). Both, high affinity potassium transporters are expressed under low external K^+ ion concentrations to ensure the required intracellular ion level which is essential for bacterial growth. In contrast, under high external K^+ ion concentration the low affinity transporter KtrCD is expressed. A high external K^+ ion concentration was described to activate the accumulation of c-di-AMP which in turn leads to a reduced K^+ ion uptake (Gundlach et al. 2017b). It has been reported that c-di-AMP binds to the RCK_C domains (regulator of conductance of K^+) of KtrAB and KtrCD forming a gating component of potassium ion channels. RCK_C domains have been described as c-di-AMP binding domains also present in other proteins. So far five proteins were identified in *B. subtilis* to possess an RCK_C domain, many of these proteins are described to be potential K^+ ion transporters. The RCK_C domain containing KhtSTU complex and CpaA from *S. aureus* for instants which are known to bind c-di-AMP are suggested to be involved in potassium ion export (Fujisawa et al. 2007; Gundlach et al. 2019). In group B Streptococcus, bacteria that have been identified for neonatal septicaemia and meningitis and in *L. lactis* c-di-AMP binds to the RCK_C domain containing transcription regulator BusR. Upon binding of c-di-AMP, BusR has been shown to negatively regulate the expression of the glycine betaine transporter BusAB (Devaux et al. 2018; Pham et al. 2018).

Only recently it has been shown that c-di-AMP also negatively effects the potassium ion transport in *L. lactis* upon binding to the high affinity K^+ ion transporters KupA and KupB (Quintana et al. 2019).

The human pathogen *S. pneumoniae* was also reported to modulate K^+ ion homeostasis via c-di-AMP signaling. CabP was identified to specifically bind c-di-AMP which interacts with the K^+ ion importer SPD_0076 and as a result reduces ion uptake (Bai et al. 2014). Yet c-di-AMP is not only involved in controlling the cellular potassium transport but osmolyte homeostasis in general. One class of proteins that were also identified to bind c-di-AMP are the so-called CBS domain containing proteins. These domains are also known as Bateman domains named after Alexander Bateman who firstly described this specific CBS domain fold of cystathionine-β-synthases (Bateman 1997). CBS domains are able to bind a great variety of different adenine derivatives (Day et al. 2007; Baykov et al. 2011; Ereño-Orbea et al. 2013). Hence, it should be kept in mind that not all CBS domains bind the secondary dinucleotide. Indeed, in *B. subtilis* the majority of CBS domains do not bind c-di-AMP (Devaux et al. 2018; Gundlach et al. 2019). Only three out of sixteen CBS domain containing proteins were observed so far to bind c-di-AMP: the Mg^{2+} ion transporter MgtE, YkuL/DarB (CbpB in *L. monocytogenes*), a protein of unknown function, and the glycine betaine-carnitine transporter OpuCA. Whereas the latter has also been confirmed to be inhibited upon c-di-AMP binding in *L. monocytogenes* and *S. aureus* resulting in an impaired carnitine uptake (Schuster et al. 2016; Gundlach et al. 2019). Interestingly the deletion of the sole DAC CdaA in *L. monocytogenes* resulted in the development of suppressor mutants in rich medium carrying mutations in CbpB (*B. subtilis* DarB/YkuL) and PstA (*B. subtilis* DarA) (Sureka et al. 2014). CbpB is subordinated to the proteins possessing the highly conserved CBS domain whereas PstA/DarA was described to be similar to the PII-like domain proteins (Gundlach et al. 2015b). Both proteins have been identified to bind c-di-AMP, but their function still needs to be elucidated. Furthermore, the pyruvate carboxylase (PycA) was identified as a potential c-di-AMP binding protein. As described for other c-di-AMP interacting proteins, the binding to PycA has a negative effect on its activity through allosteric inhibition (Sureka et al. 2014). Therefore it was suggested that c-di-AMP also plays an important role in linking osmoregulation and metabolic homeostasis (Whiteley et al. 2017).

The fact that c-di-AMP binds to different proteins in the bacterial cells most of which are osmotransporters emphasizes the importance to keep the osmotic level in balance in order to regulate the cellular turgor (Commichau et al. 2017).

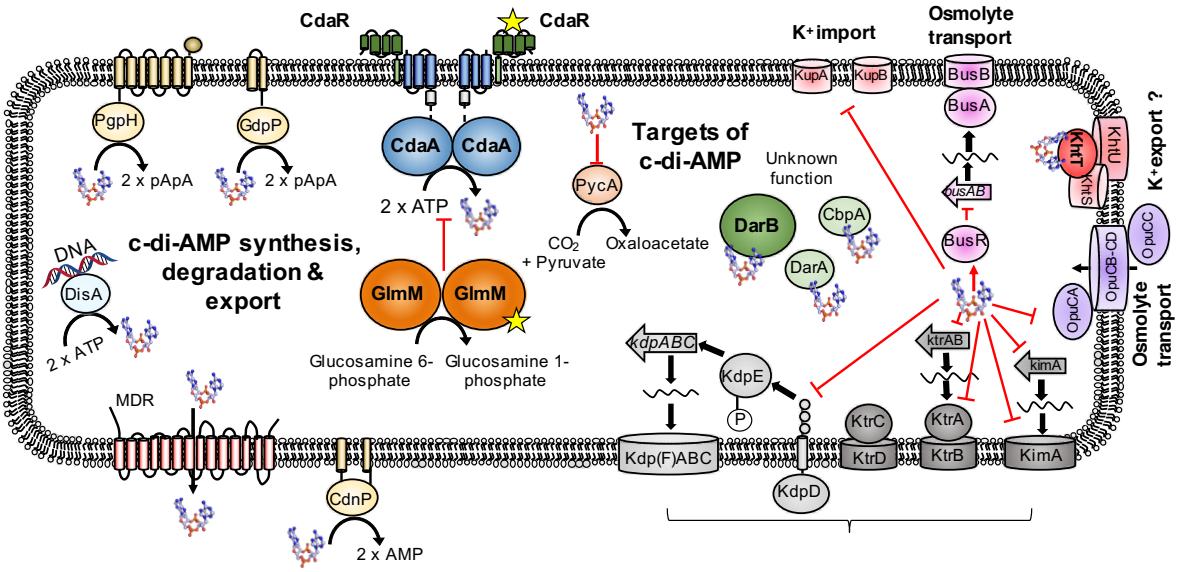

Figure 5: c-di-AMP synthesis, degradation and its interaction partners. The nucleotide-based second messenger c-di-AMP is synthesized by proteins containing a DAC domain. In this figure the two main DACs (CdaA and DisA) are shown. The DAC activity of the membrane bound CdaA is modulated by the extracellular located CdaR and the glucosamine mutase GlmM. c-di-AMP can be degraded into pApA by specific phosphodiesterases. Here only the membrane bound PDEs are shown that degrade c-di-AMP either to pApA or AMP. The cytosolic DhhP-type PDEs are not shown. However, c-di-AMP is not only removed from the cell by degradation but also by secretion through secretion systems like MDR, a multidrug resistance transporter. In addition, targets are displayed that have been shown to bind c-di-AMP. Some of these targets are of unknown function like DarA and DarB but many others were identified to bind to osmolyte transporters and therefore regulate the uptake and export of osmolytes. c-di-AMP not only binds directly to the protein itself. It has also been shown to regulate protein expression as it was reported for KimA. The red arrow represents activation and the arrow with a flat end represents the inhibition through c-di-AMP binding (modified from Commichau et al. 2019).

1.7 CdaA as a new antibiotic target?

Due to the rapid adaptation of bacteria to environmental changes and as a result to antibiotics many bacteria developed resistances to the available repertoire of antimicrobial drugs. The WHO declares antibiotic resistance as a “global health concern” since bacteria spread easily around the world and are not stopped by national borders (Ventola 2015; Wang et al. 2018). According to the German federal government each year in Germany 400,000 to 600,000 people become infected by antibiotic resistant bacteria (German Federal Government 2020). It has been reported that 10,000 to 15,000 patients die due to the lack of effective antibiotic agents. The Director-General of the WHO Dr. Tedros Adhanom Ghebreyesus said “Never has a thread of antimicrobial resistance been more immediate and the need for solutions more urgent” emphasizing the desperate need of new substances to combat against resistant bacteria (WHO 2020). However, it is not enough to come up with new antibiotic targets or the development of

new antimicrobial substances. The overuse and misuse of antibiotic drugs needs to be drastically reduced (Phillips et al. 2004; Hume 2011; Michael et al. 2014). In 2017 the WHO published a "priority pathogen" list filing bacterial pathogens that have an increased risk to the human health due to the lack of effective drugs (WHO 2017; Asokan et al. 2019).

Hence, there is an urgent need of identifying new drug targets and antibacterial substances. One major challenge of developing new effective antibiotics is the identification of suitable drug targets. A pivotal aspect of an auspicious target is its conservation as well as its essential function for a wide range of different bacterial species. An interaction with the potential target through stimulation or inhibition should result in a decreased growth of the bacteria in order to be considered as a drug target. In addition, it is of great importance not to neglect that a potential target lacks structural and functional homology to human proteins in order to avoid side effects (Silver 2011). The c-di-AMP synthesizing enzymes DACs were suggested in many studies to function as a promising target for novel antibiotic agents (Corrigan R. M. and Gründling 2013; Rosenberg et al. 2015; Commichau et al. 2019). So far DACs as well as its product c-di-AMP could not be detected in humans. It has been reported that the synthesis of c-di-AMP in bacteria that possess a DAC is essential under standard conditions due to its regulatory function in osmolyte homeostasis (Gundlach et al. 2015a; Commichau et al. 2017; Gundlach et al. 2017a). An uncontrolled transport of osmolytes which is triggered due to loss of c-di-AMP in the cell was identified to result in cell lysis (Luo Yun and Helmann 2012; Mehne et al. 2013; Rismondo et al. 2016). Interestingly, the intracellular excess as well as a reduced amount of c-di-AMP have been linked to either increased resistance or susceptibility to β-lactam antibiotics, respectively. On the one hand it has been shown in several studies that mutation that lead to a reduced intracellular c-di-AMP level get more susceptible to methicillin, oxacillin and cefuroxime. The increased susceptibility might be a result of a reduced structural stability of the bacterial cell wall (Dengler et al. 2013; Witte et al. 2013; Cheng et al. 2016; Rismondo et al. 2016). On the other hand, it has been reported that a deletion or depletion of the c-di-AMP specific PDEs resulted in a higher resistance to β-lactam antibiotics due to the increased c-di-AMP level (Corrigan et al. 2011; Luo Yun and Helmann 2012; Witte et al. 2013). In *S. aureus* an elevated cellular c-di-AMP level resulted in a significantly increased number of cross-linked peptidoglycans which in fact emerged an increased resistance to cell wall targeting enzymes (Corrigan et al. 2011). In addition, several known human pathogens were identified to express DACs, like *Mycobacterium tuberculosis*, *S. aureus*, Group B *Streptococcus* and *S. pneumoniae*, some of these bacteria listed here are also constituents of the WHO "priority pathogen" list (Song et al. 2005; Woodward et al. 2010; Corrigan et al. 2011; Luo Yun and Helmann 2012; Andrade et al. 2016; WHO 2017; Devaux et al. 2018; Asokan et al. 2019). Taken together all these aspects, it might be worth to consider DACs, in particular CdaA/DacA, as a potential new antibiotic target.

1.8 Diadenylate cyclase inhibitors

DAC domain containing enzymes are potential targets for the development of new antibiotic agents owing to their synthesis of c-di-AMP. Inhibiting substances were already described for the DAC class DisA but no CdaA inhibitors have been reported so far (Zheng et al. 2014; Opoku-Temeng and Sintim 2016a). The ATP analogue 3'-deoxyATP misses its 3'OH group and is therefore unable to from c-di-AMP. Hence it inhibits synthesis as a completive inhibitor with an IC_{50} (50 % inhibitor concentration) at 3.8 µM (Müller et al. 2015). The screening of two compound libraries unveiled two additional DisA inhibitors: bromophenol thiohydantoin (Br-TH) with an IC_{50} of 56 µM and suramin an antiparasitic drug with an IC_{50} of 1.1 µM (Zheng et al. 2014; Opoku-Temeng and Sintim 2016b). The last molecule which is known to inhibit cyclase activity in DisA is theaflavin digallate with an IC_{50} of 3.4 µM. It was shown, that its inhibitory effect is non-competitive with ATP (Opoku-Temeng and Sintim 2016a; Commichau et al. 2019).

1.9 Objective of this thesis

Infections caused by antimicrobial resistant bacteria are one major health concern of humanity. Bacteria use their ability of rapid adaptation to environmental changes in order to combat against antibiotics. This enables bacteria to develop resistances and to survive even under usually life-threatening conditions. The misuse e.g. in agriculture and overuse due to insufficient education on how and when antibiotics should be used leads to an increase of bacterial species that are resistant to one or more antibiotic substances (Phillips et al. 2004; Hume 2011; Michael et al. 2014; Woolhouse et al. 2016). The number of resistant bacteria increases, while the number of effective antibiotics decreases. The identification of new targets to stop bacterial growth is difficult since these need to be essential for the bacterial survival and structural homologs should rather be absent in humans (Silver 2011).
The second messenger c-di-AMP was reported to be essential for the survival of different pathogenic bacteria and it is not synthesized by mammals (Gundlach et al. 2015a; Commichau et al. 2017; Gundlach et al. 2017a). Hence its synthesizing enzymes, the DAC domain containing proteins, were assumed to be a good target for novel antibiotics (Corrigan R. M. and Gründling 2013; Rosenberg et al. 2015; Heidemann et al. 2019). This work focuses on the structural and biochemical characterization of the most abundant DAC class CdaA from *L. monocytogenes*. Both, crystallization and biochemical experiments, might give further insights into the functionality of CdaA, how its synthesis is inhibited in the cell and how it can be synthetically inhibited. In addition, c-di-AMP binding receptors are structurally and biochemically characterized in order to better understand the interaction network of c-di-AMP and its effect on effector proteins.

Chapter 2: Crystal structure of the c-di-AMP-synthesizing enzyme CdaA

This manuscript has originally been published in the Journal of Biological Chemistry

Crystal structure of the c-di-AMP- synthesizing enzyme CdaA

Jana L. Heidemann[1], Piotr Neumann[1], Achim Dickmanns[1] and Ralf Ficner[1]

From the [1]Department of Molecular Structural Biology, Institute for Microbiology and Genetics, GZMB, Georg-August-University Goettingen, 37077 Goettingen, Germany

To whom correspondence should be addressed: Ralf Ficner, Department of Molecular Structural Biology, Institute for Microbiology and Genetics, Georg-August-University Göttingen, 37077 Göttingen, rficner@uni-goettingen.de; Tel. +49 551 3914072

Authors contribution

J.L.H.: data curation; formal analysis; validation; writing-original draft; writing review and editing

P. N.: formal analysis; validation; writing-original draft; writing review and editing

A. D.: formal analysis; writing review and editing

R. F.: formal analysis; validation; writing-original draft; writing review and editing; conceptualization; funding acquisition.

JBC ARTICLE

Crystal structures of the c-di-AMP–synthesizing enzyme CdaA

Received for publication, May 9, 2019 Published, Papers in Press, May 22, 2019, DOI 10.1074/jbc.RA119.009246

Jana L. Heidemann, Piotr Neumann, Achim Dickmanns, and Ralf Ficner[1]

From the Department of Molecular Structural Biology, Institute for Microbiology and Genetics, Göttingen Center for Molecular Biosciences, Georg-August-University Göttingen, 37077 Göttingen, Germany

Edited by Joseph M. Jez

Cyclic di-AMP (c-di-AMP) is the only second messenger known to be essential for bacterial growth. It has been found mainly in Gram-positive bacteria, including pathogenic bacteria like *Listeria monocytogenes*. CdaA is the sole diadenylate cyclase in *L. monocytogenes*, making this enzyme an attractive target for the development of novel antibiotic compounds. Here we report crystal structures of CdaA from *L. monocytogenes* in the apo state, in the post-catalytic state with bound c-di-AMP and catalytic Co^{2+} ions, as well as in a complex with AMP. These structures reveal the flexibility of a tyrosine side chain involved in locking the adenine ring after ATP binding. The essential role of this tyrosine was confirmed by mutation to Ala, leading to drastic loss of enzymatic activity.

Bacteria have the ability to perceive environmental changes, leading to rapid and effective adaptation by utilizing different proteins as well as second messengers to transduce signals in the cell. In response to external stimuli, the intracellular concentration of second messengers, like cyclic dinucleotides and linear mononucleotides, varies to regulate and coordinate cellular processes (1–3). Cyclic di-AMP (c-di-AMP)[2] is the most recently discovered bacterial signaling nucleotide and, to date, has been found mostly in Gram-positive bacteria. c-di-AMP is involved in different cellular processes, such as DNA integrity scanning, cell wall metabolism, and osmolyte homeostasis (for a review, see Refs. 4–6). c-di-AMP is the only essential second messenger in bacteria because of its role in potassium homeostasis. It regulates potassium importers at high intracellular K^+ concentrations, whereas c-di-AMP is not essential at low K^+ concentrations (7). Interestingly, c-di-AMP becomes toxic when its degradation is blocked; hence, a tightly controlled intracellular c-di-AMP concentration is required for bacterial growth (8).

Proteins containing a diadenylate cyclase (DAC) domain have been bioinformatically identified, mainly in Gram-positive bacteria of the phyla Actinobacteria and Firmicutes but also in Gram-negative Cyanobacteria, Chlamydiae, Bacteroidetes, Fusobacteria, and Deltaproteobacteria and even in archaea of the phylum Euryarchaeota (5). Several DAC domain–containing proteins from various bacterial species have also been experimentally proven to produce c-di-AMP. Many of these bacteria are well-known pathogens, *e.g. Mycobacterium tuberculosis* (9), *Staphylococcus aureus* (10) and *Listeria monocytogenes* (11). In total, eight families of diadenylate cyclases have been identified so far, sharing the highly conserved DAC domain (12). However, DACs differ in their additional domains and domain organization, suggesting that DAC enzymes are regulated by different signals (12).

The three-dimensional structure of a DAC domain was first reported for DisA, a multidomain protein with an N-terminal DAC domain (13). This structure revealed that, within the homo-octameric DisA, two adjacent and properly positioned DAC domains, each with one ATP bound, catalyze the synthesis of c-di-AMP. Based on the homology of all DAC domains, it was proposed that DAC domains with bound ATP need to dimerize in a specific arrangement to catalyze c-di-AMP formation.

The importance of c-di-AMP for the growth of several pathogenic bacteria is marked by an increased resistance to cell wall–targeting antibiotics (10, 14). Its absence in humans makes DAC enzymes an interesting target for the development of novel antibiotics by structure-based drug design. Therefore, CdaA, the only DAC of the human pathogen *L. monocytogenes*, was previously characterized biochemically and structurally. The analysis revealed that CdaA is active with Co^{2+} or Mn^{2+} ions as cofactors but inactive in the presence of Mg^{2+} ions (15). The CdaA crystal structure unveiled the monomeric and catalytically inactive enzyme–substrate complex with bound ATP and Mg^{2+}, leaving the structure of a dimeric and active form with a bound Co^{2+} or Mn^{2+} cofactor still to be determined. Such a crystal structure could shed light on the role of the metal ion in the catalytic reaction.

In this study we report two new crystal structures of CdaA from *L. monocytogenes* at 2.0 Å and 2.8 Å resolution, representing the enzyme in its apo form and the post-catalytic homodimeric enzyme–product complex, respectively. The structure of CdaA with bound c-di-AMP was obtained by co-crystallization of CdaA in the presence of ATP and Co^{2+} ions. Comparison of the CdaA structure in the apo state with the ligand-bound forms of CdaA (ATP, AMP, or c-di-AMP) revealed conformational changes of a tyrosine residue present in the active site. Mutation of this tyrosine to alanine abolishes c-di-AMP formation and, thus, demonstrates its functional importance. Furthermore, we confirmed that CdaA is active in the presence of Mn^{2+} or Co^{2+} ions, with significantly higher activity in the case of Mn^{2+}, but it is inactive in the presence of Mg^{2+} ions. These

This work was supported by Deutsche Forschungsgemeinschaft Priority Programs SPP1879 and INST186/1117. The authors declare that they have no conflicts of interest with the contents of this article.
This article contains Figs. S1–S6.
[1] To whom correspondence should be addressed. Tel.: 49-551-3914072; E-mail: rficner@uni-goettingen.de.
[2] The abbreviations used are: c-di-AMP, cyclic di-AMP; DAC, diadenylate cyclase; TM, transmembrane; r.m.s.d., root mean square deviation.

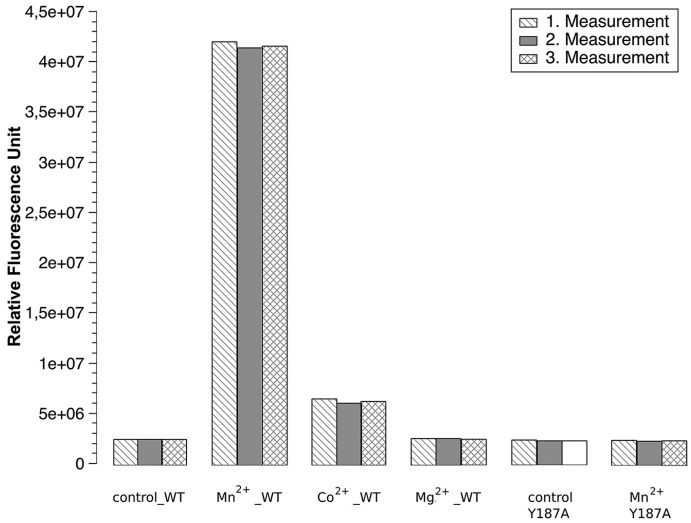

Figure 1. *In vitro* diadenylate cyclase activity of Δ100CdaA. Presented is a histogram displaying three independent measurements. A control measurement was performed using WT Δ100CdaA without addition of any divalent metal cations. The histogram represents the divalent metal cation preferences of WT Δ100CdaA. The highest amount of c-di-AMP was formed in the presence of $MnCl_2$, whereas, in the presence of $CoCl_2$, the amount of the product is significantly reduced. For $MgCl_2$ and $CaCl_2$, production of c-di-AMP could not be confirmed, as it was within the range of the control. Additionally, it represents the importance of Tyr-187 on catalysis. The mutant Y187A causes a significant reduction (5-fold) of diadenylate cyclase activity, confirming its essential role in c-di-AMP synthesis.

new CdaA structures could serve as an important starting point for future rational drug design.

Results

Structure-based development of novel antibiotic drugs requires high-resolution three-dimensional structures of the targeted enzyme and enzyme–inhibitor complexes. CdaA of the human pathogen *L. monocytogenes* appears to be an attractive target, as c-di-AMP synthesis is essential for bacterial growth and CdaA is the only DAC in this pathogenic bacterium, whereas there are no DACs in humans. For this study, truncated Δ100CdaA, missing the N-terminal transmembrane (TM) helices and the 20 amino acids linking the TM to the DAC domain, was used because the transmembrane helices hamper the solubility of the recombinant full-length protein. We have demonstrated previously that this truncated Δ100CdaA has preserved its enzymatic activity with a higher enzymatic activity for Co^{2+} compared with Mn^{2+} but no activity for of Mg^{2+} (15). Although, in this previous study, the *in vitro* activity was measured by LC-MS/MS, we now applied a direct fluorescence-based measurement of c-di-AMP formation by its binding to coralyne (16). In contrast to the results obtained with the LC-MS/MS method, more efficient c-di-AMP synthesis was observed in the presence of Mn^{2+} compared with Co^{2+} (Fig. 1*A*).

Structure of apo CdaA

One approach for identification of potential inhibitors is crystallographic fragment screening, which desires crystals of CdaA in its apo state. Therefore, Δ100CdaA was crystallized in the absence of ATP and divalent metal ions. Crystals of apo-CdaA were obtained and belong to space group $P2_12_12_1$, containing two Δ100CdaA molecules per asymmetric unit. The phase problem was solved by means of molecular replacement using the monomeric Δ100CdaA structure of *L. monocytogenes* (PDB code 4RV7) as a search model. The resulting crystal structure of apo-CdaA was determined at 2.0 Å resolution (Table 1). The CdaA monomer is composed of a slightly twisted central β-sheet made up of seven mixed-parallel and antiparallel β-strands (β1–β7), flanked on both sides by five α-helices (α1–α5) in total (Fig. 2). The two Δ100CdaA molecules in the asymmetric unit are structurally very similar, as indicated by the root mean square deviation (r.m.s.d.) of 1.19 Å between all Cα positions.

The structure of apo-CdaA closely resembles that of CdaA with bound ATP (PDB code 4RV7), as they exhibit an r.m.s.d. of 1.56 Å, but a few differences are seen in a loop region (residues 137–140) and the C-terminal residues. Careful inspection of the difference electron density map revealed a small molecule bound to the surface of one of two CdaA molecules in the asymmetric unit (Fig. S1). This electron density was interpreted as a sucrose molecule originating from the utilized cryo-protectant solution. In the apo-CdaA crystal structure, the active site is accessible from solvent channels; hence, this crystal form of apo-CdaA appears to be suitable for a fragment screen.

Structure of the CdaA–c-di-AMP complex

To gain more insight into the structure and function of CdaA, we also crystallized Δ100CdaA in the presence of ATP and the cofactor Co^{2+}. The obtained crystals belong to a differ-

Table 1
Crystallographic data collection and refinement statistics

	Δ100CdaA with AMP and c-di-AMP	Δ100CdaA-APO	Δ100CdaA_Y187A-APO
Crystallographic data			
Beamline	Petra III-P14, EMBL, Hamburg	Petra III-P14, EMBL, Hamburg	Petra III-P13, EMBL, Hamburg
Wavelength (Å)	0.97620	0.97620	0.97625
Resolution range (Å)[a]	42.27–2.80 (2.90–2.80)	45.89–2.00 (2.10–2.00)	46.49–2.23 (2.33–2.23)
Unique reflections	9,435	24,884	19,512
Redundancy	5.6 (5.7)	7.1 (7.0)	5.8 (4.2)
Completeness (%)	93.0 (95.4)	99.7 (98.5)	97.1 (79.3)
Space group	H32	$P2_12_12_1$	$P2_12_12_1$
a (Å)	121.90	42.69	46.49
b (Å)	121.90	64.67	65.13
c (Å)	141.59	129.75	131.33
R_{merge} (%)	10.9 (80.5)	9.4 (119.0)	8.0 (52.0)
I/σ (I)	12.4 (1.9)	13.6 (2.0)	15.6 (2.8)
$CC_{1/2}$	99.8 (72.6)	99.9 (77.2)	99.8 (80.5)
Refinement statistics			
R_{work}/R_{free}	0.1875/0.2337	0.1858/0.2245	0.1837/0.2258
No. of atoms	2453	2610	2740
Average B-factor (Å^2)	58.0	47.6	39.8
Root mean square deviation			
Bonds Å	0.003	0.008	0.006
Angles (°)	0.644	1.003	1.258
Ramachandran plot			
Favored (%)	98.05	98.11	98.79
Allowed (%)	1.95	1.57	1.21
Outlier (%)	0.00	0.31	0. 00
PDB codes	6HVL	6HVM	6HVN

[a] Values for the data in the highest-resolution shell are shown in parentheses.

ent space group (H32) than the previously determined structure but also contain two CdaA molecules in the asymmetric unit. The newly obtained crystal structure was determined at 2.8 Å resolution. The two CdaA molecules in the asymmetric unit superpose very well, as the r.m.s.d. calculated between all Cα positions amounts to 0.65 Å. Analysis of the protein contact surfaces in the crystal revealed that one of the two CdaA molecules in the asymmetric unit forms a dimer with a symmetry mate related by a crystallographic two-fold axis (Fig. 3*A*). This CdaA homodimer corresponds to the catalytically active DAC domain dimers seen in the DisA homo-octamer. The calculated r.m.s.d between superimposed CdaA and DisA dimers amounts to 1.72 Å (198 matched Cα positions, Fig. S4). The CdaA–CdaA dimer interface buries about 605 Å^2 of the accessible surface area (7.3%) and is stabilized by six hydrogen bonds and two salt bridges. However, additional interactions between the monomers are mediated by the ligand bound to the active site (see below). Surprisingly, the difference electron density map clearly revealed the presence of a c-di-AMP molecule and two metal ions bound in the active site of the CdaA crystallographic dimer (Fig. S2*A*). As only ATP and Co^{2+} were added to the protein right before it was subjected to crystallization, the c-di-AMP must have formed during or after crystallization droplets were set up. It appears very likely that the bound metal ion is a Co^{2+}, as no other catalytic metal cation was present in the crystallization solution. The Co^{2+} is coordinated by the phosphate moiety and the carboxylate group of Glu-224 as well as the carboxylate group of Asp-171 and the imidazole ring nitrogen of His-170 of the symmetry-related subunit (Fig. 3, *B* and *C*). The metal–oxygen distances of 2.1 Å for Asp-171 and Glu-224 and 2.3 Å for phosphate correspond to distances observed in other proteins containing a Co^{2+} ion (17). Elongated distances observed between Co^{2+} and the imidazole ring of His-170 (3.1 Å) and the c-di-AMP 3′OH group (3.8 Å) indicate that this complex corresponds to the post-catalytic state. To fulfill its catalytic role, the metal ion must be shifted. Only then it can act as Lewis acid to increase the nucleophilicity of the metal-activated 3′ hydroxyl group of ATP and enhance the electrophilicity of the phosphorus atom of the adjacent ATP molecule.

The asymmetric unit of the crystal contains a second CdaA molecule that also accommodates a nucleotide bound in the active site but no bound metal ion (Fig. 4). Based on the observed difference omit electron density map (Fig. S2*B*), the nucleotide was identified as AMP. Because previous crystal structures of DisA and CdaA with bound ATP or 3′-dATP showed well-defined electron density for the β and γ phosphates, it appears likely that the second CdaA molecule indeed has AMP bound, which must have formed out of ATP during the crystallization process. ATP hydrolysis also explains the presence of another difference electron density map peak, which has been interpreted as a free phosphate. This phosphate ion is bound in the vicinity of the c-di-AMP molecule and could potentially mark an exit route of the pyrophosphate molecule on the surface of CdaA.

Conformational rearrangements of the active site induced by ligands

The comparison of CdaA in the apo state to CdaA complexed with AMP or c-di-AMP unveils different orientations of the Tyr-187 side chain, which is located in close proximity to the adenine base. In the CdaA apo state, this tyrosine side chain is rotated outward from the active site, leading to an opening of the binding site for the adenine base (Fig. 5). In the monomeric CdaA–AMP complex, the tyrosine is rotated inward at the active site and stacks on the adenine in an almost coplanar orientation. In contrast, in the dimeric c-di-

Structures of the diadenylate cyclase CdaA

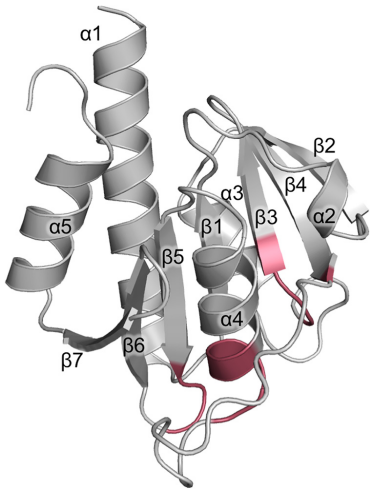

Figure 2. Crystal structure of Δ100CdaA in the apo state, refined at 2 Å resolution. The fold of the CdaA DAC domain consists of seven β-strands forming a central β-sheet surrounded by five α-helices. The positions of residues forming the active site are highlighted in *red*.

AMP complex, the tyrosine side chain is flipped outward, as the Thr-202 side chain of the other subunit packs against the adenine ring (Fig. 3*B*).

To investigate whether Tyr-187 plays an important role in c-di-AMP formation, a Y187A mutant was generated. This mutation led to a significant reduction (about 80%) in activity, confirming the functional impact of Tyr-187 (Fig. 1*B*). To exclude that the Y187A mutation perturbed the fold of CdaA, the crystal structure of Δ100CdaA_Y187A was determined as well (Table 1). Comparison with the structure of WT Δ100CdaA demonstrates no structural changes caused by the mutation.

Discussion

Synthesis of c-di-AMP requires dimerization and proper orientation of two DAC domains, each with one ATP bound and accompanied by the metal ion cofactor. In DisA, this is achieved permanently by the homo-octameric oligomerization state (13). The first structure of CdaA of *L. monocytogenes* showed that the DAC domain crystallized as a monomer even though ATP was bound to the active site (15). However, for the previous study and this one, a truncated CdaA was used. So far, the influence of the missing transmembrane domain on oligomerization and catalytic activity is unknown.

Here, a new crystal form of CdaA was obtained that contains two CdaA molecules with different nucleotides bound. One CdaA molecule forms a catalytically active dimer with a symmetry mate in the crystal. This dimer contains a c-di-AMP molecule and two metal ions in the active site; hence, it closely resembles the dimer arrangement of DAC domains seen in DisA (Fig. S4).

The c-di-AMP must have been formed during crystallization, as only ATP and Co^{2+} ions were added to CdaA. This complex corresponds to the enzyme–product complex, which is supposed to have a lower stability. However, c-di-AMP mediates multiple contacts between the monomers, increasing the interaction surface area between the monomers, and the catalytically active dimer appears to be caught in the crystalline lattice.

Conserved active-site residues of DisA and CdaA directly involved in substrate binding and catalysis have been identified previously (15, 18). Each of the mutations in DisA (D75N, R130A, RHR (108–110)AAA, T107V+T111V), and in CdaA (D171N, G172A, and T202N) led to a reduction or complete loss of enzymatic activity. However, by analyzing the structure of the monomeric CdaA in the asymmetric unit with bound AMP, we realized that the Tyr-187 side chain might also be involved in substrate binding, as it stacks on the adenine ring, but it is rotated outward in the structure of apo CdaA (Fig. 5). Hence, it appears likely that, upon binding of ATP to monomeric CdaA, Tyr-187 rotates toward the adenine moiety and locks the ATP in the active site by a $\pi-\pi$ stacking interaction, as observed for many other ATP binding proteins (19). However, upon CdaA dimerization, the tyrosine side chain is replaced by the side chain of Thr-202 of the other subunit, which then stabilizes the bound ATP. The replacement of the Tyr by a side chain from the other subunit might facilitate product release after catalysis, as, upon dimer dissociation, the product can be released more easily. By mutation of Tyr-187 to Ala, which strongly reduced the activity *in vitro*, we demonstrate that Tyr-187 indeed plays an essential role in c-di-AMP formation by CdaA. Notably, this Tyr-187 is conserved in most CdaA enzymes but not in other DAC proteins, like DisA, suggesting a slightly different mechanism of substrate binding between different classes of DACs.

A remarkable difference between DisA and CdaA concerns the metal ion specificity in the catalytic center. Although DisA appears to be active with Mg^{2+} and Mn^{2+} (20), CdaA is not active in the presence of Mg^{2+}. Such unexpected differences in metal ion preferences have also been observed for other protein families, *e.g.* the metal-dependent serine/threonine phosphoprotein phosphatase family (21). Because the catalytic mechanism of phosphoprotein phosphatase enzymes as well as that of DAC proteins does not require the redox potential of Mn^{2+} to carry out the catalyzed reaction, it is not clear why some members of the DAC family would prefer Mn^{2+} or other divalent cations over Mg^{2+} (22). Hence, the observed strict dependence of CdaA on Mn^{2+} or Co^{2+} ions raised questions concerning its structural basis. The observed metal ion dependence is most likely related to different chemical properties of the cation, *e.g.* ionic radius, and to the amino acid composition of the active site.

Comparison of the DisA and CdaA structures reveals significant differences in metal ion coordination. In the catalytically active dimer of DisA with bound ATP, the Mg^{2+} ion is coordinated by three phosphate groups and the Asp carboxylate. In CdaA, more protein residues contribute to metal binding, resulting in a more crowded active site. In addition to Asp-171 (which corresponds to Asp-75 of DisA), the side chains of Glu-224 and His-170 coordinate the Co^{2+} ion. These two residues are not structurally conserved in DisA, as

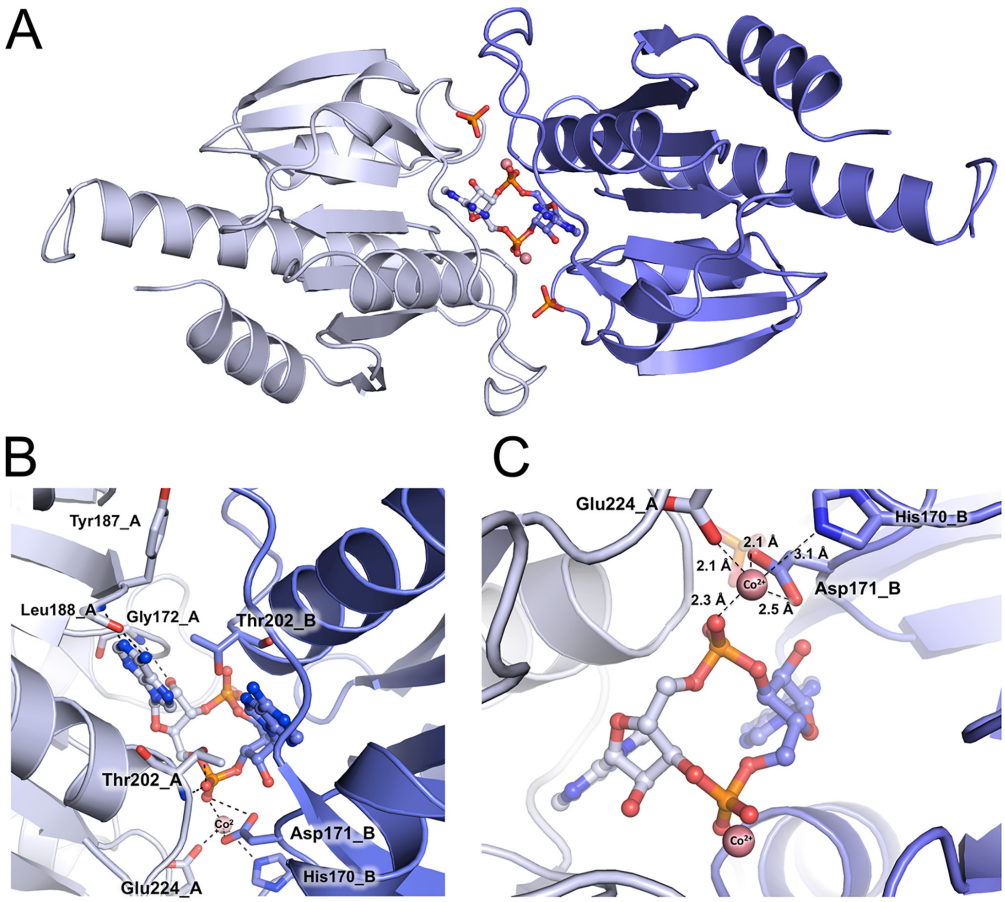

Figure 3. The active site of dimeric CdaA with bound c-di-AMP. *A*, the catalytically active Δ100CdaA homodimer is depicted as a *cartoon*, and the bound reaction product c-di-AMP is shown as *balls* and *sticks* (carbon in *pale blue* and *blue*, phosphate in *orange*, oxygen in *red*, and nitrogen in *dark blue*). The two Δ100CdaA monomers are colored according to the c-di-AMP in *pale blue* and *blue*, respectively. Co^{2+} ions are depicted as *pale red spheres*. *B*, detailed view of the CdaA active site. Amino acids involved in binding the c-di-AMP molecule (colored and depicted as in *A*) are shown as *sticks* (carbon in *pale blue* and *blue*, oxygen in *red*, and nitrogen in *dark blue*). The Co^{2+} ions are colored and depicted according to *A*. For simplicity, only one half of the two-fold symmetric CdaA active site is shown. *C*, detailed view of the Co^{2+} binding site and its coordination sphere.

there is an Arg instead of the Glu and a Met instead of the His. The side chains of both Arg and Met are rotated outward from the metal binding site, making it less crowded. Hence, the major difference appears to be presence of the His. Although Mg^{2+} strongly prefers coordination by Asp and Glu, the transition metal ions Mn^{2+} and Co^{2+} are bound as well by His, as deduced from analysis of all metal binding sites in known protein structures (23).

The reason for this difference between DisA and CdaA is most likely related to the fact that DisA contains stably associated, catalytically active dimers, whereas, for CdaA, the catalytic dimer might just exist transiently. Therefore, in DisA, Asp-171, which belongs to the second DAC domain, is sufficient for binding the substrate ATP and the metal ion. In CdaA, ATP and the metal ion are initially bound to the monomeric DAC domain by the Glu-224 side chain, and solvent molecules complete the metal coordination sphere. Upon formation of the catalytically active dimer, the metal ion needs to be slightly repositioned to be further coordinated by His-170 and Asp-171, provided by the second monomer (Fig. S3).

Recently, CdaA from *S. aureus* was characterized structurally and biochemically (24). Surprisingly, in contrast to *L. monocytogenes* CdaA, the *S. aureus* CdaA homolog shows activity not only in the presence of transition metal ions but also in the presence of Mg^{2+}. Comparison of the active sites of both available CdaA structures unveils identical positioning of the amino acids directly involved in c-di-AMP and

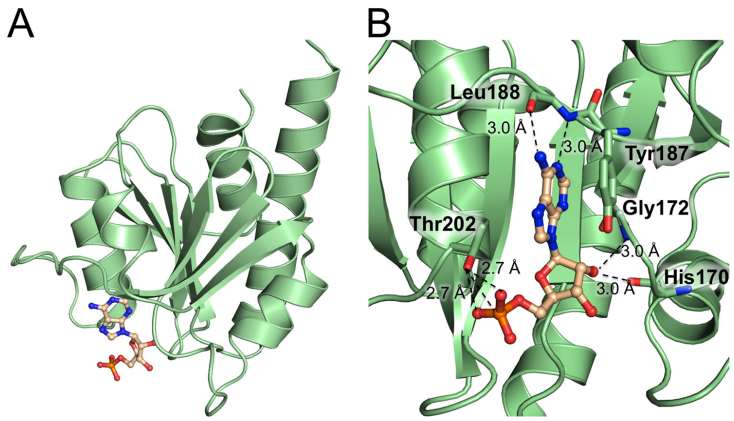

Figure 4. Structure of the CdaA-AMP complex. *A*, CdaA monomer (*cartoon*, *pale green*) with a bound AMP molecule depicted as *balls* and *sticks*. *B*, a detailed view of the active site showing the amino acids (*sticks*, carbon in *pale green*, oxygen in *red*, and nitrogen in *blue*) involved in AMP binding. The bound AMP is shown as a *ball-and-stick model* (carbon in *wheat*, phosphate in *orange*, oxygen in *red*, and nitrogen in *dark blue*).

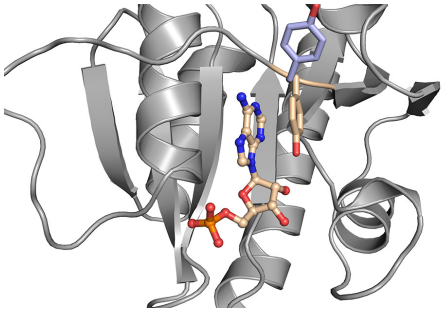

Figure 5. Conformational switch of Tyr-187 during c-di-AMP synthesis. For convenience, only the Δ100CdaA monomer (*gray*) with bound AMP (carbon in *wheat*, phosphate in *orange*, oxygen in *red*, and nitrogen in *dark blue*) and Tyr-187 (*wheat*) is shown. AMP is depicted as a *ball-and-stick model*. The side chain of Tyr-187 (*pale blue*) of the Δ100CdaA– c-di-AMP complex structure is superimposed. Upon ATP binding to monomeric CdaA, Tyr-187 stacks parallel on the adenine base (π–π interaction) and stabilizes the protein–substrate complex. Upon homodimer formation, the side chain of Tyr-187 rotates outwards as it is replaced by the Thr-202 side chain of the second monomer in the catalytically active homodimer.

metal ion coordination (Fig. S5). The largest structural differences can be observed for N- and C-terminal α-helices and a loop connecting β-strand 4 and α-helix 4. The latter is located in close proximity to the phosphate moiety of ATP and could indirectly alter the metal binding preferences or even metal catalytic efficiency. This could serve as a potential explanation for the metal ion promiscuity of CdaAs showing strict conservation of three residues (His-170, Asp-171, and Glu-224) directly involved in metal binding, as revealed by sequence alignment of ten bacterial CdaAs (Fig. S6). The chemical properties of these three residues are most likely the structural basis for the observed metal ion promiscuity of CdaAs, which has also been observed for other enzymes, *e.g.* mannosylglycerate synthase (25). The observed capability of utilizing several ions by one enzyme is still one of many not well-understood marvels of enzymology that require further investigation.

Experimental procedures

Bacterial strains and growth conditions

For cloning procedures and protein overexpression, *Escherichia coli* strains DH5α and BL21(DE3) were used. The *E. coli* strains were cultivated in 2xYT ((trypton 1.6% (w/v), yeast extract 1.0% (w/v), NaCl 0.5% (w/v)) medium, whereas transformed cells were selected on lysogeny broth-medium plates containing ampicillin (100 μg/ml).

Plasmid construction

For purification, the DAC-type CdaA was equipped with a GST tag. CdaA is known to be a transmembrane protein. The Δ*300cdaA* allele, which lacks the TM domain, was amplified using the primer pairs JH004 forward (5′-CCGGATCCTATGGATCAAGAATTGAGCG-3′)/JH005 reverse (5′ GGCTCGAG TCATTCGCTTTTGCCTCCTTTCC-3′). As a template, the plasmid pBP33 was used (15). The resulting PCR products were cloned in the pGEX-6P-1 (GE Healthcare) expression vector using the restriction sites XhoI and BamHI, leading to plasmid pGEXpBP33, which encodes for the truncated Δ100CdaA protein with an N-terminal GST tag.

Site-directed mutagenesis

Δ100CdaA mutants were generated with site-directed mutagenesis to identify amino acid residues that have an important function in the catalytic reaction mechanism. The CdaA mutant Y187A was created by PCR using the mutagenesis primer pairs JH_Y187A_forward (5′-CAGCAAGTGCCTTGCCA CTTTCAGATAGCCCGTTCTTATCCAAAGAAC-3′) and JH_Y187A_reverse (5′-GTGGCAAGGCACTTGCTGCCGATGC AATTTCGTTTCCTTTAATAATAACTGC-3′), resulting in the plasmid encoding the truncated mutant variant Δ100CdaA_Y187A.

Protein expression and purification

E. coli BL21(DE3) was used for expression of the fusion protein GST-Δ100CdaA. The cells were grown in 1 liter of 2xYT medium at 37 °C. Protein expression was induced after the culture reached an A_{600} of ~ 0.6 by addition of 1 mM isopropyl 1-thio-β-D-galactopyranoside and incubated at 16 °C for 18 h. After harvesting and subsequent to cell disruption with a microfluidizer (M-110S Microfluidizer, Microfluidics) and centrifugation at 15,600 × *g* for 30 min to remove cell debris, the lysate was loaded onto a GSH-Sepharose column (GE Healthcare) in 300 mM NaCl, 20 mM Tris/HCl (pH 7.5), and 10 mM EDTA. The target protein GST-Δ100CdaA was eluted from the column with 40 mM reduced GSH. The eluate was incubated overnight with PreScission protease (1:100 (w/w)) in cellulose tubing placed in dialysis buffer (100 mM NaCl and 20 mM Tris/HCl (pH 7.5)) at 4 °C to remove the high GSH concentration and to dissect the GST tag from Δ100CdaA. To remove the cleaved-off tag from the truncated CdaA, a second GSH-Sepharose purification step was included.

Crystallization and cryoprotecion

For crystallization, the sitting-drop vapor diffusion method was applied. Initial crystallization trials were performed at 20 °C using Δ100CdaA at a concentration of 4.0 mg/ml supplemented with 500 μM $CoCl_2$ and 500 μM ATP. Rectangular crystals grew after approximately 48 h in a 2-μl droplet composed of the aforementioned protein solution mixed with reservoir in a 1:1 ratio. The reservoir was composed of 0.2 M $Ca(CH_3COO)_2$, 0.1 M Na-HEPES (pH 7.5), and 10% (w/v) PEG8000. Crystals were cryoprotected by soaking them in a reservoir solution supplemented with 25% PEG8000.

For crystallization of the apo form and the Y187A variant of Δ100CdaA, a protein concentration of 6.0 mg/ml was used, keeping the 2-μl droplet size and 1:1 protein-to-reservoir ratio. To facilitate crystal growth, microseeding was performed in combination with small alterations of NaCl concertation. Thin crystal plates were obtained after approximately 18 h in a salt concentration ranging between 3.7–4.5 M NaCl and 0.1 M Na-HEPES (pH 8.5). Crystals were cryoprotected by soaking them in a saturated sucrose solution obtained by solubilizing sucrose in reservoir solution.

X-ray data collection and processing

Diffraction images were collected at PETRA III EMBL beamlines P13 and P14 (DESY, Hamburg, Germany) and processed with the XDS package (26, 27). Data collection and processing statistics are summarized in Table 1. A trigonal lattice with unit cell parameters of $a = b = 121.90$ Å, $c = 141.59$ Å was determined for the crystals containing the CdaA–c-di-AMP complex. Cell content analysis indicated the presence of two CdaA molecules occupying the asymmetric unit ($V_m = 2.89$ Å^3/Da, corresponding solvent content of 57.4%). The crystals of apo CdaA and the Y187A mutant exhibited an orthorhombic lattice and the unit cell parameters of $a = 42.96$ Å, $b = 64.67$ Å, $c = 129.75$ Å and $a = 46.49$ Å, $b = 65.13$ Å, $c = 131.33$ Å, respectively. The Matthews coefficient ($V_m = 2.55$ Å^3/Da, corresponding solvent content of 51.78%) implicates two molecules occupying the asymmetric unit.

Structure determination and refinement

The crystallographic phase problem was solved by molecular replacement with PHASER (28) using the structure of the DAC Δ100CdaA from *L. monocytogenes* (PDB code 4RV7) as a search model. Manual model building was preformed with Coot (29), and the structure was refined with Refmac (30) and PHENIX (31). To monitor the refinement progress using R_{free}, 5% of the reflections were selected randomly and excluded from refinement. During the refinement process, the coordination distance for the Co^{2+} ion in the ligand-bound structure was restrained to 2.1 Å for the Glu-224 and Asp-171 side chains and to 2.3 Å for the cyclic di-AMP phosphate. The final structure of the CdaA–c-di-AMP complex was refined at a resolution of 2.8 Å to R_{work} of 18.7% and R_{free} of 23.4%. The apo-CdaA was refined at a resolution of 2.0 Å to R_{work} of 18.6% and R_{free} of 22.5%. The structure of the Y187A mutant was determined at 2.32 Å resolution and refined to 17.5% and 22.0% for R_{work} and R_{free}, respectively. Protein contact areas in the crystals were analyzed using "Protein interfaces, surfaces and assemblies" services at the European Bioinformatics Institute using standard settings (32).

In vitro DAC activity assay

Diadenylate cyclase activity was measured with a quantitative fluorescence assay based on an increased fluorescence signal because of the specific interaction of the fluorescent dye coralyne with c-di-AMP (16). A 200-μl reaction mixture contained 40 mM Tris/HCl (pH 7.5), 100 mM NaCl, 10 mM XCl_2 (X = Mg, Co, Mn, or Ca) and 100 μM ATP. The reaction was started by addition of 10 μM Δ100CdaA and incubated for 1 h at 37 °C. To stop the reaction, the reaction mixture was boiled for 5 min and centrifuged for another 5 min at 13,400 × *g* to remove the precipitated protein. For quantification of the synthesized c-di-AMP, 250 mM KBr and 10 μM coralyne were added to the reaction mixture. After incubating the samples for 30 min in the dark, c-di-AMP concentration was determined by excitation at a wavelength of 420 nm and measuring the fluorescence emission at a wavelength of 475 nm using a microplate reader (Victor Nivo multimode microplate reader, PerkinElmer Life Sciences).

Author contributions—J. L. H. data curation; J. L. H., P. N., A. D., and R. F. formal analysis; J. L. H. and P. N. validation; J. L. H., P. N., and R. F. writing-original draft; J. L. H., P. N., A. D., and R. F. writing-review and editing; R. F. conceptualization; R. F. funding acquisition.

Acknowledgments—We thank the EMBL-Outstation Hamburg (DESY PETRA III beamlines P13 and P14, Germany) for allocation of beam time and Isabel Bento, Johanna Hakanpää, as well as Saravanan Panneerselvam for excellent support at the beamline. We also thank Johannes Gibhardt, Fabian Commichau, and Jörg Stülke for fruitful discussions.

References

1. Gomelsky, M. (2011) cAMP, c-di-GMP, c-di-AMP and now cGMP: bacteria use them all!. *Mol. Microbiol.* **79,** 562–565 CrossRef Medline

Structures of the diadenylate cyclase CdaA

2. Kalia, D., Merey, G., Nakayama, S., Zheng, Y., Zhou, J., Luo, Y., Guo, M., Roembke, B. T., and Sintim, H. O. (2013) Nucleotide, c-di-GMP, c-di-AMP, cGMP, cAMP, (p)ppGpp signaling in bacteria and implications in pathogenesis. *Chem. Soc. Rev.* **42,** 305–341 CrossRef Medline
3. Hengge, R., Gründling, A., Jenal, U., Ryan, R., and Yildiz, F. (2016) Bacterial signal transduction by cyclic di-GMP and other nucleotide second messengers. *J. Bacteriol.* **198,** 15–26 CrossRef Medline
4. Commichau, F. M., Dickmanns, A., Gundlach, J., Ficner, R., and Stülke, J. (2015) A jack of all trades: the multiple roles of the unique essential second messenger cyclic di-AMP. *Mol. Microbiol.* **97,** 189–204 CrossRef Medline
5. Corrigan, R. M., and Gründling, A. (2013) Cyclic di-AMP: another second messenger enters the fray. *Nat. Rev. Microbiol.* **11,** 513–524 CrossRef Medline
6. Witte, C. E., Whiteley, A. T., Burke, T. P., Sauer, J. D., Portnoy, D. A., and Woodward, J. J. (2013) Cyclic di-AMP is critical for *Listeria monocytogenes* growth, cell wall homeostasis, and establishment of infection. *MBio* **4,** e00282–00213 Medline
7. Gundlach, J., Herzberg, C., Kaever, V., Gunka, K., Hoffmann, T., Weiß, M., Gibhardt, J., Thürmer, A., Hertel, D., Daniel, R., Bremer, E., Commichau, F. M., and Stülke, J. (2017) Control of potassium homeostasis is an essential function of the second messenger cyclic di-AMP in *Bacillus subtilis*. *Sci. Signal.* **10,** eaal3011 CrossRef Medline
8. Gundlach, J., Dickmanns, A., Schröder-Tittmann, K., Neumann, P., Kaesler, J., Kampf, J., Herzberg, C., Hammer, E., Schwede, F., Kaever, V., Tittmann, K., Stülke, J., and Ficner, R. (2015) Identification, characterization, and structure analysis of the cyclic di-AMP-binding PII-like signal transduction protein DarA. *J. Biol. Chem.* **290,** 3069–3080 CrossRef Medline
9. Bai, Y., Yang, J., Zhou, X., Ding, X., Eisele, L. E., and Bai, G. (2012) *Mycobacterium tuberculosis* Rv3586 (DacA) is a diadenylate cyclase that converts ATP or ADP into c-di-AMP. *PLoS ONE* **7,** e35206 CrossRef Medline
10. Corrigan, R. M., Abbott, J. C., Burhenne, H., Kaever, V., and Gründling, A. (2011) c-di-AMP is a new second messenger in *Staphylococcus aureus* with a role in controlling cell size and envelope stress. *PLoS Pathog.* **7,** e1002217 CrossRef Medline
11. Woodward, J. J., Iavarone, A. T., and Portnoy, D. A. (2010) c-di-AMP secreted by intracellular *Listeria monocytogenes* activates a host type I interferon response. *Science* **328,** 1703–1705 CrossRef Medline
12. Commichau, F. M., Heidemann, J. L., Ficner, R., and Stülke, J. (2019) Making and breaking of an essential poison: the cyclases and phosphodiesterases that produce and degrade the essential second messenger cyclic di-AMP in bacteria. *J. Bacteriol.* **201,** e00462–18 Medline
13. Witte, G., Hartung, S., Büttner, K., and Hopfner, K. P. (2008) Structural biochemistry of a bacterial checkpoint protein reveals diadenylate cyclase activity regulated by DNA recombination intermediates. *Mol. Cell* **30,** 167–178 CrossRef Medline
14. Cho, K. H., and Kang, S. O. (2013) *Streptococcus pyogenes* c-di-AMP phosphodiesterase, GdpP, influences SpeB processing and virulence. *PLoS ONE* **8,** e69425 CrossRef Medline
15. Rosenberg, J., Dickmanns, A., Neumann, P., Gunka, K., Arens, J., Kaever, V., Stülke, J., Ficner, R., and Commichau, F. M. (2015) Structural and biochemical analysis of the essential diadenylate cyclase CdaA from *Listeria monocytogenes*. *J. Biol. Chem.* **290,** 6596–6606 CrossRef Medline
16. Zhou, J., Sayre, D. A., Zheng, Y., Szmacinski, H., and Sintim, H. O. (2014) Unexpected complex formation between coralyne and cyclic diadenosine monophosphate providing a simple fluorescent turn-on assay to detect this bacterial second messenger. *Anal. Chem.* **86,** 2412–2420 CrossRef Medline
17. Harding, M. M. (2006) Small revisions to predicted distances around metal sites in proteins. *Acta Crystallogr. D Biol. Crystallogr.* **62,** 678–682 CrossRef Medline
18. Müller, M., Deimling, T., Hopfner, K. P., and Witte, G. (2015) Structural analysis of the diadenylate cyclase reaction of DNA-integrity scanning protein A (DisA) and its inhibition by 3′-dATP. *Biochem. J.* **469,** 367–374 CrossRef Medline
19. Mao, L., Wang, Y., Liu, Y., and Hu, X. (2004) Molecular determinants for ATP-binding in proteins: a data mining and quantum chemical analysis. *J. Mol. Biol.* **336,** 787–807 CrossRef Medline
20. Manikandan, K., Sabareesh, V., Singh, N., Saigal, K., Mechold, U., and Sinha, K. M. (2014) Two-step synthesis and hydrolysis of cyclic di-AMP in *Mycobacterium tuberculosis*. *PLoS ONE* **9,** e86096 CrossRef Medline
21. Shi, L. (2004) Manganese-dependent protein *O*-phosphatases in prokaryotes and their biological functions. *Front. Biosci.* **9,** 1382–1397 CrossRef Medline
22. Samol, I., Shapiguzov, A., Ingelsson, B., Fucile, G., Crèvecoeur, M., Vener, A. V., Rochaix, J. D., and Goldschmidt-Clermont, M. (2012) Identification of a photosystem II phosphatase involved in light acclimation in *Arabidopsis*. *Plant Cell* **24,** 2596–2609 CrossRef Medline
23. Putignano, V., Rosato, A., Banci, L., and Andreini, C. (2018) MetalPDB in 2018: a database of metal sites in biological macromolecular structures. *Nucleic Acids Res.* **46,** D459–D464 CrossRef Medline
24. Tosi, T., Hoshiga, F., Millership, C., Singh, R., Eldrid, C., Patin, D., Mengin-Lecreulx, D., Thalassinos, K., Freemont, P., and Gründling, A. (2019) Inhibition of the *Staphylococcus aureus* c-di-AMP cyclase DacA by direct interaction with the phosphoglucosamine mutase GlmM. *PLoS Pathog.* **15,** e1007537 CrossRef Medline
25. Nielsen, M. M., Suits, M. D., Yang, M., Barry, C. S., Martinez-Fleites, C., Tailford, L. E., Flint, J. E., Dumon, C., Davis, B. G., Gilbert, H. J., and Davies, G. J. (2011) Substrate and metal ion promiscuity in mannosylglycerate synthase. *J. Biol. Chem.* **286,** 15155–15164 CrossRef Medline
26. Kabsch, W. (2010) XDS. *Acta Crystallogr. D Biol. Crystallogr.* **66,** 125–132 CrossRef Medline
27. Kabsch, W. (2010) Integration, scaling, space-group assignment and post-refinement. *Acta Crystallogr. D Biol. Crystallogr.* **66,** 133–144 CrossRef Medline
28. McCoy, A. J., Grosse-Kunstleve, R. W., Adams, P. D., Winn, M. D., Storoni, L. C., and Read, R. J. (2007) Phaser crystallographic software. *J. Appl Crystallogr.* **40,** 658–674 CrossRef Medline
29. Emsley, P., Lohkamp, B., Scott, W. G., and Cowtan, K. (2010) Features and development of Coot. *Acta Crystallogr. D Biol. Crystallogr.* **66,** 486–501 CrossRef Medline
30. Winn, M. D., Ballard, C. C., Cowtan, K. D., Dodson, E. J., Emsley, P., Evans, P. R., Keegan, R. M., Krissinel, E. B., Leslie, A. G., McCoy, A., McNicholas, S. J., Murshudov, G. N., Pannu, N. S., Potterton, E. A., Powell, H. R., *et al.* (2011) Overview of the CCP4 suite and current developments. *Acta Crystallogr. D Biol. Crystallogr.* **67,** 235–242 CrossRef Medline
31. Adams, P. D., Afonine, P. V., Bunkóczi, G., Chen, V. B., Davis, I. W., Echols, N., Headd, J. J., Hung, L. W., Kapral, G. J., Grosse-Kunstleve, R. W., McCoy, A. J., Moriarty, N. W., Oeffner, R., Read, R. J., Richardson, D. C., *et al.* (2010) PHENIX: a comprehensive Python-based system for macromolecular structure solution. *Acta Crystallogr. D. Biol. Crystallogr.* **66,** 213–221 CrossRef Medline
32. Krissinel, E., and Henrick, K. (2007) Inference of macromolecular assemblies from crystalline state. *J. Mol. Biol.* **372,** 774–797 CrossRef Medline

Crystal structures of the c-di-AMP–synthesizing enzyme CdaA

Jana L. Heidemann, Piotr Neumann, Achim Dickmanns and Ralf Ficner

J. Biol. Chem. 2019, 294:10463-10470.
doi: 10.1074/jbc.RA119.009246 originally published online May 22, 2019

Supporting Information

Crystal structures of the c-di-AMP synthesizing enzyme CdaA

Jana L. Heidemann[1], Piotr Neumann[1], Achim Dickmanns[1], and Ralf Ficner[1*]

[1]Department of Molecular Structural Biology, Institute for Microbiology and Genetics, Georg-August-University Goettingen, 37077 Goettingen, Germany

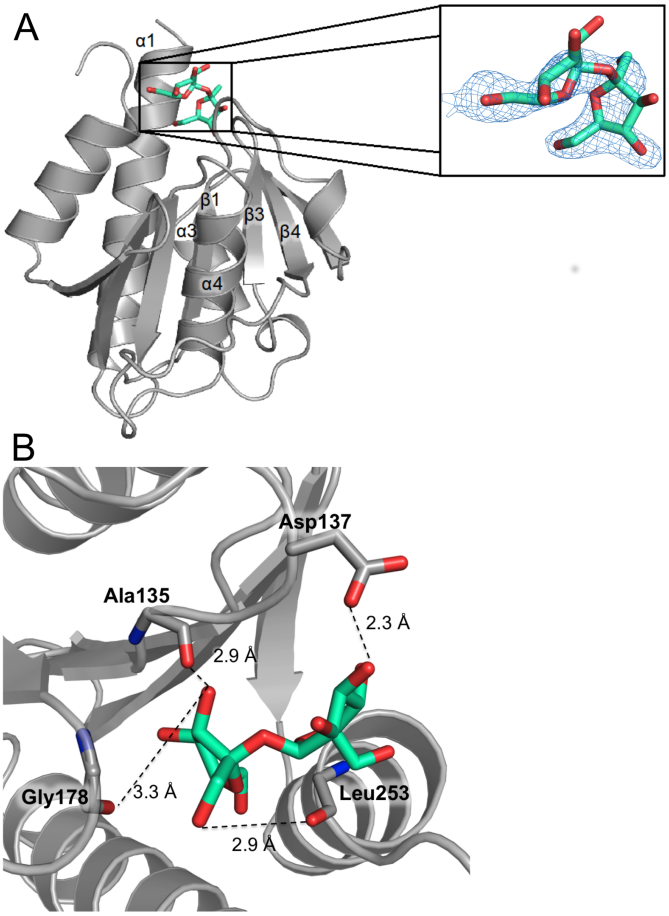

Supporting Figure S1: Crystal structure of apo Δ100CdaA with a bound sucrose molecule. (**A**) Δ100CdaA monomer is depicted in cartoon mode (light grey). The sucrose molecule (represented as sticks with carbons in green cyan and oxygen in red) is bound in a cavity formed by helix α1, loop connecting β1 and α3, loop between β3 and β4, and helix α3. An omit mFo-DFc electron density map (blue mesh) is contoured at a sigma level 3.0. (**B**) Detailed view of the sucrose binding. Amino acids (sticks, carbon in gray, oxygen in red and nitrogen in dark blue) that are involved in sucrose binding are shown in stick mode, and hydrogen bonds are indicated by dashed lines.

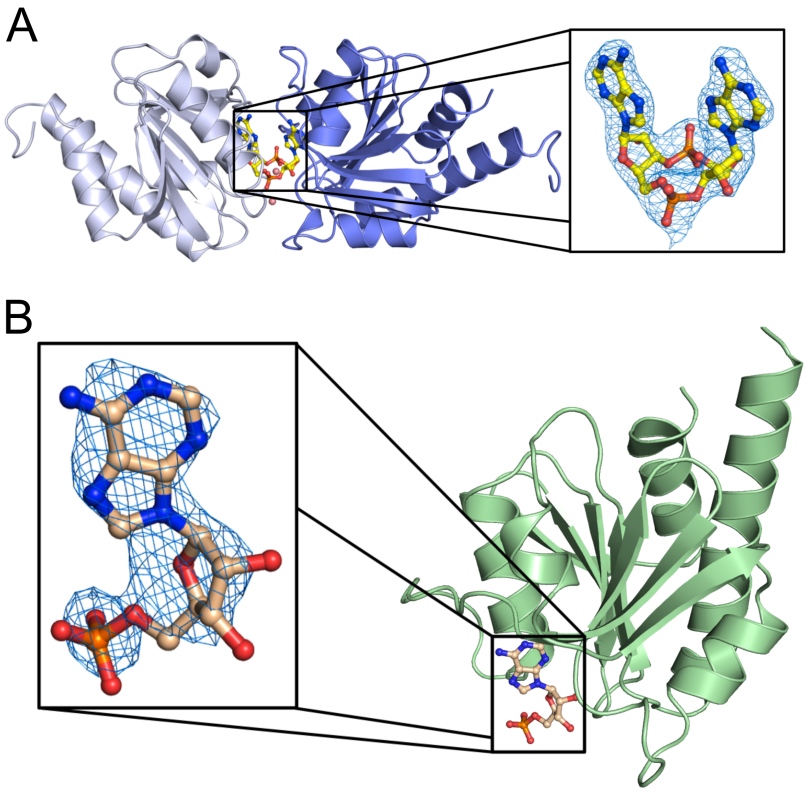

Supporting Figure S2: Crystal structure of Δ100CdaA with a bound c-di-AMP. (**A**) The crystallographic homo-dimer forming the catalytically active form of CdaA with bound c-di-AMP is depicted as ribbon cartoon (light blue and dark blue). The two monomers are related by a crystallographic two-fold symmetry axis. The difference electron density mFo-DFc omit map contoured at 3 σ revealed the presence of a c-di-AMP molecule (sticks; carbon in yellow, phosphate in orange, oxygen in red and nitrogen in blue) and a Co^{2+} ion (red sphere) in the active site. (**B**) The active site of the second CdaA molecule (light green/cartoon mode) present the asymmetric unit, which does not form an active dimer, is loaded with an AMP molecule (Carbon in wheat, rest coloured as in A). The omit mFo-DFc electron density map (blue mesh) is contoured at a 3 σ.

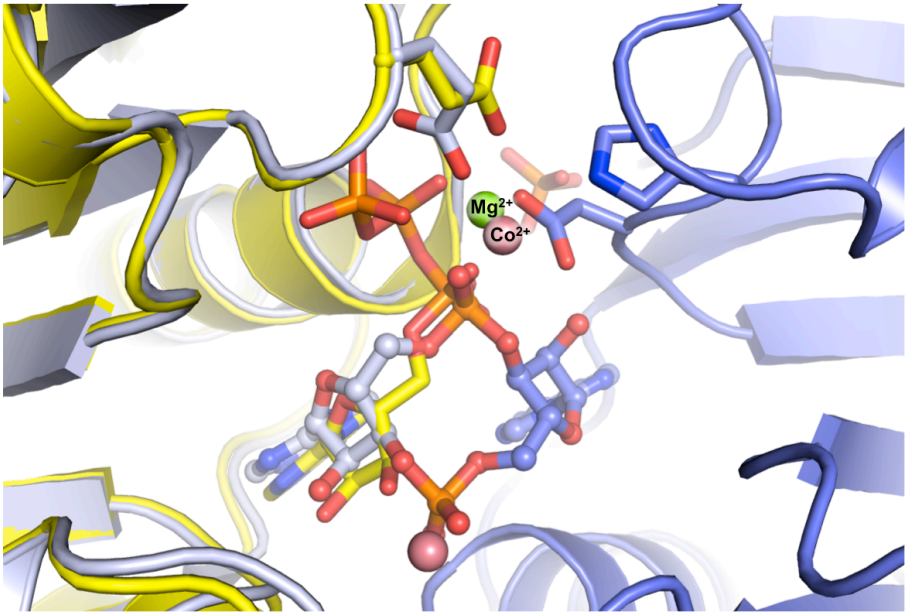

Supporting Figure S3: Superposition of a Δ100CdaA dimer with bound c-di-AMP and a Δ100CdaA monomer with bound ATP (PDB code: 4RV7). The overlay shows a slightly different positioning of the metal ions. Colouring of the Δ100CdaA dimer and the c-di-AMP is according to Figure 3. The Δ100CdaA monomer is depicted in ribbon cartoon mode (yellow). The bound ATP is shown in stick model (carbon in yellow, phosphate in orange, oxygen in red and nitrogen in dark blue) and the Mg^{2+} and Co^{2+} ions as a green and light pink sphere, respectively.

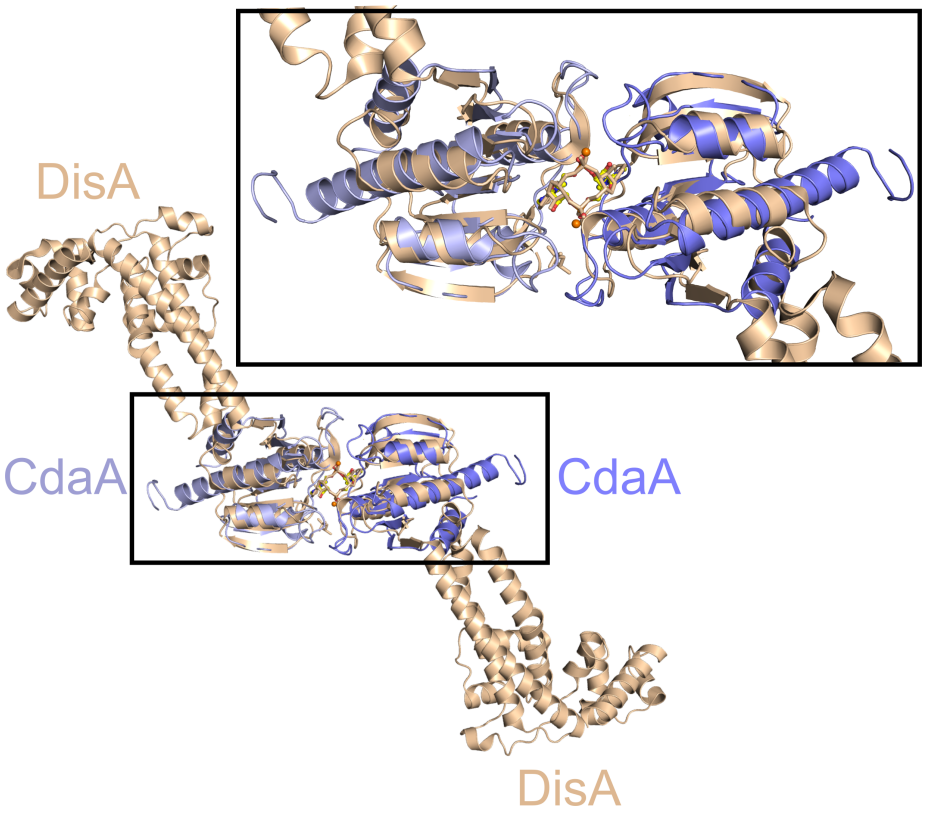

Supporting Figure S4: Superposition of DisA and Δ100CdaA homodimers. The catalytically active Δ100CdaA homo-dimer is shown as on Figure 3 (cartoon in blue and pale blue, c-di-AMP is depicted as colour coded balls and sticks, Co^{2+} ions are depicted as orange spheres). DisA homodimer is coloured wheat.

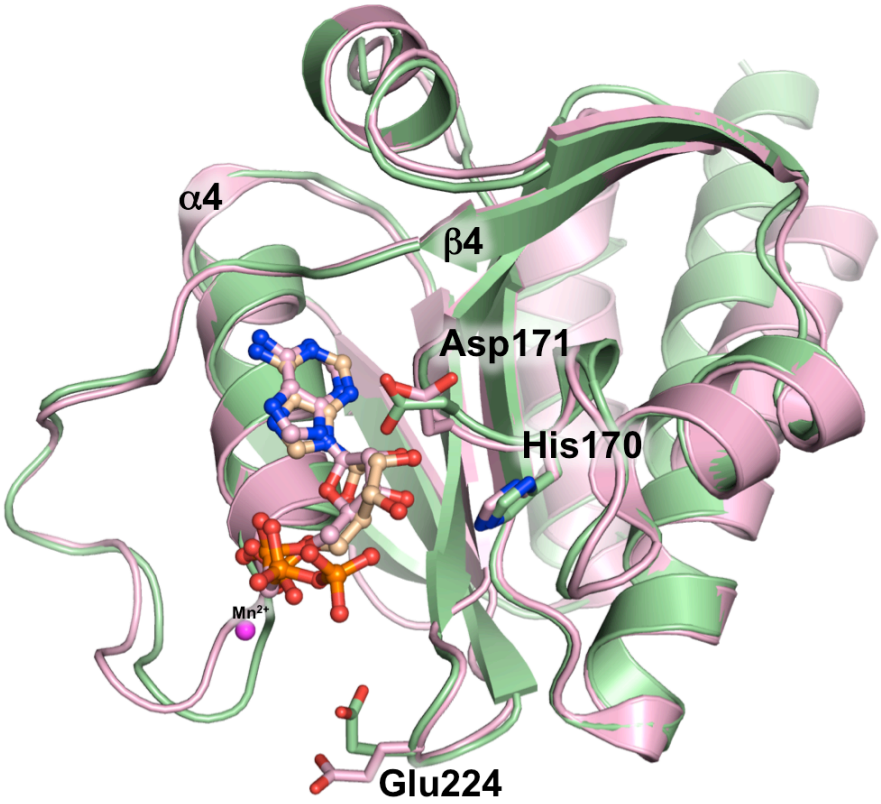

Supporting Figure S5: Superposition of *S. aureus* $DacA_{CD}$ (6GYX) and *L. monocytogenes* Δ100CdaA (6HVL) monomers. The Δ100CdaA monomer is shown as on Figure 4 (cartoon in pale green, AMP is depicted as colour coded balls and sticks. The $CacA_{CD}$ monomer is coloured pale pink, ApCpp is depicted in colour coded balls and stick mode, Mn^{2+} ion is shown as a magenta sphere. The amino acids His, Glu and Asp, which are involved in metal ion coordination and highly conserved in CdaA, are highlighted as sticks.

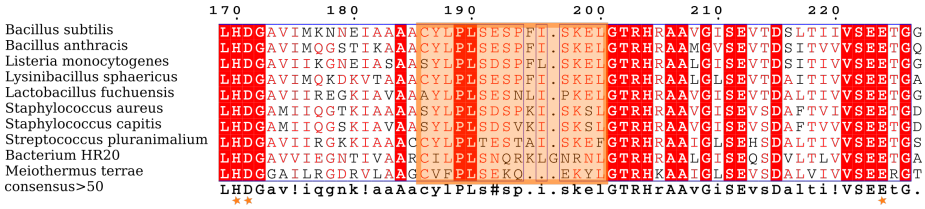

Supporting Figure S6: Sequence alignment of CdaAs from different organisms. The highly conserved residues that are involved in metal ion binding are labelled with orange stars at the bottom. The structurally divergent loop region connecting α-helix 4 and β-strand 4, which is in the close vicinity of the phosphate moiety of ATP, is marked with an orange box

Chapter 3: An extracytoplasmatic protein and a moonlighting enzyme modulate synthesis of the essential signaling nucleotide c-di-AMP in *Listeria monocytogenes*

This manuscript has originally been published in Environmental Biology

An extracytoplasmatic protein and a moonlighting enzyme modulate synthesis of the essential signaling nucleotide c-di-AMP in *Listeria monocytogenes*

Johannes Gibhardt[1,*], Jana L. Heidemann[2,*], Rica Bremenkamp[1], Jonathan Rosenberg[1], Roland Seifert[3], Volkhard Kaever[3], Ralf Ficner[2], Fabian M. Commichau[1]

[1]Department of General Microbiology, Institute for Microbiology and Genetics, University of Goettingen, 37077 Göttingen, Germany
[2]Department of Molecular Structural Biology, Institute for Microbiology and Genetics, GZMB, University of Goettingen, 37077 Göttingen, Germany
[3]Institute of Pharmacology & Research Core Unit Metabolomics, Hannover Medical School, Hannover, Germany

* The first two authors should be regarded as Joint First Authors.

Authors contribution

J.G.: data curation; formal analysis; validation; draft editing

J.L.H.: data curation; formal analysis; validation; draft editing

R.B.: data curation; formal analysis; validation; draft editing

R. F.: formal analysis; validation; draft editing; funding acquisition.

F.M.C.: formal analysis; validation; writing-original draft; writing review and editing; conceptualization; funding acquisition

An extracytoplasmic protein and a moonlighting enzyme modulate synthesis of c-di-AMP in *Listeria monocytogenes*

Johannes Gibhardt[a,b,*], Jana L. Heidemann[c,*], Rica Bremenkamp[a], Jonathan Rosenberg[a], Roland Seifert[d], Volkhard Kaever[d], Ralf Ficner[c], Fabian M. Commichau[b]

[a]Department of General Microbiology, Institute for Microbiology and Genetics, University of Goettingen, 37077 Göttingen, Germany

[b]FG Synthetic Microbiology, Institute for Biotechnology, BTU Cottbus-Senftenberg, 01968 Senftenberg

[c]Department of Molecular Structural Biology, Institute for Microbiology and Genetics, GZMB, University of Goettingen, 37077 Göttingen, Germany

[d]Institute of Pharmacology & Research Core Unit Metabolomics, Hannover Medical School, Hannover, Germany

Address correspondence to Ralf Ficner, rficner@gwdg.de, and Fabian Commichau, fabian.commichau@b-tu.de

* The first two authors should be regarded as Joint First Authors

BTU Cottbus-Senftenberg
Universitätsplatz 1
01968 Senftenberg
Germany
Phone: +49-3573-85-915; Fax: +49-3573-85-809
Fabian.commichau@b-tu.de

RUNNING TITLE: Control of CdaA activity
KEYWORDS: cyclic di-AMP, diadenylate cyclase, phosphoglucosamine mutase, CdaA, CdaR

3.1 Abstract

The second messenger cyclic di-AMP (c-di-AMP) is essential for growth of many bacteria as it controls the cellular osmolyte homeostasis. c-di-AMP can regulate the synthesis of potassium uptake systems in some bacteria and also directly inhibits and activates potassium import and export systems, respectively. Therefore, c-di-AMP production and degradation have to be tightly regulated depending on the environmental osmolarity. The Gram-positive pathogen *Listeria monocytogenes* relies on the membrane-bound diadenylate cyclase CdaA for c-di-AMP production and degrades the nucleotide with two phosphodiesterases. While the enzymes producing and degrading the dinucleotide have been reasonably well examined, the regulation of c-di-AMP production is not well understood yet. Here we demonstrate that the extracytoplasmic regulator CdaR interacts with CdaA *via* its transmembrane helix to modulate c-di-AMP production. Moreover, we show that the phosphoglucosamine mutase GlmM forms a complex with CdaA and inhibits the diadenylate cyclase activity *in vitro*. We also found that GlmM inhibits c-di-AMP production in *L. monocytogenes* when the bacteria encounter osmotic stress. Thus, GlmM is the major factor controlling the activity of CdaA *in vivo*. GlmM can be assigned to the class of moonlighting proteins because it is active in metabolism and adjusts the cellular turgor depending on environmental osmolarity.

3.2 Introduction

The Gram-positive bacterium *Listeria monocytogenes* thrives in diverse environmental niches and has the remarkable ability to invade and reproduce inside human cells when ingested with contaminated food (Hamon et al., 2006; Radoshevich and Cossart, 2018). Depending on where a *L. monocytogenes* cell is growing, the extracellular osmolarity can vary greatly. Therefore, the bacterium must be endowed with sophisticated regulatory systems allowing the cells to adjust the cellular turgor to the extracellular osmolarity (Bremer and Krämer, 2019). *L. monocytogenes* indeed possess regulatory systems to respond to osmotic stress, especially elevated osmolarity (Wood, 1999; Sleator and Hill, 2002; Wood, 2011).

Cyclic di-AMP (c-di-AMP) plays a central role in the adaptation of bacteria to the environmental osmolarity (Commichau et al., 2015, 2018, 2019; Corrigan and Gründling, 2013; Fahmi et al., 2017; Stülke and Krüger, 2020; Witte et al., 2008). The dinucleotide is in fact essential for *Bacillus subtilis*, *Lactococcus lactis*, *L. monocytogenes* and other Gram-positive bacteria since the dinucleotide prevents the uptake of potassium and other osmolytes to toxic levels by direct binding to the respective transport systems (Bai et al., 2013, 2014; Blötz et al., 2017; Commichau et al., 2018, 2019; Corrigan et al., 2011, 2013; Devaux et al., 2018; Gibhardt et al., 2019; Gundlach et al., 2017; Gundlach et al. 2019; Huynh et al., 2016; Kim et al., 2015;

Luo and Helmann, 2012; Mehne et al., 2013; Pham et al., 2018; Pham and Turner, 2019; Quintana et al., 2019; Rismondo et al., 2016; Schuster et al., 2016; Whiteley et al., 2015, 2017; Witte et al., 2013; Woodward et al., 2010; Zarella et al., 2018; Zeden et al., 2018).

Recently, it has been shown that c-di-AMP is also involved in osmoadaptation of cyanobacteria and archaea (Braun et al., 2019; Rubin et al., 2018). Beside its role in modulating osmolyte transport, c-di-AMP regulates the expression of genes encoding osmolyte transporters by binding to OFF-riboswitches in *B. subtilis* and *Bacillus thuringiensis* (Jones et al., 2014; Gao and Serganov, 2014; Gundlach et al., 2017; Nelson et al., 2013; Ren and Patel, 2014; Wang et al., 2019), the sensor kinase KdpD of the KdpDE two-component system in *S. aureus* (Moscoso et al., 2015) and the transcription factor BusR in *L. lactis* and *S. agalactiae* (Pham et al., 2018; Devaux et al., 2018). Thus, archaea and bacteria have evolved species-specific mechanisms to regulate the cellular turgor by employing different osmolyte transporters, but all organisms use c-di-AMP in this essential process (Commichau et al., 2018).

In the past years, several additional c-di-AMP targets of which some are also involved in osmoadaptation have been identified. For instance, c-di-AMP controls the synthesis of cell wall-lytic enzymes in *Streptomyces coelicolor* (St Onge and Elliot, 2017; St-Onge et al., 2015; Sexton et al., 2015). Moreover, c-di-AMP stimulates the DNA-binding activity of the *M. smegmatis* transcription factor DarR, which controls the expression of three genes (Zhang et al., 2013). Furthermore, c-di-AMP binds to and inhibits the pyruvate carboxylase in *L. lactis* and *L. monocytogenes* (Choi et al., 2017; Sureka et al., 2014). In the latter organism, c-di-AMP also binds to the cystathione-beta-synthase domain-containing (CBS) proteins CbpA and CbpB as well as to the PII-like signal transduction protein PstA (also designated as DarA) (Choi et al., 2015; Sureka et al., 2014). Like *L. monocytogenes* PstA, the homologs from *B. subtilis* and *S. aureus* have been biochemically and structurally characterized (Campeotto et al., 2015; Gundlach et al., 2015; Müller et al., 2015). A recent study revealed that c-di-AMP also binds to the *B. subtilis* DarB protein, a homolog of CbpB from *L. monocytogenes* (Gundlach et al., 2019). The same study confirmed that c-di-AMP binds to the osmoprotectant transporter subunit OpuCA. Moreover, the K^+/H^+ antiporter KhtT, the Mg^{2+} importer MgtE and CpaA were shown to be *bona fide* c-di-AMP-binding proteins. However, the impact of c-di-AMP binding on the function of these proteins in *B. subtilis,* of CbpA in *L. monocytogenes*, and of the CbpB and PstA homologs remains to be elucidated.

c-di-AMP is synthesized by diadenylate cyclases from two molecules of ATP (Commichau et al., 2019; Corrigan and Gründling, 2013; Witte et al., 2008). All diadenylate cyclases share the diadenylate cyclase (DAC) domain that is fused to regulatory domains, controlling c-di-AMP synthesis (Commichau et al., 2019; Corrigan and Gründling, 2013; Witte et al., 2008). So far, five different types of diadenylate cyclases have been described (Commichau et al., 2019). Bacteria like *B. subtilis* possess three diadenylate cyclases: the vegetative enzymes DisA and CdaA, and the sporulation-specific enzyme CdaS (Luo and Helmann, 2012; Oppenheimer-

Shanaan et al., 2011; Bejerano-Sagie et al., 2006; Mehne et al., 2013, 2014). DisA is a soluble enzyme while CdaA is attached to the membrane *via* three transmembrane helices (FIG 1B) (Witte et al., 2008; Rismondo et al., 2016). In contrast to *B. subtilis* and its close relatives, the majority of bacteria that are known to produce c-di-AMP have only one diadenylate cyclase, either DisA or CdaA (Corrigan and Gründling, 2013).

CdaA is the most-abundant cyclase that is present in many pathogenic bacteria, including *L. monocytogenes* (Woodward et al., 2010; Corrigan et al., 2011; Kamegaya et al., 2011; Dengler et al., 2013; Barker et al., 2013; Du and Sun, 2015). Therefore, the diadenylate cyclase CdaA, which has been biochemically and structurally characterized, is considered to be an interesting target for novel antibiotics (Rosenberg et al., 2015; Heidemann et al., 2019; Tosi et al., 2019). c-di-AMP must also be removed from the cell to enable the bacteria to take up osmolytes under hyperosmotic conditions, or to re-establish an equilibrium after exceeded c-di-AMP synthesis. Indeed, several studies revealed that bacteria can secrete c-di-AMP *via* multidrug resistance transporters (Woodward et al., 2010; Schwartz et al., 2012; Kaplan Zeevi et al., 2013; Barker et al., 2013). However, c-di-AMP is mainly degraded by specific phosphodiesterases (PDEs) that can be assigned to different classes (Commichau et al., 2019; Huynh and Woodward, 2016). The GdpP- and PgpH-type PDEs are localized at the membrane and contain domains that are involved in signaling and c-di-AMP degradation (Rao et al., 2010; Tan et al., 2013; Hyunh et al., 2015; Huynh and Woodward, 2016; Wang et al., 2018). The DhhP-type PDEs are soluble and form the third class of c-di-AMP-degrading enzymes (Huynh and Woodward, 2016; Drexler et al., 2017). As described above, c-di-AMP plays a central role in osmoadaptation. Therefore, the cellular c-di-AMP levels have to be tightly adjusted to the environmental osmolarity (Pham et al., 2016). Indeed, perturbation of c-di-AMP metabolism negatively affects growth of a variety of bacteria (Witte et al., 2013; Mehne et al., 2013; Rismondo et al., 2016; Gundlach et al., 2015, 2016; Bowman et al., 2016; Commichau et al., 2018; I et al., 2019).

The *cdaA* gene located within the conserved *cdaA-cdaR-glmM* module (FIG 1B). The *cdaR* and *glmM* genes encode the CdaR protein and the phosphoglucosamine mutase GlmM, respectively, of which the latter is essential for cell wall biosynthesis. CdaR inhibits the diadenylate cyclase CdaA in *L. lactis*, *L. monocytogenes* and *S. aureus* (Rismondo et al., 2016; Zhu et al., 2016; Tosi et al., 2019). Moreover, GlmM interacts and inhibits CdaA in *L. lactis* and *S. aureus in vivo* (Zhu et al., 2016; Tosi et al., 2019). The interaction between GlmM and CdaA was also confirmed in *B. subtilis* (Gundlach et al., 2015). Recently, it was demonstrated that GlmM inhibits CdaA *in vitro* and both enzymes form a complex in *S. aureus* (Tosi et al., 2019). Thus, GlmM is a moonlighting enzyme because it is active in cell wall biosynthesis and involved in the regulation of osmolyte homeostasis (Jefferey, 1999; Jeffery 2019).

In this study, we have analysed how CdaR and GlmM affect the activity of CdaA in *L. monocytogenes.* We show that CdaR is an extracytoplasmic protein that is attached to the membrane,

modulating CdaA activity and therefore the adaptation of the bacteria to hyperosmotic growth conditions. We also demonstrate that GlmM forms a complex with CdaA and that the cell wall enzyme inhibits the diadenylate cyclase *in vivo* and *in vitro*. Furthermore, we detected an inhibitory effect of GlmM on CdaA activity when the cells experience a hyperosmotic shock. The fact that GlmM and CdaA also form a complex in *L. monocytogenes* suggest that the GlmM- and CdaR-dependent modulation of the CdaA cyclase activity is conserved among Gram-positive bacteria possessing the *cdaA-cdaR-glmM* module.

3.3 Results

3.3.1 Cellular localization of CdaA, CdaR and GlmM and CdaR membrane topology analysis.

Previous studies revealed that CdaR and GlmM interact with CdaA and control its DAC activity (Mehne et al., 2013; Bharat Siva Varma et al., 2015; Rismondo et al., 2016; Bowman et al., 2016). CdaR is most likely attached to the membrane because the protein contains a transmembrane I domain (FIG 1A), while GlmM is supposed to be a soluble protein. So far, it has remained elusive whether GlmM localizes at the membrane. To address this question, we separated whole cell-lysates into cytosolic and membrane fractions and analysed the subcellular localization of CdaA, CdaR and GlmM by Western blotting using polyclonal antibodies that were raised against the three *L. monocytogenes* proteins (see *Materials and Methods*). As a control, we detected the soluble PrfA protein, the key regulator of virulence gene expression in *L. monocytogenes* (Brehm et al., 1996). The Δ*cdaA* and Δ*cdaR* mutant strains BPL77 and LMR45, respectively, were included to evaluate whether CdaA and CdaR affect synthesis and membrane localization of GlmM. As expected, CdaA, CdaR, GlmM and PrfA were detectable in the whole cell-lysates of the wild type strain (FIG 1C). Moreover, CdaR and CdaA were enriched in the membrane fractions and GlmM and PrfA both localize mainly in the cytosolic fraction (FIG 1C). The lack of CdaA and CdaR did not affect the cellular localization of GlmM and PrfA. CdaR was not detectable in the Δ*cdaA* mutant strain probably because of a negative polar effect on *cdaR* due to *cdaA* deletion. To conclude, under the conditions tested, GlmM is a soluble protein that localizes mainly in the cytoplasm.

The membrane topology of CdaR was previously predicted *in silico* (Corrigan and Gründling, 2013; Rismondo et al., 2016; Bowman et al., 2016). However, it was never analysed experimentally whether the YbbR domains of CdaR are located in the extracytoplasmic space. To address this question, we made use of the plasmid pKTop encoding a dual *phoA-lacZ* reporter system (Karimova et al., 2009). The reporter system of the *E. coli* alkaline phosphatase fragment PhoA 22-472 fused in frame with the α-peptide of the *E. coli* β-galactosidase, LacZ 4-60

(Alexeyev and Winkler, 1999). In this fusion approach, an extracytoplasmic localization results in high alkaline and low β-galactosidase activity, while a cytoplasmatic localization of the reporter results in low alkaline and high β-galactosidase activity (Karimova et al., 2009). The full-length *cdaR* gene as well as the *cdaR* ΔTM and *cdaR* ΔybbR fragments encoding the truncated CdaR variants CdaR ΔTM (34-452) and CdaR ΔybbR (1-33) variants, respectively, were introduced into the plasmid pKTop (FIG 1D). We also cloned the *prfA* (*lmo0200*) and *prkA* (*lmo1820*) genes encoding the soluble transcription factor PrfA and the membrane-associated serine/threonine kinase PrkA (FIG 1D) (Lima et al., 2011). Next, *E. coli* DH5α was transformed with the newly constructed plasmids and the empty plasmid (control), and the transformants were analysed on dual-indicator LB plates containing both a blue chromogenic substrate for phosphatase activity (X-Phos) and a red chromogenic substrate for β-galactosidase activity (Red-Gal). As expected, the cells carrying the empty plasmid and producing the PrfA fusion protein exhibited a red phenotype (Lac^+), indicating a cytosolic localization of the PhoA-LacZ reporter and the PrfA-PhoA-LacZ fusion (FIG 1E). By contrast, the cells producing the PrkA- and CdaR-PhoA-LacZ fusion proteins exhibited a blue phenotype (Pho^+), indicating that the C-termini of both proteins are located in the extracytoplasmic space (FIG 1E). The cells producing the CdaR ΔTM and CdaR ΔybbR hybrid proteins exhibited high β-galactosidase and high phosphatase activities, respectively (FIG 1E). Thus, the TM domain is required for membrane-association of CdaR and sufficient to promote extracytoplasmic localization of the PhoA-LacZ fusion. The transmembrane orientation of PrfA, PrkA, CdaR and the truncated CdaR variants was also confirmed by assaying the enzymatic activities of the hybrid proteins using cell-free crude extracts (FIG 1F) (see *Materials and Methods*). To conclude, the PhoA-LacZ experiment revealed that the YbbR domains of CdaR are located in the extracytoplasmic space.

3.3.2 *In vivo* CdaA-CdaR-GlmM complex formation.

To test whether the phosphoglucosamine mutase GlmM and the diadenylate cyclase CdaA from *L. monocytogenes* form a complex *in vivo*, we performed a bacterial two-hybrid (B2H) experiment, which is based on the interaction-mediated reconstitution of the *Bordetella pertussis* adenylate cyclase in *E. coli* (Karimova et al., 1998). We also included CdaR that was previously shown to interact with CdaA (Gundlach et al., 2015; Rismondo et al., 2016). The B2H experiment revealed that all proteins showed self-interaction and confirmed the formation of a CdaR-CdaA complex, which is likely mediated by the TM domains (FIG 2) (Rismondo et al., 2016). The experiment also revealed that the phosphoglucosamine mutase GlmM and the diadenylate cyclase CdaA from *L. monocytogenes* form a complex. Thus, the CdaA-CdaR-GlmM complex formation and the GlmM- and CdaR-dependent modulation of the CdaA

cyclase activity seems to be conserved among bacteria possessing the *cdaA-cdaR-glmM* module.

3.3.3 *In vitro* CdaA-GlmM complex formation.

To assess whether GlmM and CdaA of *L. monocytogenes* form a complex *in vitro*, we purified the His-tagged and GST-tagged GlmM and Δ100CdaA proteins, respectively, from *E. coli* and performed a pull-down assay. The Δ100CdaA cyclase variant lacks the N-terminal TM domains and 20 additional amino acids forming the linker between TM and DAC domain, which facilitates the purification success of the membrane protein (Rosenberg et al., 2015; Heidemann et al., 2019). The elution fraction containing the GST-Δ100CdaA fusion protein was incubated with the PreScission protease to cut off the GST-tag (see *Materials and Methods*). The proteins were mixed in a 1:1 ratio and added to a gravity flow column containing TALON-cobalt beads. As a control, the Δ100CdaA was pipetted alone onto a column. Both columns were washed, the proteins were eluted with imidazole and the fractions were analysed by SDS page. While GlmM disappeared from the washing fractions, Δ100CdaA was present in each of the fractions (FIG 3A). By contrast, Δ100CdaA was only detectable in the first washing fraction of the control batch, indicating that the protein does not bind to the beads (FIG 3B). The presence of Δ100CdaA in the washing and elution fractions that were obtained from the column containing both proteins indicates that the immobilized GlmM protein interacts and retains the cyclase. To conclude, GlmM and Δ100CdaA from *L. monocytogenes* form an unstable complex *in vitro*. We also performed size exclusion chromatography to get further experimental evidence for the formation of GlmM-Δ100CdaA complex. When the two proteins were purified separately, two peaks appeared due to the presence of GlmM and Δ100CdaA (FIG 4A). By contrast, when the proteins were co-purified, two faster eluting peaks appeared, indicating the formation of high-molecular weight complexes consisting of GlmM and Δ100CdaA (elution peaks 1 and 2; FIG 4A). The subsequent SDS page analysis of the elution fractions confirmed that both proteins co-eluted from the column, indicating the formation of a GlmM-Δ100CdaA complex (FIG 4B). To estimate the size and stoichiometry of the GlmM-Δ100CdaA complex, we performed SEC-MALS and ITC. Based on the SEC-MALS elution profile, the GlmM-Δ100CdaA complex had an estimated molecular weight of 105.0 kDa ± 2.18 % (FIG 5A, Table 1). These data are consistent with a GlmM-Δ100CdaA complex comprising one GlmM dimer (estimated mass 85.63 kDa ± 2.072 %) interacting with one Δ100CdaA dimer (estimated mass of the dimer 36.27 kDa ± 1.7 %), with a theoretical molecular weight of 134.7 kDa (Table 1). The ITC analysis further supports the formation of a weak GlmM-Δ100CdaA complex (K_D = 1.09 µM ± 66.5 nM) consisting of GlmM and Δ100CdaA in 1:1 ratio (FIG 5B and 5C). The parameters for the titration

series of the ITC analysis are given in Table S3. Taken together, the biochemical analyses show that GlmM and Δ100CdaA from *L. monocytogenes* form a complex.

3.3.4 Role of CdaR in salt adaptation and in controlling cellular c-di-AMP levels.

To evaluate whether CdaR is involved in osmotic stress tolerance in *L. monocytogenes*, we performed a high-throughput screen based on the Biolog phenotype microarray technology (Biolog Inc.; Bochner et al., 2001). The Biolog assay allows assessing and comparing the responses of bacterial strains to more than 1000 distinct growth conditions by cultivating strains in 96-well microplates, with each well presenting a different culture condition. The metabolic activity of the cells is determined by measuring their respiration, which converts the colourless tetrazolium into a purple dye. The colour intensity, which corresponds to the metabolic activity of the cell, can be measured. We determined the metabolic activities of the *L. monocytogenes* wild type and Δ*cdaR* strains in the microarray plates PM 1 – 10 and 13B (see FIG S1). The Biolog assay revealed strong metabolic differences among the strains in the plate PM9, which is supplemented with increasing amounts of the osmolyte sodium chloride and other salts, and in the plates PM 6-8, which are supplemented with di- or tri-peptides (especially if containing aromatic amino acids) that are known to be important osmolytes for *L. monocytogenes* (Whiteley et al., 2015, 2017, FIG 6A, FIG S1).

To uncover whether the lack of CdaR also affects growth of *L. monocytogenes* in the presence of osmolytes, we cultivated the strains in BHI broth with increasing amounts of sodium chloride, potassium chloride or sorbitol. As shown in FIG 6B, the wild type was more resistant to osmotic stress than the Δ*cdaR* strain. This indicates that CdaR, which was shown to inhibit CdaA and thus c-di-AMP production in *L. monocytogenes* (Rismondo et al., 2016), is indeed involved in the adaptation of the bacterium to osmotic stress during growth in BHI rich medium.

Next, we assessed to role of CdaR and truncated variants ΔTM and ΔybbR 1-4 lacking the transmembrane and the four YbbR domains, respectively, in modulating c-di-AMP production in *L. monocytogenes* during adaptation to osmotic stress. For this purpose, we introduced plasmids allowing the IPTG-dependent expression of the full-length and truncated *cdaR* alleles into the genome and deleted the native *cdaR* gene see (*Materials and Methods*). The wild type strain carrying the integrated empty vector served as a control. The strains were cultivated in LSM medium until an OD_{600} of 0.5-0.6 and samples for determining the cellular c-di-AMP levels were taken. The cultures were split and diluted with pre-warmed LSM medium containing sodium chloride to a final concentration of 0.5 M, or with equal amounts of standard LSM medium as a control. The cultures were further incubated for 25 minutes and samples for determining the cellular c-di-AMP levels were taken (FIG 6C).

As shown in FIG 6D, in all strains the c-di-AMP levels did not change when the cultures were diluted with standard LSM medium. Previously, it has been observed that the overexpression of the *cdaR* gene in *L. monocytogenes* during growth in BHI rich medium inhibits c-di-AMP production. Here we show that CdaR has a positive effect on the cellular c-di-AMP levels when the bacteria are grown in LSM medium (FIG 6D, middle panel). Thus, the effect of CdaR on c-di-AMP production seems to depend on the medium and growth conditions. The c-di-AMP levels were similar in the Δ*cdaR* strains carrying the empty vector and the vector encoding the CdaR ΔTM variant. Thus, CdaR has to be attached to the cell surface to be able to regulate the activity of CdaA.

Surprisingly, the c-di-AMP levels were strongly reduced in bacteria producing only the TM domain of CdaR (ΔybbR 1-4 variant). This could indicate that the TM domain of CdaR controls the dimerization of CdaA, which is crucial for c-di-AMP synthesis. Except for the strain producing only the TM domain of CdaR, the c-di-AMP levels dropped upon osmotic stress, especially in the case of the wild type and CdaR overexpressing strains (FIG 6 D). To conclude, CdaR influences c-di-AMP production in *L. monocytogenes* during growth in LSM medium. However, CdaR does not seem to be the sole regulator of CdaA activity. Under osmotic stress the bacteria can adjust the cellular levels of the signaling nucleotide independent of CdaR, as demonstrated by the reduction of c-di-AMP in the *cdaR* deletion mutant.

3.3.5 Control c-di-AMP synthesis by CdaR and GlmM in *E. coli*.

Next, we assessed the ability of GlmM, CdaR, and of the N- and C-terminally truncated CdaR variants ΔTM, ΔybbR 4, ΔybbR 3-4, ΔybbR 2-4 ΔybbR 1-4 to modulate the activity of CdaA in a heterologous system. For this purpose, we introduced the plasmid pBP384 allowing the expression of the *L. monocytogenes kimA* potassium transporter gene *E. coli* strain LB2003 lacking the native potassium transporters. Expression of the *kimA* gene allows the *E. coli* strain to grow in minimal medium under potassium limitation (Gibhardt et al., 2019). Since c-di-AMP inhibits KimA when CdaA is also synthesized by the *E. coli* strain, the growth rate of the bacteria serves as a read out to evaluate whether proteins activate or inhibit the cyclase (FIG 6E).

Indeed, while the wild type CdaA reduced the growth rate of the reporter strain, the growth rate was about 2-fold higher when the catalytically inactive CdaA D171N variant was produced (FIG 6F). The growth was also faster when the full-length and the C-terminally truncated CdaR variants were synthesized. Thus, CdaR inhibits CdaA but the YbbR domains are not crucial for regulating the cyclase in a heterologous system. When the N-terminally truncated CdaR variant ΔTM was produced, CdaA was only slightly inhibited. Thus, the ability of CdaR to inhibit CdaA depends on the cellular localization (see FIG 6D). The growth rate of the *E. coli* strain

synthesizing GlmM was also increased, indicating that the cell wall enzyme is also capable of modulating the activity of CdaA in *L. monocytogenes* (FIG 6F). However, at least in *E. coli*, CdaR has as a stronger ability of modulating the cyclase activity than GlmM alone (Fig. 6F). To conclude, CdaR as well as GlmM can modulate the enzymatic activity of CdaA, if expressed in a heterologous system.

3.3.6 GlmM negatively regulates CdaA activity *in vitro*.

A previous suppressor screen with *L. lactis* revealed that GlmM inhibits the cyclase activity of CdaA *in vivo* (Zhu et al., 2015). It has also been observed that the replacement of isoleucine 154 by phenylalanine within a region of high sequence conservation in GlmM enabled the enzyme to stronger inhibit CdaA (Zhu et al., 2015) (FIG 7A). Moreover, a recent study showed that GlmM inhibits CdaA in *S. aureus* (Tosi et al., 2019).

To assess whether GlmM also inhibits Δ100CdaA *in vitro*, we purified the *L. monocytogenes* enzymes and determined the activity of the cyclase using the coralyne assay for c-di-AMP quantification (Zheng et al., 2014; Heidemann et al., 2019). To evaluate whether the tyrosine 153 and phenylalanine 154 residues are important for the GlmM-dependent regulation of Δ100CdaA, we also purified the GlmM Y153A, F154I and F154A variants (see *Materials and Methods*) (FIG 7A). As previously described, Δ100CdaA was only capable of producing c-di-AMP in the presence of Mn^{2+} and Co^{2+} ions (Rosenberg et al., 2015; Heidemann et al., 2019) (FIG 7B). As expected, no c-di-AMP was formed in the control sample when only GlmM and Mn^{2+} ions were present. However, a decrease in c-di-AMP production was detected in these samples containing CdaA and Mn^{2+} upon addition of increasing amounts of GlmM (FIG 7B). No c-di-AMP was detected when Δ100CdaA was mixed at a 1:2 molar ration with GlmM. The inhibition of CdaA by GlmM variants with the amino acid replacements at position 154 was slightly reduced. The amino acid replacement at position 153 did not affect the GlmM-dependent inhibition of Δ100CdaA (FIG 7B).

To conclude, GlmM inhibits CdaA from *L. monocytogenes* and the phenylalanine residue at position 154 in GlmM is important for controlling the activity of the cyclase.

3.3.7 Inhibition of CdaA by GlmM in *L. monocytogenes*.

To evaluate whether GlmM also inhibits the activity of CdaA in *L. monocytogenes in vivo*, we constructed strains allowing the IPTG-dependent overproduction of the wild type GlmM and the GlmM F154I variants. As shown above, the GlmM F154I variant does not inhibit CdaA as strong as the wild type GlmM enzyme (see above) (FIG 7B).

To assess whether a GlmM from a bacterium that does not produce c-di-AMP is capable of inhibiting CdaA, we replaced the native *glmM* gene with the *glmM* gene from *E. coli*. The wild type *L. monocytogenes* strain carrying the integrated empty vector served as a control. As shown in FIG 7C, growth of the strains was not affected when the GlmM variants were over-produced after the addition of IPTG. Surprisingly, the strain carrying the inducible *E. coli glmM* allele grew also in the absence of IPTG. It is tempting to speculate that GlmM from *E. coli* is more active than the *L. monocytogenes* enzyme, thereby allowing the bacteria to produce sufficient amounts of precursors for cell wall biosynthesis in the absence of IPTG. By contrast, the strains in which the native GlmM variants were depleted grew much slower than the wild type strain (FIG 7C). To conclude, the native GlmM can be replaced by the F154I variant and by the homolog from *E. coli* in *L. monocytogenes* without affecting bacterial growth.

Next, we determined the intracellular c-di-AMP levels in the *L. monocytogenes* strains producing the different GlmM variants during growth in LSM medium. As shown in FIG 7D, the c-di-AMP levels were only slightly reduced in the strains overproducing the GlmM variants. Thus, the overproduction of GlmM *per se* is not sufficient for inhibiting CdaA *in vivo*. To assess whether the GlmM variants modulate the production of c-di-AMP in *L. monocytogenes* during adaptation to osmotic stress, we cultivated the strains in LSM medium until an OD_{600} of 0.5-0.6 and samples for determining the cellular c-di-AMP levels were taken. The cultures were split and diluted with pre-warmed LSM medium containing sodium chloride to a final concentration of 0.5 M, or with equal amounts of standard LSM medium as a control. The cultures were further incubated for 25 minutes and the c-di-AMP levels were compared with those obtained from culture samples prior to the dilution step.

As shown in FIG 7D, in all strains the c-di-AMP levels did not change when the cultures were diluted with LSM medium. By contrast, the cellular c-di-AMP levels strongly decreased in the strains overproducing the native GlmM enzyme after salt stress (FIG 7D). The decrease of the c-di-AMP level was less pronounced in a strain producing the GlmM F154I variant, indicating that the phenylalanine residue at position 154 in GlmM is important for controlling CdaA activity *in vivo*.

The *E. coli* GlmM enzyme did not inhibit the production of c-di-AMP in *L. monocytogenes* during adaptation to osmotic stress. To conclude, GlmM also inhibits CdaA in *L. monocytogenes* and the GlmM-dependent control of c-di-AMP synthesis depends on osmotic stress.

3.4 Discussion

In the present study, we have confirmed that CdaR directly interacts with CdaA and modulates the activity of the diadenylate cyclase of *L. monocytogenes* (FIG 2). As previously reported, CdaR and CdaA form a complex in *B. subtilis* and *L. monocytogenes* (Gundlach et al., 2015; Rismondo et al., 2016; Zhu et al., 2016). However, due to the fact that the membrane topology of CdaR was unknown, it was unclear which domain of the regulatory protein interacts with CdaA. Our topology analysis suggests that the YbbR domains of CdaR are exposed to the peptidoglycan layer of the cell envelope (FIG 1, FIG 8). Therefore, the interaction between CdaR and CdaA, and thus the control of the diadenylate cyclase, is very likely to be mediated through the transmembrane helices. Indeed, the cellular c-di-AMP levels were strongly reduced in a *L. monocytogenes cdaR* mutant strain overproducing only the transmembrane helix of CdaR (FIG 6D). The molecular details underlying the inhibition of CdaA by the transmembrane helix and the extracytoplasmic signal perceived by the YbbR domains remain to be elucidated.

Previously, we have reported that CdaR inhibits CdaA in *L. monocytogenes* cells that were cultivated in BHI rich medium (Rismondo et al., 2016). The inhibition of CdaA by CdaR was also shown in *S. aureus* (Bowman et al., 2016). Interestingly, the inhibitory effect of CdaR was increased under acidic conditions, a phenomenon that remains to be resolved. CdaR of *S. aureus* is also capable of reducing c-di-AMP production by CdaA in the environment of an *E. coli* cell (FIG 6F) (Zhu et al., 2016).

Here we have observed that the overproduction of CdaR may also stimulate c-di-AMP synthesis in *L. monocytogenes* cells that were cultivated in LSM defined medium (FIG 6D). Moreover, for *B. subtilis* it has been shown that CdaR stimulates the activity of CdaA when the *cdaR* and *cdaA* genes are co-expressed in *E. coli* (Mehne et al., 2013). Thus, depending on the growth conditions and the cellular environment, CdaR either inhibits or activates the diadenylate cyclase CdaA. Since CdaR is facing towards the peptidoglycan layer of the cell envelope it is tempting to speculate that the YbbR domains perceive mechanical shear forces arising as a result of a displacement of the membrane and the peptidoglycan in response to an osmotic up- or downshift (FIG 8). This model implies that the YbbR domains of CdaR interact with the peptidoglycan, or with proteins that are embedded in the cell wall, or that the reported self-interaction of the YbbR domains effect the interaction of CdaA via the transmembrane domains (Rismondo et al., 2016).

However, so far, we were unable to detect an interaction between the YbbR domains and the peptidoglycan layer (unpublished data). Thus, the signals that are perceived by the YbbR domains of CdaR and transmitted by the transmembrane helix to CdaA remain to be identified. Structural studies of the YbbR domains I and IV of the CdaR protein from *Desulfitobacterium hafniense* Y51 uncovered similarities to the C-terminal domains of the TL5 and L25 ribosomal proteins (Barb et al., 2011). However, the potential interaction partners of C-terminal domains,

which are exposed to the surface of the ribosome are currently unknown. It will be interesting to find out whether the YbbR domains of different proteins respond to similar or different stimuli.

In the present study, we have also demonstrated that the phosphoglucosamine mutase GlmM directly interacts with CdaA and inhibits the activity of the cyclase *in vitro* and *in vivo* (FIG 7B and 7D). Furthermore, we could show that only the native phosphoglucosamine mutase is capable of inhibiting CdaA when the cells encounter hyperosmotic growth conditions (FIG 7D). Since the formation of a CdaA-GlmM complex has also been reported to occur in bacteria like *B. subtilis*, *L. lactis* and *S. aureus*, which are phylogenetically related to *L. monocytogenes* (Gundlach et al., 2015; Zhu et al., 2016; Tosi et al., 2019), the GlmM-dependent control of CdaA seems to be specific and a conserved among species possessing the *cdaA-cdaR-glmM* module. The specificity of the interaction between GlmM and CdaA is further supported by the observation that the replacement of the phenylalanine (F) at position 154 in GlmM by either isoleucine (I) or alanine (A) decreases the ability of the enzyme to inhibit CdaA (FIG 7B). The amino acid at the position 154 was previously reported to be important for the GlmM-dependent control of CdaA activity in the *L. lactis* strain MG1363 (FIG 7A) (Zhu et al., 2016). However, albeit to a lesser extent, the GlmM F154I and F154A variants of *L. monocytogenes* still inhibited CdaA, indicating that additional residues of the phosphoglucosamine mutase are involved in the formation of the protein complex. Indeed, a recent structural model of the CdaA-GlmM complex from *S. aureus* revealed that other amino acid residues surrounding the phenylalanine 154 might be important for the regulatory protein-protein interaction (Tosi et al., 2019). However, a more comprehensive mutational study and a structural analysis of the CdaA-GlmM complex might provide insights into the molecular details of the interaction.

Given the fact that the GlmM enzyme has an additional function beside its role in providing precursors for cell wall biosynthesis, the phosphoglucosamine mutase can be assigned to the class of "moonlighting proteins" (Jeffery, 2019). In general, moonlighting proteins perform two or more distinct and physiologically relevant biochemical or biophysical functions in the cell (Jeffery, 2019). Research in recent years has shown that the phenomenon of moonlighting is widespread among bacterial proteins. For instance, the *B. subtilis* and *E. coli* UDP-glucose diacylglycerol glucosyltransferases UgtP and OpgH, respectively, which are active in lipid metabolism, act as metabolic sensors coupling the nutritional availability to cell division and thus cell size (Weart et al., 2007; Hill et al., 2013). The glutamate dehydrogenases RocG and GudB1 of *B. subtilis* are active in glutamate degradation and in controlling *de novo* synthesis of glutamate (Commichau et al., 2007a; Stannek et al., 2015). For many moonlighting enzymes, the signals controlling the secondary function of the enzymes have been identified (Commichau and Stülke, 2008). However, this is not the case for GlmM, which controls the activity of CdaA and thus the uptake of osmolytes *via* transporters whose activities are regulated by c-di-AMP

(Stülke and Krüger, 2020). Even though osmoregulation has been intensively studied in bacteria, it is still rather unclear how the cell senses the environmental osmolarity to adjust the turgor accordingly. The present study and a previous report revealed that GlmM alone is sufficient to inhibit CdaA (Tosi et al., 2019) and the membrane bound CdaR protein rather plays a minor role in modulating the CdaA activity in these coccoid bacteria. This idea is supported by the finding that some bacterial isolates like the *L. lactis* strain MG1363, which does not produce a functional CdaR protein, still adjusts the cellular c-di-AMP levels by employing GlmM (Zhu et al., 2016).

So how does a cell synthesizing CdaA and GlmM sense osmotic up- and downshifts and how is c-di-AMP production regulated by employing the phosphoglucosamine mutase? Over the past years it has been observed that in many bacteria c-di-AMP is controlling the uptake and efflux of potassium ions to adjust the cellular turgor (Stülke and Krüger, 2020). Thus, the cellular potassium concentration could control the regulatory interaction between GlmM and CdaA. However, in addition to potassium, other osmolytes like glycine betaine and carnitine are taken up by c-di-AMP-regulated transporters (Commichau et al., 2018; Stülke and Krüger, 2020). Therefore, it can be assumed that a mechanism, which is independent of a specific osmolyte, ensures the adjustment of the cellular turgor.

It would be an attractive idea to assume that the volume changes in response to an osmotic up- or downshift would result in a transient change in the cellular GlmM concentration, which in turn could affect c-di-AMP synthesis. The adjustment of the c-di-AMP levels would then lead to an inhibition and activation of osmolyte uptake and export, respectively, to adjust the cellular turgor to the environment. However, the most exciting question of how the cell uses c-di-AMP to adapt the turgor to the environmental osmolarity remains to be answered.

3.5 Experimental Procedure

3.5.1 Chemicals, media, bacterial strains and growth conditions.

Chemicals and media were purchased from Sigma-Aldrich (Munich, Germany), Carl Roth (Karlsruhe, Germany) and Becton Dickinson (Heidelberg, Germany). Primers were purchased from Sigma-Aldrich (Munich, Germany) and are listed in Table S1. *E. coli* strains were grown in lysogeny broth (LB) and in M9 minimal medium, as previously described (Gibhardt et al., 2019). Agar plates were prepared with of 15 g agar/l (Roth, Germany). *E. coli* transformants were selected on LB plates containing kanamycin (50 µg/ml) or ampicillin (100 µg/ml). *L. monocytogenes* was grown in brain-heart-infusion (BHI) medium (Sigma-Aldrich, Germany) or in Listeria Synthetic Medium (LSM; Whiteley et al., 2017), as previously described (Gibhardt et al., 2019). All bacteria used in this study are listed in Table S2.

Potassium transporter deficient *E. coli* strains LB650 and LB2003 were cultivated in LB-K medium (NaCl substituted by 1 % KCl (w/v)) (Stumpe and Bakker 1997). M9 medium was used for *E. coli* growth experiments with the following composition: 37.85 mM Na_2HPO_4, 22.05 mM KH_2PO_4, 18.75 mM NH_4Cl, 1 mM MgSO4, 0.1 mM $CaCl_2$, 0.5 µM $FeCl_3$, 28 mM D-glucose or glycerol as sources of carbon (Gibhardt et al., 2019). For the *E. coli* strain LB650 the M9 medium was supplemented with amino acids L-valine, L-isoleucine, L-methionine, L-proline, L-serine (each 0.02 % (w/v)) and 3 µM thiamine. For the *E. coli* strain LB2003 the M9 medium was supplemented with 0.0066 % (w/v) casein hydrolysate (acid) (Oxoid), 0.004 % (w/v) L-proline and 3 µM thiamine. For experiments with defined potassium concentrations, the KH_2PO_4 salt was replaced by NaH_2PO_4 and KCl was added as indicated. If not specified different, IPTG was used at a concentration of 50 µM and L-arabinose at 0.005 % (w/v). Growth in liquid medium was monitored using 96-well plates (Microtest Plate 96-Well,F, Sarstedt) at 37°C and medium orbital shaking at 237 cpm (4 mm) in an Epoch 2 Microplate Spectrophotometer, equipped with the Gen5 software (02.09.2001; BioTek Instruments) and the OD_{600} was measured in 15 min intervals.

To evaluate the growth of the Δ*cdaR* mutant (LMJR45) compared to the EGD-e wt under osmotic stress conditions, bacteria were grown overnight from single colonies in 5 ml BHI medium at 37°C and 220 rpm. 10 ml BHI were inoculated from the pre-cultures to an OD_{600} of 0.1 and grown at 37°C and 220 rpm until they reached an OD_{600} of 0.4-0.8. The optical density was adjusted to 0.2 and 100 µl of the cell suspension was pipetted into 96-well plates, containing 100 µl BHI medium with 0, 0.25, 0.5, 0.75, 1, 1.5 and 2 M of NaCl, KCl, or D-sorbitol. Bacteria were grown using an Epoch2 multiwell platereader as described above. The growth rates of the exponential phases were determined as described previously (Gibhardt et al., 2019) and plotted against the osmolyte concentration.

The essentiality of the GlmM variants for growth of the *L. monocytogenes* strains BPL63, BPL64 and BPL65 lacking the native *glmM* copy was analysed as follows. The strain BPL45

served as a control. 5 ml BHI medium were inoculated with the strains and incubated over night at 37°C at 220 rpm. The 2 ml of the cultures were centrifuged for 1 min at 20,000 g, the cells were washed twice in BHI and used to inoculate the next cultures (5 ml each) at an OD_{600} of about 0.1. The cultures were incubated for 24 h, the cells were washed again three times in BHI medium and used to inoculate 96 well plates containing 200 µl BHI medium without and with 1 mM IPTG to an OD_{600} of about 0.1. Growth was monitored in a microplate reader at 37°C.

3.5.2 DNA manipulation, construction of plasmids and mutant strains.

The plasmids that were used and constructed in this study are listed in Table S2. Transformation of *E. coli* was performed using standard procedures (Sambrook et al., 1989). Plasmids were isolated from *E. coli* using the Nucleospin Extract Kit (Macherey and Nagel, Germany). PCR products were purified using the PCR Purification Kit (Qiagen, Germany). DNA polymerases, restriction enzymes, DNA ligases were purchased from Thermo Scientific (Germany) and used according to the manufacturer's instructions. Other DNA sequencing performed the SeqLab Sequence Laboratories (Göttingen, Germany). *L. monocytogenes* chromosomal DNA was isolated using the NucleoSpin Microbial DNA Kit (Macherey and Nagel, Germany).
L. monocytogenes mutant strains were constructed using the pMAD plasmid system (Arnaud et al., 2004), as previously described (Gibhardt et al., 2019). Deletion of genes in *L. monocytogenes* was confirmed by colony PCR (Dussurget et al., 2002) and DNA sequencing. The insertion of pIMK3-derived plasmids (Monk et al., 2008) into the *attB* site of the $tRNA^{Arg}$ locus in the *L. monocytogenes* genome was confirmed by PCR (Rismondo et al., 2016). The plasmid pBP1002 was constructed for the deletion of the *glmM* gene in *L. monocytogenes.* The DNA fragments surrounding the *glmM* gene were amplified by PCR with the primer pairs RB6/RB7 and RB8/RB9, fused in a second PCR. The fusion product was digested with the enzymes *Eco*RI and *Bam*HI, and ligated to the plasmid pMAD (Arnaud et al., 2004).
The plasmid pBP223 was constructed for the overexpression and purification of N-terminally Strep-tagged CdaR protein lacking the amino acids 1-28. The *cdaR* fragment was amplified by PCR using the primer pair JR28/JR56. The PCR product was digested with *Sac*I and *Bam*HI and ligated to the plasmid pGP172 (Merzbacher et al., 2004). The plasmids pBP260 (*cdaA-cdaR* ΔTM), pBP261 (*cdaA-cdaR* ΔybbR 4), pBP262 (*cdaA-cdaR* ΔybbR 3-4), pBP263 (*cdaA-cdaR* ΔybbR 2-4), pBP264 (*cdaA-cdaR* ΔybbR 1-4) and pBP387 (*cdaA-cdaR*) were constructed for the arabinose-dependent expression of CdaA together with CdaR variants in the *E. coli* strain LB2003.
The *cdaA-cdaR* ΔTM, *cdaA-cdaR* ΔybbR 4, *cdaA-cdaR* ΔybbR 3-4, *cdaA-cdaR* ΔybbR 2-4, *cdaA-cdaR* ΔybbR 1-4 and *cdaA-cdaR* operons were amplified by PCR using the primers

JH51/JH135//JH136/JH103 (fragments joined by SOE PCR; Horton et al., 1990), JH51/JH138, JH51/JH139, JH51/JH140, JH51/JH137, and JH51/JH103, respectively, digested with *Xba*I and *Hind*III and ligated to the plasmid pBAD33 (Guzman et al., 1995). The plasmids pBP388 (*cdaA-cdaR-glmM*) and pBP389 (*cdaA-glmM*) were constructed for the expression of CdaA together with CdaR/GlmM and with GlmM, respectively, in the *E. coli* strain LB2003. For this purpose, the *glmM* gene was amplified by PCR using the primer pair JH104/JH105, digested with *Hind*III and *Pst*I, and ligated to pBP387 and pBP370 (Gibhardt et al., 2019) yielding in the plasmids pBP388 and pBP389, respectively. The plasmids pBP255 and pBP259 were constructed for the expression of the *cdaR* ΔTM and *cdaR* ΔYbbR 1-4 genes in *L. monocytogenes*, respectively. The *cdaR* fragments were amplified using the primer pairs JH130/JH22 and JH21/JH131, digested with *Nco*I and *Sal*I, and ligated to the plasmid pIMK3 (Monk et al., 2008).

The plasmids pBP1000, pBP1001 and pBP1003 were constructed for the expression of the *glmM-E. coli*, *glmM-L. monocytogenes* and *glmM T460A-L. monocytogenes* phosphoglucosamine mutase genes in *L. monocytogenes.* The *glmM* genes were amplified by PCR using chromosomal DNA from *E. coli* W3110 and *L. monocytogenes* and the primer pairs RB3/RB4 and RB1/RB2 and (Table S1 and S2). The PCR products were digested with *Pst*I/*Nco*I and ligated to the plasmid pIMK3 (Monk et al., 2008). The T460A nucleotide exchange was introduced using the mutagenic primer RB5 as described previously (Commichau et al., 2007a).

The plasmids pBP366 and pBP369 were constructed for the overexpression and purification of His-tagged GlmM and GST-tagged GlmM proteins, respectively. The *glmM* gene was amplified by PCR using the primer pairs FC334/FC335 and JR72/JR73 and chromosomal DNA from *L. monocytogenes*. The *glmM* genes were digested with *Bsa*I/*Xho*I and *Bam*HI/*Xho*I and ligated with the plasmids pET SUMOadapt and pGEX-6P1, respectively, that were digested with the same enzyme pairs.

The plasmids GlmM_Y153A, GlmM_F154A and GlmM_F154I for the overexpression GlmM variants GlmM Y153A, GlmM F154A and GlmM F154I for the *in vitro* DAC assay were constructed by site-directed mutagenesis (Heidemann et al., 2019) using the primer pairs GlmM_Y153A_F/GlmM_Y153A_R, GlmM_F154A_F/GlmM_F154A_R and GlmM_F154I_F/GlmM_F154I_R (Table S1) and the plasmid pBP366 as a template (Table S2).

3.5.3 Determination of membrane topology.

To determine the membrane topology of CdaR, the plasmids pBP250 (CdaR), pBP251 (CdaR ΔYbbR 1-4), pBP252 (CdaR ΔTM), pBP253 (PrkA) and pBP254 (PrfA) were constructed. The full-length *cdaR*, *prkA* and *prfA* genes were amplified with the primer pairs JH121/JH122, JH126/JH127 and JH128/JH129, respectively. The *cdaR* Δ*ybbR* 1-4 and *cdaR* Δ*TM* fragments encoding truncated CdaR variants were amplified with the primer pairs JH121/JH124 and JH123/JH122, respectively. The PCR products were digested with *Bam*HI and *Kpn*I, and ligated to the pKTop plasmid (Karimova et al., 2009) digested with the same enzymes. Next, the plasmids pBP250, pBP251, pBP252, pBP253, pBP254 and pKTop were introduced into *E. coli* DH5α by transformation. The strains were grown in LB medium from an OD_{600} of 0.1 to 0.3-0.6 from overnight cultures. The OD_{600} was adjusted to 0.1 and 5 µl of the cell suspensions were propagated on LB plates containing kanamycin, 1 mM IPTG, 80 µg/ml 5-bromo-4-chloro-3-indolyl phosphate (X-Phos, Sigma-Aldrich), 100 µg/ml 6-chloro-3-indolyl-β-D-galactopyranoside (Red-Gal, Sigma-Aldrich) and 50 mM sodium phosphate buffer (pH 7). The plates were incubated for 24 h at 37°C (Karimova *et al.*, 2009).
For the quantification of the alkaline phosphatase and β-galactosidase activity a slightly modified procedure as described by (Thongsomboon et al., 2018) was applied. DH5α cells that were grown in LB medium to an OD_{600} of 0.5-0.6 at 37°C and 220 rpm were harvested (1.5 ml) by centrifugation at 20,000 g at 4°C for 2 min. Two of the cell pellets were washed in 1 ml Z buffer (60 mM Na_2HPO_4, 40 mM NaH_2PO_4, 10 mM KCl, 1 mM $MgSO_4$) and the remaining two pellets were washed in 1 ml 10 mM Tris (pH 8). Next, the cell pellets were re-suspended in 1 ml of the washing buffers and lysed by adding 50 µl 0.1 % (w/v) SDS and 50 µl chloroform and by vortexing for 10 s followed by a 10 min long incubation at room temperature. To determine the β-galactosidase activity, 200 µl of Z buffer containing 4 mg/ml o-nitrophenyl-β-D-galactopyranoside (ONPG, Sigma-Aldrich) was added. Reactions were stopped by adding 500 µl 1 M Na_2CO_3 when samples turned yellow and the time was noted. The OD_{415} was determined after centrifugation for 10 min at 20,000 g. The specific β-galactosidase activity [µmol/min/mg] was calculated. For determining the alkaline phosphatase activity, 800 µl of the cells that were lysed in 10 mM Tris (pH 8) were added to 100 µl pNPP solution (SigmaFast solution 1 mg/ml p-nitrophenyl phosphate in 200 mM Tris pH 8, Sigma-Aldrich). The samples were incubated at 37°C until they turned yellow. Reactions were stopped by adding 100 µl 3 M NaOH, the time was noted. The OD_{415} was determined after centrifugation for 10 min at 20,000 g. The specific alkaline phosphatase activity [µmol/min/mg] was calculated.

3.5.4 Bacterial two-hybrid (B2H) assay.

The primary protein-protein interactions were analysed using the (B2H) system (Claessen et al., 2008; Karimova et al., 1998). Plasmid pairs pUT18C/pKT25 and pUT18/p25-N were used for the expression of proteins fused to the C and N termini, respectively, of the T18 and T25 fragments of CyaA (Karimova et al., 1998). The plasmids constructed for the B2H analysis are listed in Table S2. The genes were amplified using the oligonucleotides listed in Table S1 and cloned between the *Xba*I and *Kpn*I sites of the plasmids pUT18, pUT18C, p25-N, and pKT25. pUT18C-zip and pKT25-zip served as controls. The construction of the plasmids for the expression of the *cdaA* and *cdaR* genes has been described previously (Rismondo et al., 2016). The *glmM* gene was amplified using the primer pair FC336/FC337. The DNA sequences were verified using the oligonucleotides FC146, FC147, FC148, and FC150. Plasmids were used for the co-transformation of *E. coli* BTH101, and the protein-protein interactions were then analysed by plating the cells on LB plates containing 100 µg/ml ampicillin, 50 µg/ml kanamycin, 100 µg/ml X-Gal, and 0.5 mM IPTG. The plates were incubated for a maximum of 36 h at 30°C.

3.5.5 Protein expression and purification.

Derivatives of the *E. coli* strain BL21(DE) carrying plasmids for the overexpression of Δ100CdaA and GlmM were cultivated in 1 l 2 x YT medium at 37°C (Heidemann et al., 2019). Protein expression was induced by the addition of 1 mM isopropyl-β-D-thiogalactopyranoside (IPTG) when the cultures had reached an OD_{600} of about 0.6. The cultures were further incubated for 18 h at 16°C. The cells were disrupted in lysis buffer (20 mM Tris-HCl pH 7.5, 200 mM NaCl, 20 mM imidazole) using the M-11S Microfluidizer (Microfluidics) and the soluble fraction was separated from the cell debris by centrifugation for 30 min at 15,600 g. His_6-tagged GlmM protein from *L. monocytogenes* was purified using a Ni-sepharose column (GE Healthcare) and the S200 16/60 gel filtration system (GE Healthcare). Proteins were eluted from the column using elution buffer (20 mM Tris-HCl pH 7.5, 200 mM NaCl, 350 mM imidazole). The GST-tagged GlmM and Δ100CdaA proteins were purified as described previously (Heidemann et al., 2019). Protein concentrations were determined using the Bradford assay (Bradford, 1976) or a Nanodrop spectrophotometer at a wavelength of 280 nm (Desjardins et al., 2009). The plasmid pBP223 was used to overexpress the N-terminally Strep-tagged CdaR (ΔTM 1-28) from *L. monocytogenes* using BL21(DE3) as described previously for CdaA (Rosenberg *et al.*, 2015).

3.5.6 Isolation of protein fractions and Western blotting.

Purified Strep-CdaR and GST-tag-free GlmM proteins were used to generate rabbit polyclonal antibodies, as previously described (Rosenberg et al., 2015). *L. monocytogenes* strains were cultivated in 300 ml shake flasks containing 100 ml LSM medium at 37°C and 220 rpm until an OD_{600} of about 0.5. The cells were harvested by centrifugation at 4°C for 10 min at 3300 g washed once with 10 ml ZAP buffer (10 mM Tris-HCl pH 7.5, 200 mM NaCl). The cell pellets were resuspended in 400 µl ZAP buffer containing DNase I (0.5 U/ml, Sigma-Aldrich) and cOmplete EDTA-free Protease Inhibitor Cocktail (1 tablet/50 ml, Sigma-Aldrich). 200 µl of the cell suspensions were added to 0.5 g glass beads (0.1 mm diameter, Carl Roth) and disrupted using a TissueLyser II (Qiagen) for 15 min at 30 Hz and 4°C. 600 µl of the buffer was added and the tubes were incubated for 10 min on ice. Samples were centrifuged for 2 min at 20000 g and 4°C and the supernatant transferred to a new tube (whole cell lysate). 1 ml of each supernatant was subjected to ultracentrifugation at 235,000 g for 1 h at 4°C. The supernatants were transferred to new tubes (cytosolic fraction) and the pellets were resuspended in 1 ml of ZAP buffer.

After a second ultracentrifugation for 30 min, the supernatants were transferred to a new tube and the pellets were resuspended (membrane fractions) in 100 µl of the ZAP buffer containing

17 mM 3-[(3-cholamidopropyl)-dimethylammonio]-1-propanesulfonate hydrate (CHAPS; Sigma-Aldrich). The protein concentrations were determined by Bradford assay (Bradford, 1976) and 10 µg of the protein extracts were separated using 12 % SDS PAGE gels. Proteins were transferred on a polyvinylidene difluoride membrane (Bio-Rad) by electroblotting (Commichau et al., 2007b). Proteins were detected using polyclonal antibodies (1:1000 dilutions) raised against CdaA (Rosenberg et al., 2015), CdaR, GlmM and PrfA (Dormeyer et al., 2018). The primary antibodies were visualized by using anti-rabbit IgG (immunoglobulin G) AP (alkaline phosphatase) secondary antibodies (Promega) and the CDP* detection system (Roche Diagnostics). Images were taken using the Inta chemo cam (Intas).

3.5.7 Protein pull-down assay.

The pull-down assay to analyse the interaction between His-tagged GlmM and Δ100CdaA was performed as described previously (Tosi et al., 2019) using 1 ml TALON-cobalt beads (GE Healthcare) and gravity flow columns as described previously (Merzbacher et al., 2004). The proteins (50 µM each) were premixed on ice and incubated for 20 min. The beads were washed five times with 1 ml washing buffer (20 mM Tris-HCl pH 7.5, 200 mM NaCl) and the proteins were eluted in two steps using 1 ml elution buffer (20 mM Tris-HCl pH 7.5, 200 mM NaCl, 500 mM imidazole). Aliquots of the load, flow-through, washing and elution fractions were run on a 15 % SDS PAGE gel and proteins were visualized by Coomassie staining.

3.5.8 Size exclusion chromatography and multiangle light scattering (SEC-MALS).

The SEC-MALS analysis was three times performed as described previously (Rosenberg et al., 2015). The GST-tag-free GlmM and Δ100CdaA proteins were mixed 1:1 (1 mg/ml each) and 500 µl of the protein mixture were loaded onto the column.

3.5.9 Isothermal calorimetry (ITC).

The ITC experiments were carried out with an VP-ITC microcalorimeter (MicroCal Inc., Northampton, MA) in order to determine the affinity of GlmM to Δ100CdaA and the oligomerization state using tag-free proteins. In a typical setup, Δ100CdaA (34 µM in 20 mM Tris-HCl, pH 7.5, 200 mM NaCl) was placed in the sample cell, and GlmM (290 µM in the same buffer) was placed in the titration syringe. All experiments were carried out at 20 °C with and a stirring speed of 307 rpm. The parameters used for the titration series are given in Table S3. Data analysis was carried out using MicroCal PEQ-ITC Analysis, Malvern Panalytical software.

3.5.10 Phenotypic microarray assay.

The Phenotype MicroArray assay (PM; Biolog Inc.; Bochner et al., 2001) was employed to screen for a phenotype of the Δ*cdaR* mutant (LMJR45). The *L. monocytogenes* wild type strain and the Δ*cdaR* mutant were streaked on BHI plates and incubated over night at 37°C. Single colonies were used to inoculate 10 ml of BHI medium and the cultures were grown at 37°C and 220 rpm to an OD_{600} of 0.4-0.5. 9 ml of the cultures were harvested by centrifugation at 3300 g for 10 min at 4°C and the pellet were resuspended in 1 ml BHI with 25 % (w/v) glycerol, frozen in liquid nitrogen and stored at -80°C. A 10 µl inoculation loop was used to freshly restreak the bacteria from the cryocultures on BHI agar plates, prior to each PM and incubated for 20 h at 37°C. The cells were scratched evenly from the bacterial lawn, resuspended in the manufactures inoculation fluid and adjusted to an OD_{600} of 0.3 in 1 ml of the inoculation fluid. The remaining treatment was performed according to the recommendations of the manufacturer. The cells were incubated on the different PM 96-well plates with 100 µl of cells per well for 48 hours at 37°C with orbital shaking (237 cpm, 4 mm) and the OD_{590} was measured in 30 min intervals using an Epoch2 multiwell reader, equipped with the Gen5 software (02.09.2001; BioTek Instruments) .

3.5.11 Analysis of the c-di-AMP pools.

L. monocytogenes was cultivated overnight in 10 ml LSM with kanamycin. The pre-cultures were used to inoculate 75 ml LSM with kanamycin and 1 mM IPTG to an OD_{600} of 0.1. Bacteria were incubated at 37°C with agitation (220 rpm) until they reached an OD_{600} of 0.5-0.6. At this time point (time 0 min) two times 10 ml samples for the determination of the c-di-AMP concentration and two times 1 ml samples for the determination of the protein concentration were taken (see below). Two times 24 ml of each culture were transferred into new flasks with either

6 ml of LSM or 6 ml of LSM with 2.5 M NaCl (- and + 0.5 M NaCl, respectively). Cultures were incubated for another 25 min and once more samples were taken for c-di-AMP and protein amount determination (time 25 min). The 1 ml samples for protein concentration determination were harvested by centrifugation at 20000 g for 1 min at 4°C and further processed as described earlier (Rismondo *et al.*, 2016). The 10 ml samples for determination of the c-di-AMP concentration, were rapidly cooled by swirling in liquid nitrogen, centrifuged for 5 min at 3300 g and 4°C and the pellets frozen in liquid nitrogen. Samples were further processed and analysed *via* HPLC/MS-MS as described previously (Rismondo *et al.*, 2016).

3.5.12 *In vitro* diadenylate cyclase (DAC) assay.

The DAC assay to monitor the activity of Δ100CdaA and the effect of the wild type and the GlmM mutant variants on the diadenylate cyclase was performed as described previously (Heidemann et al. 2019). The enzyme reaction mixtures were incubated at 30°C.

Acknowledgements

This work was supported by grants from the Deutsche Forschungsgemeinschaft *via* Priority Programme SPP1879 (to R.F., F.M.C, V.K. and R.S.), by the Fonds der Chemischen Industrie (FCI), the Göttingen Center for Molecular Biosciences (GZMB), and by the University of Göttingen. We are grateful to Jörg Stülke for fruitful discussions. We thank Ole Hinrichs, Lisa Maria Schulz, Sandra Klama, Veronika Lutz and Birthe Nordmann for the help with some experiments. Anna Lena Hagemann is acknowledged for experimental support.

Conflict of interest statement

The authors certify that there is no potential conflict of interest.

References

Alexeyev MF, Winkler HH. 1999. Membrane topology of the *Rickettsia prowazekii* ATP/ADP translocase revealed by novel dual *pho-lac* reporters. J Mol Biol 285:1503-1513.

Arnaud M, Chastanet A, Débarbouille M. 2004. New vector for efficient allelic replacement in naturally transformable, low-GC content, Gram-positive bacteria. Appl. Environ Microbiol 70:6887-6891.

Bai Y, Yang J, Zarella TM, Zhang Y, Metzger DW, Bai G. 2014. Cyclic di-AMP impairs potassium uptake mediated by a cyclic di-AMP binding protein in *Streptococcus pneumoniae.* J Bacteriol 196:614-623.

Bai Y, Yang J, Eisele LW, Underwood AJ, Koestler BJ, Waters CM, Metzger DW, Bai G. 2013. Two DHH1 subfamily 1 proteins in *Streptococcus pneumoniae* possess cyclic di-AMP phosphodiesterase activity and affect bacterial growth and virulence. J Baceriol 195:5123-5132.

Barb AW, Cort JR, Seetharaman J, Lew S, Lee HW, Acton T, Xiao R, Kennedy MA, Tong L, Montelione GT, Prestegard JH. 2011. Structures of domains I and IV from YbbR are representative of a widely distributed protein family. Protein Sci. 20:396-405.

Barker JR, Koestler BJ, Carpenter VK, Burdette DL, Waters CM, Vance RE, Valdivia RH. 2013. STING-dependent recognition of cyclic di-AMP mediates type I interferon responses during *Chlamydia trachomatis* infection. MBio 4:e00018-13.

Bharat Siva Varma P, Adimulam YB, Kodukula S. 2015. *In silico* functional annotation of a hypothetical protein from *Staphylococcus aureus*. J Infect Public Health 8:526-532.

Bejerano-Sagie M, Oppenheimer-Shaanan Y, Berlatzky I, Rouvinski A, Meyerovich M, Ben-Yehuda S. 2006. A checkpoint protein scans the chromosome for damage at the start of sporulation in *Bacillus* subtilis. Cell 125:679-690.

Blötz C, Treffon K, Kaever V, Schwede F, Hammer E, Stülke J. 2017. Identification of the components involved in cyclic di-AMP signaling in *Mycoplasma pneumoniae*. Front Microbiol 8:1328.

Bochner BR, Gadzinski P, Panomitros E. 2001. Phenotype microarrays for high-throughput phenotypic testing and assay of gene function. Genome Res 11:1246-1255.

Bowman L, Zeden MS, Schuster CF, Kaever V, Gründling A. 2016. New insights into the cyclic di-adenosine monophosphate (c-di-AMP) degradation pathway and the requirement of the cyclic dinucleotide for acid stress resistance in *Staphylococcus aureus*. J Biol Chem 291:26970-26986.

Bradford MM. 1976. A rapid and sensitive method for the quantification of microgram quantities of protein utilizing the principle of protein-dye binding. Anal Biochem. 72:248-254.

Braun F, Thomalla L, van der Does C, Quax TEF, Allers T, Kaever V, Albers SV. 2019. Cyclic nucleotides in archaea: cyclic di-AMP in the archaeon *Haloferax volcanii* and its putative role. Microbiologyopen 18:e829.

Brehm K, Kreft J, Ripio MT, Vázquez-Boland JA. 1996. Regulation of virulence gene expression in pathogenic Listeria. Microbiologia 12:219-236.

Bremer E, Krämer R. 2019. Responses of microorganisms to osmotic stress. Annu Rev Microbiol 73:313-334 .

Campeotto I, Zhang Y, Mladenov MG, Freemont PS, Gründling A. 2015. Complex structure and biochemical characterization of the *Staphylococcus aureus* cyclic diadenylate monophosphate (c-di-AMP)-binding protein PstA, the founding member of a new signal transduction protein family. J Biol Chem 290:2888-2901.

Chin KH, Liang JM, Yang JG, Shih MS, Tu ZL, Wang YC, Sun XH, Hu NJ, Liang ZX, Dow JM, Rayn RP, Chou SH. 2015. Structural insights into the distinct binding mode of cyclic di-AMP with SaCpaA_RCK. Biochemistry 54:4936-4951.

Choi PH, Vu TMN, Pham HT, Woodward JJ, Turner MS, Tong L. 2017. Structural and functional studies of pyruvate carboxylase regulation by cyclic di-AMP in lactic acid bacteria. Proc Natl Acad Sci USA 114: E7226-E7235.

Choi PH, Sureka K, Woodward JJ, Tong L. 2015. Molecular basis for the recognition of cyclic di-AMP by PstA, a PII-like signal transduction protein. Microbiologyopen 4:361-374.

Commichau FM, Heidemann JL, Ficner R, Stülke J. 2019. Making and breaking of an essential poison: the cyclases and phosphodiesterases that produce and degrade the essential second messenger cyclic di-AMP in bacteria. J Bacteriol 201: pii: e00462-18.

Commichau FM, Stülke J. 2008. Trigger enzymes: bifunctional proteins active in metabolism and in controlling gene expression. Mol Microbiol 67:692-702.

Commichau FM, Stülke J. 2018. Coping with an essential poison: a genetic suppressor analysis corroborates a key function of c-di-AMP in controlling potassium ion homeostasis in Gram-positive bacteria. J Bacteriol 200: pii: e00166-18.

Commichau FM, Gibhardt J, Halbedel S, Gundlach J, Stülke J. 2018. A delicate connection: c-di-AMP affects cell integrity by controlling osmolyte transport. Trends Microbiol 26:175-185.

Commichau FM, Dickmanns A, Gundlach J, Ficner R, Stülke J. 2015. A jack of all trades: the multiple roles of the unique essential second messenger cyclic di-AMP. Mol Microbiol 97:189-204.

Commichau FM, Herzberg C, Tripal P, Valerius O, Stülke J. 2007a. A regulatory protein-protein interaction governs glutamate biosynthesis in *Bacillus subtilis*: the glutamate dehydrogenase RocG moonlights in controlling the transcription factor GltC. Mol Micro 65:642-654.

Commichau FM, Wacker I, Schleider J, Blencke HM, Reif I, Tripal P, Stülke J. 2007b. Characterization of *Bacillus subtilis* mutants with carbon source-independent glutamate biosynthesis. J Mol Microbiol Biotechnol 12:106-113.

Corrigan RM, Gründling A. 2013. Cyclic di-AMP: another second messenger enters the fray. Nat Rev Microbiol 11:513-524.

Corrigan RM, Campeotto I, Jeganathan T, Roelofs KG, Lee VT, Gründling A. 2013. Systematic identification of conserved bacterial c-di-AMP receptor proteins. Proc Natl Acad Sci USA 110: 9084-9089.

Corrigan RM, Abbott JC, Burhenne H, Kaever V, Gründling A. 2011. c-di-AMP is a new second messenger in *Staphylococcus aureus* with a role in controlling cell size and envelope stress. PLoS Pathog 7:e1002217.

Dengler V, McCallum N, Kiefer P, Christen P, Patrignani A, Vorholt JA, Berger-Bächi B, Senn MM. 2013. Mutation in the c-di-AMP cyclase dacA affects fitness and resistance of methicillin resistant *Staphylococcus aureus*. PLoS One. 8:e73512.

Desjardins P, Hansen JB, Allen M. 2009. Microvolume protein concentration determination using the NanoDrop 2000c Spectrophotometer. J Vis Exp 33:1610.

Devaux L, Sleiman D, Mazzuoli MV, Gominet M, Lanotte P, Trieu-Cuot P, Kaminski PA, Firon A. 2018. Cyclic di-AMP regulation of osmotic homeostasis is essential in group B *Streptococcus*. PLoS Genet 14(4):e1007342.

Dormeyer M, Lentes S, Ballin P, Wilkens M, Klumpp S, Kohlheyer D, Stannek L, Grünberger A, Commichau FM. 2018. Visualization of tandem repeat mutagenesis in *Bacillus subtilis*. DNA Repair (Amst) 63:10-15.

Drexler DJ, Müller M, Rojas-Cordova CA, Bandera AM, Witte G. 2017. Structural and biophysical analysis of the soluble DHH/DHHA1-type phosphodiesterase TM1595 from *Thermotoga maritima*. Structure 25:1887-1897.

Du B, Sun JH. 2015. Diadenylate cyclase evaluation of ssDacA (SSU98_1483) in *Streptococcus suis* serotype 2. Genet Mol Res 14:6917-6924.

Dussurget O, Cabanes D, Dehoux P, Lecuit M, Buchrieser C, Glaser P, Cossart P; European Listeria Genome Consortium. 2002. *Listeria monocytogenes* bile salt hydrolase is a PrfA-regulated virulence factor involved in the intestinal and hepatic phases of listeriosis. Mol Microbiol 45:1095-1106.

Fahmi T, Port GC, Cho KH. 2017. c-di-AMP: an essential molecule in the signaling pathways that regulate the viability and virulence of Gram-positive bacteria. Genes (Basel) 8: pii: E197.

Gao A, Serganov A. 2014. Structural insights into recognition of c-di-AMP by the *ydaO* riboswitch. Nat Chem Biol 10:787-792.

Gibhardt J, Hoffmann G, Turdiev A, Wang M, Lee VT, Commichau FM. 2019. c-di-AMP assists osmoadaptation by regulating the *Listeria monocytogenes* potassium transporters KimA and KtrCD. J Biol Chem 294:16020-16033.

Gundlach J, Herzberg C, Kaever V, Gunka K, Hoffmann T, Weiß M, Gibhardt J, Thürmer A, Hertel D, Daniel R, Bremer E, Commichau FM, Stülke J. 2017. Control of potassium homeostasis is an essential function of the second messenger cyclic di-AMP in *Bacillus subtilis* Sci Signal 10: pii: eaal3011.

Gundlach J, Krüger L, Herzberg C, Turdiev A, Poehlein A, Tascón I, Weiss M, Hertel D, Daniel R, Hänelt I, Lee VT, Stülke J. 2019. Sustained sensing in potassium homeostasis: cyclic di-AMP controls potassium uptake by KimA at the levels of expression and activity. J Biol Chem 294:9605-9614.

Gundlach J, Rath H, Herzberg C, Mäder U, Stülke J. 2016. Second messenger signaling in *Bacillus subtilis*: accumulation of cyclic di-AMP inhibits biofilm formation. Front Microbiol 7:804.

Gundlach J, Mehne FM, Herzberg C, Kampf J, Valerius O, Kaever V, Stülke J. 2015. An essential poison: synthesis and degradation of cyclic di-AMP in *Bacillus subtilis*. J Bacteriol 197:3265-3274.

Gundlach J, Dickmanns A, Schröder-Tittmann K, Neumann P, Kaesler J, Kampf J, Herzberg C, Hammer E, Schwede F, Kaever V, Tittmann K, Stülke J, Ficner R. 2015. Identification, characterization, and structure analysis of the cyclic di-AMP-binding PII-like signal transduction protein DarA. J Biol Chem 290:3069-3080.

Guzman LM, Belin D, Carson MJ, Beckwith J. 1995. Tight regulation, modulation, and high level expression by vectors containing the arabinose pBAD promoter. J Bacteriol 177:4121-4130.

Hamon M, Bierne H, Cossart P. 2006. *Listeria monocytogenes*: a multifaceted model. Nat Rev Microbiol 4:423-434.

Heidemann JL, Neumann P, Dickmanns A, Ficner R. 2019. Crystal structures of the c-di-AMP-synthesizing enzyme CdaA. J Biol Chem 294:10463-10470.

Hill NS, Buske PJ, Levin PA. 2013. A moonlighting enzymes links *Escherichia coli* cell size with central metabolism. PLoS Genet 9:e10003663.

Horton RM, Cai ZL, Ho SN, Pease LR. 1990. Gene splicing by overlap extension: tailormade genes using the polymerase chain reaction. Biotechniques 8:528-535.

Huynh TN, Choi PH, Sureka K, Ledvina HE, Campillo J, Tong L, Woodward JJ. 2016. Cyclic di-AMP targets the cystathione beta-synthase domain of the osmolyte transporter OpuC. Mol Microbiol 102:233-243.

Huynh TN, Woodward JJ. 2016. Too much of a good thing: regulated depletion of c-di-AMP in the bacterial cytoplasm. Curr Opin Microbiol 30:22-29.

Huynh TN, Luo S, Pensinger D, Sauer JD, Tong L, Woodward JJ. 2015. An HD-domain phosphodiesterase mediates cooperative hydrolysis of c-di-AMP to affect bacterial growth and virulence. Proc Natl Acad Sci USA 112:E747-756.

Jeffery CJ. 1999. Moonlighting proteins. Trends Biochem Sci 24:8-11.

Jeffery CJ. 2019. Multitalented actors inside and outside the cell: recent discoveries add to the number of moonlighting proteins. Biochem Soc Trans 47:1941-1948.

Jones CP, Ferré-D'Amaré AR. 2014. Crystal structure of a c-di-AMP riboswitch reveals an internally pseudo-dimeric RNA. EMBO J 33:2692-2703.

Kaplan Zeevi M, Shafir NS, Shaham S, Friedman S, Sigal N, Nir Paz R, Boneca IG, Herskovits AA. 2013. *Listeria monocytogenes* multidrug resistance transporters and cyclic di-AMP, which contributes to type I interferon induction, play a role in cell wall stress. J Bacteriol 195:5250-5261.

Kamegaya T, Kuroda K, Hayakawa Y. 2011. Identification of a *Streptococcus pyogenes* SF370 gene involved in production of c-di-AMP. Nagoya J Med Sci 73:49-57.

Karimova G, Pidoux J, Ullmann A, Ladant D. 1998. A bacterial two-hybrid system based on a reconstituted signal transduction pathway. Proc Natl Acad Sci USA 95:5752-5756.

Karimova G, Robichon C, Ladant D. 2009. Characterization of YmgF, a 72-residue inner membrane protein that associates with the *Escherichia coli* cell division machinery. J Bacteriol 191:333-346.

Kim H, Youn SJ, Kim SO, Ko J, Lee OJ, Choi BS. 2015. Structural studies of potassium transport protein KtrA regulator of conductance of K+ (RCK)_C domain in complex with cyclic diadenosine monophosphate (c-di-AMP). J Biol Chem 290:16393-16402.

Lima A, Durán R, Schujman GE, Marchissio MJ, Portela MM, Obal G, Pritsch O, de Mendoza D, Cerveñansky C. 2011. Serine/threonine protein kinase PrkA of the human pathogen *Listeria monocytogenes*: biochemical characterization and identification of interacting partners through proteomic approaches. J Proteomics 74:1720-1734.

Luo Y, Helmann JD. 2012. Analysis of the role of *Bacillus subtilis* σ(M) in β-lactam resistance reveals an essential role for c-di-AMP in peptidoglycan homeostasis. Mol Microbiol 83:623-639.

Mehne FM, Schröder-Tittmann K, Eijlander RT, Herzberg C, Hewitt L, Kaever V, Lewis RJ, Kuipers OP, Tittmann K, Stülke J. 2014. Control of the diadenylate cyclase CdaS in *Bacillus subtilis*: an autoinhibitory domain limits cyclic di-AMP production. J Biol Chem 289:21098-21107.

Mehne FM, Gunka K, Eilers H, Herzberg C, Kaever V, Stülke J. 2013. Cyclic di-AMP homeostasis in *Bacillus subtilis*: both lack and high level accumulation of the nucleotide are detrimental for cell growth. J Biol Chem 288:2004-2017.

Merzbacher M, Detsch C, Hillen W, Stülke J. 2004. *Mycoplasma pneumoniae* HPr kinase/phosphorylase. Eur J Biochem 271:367-374.

Monk IR, Gahan CGM, Hill C. 2008. Tools for functional postgenomic analysis of *Listeria monocytogenes*. Appl Environ Microbiol 74:3921-3934.

Moscoso JA, Schramke H, Zhang Y, Tosi T, Dehbi A, Jung K, Gründling A. 2015. Binding of cyclic di-AMP to the *Staphylococcus aureus* sensor kinase KdpD occurs via the universal stress protein domain and downregulates the expression of the Kdp potassium transporter. J Bacteriol 198:98-110.

Müller M, Hopfner KP, Witte G. 2015. c-di-AMP recognition by *Staphylococcus aureus* PstA. FEBS Lett 589:45-51.

Nelson JW, Sudarsan N, Furukawa K, Weinberg Z, Wang JX, Breaker RR. 2013. Riboswitches in eubacteria sense the second messenger c-di-AMP. Nat Chem Biol 9:834-839.

Oppenheimer-Shaanan Y, Wexselblatt E, Katzhendler J, Yavin E, Ben-Yehuda S. 2011. C-di-AMP reports DNA integrity during sporulation in *Bacillus subtilis*. EMBO Rep 12:594-601.

Pham HT, Turner MS. 2019. Onward and [K+]upward: a new potassium importer under the spell of cyclic di-AMP. J Bacteriol 201: pii: e00150-19.

Pham HT, Nhiep NTH, Vu TNM, Huynh TN, Zhu Y, Huynh ALD, Chakrabortti A, Marcellin E, Lo R, Howard CB, Bansal N, Woodward JJ, Liang ZX, Turner MS. 2018. Enhanced uptake of potassium or glycine betaine or export of cyclic-di-AMP restores osmoresistance in a high cyclic-di-AMP *Lactococcus lactis* mutant. PLoS Genet 14(8):e1007574.

Pham HT, Liang ZX, Marcellin E, Turner MS. 2016. Replenishing the cyclic-di-AMP pool: regulation of diadenylate cyclase activity in bacteria. Curr Genet 62:731-738.

Radoshevich L, Cossart P. 2018. *Listeria monocytogenes*: towards a complete picture of its physiology and pathogenesis. Nat Rev Microbiol 16:32-46.

Rao F, See RY, Zhang D, Toh DC, Ji Q, Liang ZX. 2010. YybT is a signaling protein that contains a cyclic dinucleotide phosphodiesterase domain and a GGDEF domain with ATPase activity. J Biol Chem 285:473-482.

Ren A, Patel DJ. 2014. c-di-AMP binds the *ydaO* riboswitch in two pseudo-symmetry-related pockets. Nat Chem Biol 10:780-786.

Rismondo J, Gibhardt J, Rosenberg J, Kaever V, Halbedel S, Commichau FM. 2016. Phenotypes associated with the essential diadenylate cyclase CdaA and its potential regulator CdaR in the human pathogen *Listeria monocytogenes*. J Bacteriol 198:416-426.

Rosenberg J, Dickmanns A, Neumann P, Gunka K, Arens J, Kaever V, Stülke J, Ficner R, Commichau FM. 2015. Structural and biochemical analysis of the essential diadenylate cyclase CdaA from *Listeria monocytogenes*. J Biol Chem 290:6596-6606.

Rubin BE, Huynh TN, Welkie DG, Diamond S, Simkovsky R, Pierce EC, Taton A, Lowe LC, Lee JJ, Rifkin SA, Woodward JJ, Golden SS. 2018. High-throughput interaction screens illuminate the role of c-di-AMP in cyanobacterial nighttime survival. PLoS Genet 14: e1007301.

Sambrook J, Maniatis T, Fritsch EF. 1989. Molecular cloning: a laboratory manual. 2nd edition, Cold Spring Harbour Laboratory Press, New York.

Schuster CF, Bellows LE, Tosi T, Campeotto RM, Freemont P, Gründling A. 2016. The second messenger c-di-AMP inhbits the osmolyte uptake system OpuC in *Staphylococcus aureus*. Sci Signal 9:ra81.

Schwartz KT, Carleton JD, Qullin SJ, Rollins SD, Portnoy DA, Leber JH. 2012. Hyperinduction of host beta interferon by a *Listeria monocytogenes* strain naturally overexpression the multidrug efflux pump MdrT. Infect Immun 80:1537-1545.

Sexton DL, St-Onge RJ, Haiser HJ, Yousef MR, Brady L, Gao C, Leonard J, Elliot MA. 2015. Resuscitation-promoting factors are cell wall-lytic enzymes with important roles in the germination and growth of *Streptomyces coelicolor*. J Bacteriol 197:848-860.

Sleator RD, Hill C. 2002. Bacterial osmoadaptation: the role of osmolytes in bacterial stress and virulence. FEMS Microbiol Rev 26:49-71.

Stannek L, Thiele MJ, Ischebeck T, Gunka K, Hammer E, Völker U, Commichau FM. 2015. Evidence for synergistic control of glutamate biosynthesis by glutamate dehydrogenases and glutamate in *Bacillus subtilis*. Environ Microbiol 17:3379-3390.

St-Onge RJ, Elliot MA. 2017. Regulation of a muralytic enzyme-encoding gene by two noncoding RNAs. RNA Biol 14:1592-1605.

St-Onge RJ, Haiser HJ, Yousef MR, Sherwood E, Tschowri N, Al-Bassam M, Elliot MA. 2015. Nucleotide second messenger-mediated regulation of a muralytic enzyme in *Streptomyces*. Mol Microbiol 96:779-795.

Stülke J, Krüger L 2020. Cyclic di-AMP signaling in bacteria. Annu Rev Microbiol. *In press.*

Sureka K, Choi PH, Precit M, Delince M, Pensinger DA, Huynh TN, Jurado AR, Goo YA, Sadilek M, Lavarone AT, Sauer JD, Tong L, Woodward JJ. 2014. The cyclic dinucleotide c-di-AMP is an allosteric regulator of metabolic enzyme function. Cell 158:1389-1401.

Tan E, Rao F, Pasunooti S, Pham TH, Soehano I, Turner MS, Liew CW, Lescar J, Pervushin K, Liang ZX. 2013. Solution structure of the PAS domain of a thermophilic YybT protein homolog reveals a potential ligand-binding site. J Biol Chem 288:11949-11959.

Teh WK, Dramsi S, Tolker-Nielsen T, Yang L, Givskov M. 2019. Increased intracellular cyclic di-AMP levels sensitize *Streptococcus gallolyticus subsp. gallolyticus* to osmotic stress and reduce biofilm formation and adherence on intestinal cells. J Bacteriol 201: pii: e00597-18.

Thongsomboon W, Serra DO, Possling A, Hadjineophytou C, Hengge R, Cegelski L. 2018. Phosphoethanolamine cellulose: a naturally produced chemically modified cellulose. Science. 359:334-338.

Toledo-Arana A, Dussurget O, Nikitas G, Sesto N, Guet-Revillet H, Balestrino D, Loh E, Gripenland J, Tiensuu T, Vaitkevicius K, Barthelemy M, Vergassola M, Nahori MA, Soubigou G, Rénault B, Copée JY, Lecuit M, Johansson J, Cossart P. 2009. The *Listeria* transcriptional landscape from saprophytism to virulence. Nature. 459:950-956.

Tosi T, Hoshiga F, Millership C, Singh R, Eldrid C, Patin D, Mengin-Lecreulx D, Thalassinos K, Freemont P, Gründling A. 2019. Inhibition of the *Staphylococcus aureus* c-di-AMP cyclase DacA by direct interaction with the phosphoglucosamine mutase GlmM. PLoS Pathog 15:e1007537.

Quintana IM, Gibhardt J, Turdiev A, Hammer E, Commichau FM, Lee VT, Magni C, Stülke J. 2019. The KupA and KupB proteins of *Lactococcus lactis* IL1403 are novel c-di-AP receptor proteins responsible for potassium uptake. J Bacteriol 201: pii: e00028-19.

Wang F, He Q, Su K, Wei T, Xu S, Gu L. 2018. Structural and biochemical characterization of the catalytic domains of GdpP reveals a unified hydrolysis mechanism for the DHH/DHHA1 phosphodiesterase. Biochem J 475:191-205.

Wang X, Cai X, Ma H, Yin W, Zhu L, Li X, Lim HM, Chou SH, He J. 2019. A c-di-AMP riboswitch controlling *kdpFABC* operon transcription regulates the potassium transporter system in *Bacillus thuringiensis*. Commun Biol 2:151.

Weart RB, Lee AH, Chien AC, Haeusser DP, Hill NS, Levin PA. 2007. A metabolic sensor governing cell size in bacteria. Cell 130:335-347.

Whiteley AT, Garelis NE, Peterson BN, Choi PH, Tong L, Woodward JJ, Portnoy DA. 2017. c-di-AMP modulates *Listeria monocytogenes* central metabolism to regulate growth, antibiotic resistance and osmoregulation. Mol Microbiol 104:212-233.

Whiteley AT, Pollock AJ, Portnoy DA. 2015. The PAMP c-di-AMP is essential for *Listeria monocytogenes* growth in rich but not in minimal media due to a toxic increase in (p)ppGpp. Cell Host Microbe 17:788-798.

Witte CE, Whiteley AT, Burke TP, Sauer JD, Portnoy DA, Woodward JJ. 2013. Cyclic di-AMP is critical for *Listeria monocytogenes* growth, cell wall homeostasis, and establishment of infection. MBio 4: e00282-13.

Witte G, Hartung S, Büttner K, Hopfner KP. 2008. Structural biochemistry of a bacterial checkpoint protein reveals diadenylate cyclase activity regulated by DNA recombination intermediates. Mol Cell 30:167-178.

Wood JM. 1999. Osmosensing by bacteria: signals and membrane-based sensors. Microbiol Mol Biol Rev 63:230-262.

Wood JM. 2011. Bacterial osmoregulation: a paradigm for the study of cellular homeostasis. Annu Rev Microbiol 65:215-238.

Woodward JJ, Lavarone AT, Portnoy DA. 2010. C-di-AMP secreted by *Listeria monocytogenes* activates a host type I interferon response. Science 328:1703-1705.

Zarella TM, Metzger DW, Bai G. 2018. Stress suppressor screening leads to detection of regulation of cyclic di-AMP homeostasis by a Trk family effector protein in *Streptococcus pneumoniae.* J Bacteriol 200: pii: e00045-18.

Zeden MS, Schuster CF, Bowman L, Zhong Q, Williams HD, Gründling A. 2018. Cyclic di-adenosine monophosphate (c-di-AMP) is required for osmotic regulation in *Staphylococcus aureus* but dispensable for viability in anaerobic conditions. J Biol Chem 293:3180-3200.

Zhang L, Li W, He ZG. 2013. DarR, a TetR-like transcriptional factor, is a cyclic di-AMP-responsive repressor in *Mycobacterium smegmatis*. J Biol Chem 288:3085-3096.

Zheng Y, Zhou J, Sayre DA, Sintim HO (2014) Identification of bromophenol thiohydantoin as an inhibitor of DisA, a c-di-AMP synthase, from a 1000 compound library, using the coralyne assay. Chem Commun (Camb). 50:11234-7.

Zhu Y, Pham TH, Nhiep TH, Vu NM, Marcellin E, Chakrabortti A, Wang Y, Waanders J, Lo R, Huston WM, Bansal, Nielsen LK, Liang ZX, Turner MS. 2016. Cyclic-di-AMP synthesis by the diadenylate cyclase CdaA is modulated by the peptidoglycan biosynthesis enzyme GlmM in *Lactococcus lactis*. Mol Microbiol 99:1015-1027.

Figure Legends

FIG 1 The domains of CdaA and CdaR, the genomic context of the cdaR, cdaR and glmM genes, localization of the encoded proteins and topology analysis. (A) CdaA contains three transmembrane domains (TM) and a diadenylate cyclase domain (DAC) that is surrounded by coiled-coil (CC) domains (Rosenberg et al., 2019; Heidemann et al., 2019). CdaR contains a TM domain and four YbbR domains of unknown function (Barb et al., 2011). (B) The bi-cistronic cdaAR operon encodes the diadenylate cyclase CdaA and its regulator CdaR. The glmM gene encodes the essential phosphoglucosamine mutase GlmM. The lmo2121 and lmo2117 genes of unknown function surround the cdaAR-glmM module. Arrows and circles indicate transcription start sites and terminators, respectively (Toledo-Arana et al., 2009). (C) Western blot analysis to analyse the subcellular localization of CdaA, CdaR and GlmM. The preparation of the whole cell lysate, the cytosolic fraction and the membrane fraction is described in the Materials and Methods section. The proteins were separated using 12 % SDS PAGE gels. CdaA, CdaR, GlmM and PrfA (control) were detected using the polyclonal antibodies α-CdaA, α-CdaR, α-GlmM and α-PrfA, respectively. (D) Schematic illustration of the PhoA-LacZ fusion proteins that were used to analyse the topology of CdaR. The membrane-attached PASTA kinase PrkA and the cytosolic PrfA protein served as controls. (E) The E. coli strain DH5α carrying the plasmids pKTop (empty plasmid), pBP253 (PrkA), pBP252 (PrfA), pBP250 (CdaR), pBP251 (CdaR ΔTM) and pBP251 (CdaR ΔYbbR), were propagated on LB kanamycin plates containing the chromogenic substrates X-Phos and Red-Gal for PhoA and LacZ, respectively. (F) Quantification of the LacZ and PhoA activities detectable in the E. coli strains that were propagated on the agar plate shown in (E). The bacteria were cultivated in LB medium and the enzyme activities were determined as described in the Materials and Methods section. Data points represent biologically independent replicates (n = 4). Bars indicate means of replicates and the standard deviations are shown.

FIG 2 B2H assay to study the interactions among CdaA, CdaR and GlmM. The cdaA, cdaR and glmM genes were introduced into the plasmids pUT18, pUT18C, p25-N and pKT25. Plasmids pUT18 and pUT18C allow the expression of the proteins fused either to the N- or the C-terminus of the T18 domain of the B. pertussis adenylate cyclase respectively. Plasmid p25-N and pKT25 allow the expression of the proteins fused to the N- or the C-terminus of the T25 domain of the adenylate cyclase. The E. coli transformants were spotted onto LB plates supplemented with X-Gal and IPTG and incubated for 36 h at 30°C.

FIG 3 In vitro pull-down assay to analyse the interaction between Δ100CdaA and GlmM. (A) The tag-less Δ100CdaA and the His-tagged GlmM proteins were mixed in a 1:1 ratio (50 µM

each) incubated for 20 min on ice and loaded onto the gravity flow column containing TALON-cobalt beads. The flow-through was collected and the beads were washed five times to remove the unbound proteins. The proteins were eluted in two steps. The proteins in 7 µl of the fractions were separated using a 15 % SDS PAGE gel and the proteins were visualized by Coomassie staining. (B) Control experiment to assess whether the same amount of the tag-less Δ100CdaA alone binds to the TALON-cobalt beads. S, size standard (Page Ruler Plus Prestained, Thermo Scientific).

FIG 4 Size exclusion chromatography to analyse the interaction between Δ100CdaA and GlmM. (A) Size exclusion chromatography profiles of the tag-less GlmM (blue line) and Δ100CdaA (black line) proteins and the GlmM-Δ100CdaA complex (red line). The proteins (1 mg/l each) were either analysed individually or in a mixture. The elution peaks were analysed using the ASTRA software version 6.1. (B) Coomassie-stained SDS PAGE gels (15 %) containing 7 µl aliquots of the elution peaks obtained with the individual proteins or of the GlmM-Δ100CdaA complex. S, size standard (Page Ruler Plus Prestained, Thermo Scientific).

FIG 5 Assessment of the molecular mass of the GlmM-Δ100CdaA complex and of the stoichiometry of the protein-protein interaction. (A) The SEC-MALS was performed as described in the *MATERIALS AND METHODS* section. The elution volumes and the molecular masses calculated from the scattered signals indicate the formation of dimers of the Δ100CdaA and GlmM proteins and of dimers of Δ100CdaA and GlmM in the GlmM-Δ100CdaA complex. The UV light detector signals for GlmM, Δ100CdaA and the GlmM-Δ100CdaA complex are shown in dark blue, red and black, respectively. The estimated molecular masses that were calculated by analysing the light that was scattered (LS) by GlmM, Δ100CdaA and the GlmM-Δ100CdaA complex are indicated by the short light blue, pink and grey lines, respectively. (B) Binding of GlmM to Δ100CdaA was studied by means of ITC. The cell and the syringe contained 34.1 µM Δ100CdaA and 290.6 µM GlmM, respectively, see *Materials and Methods* section for details. (C) Assessment of the molar ration of the interaction between GlmM and Δ100CdaA.

FIG 6 Phenotypes associated with CdaR in *L. monocytogenes* and regulation of c-di-AMP synthesis by CdaR and GlmM in *E. coli*. (A) Phenotype microarray results of *L. monocytogenes* EGD-e wild type strain versus the Δ*cdaR* strain LMJR45 on Biolog PM9 wells A1-A9. Yellow colour indicates identical metabolic activities of the wild type and the Δ*cdaR* mutant. Red and

green colours indicate higher metabolic activities of the wild type and the Δ*cdaR* mutant, respectively. (B) Influence of NaCl, KCl and sorbitol on the growth rates of the *L. monocytogenes* EGD-e wild type strain and the Δ*cdaR* strain LMJR45 in BHI medium. The growth rates of the strains in the absence of NaCl, KCl and sorbitol were set to 100 %. (C) Schematic illustration of the experimental approach to assess the role of CdaR and truncated CdaR variants in modulating c-di-AMP synthesis in *L. monocytogenes* upon salt shock. The strains BPL45 (wild type + empty vector (EV)), BPL46 (Δ*cdaR* + empty vector (EV)), BPL16 (Δ*cdaR* + CdaR), BPL47 (Δ*cdaR* + CdaR ΔTM) synthesizing CdaR without the transmembrane (TM) helix (see Fig. 1A), and BPL47 (Δ*cdaR* + CdaR ΔYbbr1-4) synthesizing only the TM helix of CdaR (see Fig. 1A) were grown in LSM medium at 37°C and the salt shock was performed by adding prewarmed LSM medium supplemented with NaCl. As the control, the same amount of the medium without NaCl supplementation was added to a culture. The c-di-AMP intracellular levels of were determined before and after diluting the cultures (see *Materials and Methods*). (D) Effect of NaCl on the CdaR-dependent c-di-AMP production in *L. monocytogenes.* (E) Schematic illustration of the *E. coli* strain LB2003 lacking the native potassium transporters to study the effect of CdaR variants, GlmM, and CdaR in combination with GlmM on the CdaA-dependent production of c-di-AMP that inhibits potassium uptake *via* KimA and thus growth. (F) The derivatives of the *E. coli* strain LB2003 carrying the plasmid pBP384 (KimA) in combination with either pBP370 (CdaA), pBP373 (CdaA D171N), pBP387 (CdaA-CdaR), pBP389 (CdaA-GlmM), pBP388 (CdaA-CdaR-GlmM), pBP260 (CdaA-CdaR ΔTM), pBP261 (CdaA-CdaR ΔYbbR4), pBP262 (CdaA-CdaR ΔYbbR3-4), pBP263 (CdaA-CdaR ΔYbbR2-4), or pBP264 (CdaA-CdaR ΔYbbR1-4) were grown at 37°C in M9 minimal medium supplemented with 350 µM KCl. 0.005 % L-arabinose and 50 µM IPTG were added to induce the expression of the *cdaA* genes/operons and the *kimA* gene, respectively. Data points represent biologically independent replicates (n = 3). Bars indicate means of replicates and the standard deviations are shown.

FIG 7 Control of CdaA-dependent c-di-AMP production by GlmM. (A) Sequence alignment of a part of GlmM and the overall sequence identities of the homologs from *L. monocytogenes* EGD-e (UniProt: Q8Y5E6), *B. subtilis* 168 (UniProt: O34824), *S. aureus* COL (UniProt: Q5HE43), *L. lactis* MG1363 (UniProt: A2RIG0), *S. pneumoniae* (UniProt: Q04JI8), and *E. coli* K-12 MG1655 (UniProt: P31120). The *L. lactis* MG1363 GlmM I154F variant was shown to inhibit CdaA stronger *in vivo* (Zhu et al., 2016). The residues that were exchanged in *L. monocytogenes* GlmM are labelled with blue arrows. (B) Control of CdaA activity by GlmM and the GlmM variants Y153A, F154I and F154A *in vitro*. The reactions were started by adding 10 µM Δ100CdaA, incubated for 1 h at 30°C and stopped by heating for 5 min at 95°C as described previously (Heidemann et al., 2019). The reaction buffer contained 10 mM MnCl.

(C) Growth of the *L. monocytogenes* Δ*glmM* mutant strains synthesizing different GlmM enzymes and effect of GlmM depletion. The strains BPL45 (wild type + empty vector (EV)), BPL63 (Δ*glmM* + *E. coli* $GlmM^{Eco}$), BPL64 (Δ*glmM* + native GlmM), and BPL65 (Δ*glmM* + GlmM F154I) were grown in BHI medium without and with 1 mM IPTG (see *Materials and Methods* section for details). Data points indicate means of replicates. (D) Effect of NaCl on the GlmM-dependent c-di-AMP production in the *L. monocytogenes* strains BPL45 (wild type + empty vector (EV)), BPL63 (Δ*glmM* + *E. coli* $GlmM^{Eco}$), BPL64 (Δ*glmM* + native GlmM), and BPL65 (Δ*glmM* + GlmM F154I). The experiment was carried out as described in the legend to Fig. 6C. Data points represent biologically independent replicates (n = 3). Bars indicate means of replicates and the standard deviations are shown.

FIG 8 Schematic illustration of c-di-AMP signaling in *L. monocytogenes*. c-di-AMP was shown to bind to the sensor kinase KdpD of the KdpDE two-component system, which might be involved in controlling the expression of the putative *kdpABC* potassium transporter genes (Gibhardt et al., 2019). c-di-AMP can be secreted *via* multi drug resistance (MDR) proteins (Woodward et al., 2010; Schwartz et al., 2012).

Figures

Figure 1

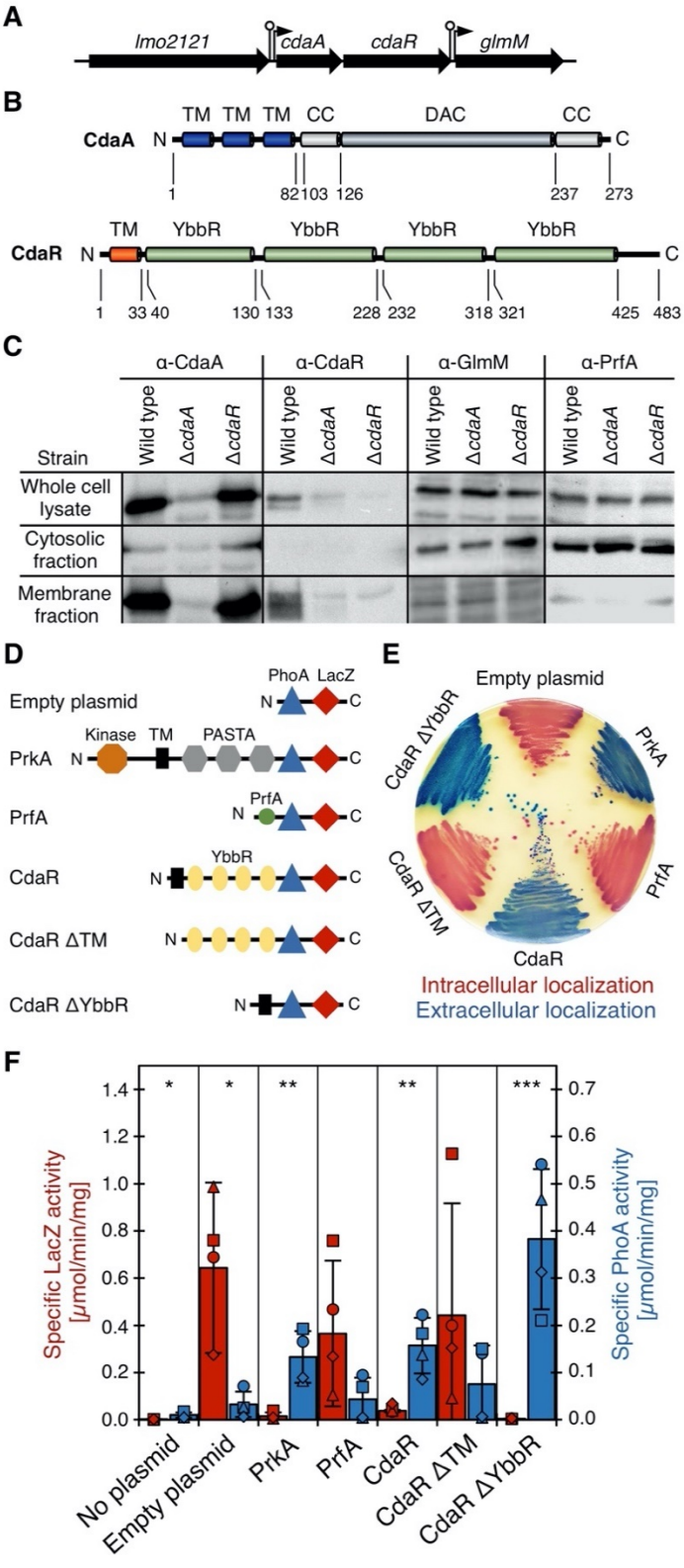

Figure 2

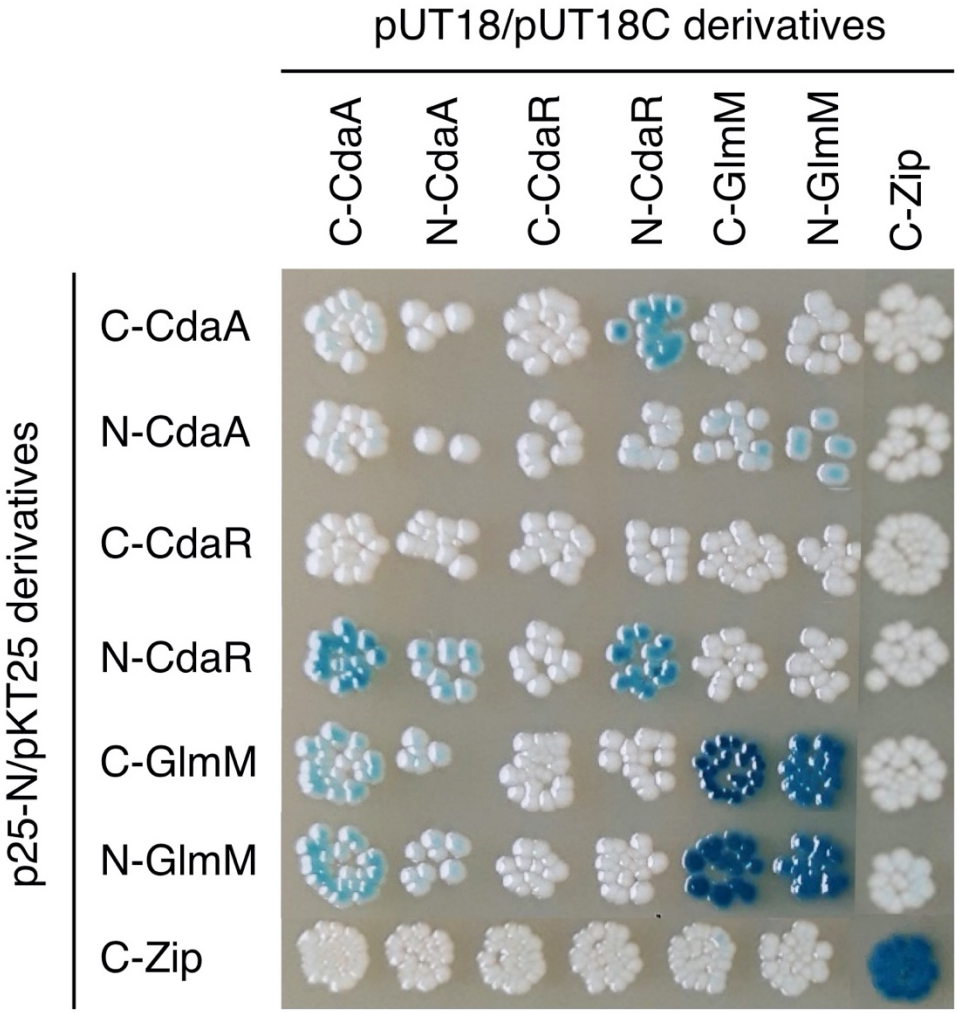
pUT18/pUT18C derivatives
C-CdaA
N-CdaA
C-CdaR
N-CdaR
C-GlmM
N-GlmM
C-Zip
p25-N/pKT25 derivatives
C-CdaA
N-CdaA
C-CdaR
N-CdaR
C-GlmM
N-GlmM
C-Zip

Figure 3

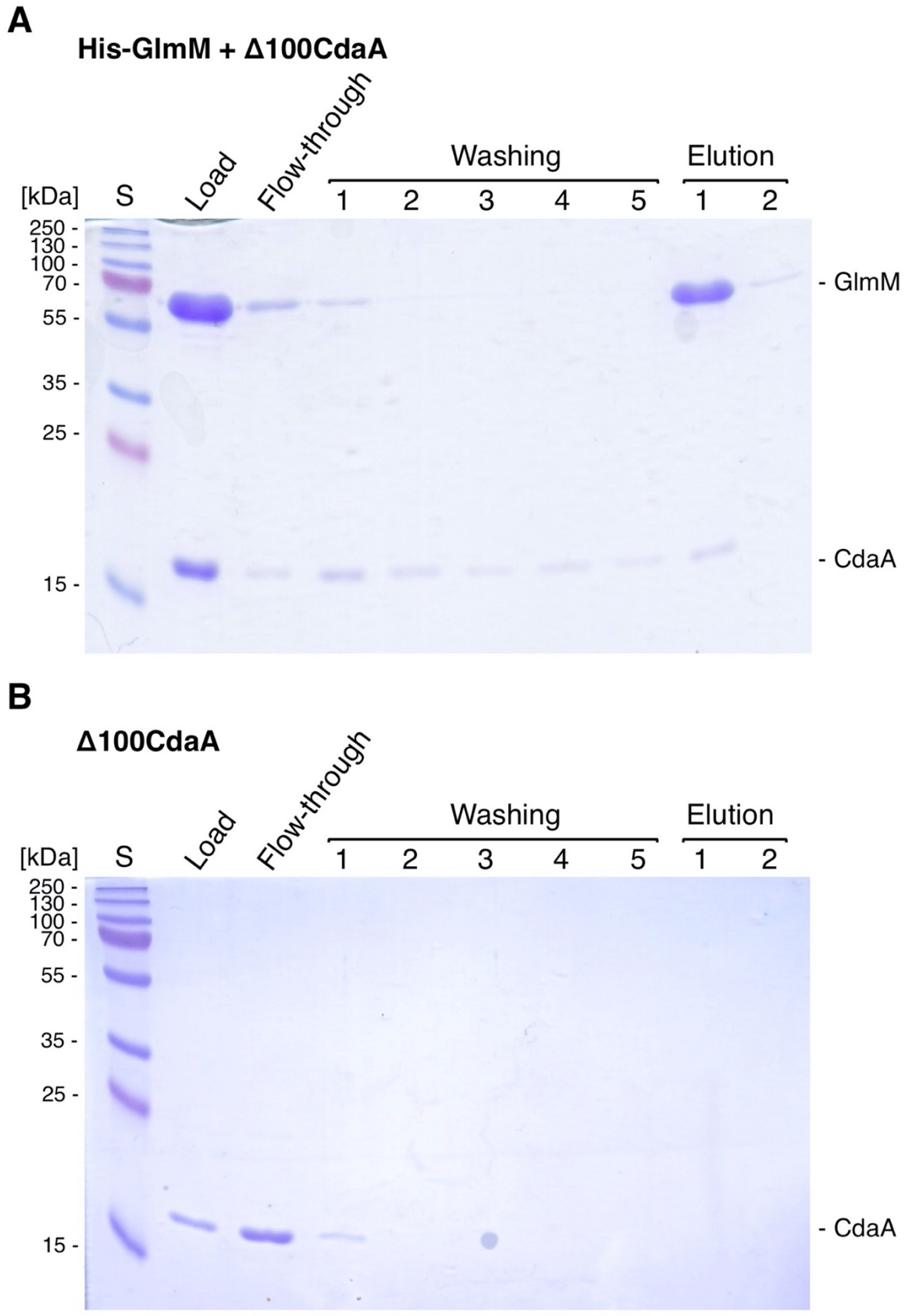
A
His-GlmM + Δ100CdaA
[kDa]
S
Load
Flow-through
Washing
1
2
3
4
5
Elution
1
2
250 -
130 -
100 -
70 -
55 -
35 -
25 -
15 -
- GlmM
- CdaA
B
Δ100CdaA
[kDa]
S
Load
Flow-through
Washing
1
2
3
4
5
Elution
1
2
250 -
130 -
100 -
70 -
55 -
35 -
25 -
15 -
- CdaA

Figure 4

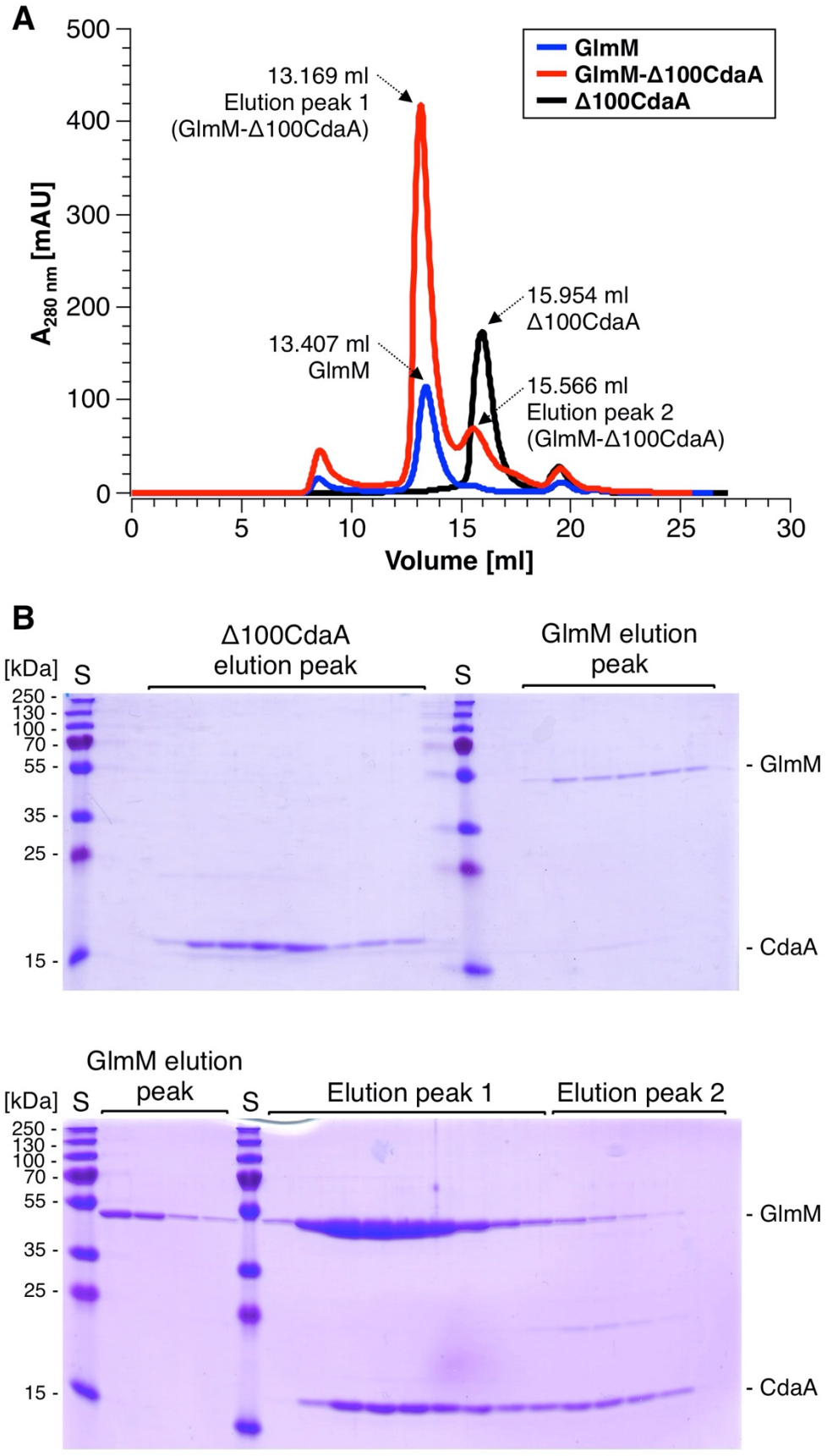
A
GlmM
GlmM-Δ100CdaA
Δ100CdaA
13.169 ml
Elution peak 1
(GlmM-Δ100CdaA)
13.407 ml
GlmM
15.954 ml
Δ100CdaA
15.566 ml
Elution peak 2
(GlmM-Δ100CdaA)
A280 nm [mAU]
Volume [ml]
B
[kDa]
S
Δ100CdaA
elution peak
GlmM elution
peak
- GlmM
- CdaA
Elution peak 1
Elution peak 2

Figure 5

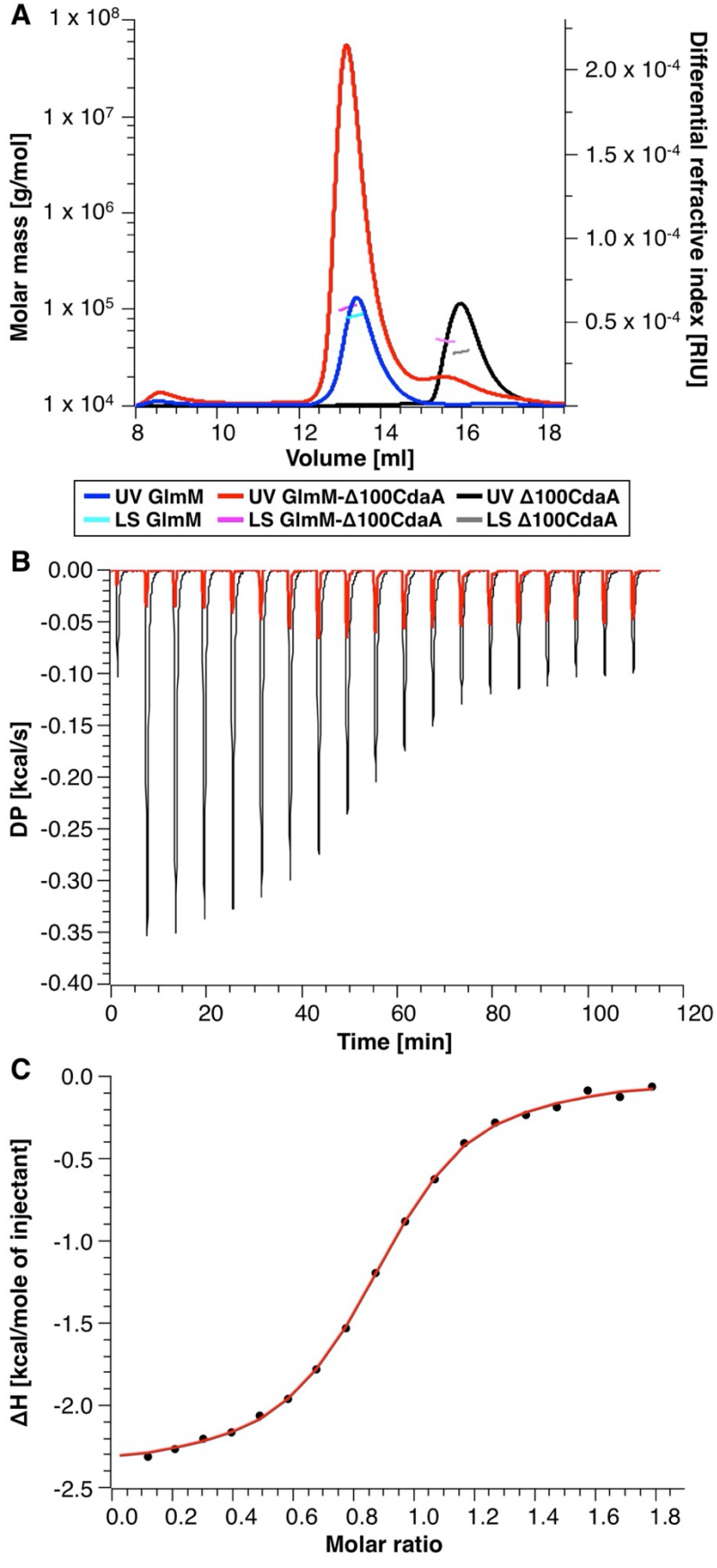
A
Molar mass [g/mol]
Differential refractive index [RIU]
Volume [ml]
UV GlmM
UV GlmM-Δ100CdaA
UV Δ100CdaA
LS GlmM
LS GlmM-Δ100CdaA
LS Δ100CdaA
B
DP [kcal/s]
Time [min]
C
ΔH [kcal/mole of injectant]
Molar ratio

Figure 6

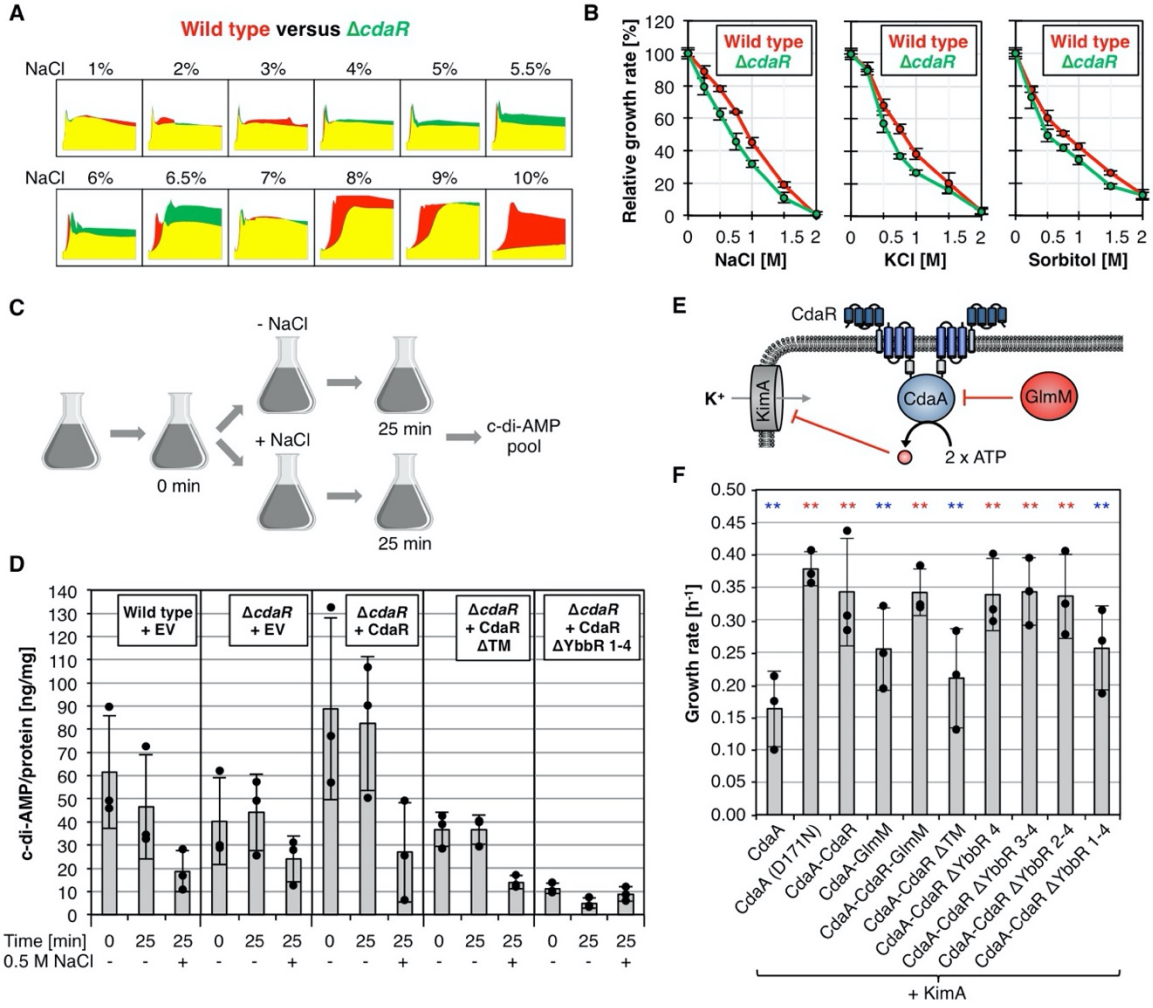
A
Wild type versus ΔcdaR
NaCl 1% 2% 3% 4% 5% 5.5%
NaCl 6% 6.5% 7% 8% 9% 10%
B
Relative growth rate [%]
Wild type ΔcdaR
NaCl [M]
KCl [M]
Sorbitol [M]
C
- NaCl
+ NaCl
0 min
25 min
25 min
c-di-AMP pool
D
c-di-AMP/protein [ng/mg]
Wild type + EV
ΔcdaR + EV
ΔcdaR + CdaR
ΔcdaR + CdaR ΔTM
ΔcdaR + CdaR ΔYbbR 1-4
Time [min]
0.5 M NaCl
E
CdaR
K+
KimA
CdaA
GlmM
2 x ATP
F
Growth rate [h-1]
CdaA
CdaA (D171N)
CdaA-CdaR
CdaA-GlmM
CdaA-CdaR-GlmM
CdaA-CdaR ΔTM
CdaA-CdaR ΔYbbR 4
CdaA-CdaR ΔYbbR 3-4
CdaA-CdaR ΔYbbR 2-4
CdaA-CdaR ΔYbbR 1-4
+ KimA

Figure 7

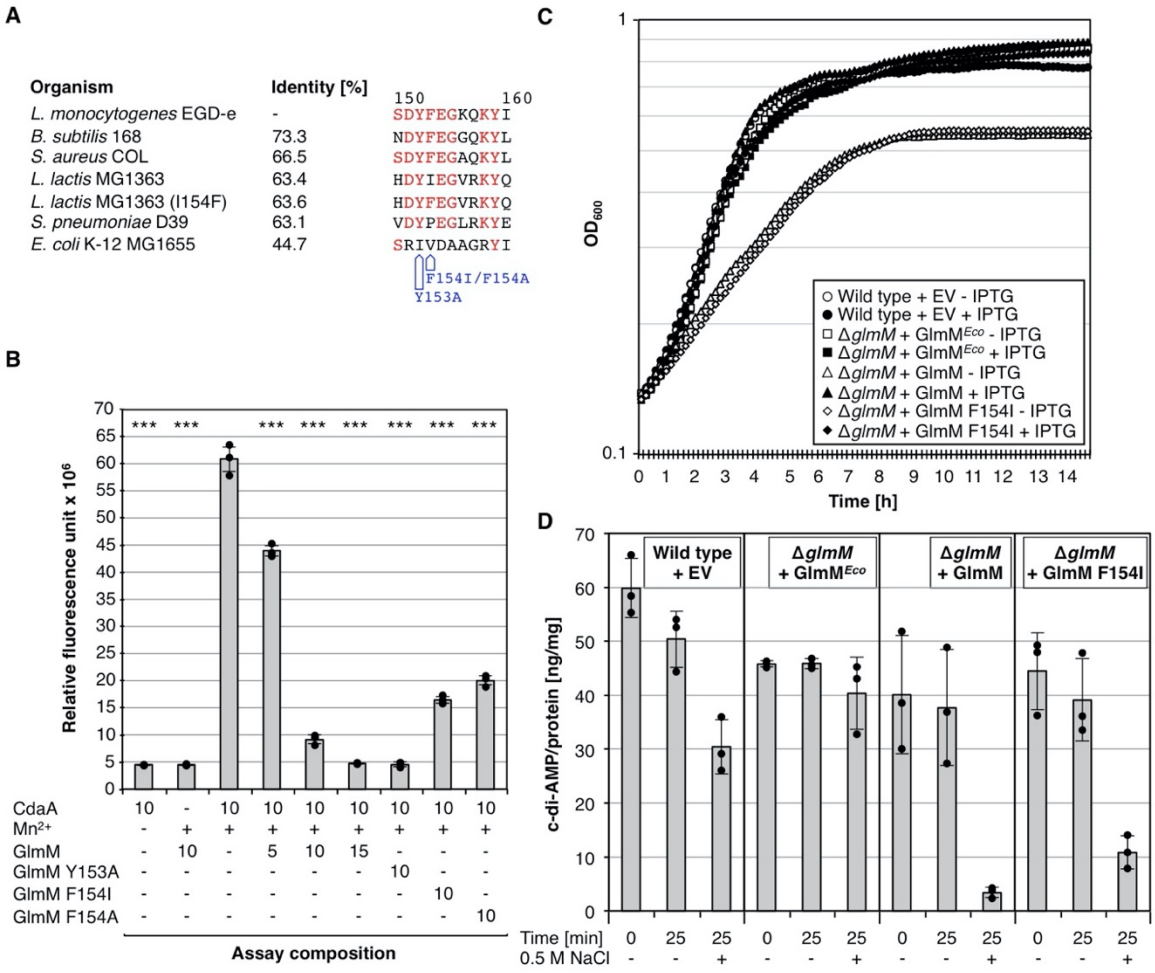

Figure 8

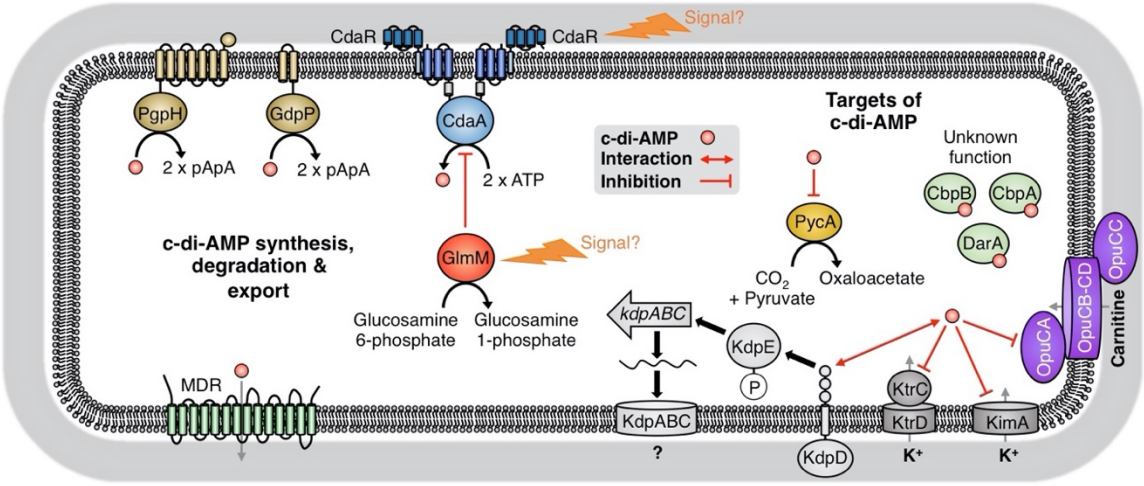

Table 1. Theoretical and calculated masses of the Δ100CdaA, GlmM and of the complex.

Proteins	**Theoretical mass [kDa]**	**Calculated mass [kDa]**
Δ100CdaA-GlmM complex	134.7	105.0 ± 2.18 %
Δ100CdaA dimer	37.8	36.27 ± 1.7 %
GlmM dimer	96.9	85.63 ± 2.072 %

Supporting Information

Additional supporting information may be found in the online version of this article at the publisher's website.

Table S1. Primer

Primer	**Sequence[a] (5' - 3')**	**Plasmid, purpose**
FC146	CGATGCGTTCGCGATCCAGGC	Sequencing
FC147	CCAGCCTGATGCGATTGCTGCAT	Sequencing
FC148	GTCACCCGGATTGCGGCGG	Sequencing
FC150	GATTCGGTGACCGATTACCTGGC	Sequencing
FC334	CCGGTCTCATGGTATGGGTAAATATTTCGG-TACGGATGGAGTTAG	pBP366
FC335	TTTCTCGAGTTAATCGTTAAGTGCCATTTCT-GAACGAACAACCG	pBP366
FC336	AAATCTAGAGATGGGTAAATATTTCGG-TACGGATGGAGTTAG	pBP359-pBP362
FC337	TTTGGTACCCGATCGTTAAGTGCCATTTCT-GAACGAACAACCG	pBP359-pBP362
GlmM_Y153A_F	CCTCGACCAAGTGGTGAAGGGCTTGGGAC-GGTTAGCGATGCTTTTGAAGGTAAAC	GlmM_Y153A
GlmM_Y153A_R	GTTTTAAGTATTGAATATATTTTTGTTTAC-CTTCAAA AGCATCGC	GlmM_Y153A
GlmM_F154A_F	CCTCGACCAAGTGGTGAAGGGCTTGGGAC-GGTTAGCGATTATGCTGAAGGTAAAC	GlmM_F154A
GlmM_F154A_R	GTTTTAAGTATTGAATATATTTTTGTTTAC-CTTCAGCATAATCGC	GlmM_F154A
GlmM_F154I_F	CCTCGACCAAGTGGTGAAGGGCTTGGGAC-GGTTAGCGATTATATTGAAGGTAAAC	GlmM_F154I
GlmM_F154I_R	GTTTTAAGTATTGAATATATTTTTGTTTAC-CTTCAATATAATCGCTAACCG	GlmM_F154I
JH21	AAACCATGGATCGAATTTTAAATAATAAAT-GGTCGATTC	pBP259
JH22	TTTGTCGACTTATGTGCTTTTGGAAGGTACTTCAATGG	pBP255
JH51	AAATCTAGACACGGAGGTGAAGTGATG-GATTTTTCCAATATGTCGATATTGCAT	pBP260-264, pBP387
JH103	TTTCTGCAGTTATGTGCTTTTGGAAGG-TACTTCAATGGATG	pBP260, pBP387
JH104	AAACTGCAGAGAAGGAGAGTAATGAAAT-GGGTAAATATTTCG	pBP388, pBP389
JH105	TTTAAGCTTTTAATCGTTAAGTGCCATTTCT-GAACGAACAAC	pBP388, pBP389
JH121	AAAGGATCCCATGGATCGAATTTTAAATAA-TAAATGGTCGATTCGAAT	pBP250
JH122	TTTGGTACCGCTGTGCTTTT-GGAAGGTACTTCAATGGATGC	pBP250
JH123	AAAGGATCCCATGACGACTTTTTCTACGAC-GTCTTCTAGTGATTC	pBP252
JH124	TTTGGTACCGCGGCGTTATTATTATTT-GCATTAACTGATGTAAAAAGG	pBP251

JH126	AAAGGATCCCATGATGATTGGTAAGCGAT-TAAGCGATCG	pBP253
JH127	TTTGGTACCGCATTTGGATAAGGGACTGTAC-CTTCATCG	pBP253
JH128	TTTGGTACCGCATTTGGATAAGGGACTGTAC-CTTCATCG	pBP254
JH129	TTTGGTACCGCATTTAATTTTCCCCAAGTAGCAG-GACATGC	pBP254
JH130	AAACCATGGCCACGACTTTTT-CTACGACGTCTTCTAG	pBP255
JH131	TTTGTCGACTTAGGCGTTATTATTATTT-GCATTAACTGATGTAAAAAGG	pBP259
JH135	CGTAGAAAAAGTCGTCATCATTCGCTTTT-GCCTCCTTTCCATTTAG	pBP260
JH136	CAAAAGCGAATGATGACGACTTTTT-CTACGACGTCTTCTAGTGATTC	pBP260
JH137	TTTCTGCAGTTAGGCGTTATTATTATTT-GCATTAACTGATGTAAAAAGG	pBP264
JH138	TTTCTGCAGTTAGTTATTTGCTTCAGACTTTT-TTACGGTCTTAATC	pBP261
JH139	TTTCTGCAGTTACTTGCCGACTTTTTCA-ACTGGCACG	pBP262
JH140	TTTCTGCAGTTATTCTTGTACATTTACGTT-GACTGTTGCTGGATTC	pBP263
JR28	TTTGGATCCTTATGTGCTTTTGGAAGGTAC	pBP223
JR56	AAAGAGCTCGAATAATAATAACGCCACGACT TTTTCTACG	pBP223
JR72	AAAGGATCCATGGGTAAATATTTCGGTACG-GATG	pBP369
JR73	TTTCTCGAGTTAATCGTTAAGTGCCATTTCT-GAACG	pBP369
RB1	AAACCATGGGTAAATATTTCGGTACGGAT	pBP1001
RB2	TTTCTGCAG-TTAATCGTTAAGTGCCATTTCTGAACG	pBP1001
RB3	AAACCATGGGTAGTAATCGTAAATATTTCGG-TACCG	pBP1000
RB4	TTTCTGCAGTTAAACGGCTTTTACTGCATCGG	pBP1000
RB5	5'-P-TTGGGACGGTTAGCGATTA-TATTGAAGGTAA ACAAAAATAT	pBP1003
RB6	AAAGAATTCCTTATGTAAAAGCAACAC-TCGAAAGTG	pBP1002
RB7	CGTTAAGTGCCGAGCTCCCTTTTTTAAGA-GAAAATTTCATCTCTCTGC	pBP1002
RB8	CTCTTAAAAAAGGGAGCTCGGCACTTAAC-GATTAAAACAACAAACAAAAAATC	pBP1002
RB9	TTTGGATCCCAAAATACATAA-TAAAGTTCCTGACCATTC	pBP1002

RB10	TTTACCTGGTGTGGAGATAACTCC	*glmM* sequencing
RB11	AAAGATGGTTATCAAGCTGGAACACC	Integration of pBP1002
RB12	TTTTCGTTTTCCACGCTTGATCTGC	Integration of pBP1002

[a]Restriction sites are underlined.

Table S2. Bacterial strains and plasmids

Bacterial strains	**Genotype; construction**	**Reference**
Escherichia coli		
BL21(DE3)	F$^-$ *ompT gal dcm lon hsdS$_B$*($r_B^- m_B^-$) λ(DE3 [*lacI lacUV5-T7p07 ind1 sam7 nin5*]) [*malB*$^+$]$_{K-12}$(λ^S)	Stratagene
BTH101	F$^-$ *cya-99 araD139 galE15 galK16 rpsL1* (*Str^r*) *hsdR2 mcrA1 mcrB1*	Euromedex
DH5α	f80d*lacZ* DM15 *recA1 endA1 gyrA96 relA1 thi-1 hsdR17*($r_k^- m_k^-$) *supE44 deoR* Δ*(lacZYA-argF) U169*	Laboratory collection
LB2003	F$^-$ *aroE rpsL metE thi gal rha kup1* (*trkD1*) Δ*kdpABC5* Δ*trkA aroE*$^+$	(1)
W3110	*F$^-$ λ$^-$ IN(rrnD-rrnE)1 rph-1*	Laboratory collection
Listeria monocytogenes		
EGD-e	Serovar 1/2a strain	Laboratory collection
BPL16	Δ*cdaR attB*::P$_{help}$-*lacO-cdaR lacI neo*	(2)
BPL45	*attB*::P$_{help}$-*lacO*-mcs *lacI neo*; pIMK3 into EGD-e	This study
BPL46	Δ*cdaR attB*::P$_{help}$-*lacO*-mcs *lacI neo*; pIMK3 into LMJR45	This study
BPL47	Δ*cdaR attB*::P$_{help}$-*lacO-cdaR* ΔTM *lacI neo*; pBP255 into LMJR45	This study
BPL51	Δ*cdaR attB*::P$_{help}$-*lacO-cdaR* ΔTM *lacI neo*; pBP259 into LMJR45	This study
BPL60	*attB*::P$_{help}$-*lacO-glmM^{Eco} lacI neo*; pBP1000 into EGD-e	This study
BPL61	*attB*::P$_{help}$-*lacO-glmM lacI neo*; pBP1001 into EGD-e	This study
BPL62	*attB*::P$_{help}$-*lacO-glmM* T460A *lacI neo*; pBP1003 into EGD-e	This study
BPL63	Δ*glmM attB*::P$_{help}$-*lacO-glmM^{Eco} lacI neo*; pBP1002 into BPL60	This study
BPL64	Δ*glmM attB*::P$_{help}$-*lacO-glmM lacI neo*; pBP1002 into BPL61	This study
BPL65	Δ*glmM attB*::P$_{help}$-*lacO-glmM* T460A *lacI neo*; pBP1002 into BPL62	This study
BPL77	Δ*cdaA*	(3)
LMJR45	Δ*cdaR*	(2)
Plasmids	**Construction and purpose**	**Reference**
GlmM_Y153A	*glmM* from plasmid pBP366 with GlmM_Y153A_F/GlmM_Y153A_R as described previously (8); expression of His-GlmM Y153A in *E. coli* BL21(DE)	This study

GlmM_F154A	*glmM* from plasmid pBP366 with GlmM_F154A_F/GlmM_F154A_R as described previously (8); expression of His-GlmM F154A in *E. coli* BL21(DE)	This study
GlmM_F154I	*glmM* from plasmid pBP366 with GlmM_F154I_F/ GlmM_F154I_R as described previously (8); expression of His-GlmM F154I in *E. coli* BL21(DE)	This study
pBAD33	P_{BAD}-*mcs araC cat*; expression of proteins in *E. coli*	(4)
pBP33	Expression of Strep-Δ100CdaA in *E. coli* BL21(DE)	(5)
pBP223	*cdaR* from *L. monocytogenes* EGD-e with JR28/JR56 *via Bam*HI/*Sac*I into pGP172; expression of Strep-CdaR in *E. coli* BL21(DE)	This study
pBP224	*cdaR* from *L. monocytogenes* EGD-e in pUT18	(2)
pBP225	*cdaR* from *L. monocytogenes* EGD-e in pUT18C	(2)
pBP226	*cdaR* from *L. monocytogenes* EGD-e in p25-N	(2)
pBP227	*cdaR* from *L. monocytogenes* EGD-e in pKT25	(2)
pBP232	*cdaA* from *L. monocytogenes* EGD-e in pUT18	(2)
pBP233	*cdaA* from *L. monocytogenes* EGD-e in pUT18C	(2)
pBP234	*cdaA* from *L. monocytogenes* EGD-e in p25-N	(2)
pBP235	*cdaA* from *L. monocytogenes* EGD-e in pKT25	(2)
pBP250	*cdaR* from *L. monocytogenes* EGD-e with JH121/JH122 *via Bam*HI/*Kpn*I into pKTop; expression of CdaR in *E. coli* DH5α	This study
pBP251	*cdaR* Δ*ybbR* from *L. monocytogenes* EGD-e with JH121/JH124 *via Bam*HI/*Kpn*I into pKTop; expression of CdaR ΔYbbR in *E. coli* DH5α	This study
pBP252	*cdaR* ΔTM from *L. monocytogenes* EGD-e with JH123/JH122 *via Bam*HI/*Kpn*I into pKTop; expression of CdaR ΔTM in *E. coli* DH5α	This study
pBP253	*prkA* from *L. monocytogenes* EGD-e with JH126/JH127 *via Bam*HI/*Kpn*I into pKTop; expression of PrkA in *E. coli* DH5α	This study
pBP254	*prfA* from *L. monocytogenes* EGD-e with JH128/JH129 *via Xba*I/*Kpn*I into pKTop; expression of PrfA in *E. coli* DH5α	This study
pBP255	*cdaR* ΔTM from *L. monocytogenes* EGD-e with JH130/JH22 *via Nco*I/*Sal*I into pIMK3; expression of CdaR ΔTM in *L. monocytogenes*	This study
pBP259	*cdaR* ΔYbbR 1-4 from *L. monocytogenes* EGD-e with JH21/JH131 *via Nco*I/*Sal*I into pIMK3; expression of CdaR ΔYbbR 1-4 in *L. monocytogenes*	This study
pBP260	*cdaA-cdaR* ΔTM from *L. monocytogenes* with JH51/JH135 and JH136/JH103 *via Xba*I/*Pst*I into pBAD33; expression of CdaA and CdaR ΔTM in *E. coli* LB2003	This study

pBP261	*cdaA-cdaR* ΔYbbR 4 from *L. monocytogenes* with JH51/JH138 *via Xba*I/*Pst*I into pBAD33; expression of CdaA and CdaR ΔYbbR 4 in *E. coli* LB2003	This study
pBP262	*cdaA-cdaR* ΔYbbR 3-4 from *L. monocytogenes* with JH51/JH139 *via Xba*I/*Pst*I into pBAD33; expression of CdaA and CdaR ΔYbbR 3-4 in *E. coli* LB2003	This study
pBP263	*cdaA-cdaR* ΔYbbR 2-4 from *L. monocytogenes* with JH51/JH140 *via Xba*I/*Pst*I into pBAD33; expression of CdaA and CdaR ΔYbbR 2-4 in *E. coli* LB2003	This study
pBP264	*cdaA-cdaR* ΔYbbR 1-4 from *L. monocytogenes* with JH51/JH137 *via Xba*I/*Pst*I into pBAD33; expression of CdaA and CdaR ΔYbbR 1-4 in *E. coli* LB2003	This study
pBP359	*glmM* from *L. monocytogenes* EGD-e with FC336/FC337 *via Xba*I/*Kpn*I into pUT18; B2H analysis	This study
pBP360	*glmM* from *L. monocytogenes* EGD-e with FC336/FC337 *via Xba*I/*Kpn*I into pUT18C; B2H analysis	This study
pBP361	*glmM* from *L. monocytogenes* EGD-e with FC336/FC337 *via Xba*I/*Kpn*I into p25-N; B2H analysis	This study
pBP362	*glmM* from *L. monocytogenes* EGD-e with FC336/FC337 *via Xba*I/*Kpn*I into pKT25; B2H analysis	This study
pBP366	*glmM* from *L. monocytogenes* with FC334/FC335 *via Bsa*I/*Xho*I into pET SUMOadapt	This study
pBP369	*glmM* from *L. monocytogenes* with JR72/JR73 *via Bam*HI/*Xho*I into pGEX-6P1	This study
pBP370	Expression of CdaA in *E. coli* LB2003	(3)
pBP373	Expression of CdaA D171N in *E. coli* LB2003	(3)
pBP384	Expression of KimA in *L. monocytogenes*	(3)
pBP387	*cdaAR* from *L. monocytogenes* with JH51/JH103 *via Xba*I/*Pst*I into pBAD33; expression of CdaAR in *E. coli* LB2003	This study
pBP388	*glmM* from *L. monocytogenes* with JH104/JH105 *via Hind*III/*Pst*I into pBP387; expression of CdaAR-GlmM in *E. coli* LB2003	This study
pBP389	*glmM* from *L. monocytogenes* with JH104/JH105 *via Hind*III/*Pst*I into pBP370; expression of CdaA-GlmM in *E. coli* LB2003	This study
pBP1000	*glmM* from *E. coli* W3110 with RB3/RB4 *via Pst*I/*Nco*I into pIMK3; expression of GlmM in *L. monocytogenes*	This study

pBP1001	*glmM* from *L. monocytogenes EGD-e* with RB1/RB2 *via Pst*I/*Nco*I into pIMK3; expression of GlmM in *L. monocytogenes*	This study
pBP1002	Up- and downstream fragments of *glmM* with RB6/RB7 and RB8/RB9 *via Eco*RI/*Bam*HI into pMAD; deletion of *glmM* in *L. monocytogenes*	This study
pBP1003	*glmM* T460A from *L. monocytogenes EGD-e* with RB1/RB2/RB5 *via Pst*I/*Nco*I into pIMK3; expression of GlmM F154I in *L. monocytogenes*	This study
pET SUMOadapt	P_{T7}-*lacO* 6x His SUMO thrombin site mcs *aphA3*	(7)
pGEX-6P-1	P_{lac}-*lacO bla*; expression of GST-tagged proteins in *E. coli* BL21(DE)	GE Healthcare
pGEXpBP33	Expression of GST-tagged Δ100CdaA in *E. coli* BL21(DE)	(8)
pGP172	P_{T7}-mcs *bla*; expression of N-terminally Strep-tagged proteins in *E. coli* BL21(DE)	(9)
pIMK3	P_{help}-*lacO*-mcs *lacI neo*; expression of proteins in *L. monocytogenes*	(10)
pKT25	P_{lac}-*cyaT25*-mcs *aphA3*; protein-protein interaction analysis, B2H assay	(11)
pKT25-zip	P_{lac}-*cyaT25*-yeast GCN4 leucine zipper *aphA3*; protein-protein interaction analysis, B2H assay	(11)
pKTop	P_{lac}-mcs-$phoA_{66\text{-}1416}$-$lacZ_{12\text{-}180}$ *aphA3*; topology analysis of membrane proteins	(12)
pMAD	*bla ermC bgaB*; construction of *L. monocytogenes* mutant strains	(13)
p25-N	P_{lac}-mcs-*cyaT25 aphA3*; Protein-protein interaction analysis, B2H assay	(14)
pUT18	P_{lac}-mcs-*cyaT18 bla*; protein-protein interaction analysis, B2H assay	(11)
pUT18C	P_{lac}-*cyaT18*-mcs *bla*; protein-protein interaction analysis, B2H assay	(11)
pUT18C-zip	P_{lac}-*cyaT18*-yeast GCN4 leucine zipper *bla*; protein-protein interaction analysis, B2H assay	(11)

References

(1) **Stumpe S, Bakker, EB.** 1997 Requirement of a large K+-uptake capacity and of extracytoplasmic protease activity for protamine resistance of *Escherichia coli*. Arch Microbiol. 167:126-136.

(2) **Rismondo J, Gibhardt J, Rosenberg J, Kaever V, Halbedel S, Commichau FM.** 2016. Phenotypes associated with the essential diadenylate cyclase CdaA and its potential regulator CdaR in the human pathogen *Listeria monocytogenes*. J Bacteriol 198:416-426.

(3) **Gibhardt J, Hoffmann G, Turdiev A, Wang M, Lee VT, Commichau FM.** 2019. c-di-AMP assists osmoadaptation by regulating the *Listeria monocytogenes* potassium transporters KimA and KtrCD. J Biol Chem. 294: 16020-16033.

(4) **Guzman LM, Belin D, Carson MJ, Beckwith J.** 1995. Tight regulation, modulation, and high level expression by vectors containing the arabinose pBAD promoter. J Bacteriol 177:4121-4130.

(5) **Rosenberg J, Dickmanns A, Neumann P, Gunka K, Arens J, Kaever V, Stülke J, Ficner R, Commichau FM.** 2015. Structural and biochemical analysis of the essential diadenylate cyclase CdaA from *Listeria monocytogenes*. J Biol Chem 290:6596-6606.

(6) **Quintana IM, Gibhardt J, Turdiev A, Hammer E, Commichau FM, Lee VT, Magni C, Stülke J.** 2019. The KupA and KupB proteins of *Lactococcus lactis* IL1403 are novel c-di-AMP receptor proteins responsible for potassium uptake. J Bacteriol 201: pii: e00028-19.

(7) **Mossessova E, Lima CD.** 2000. Ulp1-SUMO crystal structure and genetic analysis reveal conserved interactions and a regulatory element for cell growth in yeast. Mol Cell 5:865-876.

(8) **Heidemann JL, Neumann P, Dickmanns A, Ficner R.** 2019. Crystal structures of the c-di-AMP-synthesizing enzyme CdaA. J Biol Chem 294:10463-10470.

(9) **Merzbacher M, Detsch C, Hillen W, Stülke J.** 2004. *Mycoplasma pneumoniae* HPr kinase/phosphorylase. Eur J Biochem 271:367-374.

(10) **Monk IR, Gahan CGM, Hill C.** 2008. Tools for functional postgenomic analysis of *Listeria monocytogenes*. Appl Environ Microbiol 74:3921-3934.

(11) **Karimova G, Pidoux J, Ullmann A, Ladant D.** 1998. A bacterial two-hybrid system based on a reconstituted signal transduction pathway. Proc Natl Acad Sci USA 95:5752-5756.

(12) **Karimova G, Robichon C, Ladant D.** 2009. Characterization of YmgF, a 72-residue inner membrane protein that associates with the *Escherichia coli* cell division machinery. J Bacteriol 191:333-346.

(13) **Arnaud M, Chastanet A, Débarbouillé M.** 2004. New vector for efficient allelic replacement in naturally transformable, low-GC content, gram-positive bacteria. Appl. Environ Microbiol 70:6887-6891.

(14) **Claessen D, Emmins R, Hamoen LW, Daniel RA, Errington J, Edwards DH.** 2008 Control of the cell elongation-division cycle by shuttling PBP1 protein in *Bacillus subtilis*. Mol Microbiol. 68:1029-1046.

Table S3. Parameters used for the ITC titration series

Injection no.	Injection volume [µl]	Injection duration [sec]	Spacing [sec]	Filter period [sec]
1	5	10	360	2
2-19	15	30	360	2

Chapter 4: Crystal structures of DarB reveal a novel c-di-AMP binding mode of CBS domains

This manuscript in preparation

Crystal structures of DarB reveal a novel c-di-AMP binding mode of CBS domains

Jana L. Heidemann[1], Piotr Neumann[1], Larissa Krüger[2], Jörg Stülke[2] and Ralf Ficner[1*]

[1]Department of Molecular Structural Biology, Institute for Microbiology and Genetics, GZMB, University of Goettingen, 37077 Göttingen, Germany
[2]Department of General Microbiology, Institute for Microbiology and Genetics, University of Goettingen, 37077 Göttingen, Germany

* To whom correspondence should be addressed: Ralf Ficner, Department of Molecular Structural Biology, Institute for Microbiology and Genetics, Georg-August-University Goettingen, 37077 Goettingen, Germany; rficner@uni-goettingen.de; Tel. +49 551 3914072

Authors contribution

J.L.H.: data curation; formal analysis; validation; writing-original draft; writing review and editing

P.N.: formal analysis; validation; writing-original draft; writing review and editing

L.K.: plasmid construction and protein purification

A. D.: draft editing

J.S.: draft editing

R. F.: formal analysis; validation; writing-original draft; writing review and editing; conceptualization; funding acquisition.

Crystal structures of DarB reveal a novel c-di-AMP binding mode of CBS domains

Jana L. Heidemann[1], Piotr Neumann[1], Larissa Krüger[2], Achim Dickmanns[1], Jörg Stülke[2], Ralf Ficner[1*]

[1]Department of Molecular Structural Biology, Institute for Microbiology & Genetics, GZMB, Georg-August-University Göttingen, 37077 Göttingen, Germany

[2]Department of General Microbiology, Institute for Microbiology & Genetics, GZMB, Georg-August-University Göttingen, 37077 Göttingen, Germany

* To whom correspondence should be addressed: Ralf Ficner, Department of Molecular Structural Biology, Institute for Microbiology and Genetics, Georg-August-University Göttingen, 37077 Göttingen, rficner@uni-goettingen.de; Tel. +49 551 3914072

Running title: c-di-AMP binding by the CBS protein DarB

Keywords: second messenger, X-ray crystallography, cystathionine β–synthase (CBS) domain

4.1 Abstract

The second messenger c-di-AMP is importantly involved in a plethora of different cellular functions mainly in regulating the bacterial osmolyte homeostasis. Over the years diverse c-di-AMP binding proteins were identified like RCK_C domains, USP-like domains or CBS domains. Here we report crystal structures of the CBS domain containing protein DarB in its apo-state and in complex with either c-di-AMP, 3'3'cGAMP and AMP. We suggest a specific binding of c-di-AMP to DarB and a putative regulatory function of DarB which is most likely mediated directly through the bound c-di-AMP.

4.2 Introduction

The cystathionine β–synthase (CBS) domain is a small protein motif consisting of ca. 60 amino acids. It was first identified in several archaeal proteins and the name-giving human cystathionine β–synthase (Bateman 1997). Up to now it was found in all kingdoms of life in a plethora of proteins that exhibit a large variety of functions (Baykov et al. 2011; Ereño-Orbea et al. 2013). Some of these proteins consist only of CBS domains, while in many other proteins the CBS domains are fused to other domains. Many CBS domains possess regulatory function of

enzymes and membrane transporters which depends on a ligand bound to the CBS domain (Anashkin et al. 2017). Most CBS domains are known to bind AMP or ATP, other adenosine derivatives like NADH and SAM or the even larger cyclic di-AMP (c-di-AMP) (Schuster et al. 2016; Huynh et al. 2017). c-di-AMP is a bacterial second messenger involved in many cellular processes as it binds to several different proteins as well as to RNA riboswitches (for review sew (Corrigan R. M. and Gründling 2013; Commichau et al. 2015a). c-di-AMP is the only second messenger in bacteria known to be essential, since it regulates the activity of proteins required for potassium and osmolyte homeostasis (for review see (Commichau et al. 2017)) It was reported previously that binding of c-di-AMP to the RCK_C domains of potassium ion transporters blocks potassium import (Corrigan et al. 2013; Bai et al. 2014; Kim et al. 2015). This nucleotide based second messenger does not only bind to RCK_C domains, but also to other receptors, e.g. PII-like signal transduction protein (Gundlach et al. 2015b), KupA/B (Quintana et al. 2019), USP-like domains (Moscoso et al. 2016) and CBS domains (Sureka et al. 2014). Binding of c-di-AMP to the CBS domains of the carnitine transporter OpuC leads to an inhibition of the carnitine uptake (Schuster et al. 2016; Huynh et al. 2017). The Mg^{2+} transporter MgtE is another CBS domain protein, which binds c-di-AMP and is also involved in osmolyte transport (Gundlach et al. 2019).

All CBS domains share the same topology ($\beta_1-\alpha_1-\beta_2-\beta_3-\alpha_2$), but they often display only low sequence conservation within protein families, or even within one protein. The first two of the three β-strands are in a parallel orientation, while the third one is in an antiparallel orientation relative to the first two. The β-strands β2 and β3 are flanked by two α-helices (α1 and α2). Usually, CBS domains occur as tandem repeats associated in the form of a Bateman module or a CSB pair (for review see (Baykov et al. 2011; Ereño-Orbea et al. 2013)) . This association is often stabilized by the region positioned N-terminally to the conserved CBS motif containing a third α-helix (α0) which clamps the two CBS domains in a tandem repeat. There are three different types of homodimers formed by CBS domains, classified as parallel (head-to-head assembly), antiparallel (head-to-tail assembly) and V-shaped. The head-to-head assembly represents the most common assembly (Ereño-Orbea et al. 2013) which exhibits as the heat-to-tail assembly with a disk-like shape containing four CBS domains related by an internal D_2 pseudo-symmetry (the so-called CBS module). The tandem repeat of two CBS domains contains two canonical adenosine binding sites, hence, a dimeric protein with four CBS domains could bind up to four adenosine derivatives.

Recently, the protein DarB (previously denoted as YkuL) was identified as c-di-AMP binding protein in *B. subtilis* (Gundlach et al. 2019). DarB consists of 147 amino acids, and comprises two CBS domains, but no other domains. The cellular function of DarB is so far unknown. Here we demonstrate that DarB specifically binds c-di-AMP with a dissociation constant in the

nano-molar range, and AMP with much lower affinity. DarB also binds 3´3´cGAMP *in vitro*, however, as cGAMP does not exist in *B. subtilis*, this interaction might have no physiological relevance. In order to understand the specificity and affinity for different ligands, we determined four crystal structures of DarB (YkuL) in its apo from and its ligand bound form either with c-di-AMP, 3´3´cGAMP, or AMP, respectively. The four CBS domains of the homo-dimeric DarB bind two molecules of c-di-AMP, however, only one adenine of each c-di-AMP is specifically recognized by DarB, while the remaining adenines protrude out of the donut-like protein. No conformational changes occur in DarB upon c-di-AMP binding, hence, a putative regulatory function of DarB must directly be caused by the bound c-di-AMP, most likely by the protruding adenine.

4.3 Results

4.3.1 Nucleotide Binding and Specificity of DarB

The CBS domain containing protein DarB from *B. subtilis*, a protein of unknown function and previously denoted as YkuL, was recently identified as c-di-AMP binding protein (Gundlach et al. 2019). Since CBS domains are known to bind a plethora of adenine-containing nucleotides, ITC measurements with different mono- and di-nucleotides were performed. The results confirmed the tight binding of c-di-AMP with a K_d in the nM range (27.0 nM ± 1.98 nM) (Figure 1). No binding was detected for 2´3´cGAMP, c-di-GMP, ATP, SAM, NAD^+ and co-enzyme A (Figure S1). Interestingly, 3´3´cGAMP binds to DarB with a K_d in the low µM range (1.17 µM ± 0,97 nM), and also a weak interaction with AMP was observed (Figure 1 and S1. The direct comparison of binding constants between 3´3´cGAMP and c-di-AMP shows that DarB binds the cyclic homo-di-nucleotide with an approximately 40-fold higher affinity than the cyclic hetero-di-nucleotide. However, since 3´3´cGAMP is absent in *B. subtilis*, the binding to DarB is of no physiological relevance.

4.3.2 Overall structure of the c-di-AMP binding protein DarB

DarB was crystallized in the space group $P2_12_12_1$ with two DarB molecules occupying the asymmetric unit. The crystal structure of the ligand free DarB (apo-DarB) was determined at 1.84 Å resolution (Table 1) and superposes well with the deposited but unpublished structure of DarB/YkuL (PDB id:1YAV), as indicated by the root mean square deviation (r.m.s.d.) of 0.533 Å between all Cα atoms. The previously deposited structure of DarB has a bound sulfate ion and is represents a different crystal form.

The DarB monomer occurs as a tandem repeat composed of two CBS domains (CBS1 and CBS2), each possessing the canonical βαββα fold, and an N-terminal region that contains a short α-helix, and in case of CBS1 also a short β-strand (Figure 2A). The N-terminal region preceding the CBS1 spans over the two CBS domains and clamps them together, as the N-terminus of the polypeptide chain is close to the C-terminus of the CBS2. The N-terminal short β-strand (β0) of CBS1 packs against β-strand β6 of CBS2, extends the β-sheet of CBS2 as fourth strand and thereby stabilizing the arrangement of the two CBS domains. The core of the protein is formed by the β-sheets of CBS1 and CBS2. These two β-sheets are oriented parallel to each other and are flanked on each side by the α-helices (blue). Like the N-terminal region, the linker connecting CBS1 and CBS2 also contains an α-helix (α0-1) followed by the canonical CBS fold of CBS2 (β4-α4-β5-β6-α5).

The two molecules in the asymmetric unit form a donut-shaped homodimer related by a two-fold non-crystallographic symmetry. The dimer interface buries 1402.8 Å of the accessible surface area (17.5 %) and is stabilized by 7 hydrogen bonds between α-helices 1 and 1' as well as α-helices 4 and 4'. According to the CBS protein classification DarB forms a dimer in a parallel head-to-head assembly (Figure 2B). The donut shaped DarB dimer has a rather negatively charged outer surface, while the surface of the central pore is positively charged (Figure 2C).

4.3.3 Structure of DarB_c-di-AMP complex

DarB was also crystallized in presence of nucleotides that were identified by ITC measurements to bind to DarB (see above). First, DarB was crystallized in presence of c-di-AMP. The obtained crystals belong to the same space group as the ligand-free DarB crystals but differ slightly in unit cell dimensions. The structure of the c-di-AMP - DarB complex was determined at 1.7 Å resolution (Table 1). The two DarB molecules in the asymmetric unit form the donut-shaped dimer like the apo DarB. Upon rigid body refinement using the apo DarB structure as the model, the difference electron density map clearly revealed the presence of two c-di-AMP molecules bound inside the DarB dimer (Figure S2).

The nucleotide binding site is formed by the loop region connecting α1 and β2 as well as β-strand 2 of CBS1, α-helix 4 and β-strands 5 and 6 of CBS2 and α-helix 4 of the CBS2 of the opposite monomer (B) (Figure 3A). Residues Lys^{23}, Ala^{25}, Tyr^{45}, Thr^{46}, Ala^{47}, Arg^{132} of monomer A, and $Arg^{131'}$ of monomer B are involved in c-di-AMP binding (Figure 3B). The N6 of the adenine-1 (Ade1) forms a hydrogen bond to the main chain carbonyl O atom of Lys^{23}, and N1 to the main backbone N atom of Ala^{25}. Furthermore, Tyr^{45} positioned in the loop α1-β2 stacks against the adenine by π–π in an almost coplanar orientation. Surprisingly, the second

adenine (Ade2) does not show any direct interactions with the protein. It protrudes from the protein ring and is surrounded by several water molecules, of which two are mediating contacts between adenine-2 and the protein. The 2′-OH of the ribose attached to Ade1 is hydrogen bonded to the carbonyl O atom of Ala^{47}. The 2′-OH and the 3′-OH of the second ribose (adenosine-2) form hydrogen bonds to side chain of $Arg^{131'}$ of the other monomer. The phosphate of adenosine-1 forms hydrogen bonds with the main chain N of Arg^{132}, while the phosphate of adenosine-2 forms two hydrogen bonds with the side chain OH and the main chain amide of Thr^{46}.

The structure of the DarB_c-di-AMP complex superposes well with the ligand-free structure and the DarB structure with bound sulfate (PDB code: 1YAV), as indicated by the r.m.s.d. between all Cα atoms of 0.57 Å and 0.53 Å, respectively. Hence, binding of c-di-AMP does not induce any major conformational changes in DarB. Some minor structural changes occur in the central pore of the protein dimer. In the ligand-free state, the central pore of the donut is constricted in comparison to the c-di-AMP-bound state. This structural change is due to a movement of the loop connecting α1 and β2 which leads to a repositioning of Thr^{46}. Upon c-di-AMP binding this loop becomes less flexible as Thr^{46} forms a hydrogen bond with the phosphate of the ligand and is therefore fixed in its position. Another difference between apo and ligand-bound state concerns the side chain of Tyr^{45} which is disordered in the ligand-free state. When c-di-AMP is bound Tyr^{45} is caught in one conformation by the π–π stacking interaction with the adenine base.

4.3.4 Structure of DarB_AMP complex

Since the ITC experiments showed also a weak binding of AMP to DarB, crystallization trials of DarB in presence of AMP were performed. The obtained crystals diffracted to a resolution of 1.64 Å and belonged to the same space group as observed for the DarB-c-di-AMP and apo-DarB structures. The difference electron density maps demonstrate two AMP molecules bound in the position corresponding to the two adenosine-1 moieties in the c-di-AMP complex structure (Figure S3).

Hence, the protein-AMP contacts are the same as for the corresponding AMP of c-di-AMP (Figure 4). The comparison of the two nucleotide binding sites in the DarB-AMP complex unveiled that in one of the monomers the side chain of Arg^{132} binds the phosphate of AMP, while in the other monomer $Arg^{132'}$ is rotated outwards of the binding pocket and forms a salt bridge with the Asp^{9} of a symmetry-related protein molecule leading to the loss of the contact with AMP phosphate.

4.3.5 Structure of DarB_3′3′cGAMP complex

In addition, the ITC experiments revealed that the hetero dinucleotide 3′3′cGAMP is also bound by DarB, but not the related 2′3′cGAMP. The DarB crystals obtained in presence of 3′3′cGAMP belong also to the space group $P2_12_12_1$ and contain two protein monomers in the asymmetric unit as described for DarB in complex with c-di-AMP. The crystal structure was determined at 1.5 Å resolution, and the difference electron densities showed the presence of two 3′3′cGAMP molecules bound similar as described for c-di-AMP (Figure S4). The binding of the adenine in 3′3′cGAMP is identical to that of Ade1 of c-di-AMP, while the guanine is protruding out of the protein ring like the Ade2 in the c-di-AMP complex. Surprisingly, the difference electron density maps indicated the presence of two additional 3′3′cGAMP molecules adjacent to one of the two canonically bound 3′3′cGAMP, here denoted as cGAMP-2 (Figure S4). The third 3′3′cGAMP (cGAMP-3) molecule binds to cGAMP-2 by π–π stacking interaction between the guanines, hydrogen bonds between the guanine NH2 group of cGAMP-3 with a phosphate of cGAMP-2, and *vice versa* between the guanine NH2 group of cGAMP-2 with a phosphate of cGAMP-3, and between the guanine N1 of c-GAMP-3 and the Tyr45 OH group. The fourth 3′3′cGAMP molecule (cGAMP-4) is also bound by π–π stacking interaction of its adenine with the guanine of cGAMP-2, hence the guanine of cGAMP-2 is sandwiched between the guanine of cGAMP-3 and the adenine of cGAMP-4 (Figure 5). cGAMP-4 is also bound by several hydrogen bonds to the protein, between the phosphates and the side chains of Lys^{23}, Lys^{136}, Arg^{132}, and between the guanine and the main chain carbonyl O of Phe^{17} and Met^{18}.

Notably, the weaker electron density for cGAMP-3 and cGAMP-4 corresponds to a lower occupancy of 58 % and 59 %, respectively, meaning that a third and fourth 3′3′cGAMP is bound to only ca. 60 % of the DarB molecules in the crystal. These additional 3′3′cGAMP molecules are not involved in crystal contacts with neighboring protein molecules, hence, their binding is most likely not a crystallization artefact. However, the additional 3′3′cGAMP molecules are only found on one side of the donut shaped DarB dimer. On the other side the corresponding binding sites for the additional 3′3′cGAMP molecules are partially occupied by a neighboring protein molecule.

4.4 Experimental procedures

4.4.1 Plasmid construction

The selected gene *darB* was amplified using chromosomal DNA of *B. subtilis 168* as template and appropriate nucleotides that attached BsaI and XhoI restriction sites to the fragments and cloned between the BsaI and XhoI sites of the expression vector pET-SUMOadapt. The resulting plasmid was pGP2972.

4.4.2 Protein expression and purification

E. coli Rosetta (DE3) was transformed with the plasmid pGP2972 encoding 6x-His-SUMO-DarB. Expression of the recombinant proteins was induced by the addition of isopropyl 1-thio-β-D-galactopyranoside (final concentration, 1 mM) to exponentially growing cultures (A_{600} of 0.8) of *E. coli* carrying the relevant plasmid. Cells were lysed by three passes at 18,000 p.s.i. through an HTU DIGI-F press (G. Heinemann, Germany). After lysis (50 mM Tris/HCl pH 7.5, 150 mM NaCl), the crude extract was centrifuged at 100,000 xg for 60 min and then passed over a Ni^{2+}-nitrilotriacetic acid column (IBA, Germany). The protein was eluted with an imidazole gradient. After elution, the fractions were tested for the desired protein using 15 % SDS-PAGE. The relevant fractions were combined, and the SUMO tag was removed with the SUMO protease while overnight dialysis. The cleaved SUMO moiety and the protease were removed using a Ni^{2+}-nitrilotriacetic acid column. The protein concentration was determined according to the method of Bradford (Bradford 1976) using the Bio-Rad dye binding assay and bovine serum albumin as standard (BioRad, Germany).

4.4.3 Isothermal Calorimetry (ITC)

All ITC experiments were performed on a VP-ITC microcalorimeter (MicroCal Inc., Northampton, MA, USA). Prior the ITC measurements the buffer of the protein solution was exchanged using the "Zaba" spin desalting columns (Thermo Scientific) to 50 mM Tris/HCl pH 7.5, 200 mM NaCl. The nucleotides were individually dissolved in the exact same buffer (c-di-AMP, c-di-GMP, 3′3′c-GMP-AMP, 2′3′c-GMP-AMP, AMP, NADH, SAM, Co-A and ATP). Measurements were carried out with 10 µM DarB in the sample cell and 100 µM nucleotide in the titration syringe. All experiments were carried out at 20 °C and a stirring speed of 307 rpm. All parameters for the titration series are given in Tab.3. The data analysis was carried

out using the MicroCal PEQ-ITC Analysis, Malvern Panalytical software. The protein and ligand concentration were determined by using either the Bradford assay (Bradford 1976) or a Nanodrop spectrophotometer (NANODROP 2000 Spectrometer, Thermo Scientific).

4.4.4 Crystallization and Cryoprotection

The sitting-drop vapour diffusion method was applied for crystallization. The initial crystallization trials were performed at 20 °C using the protein at a concentration of 4.0 mg/ml. For crystallizing the DarB apo the initial droplet size (0.25µM; 1:1 ratio) was increased to 2 µl using a 1:1 protein-to-reservoir ratio. Rectangular shaped crystals grew over night in 0.2 M calcium acetate, 0.1 M MES pH 6.5, 15 % w/v polyethylene glycol 8000. For crystallization of DarB c-di-AMP complex the protein was supplemented with a 6-fold excess of ligand (Jena Bioscience, Germany). The best diffracting crystals grew after approximately 24 hours in 0.2 M calcium chloride dehydrate, 0.05 M HEPES sodium pH 7.5, 28 % v/v polyethylene glycol 400 and 0.002 M spermine (Hampton Research, USA) in a 1:1 ratio (0.25µl:0.25µl of protein/reservoir).
Both crystal types were soaked in a sucrose saturated reservoir solution for cryoprotection and flash cooled before data collection.
DarB was also crystallized in presence AMP or 3´3´cGAMP. A protein concentration of 4.5 mg/ml DarB supplemented with either an 8.5-fold excess AMP or a 6.0-fold excess of 3´3´cGAMP in a 1:1 protein-to-reservoir ratio. In case of AMP best diffracting crystals were obtained after one month, while DarB- 3´3´cGAMP containing crystals were already obtained after 24 h in 0.1 M Tris/HCl pH 8.5, 32 % w/v polyethylene glycol 4000 and 5 % v/v glycerol respectively. No additive was added to the reservoir solution for cryoprotection.

4.4.5 X-ray data collection and processing

The diffraction images were recorded at PETRAIII EMBL beamlines P13 (DarB_APO and DarB_c-di-AMP) and P14 (DarB_AMP and DarB_3´3´cGAMP) and processed with the XDS package (Kabsch 2010a; Kabsch 2010b). The data collection and processing statistics are summarized in Tab.1. For all crystals an orthorhombic lattice with similar unit cell parameters was determined. The crystals of apo DarB and in complex with AMP exhibits unit cell parameters of *a = 38.670 Å, b = 67.760 Å, c = 103.960 Å*, and *a = 41.310 Å, b = 69.260 Å, c = 105.420 Å*, respectively. The crystals in complex c-di-AMP and 3´3´cGAMP exhibit cell constants of *a = 42.150 Å, b = 65.410 Å, c = 104.850 Å* and *a = 41.840 Å, b = 65.130 Å, c = 104.210 Å*

respectively. The cell content analysis of all four structures indicated the presence of two monomers occupying the asymmetric unit (apo: V_m=2.07 Å^3/Da, corresponding solvent content, c-di-AMP V_m = 2.15 Å^3/Da, corresponding solvent content of 42.81 %, 3´3´cGAMP: V_m=2.15 Å^3/Da, corresponding solvent content 42.73 %, and AMP: V_m=2.27 Å^3/Da, corresponding solvent content 45.89 %).

4.4.6 Structure Determination and Refinement

The initial phases of DarB_c-di-AMP were obtained by molecular replacement with PHASER (McCoy et al. 2007) using the DarB structure of *B. subtilis* (PDB code 1YAV) as a search model. All other structures (DarB_apo, DarB_3´3´cGAMP and DarB_AMP) are isomorphous to the DarB_c-di-AMP crystal structure. Therefore, rigid body refinement followed by manual modelling in Coot (Emsley et al. 2010) utilizing 2mFo-DFc and mFo-DFc electron density maps was performed. Reciprocal space refinement has been conducted with Refmac5 (Winn et al. 2011) and PHENIX. In order to monitor the progress of refinement using the R_{free} a random set of 5 % reflections was excluded from the refinement. The structure of apo DarB was determined at a resolution of 1.84 Å and to R_{work} of 20.23% and R_{free} of 25.09 %. The final structure of DarB in complex with c-di-AMP was determined at a resolution of 1.70 Å to R_{work} of 18.29 % and R_{free} of 20.97 %. Finally, the structures of DarB in complex with AMP and 3´3´cGAMP were determined at 1.64 Å (R_{work} of 18.88 % and R_{free} of 22.18 %) and 1.50 Å (R_{work} of 15.33 % and R_{free} of 19.20 %) resolution, respectively. Atomic models have been verified against omit maps as calculated with PHENIX suite. The presence of bound ligands has been confirmed by calculation of omit maps using phenix.polder program (Liebschner et al. 2017). Figures have been generated using an open source version of pymol (Schrödinger 2010).

4.5 Discussion

In the recent years more and more proteins were identified to bind the essential second messenger c-di-AMP. Most of these proteins are known to be involved in processes essential for bacteria survival, e.g.: the potassium or osmolyte homeostasis (Woodward et al. 2010; Luo Y and Helmann 2012; Mehne et al. 2013; Gundlach et al. 2015a; Commichau et al. 2017; Gundlach et al. 2017a; Gundlach et al. 2017b; Commichau et al. 2019). Some of these proteins share two distinct and conserved domains, the RCK_C and CBS domains, which are responsible for binding c-di-AMP (Gundlach et al. 2019). In this study we structurally and biochemically analyzed the c-di-AMP binding receptor B (DarB) which was previously described as a CBS domain containing protein with the ability to bind c-di-AMP. So far, a functional link between c-di-AMP binding of DarB and a physiological relevance in the bacterial cell has not been observed.

Our results confirmed a tight and specific binding of c-di-AMP to each DarB monomer in the nanomolar range. Although the hetero di-nucleotide 3'3'cGAMP is absent in *B. subtilis* which indicates no physiological relevance it binds to DarB with an affinity in the micromolar range. The first crystal structure of DarB from *B. subtilis* was already deposited in the PDB in 2004. It has crystallized as a donut-shaped dimer revealing a typical CBS domain fold with two domains forming a head-to-head assembly. In contrast, the structurally and biochemical characterized CBS domain subunit from the carnitine transporter OpuC also binds c-di-AMP, yet the CBS modules are oriented in an antiparallel manner (head-to-tail assembly) (Ereño-Orbea et al. 2013; Schuster et al. 2016).

In order to get further structural insights into the specificity and affinity for different ligands four crystal structures were determined: DarB in its apo-form and in complex with either c-di-AMP, 3'3'cGAMP or AMP. Structural comparisons of different CBS domain containing proteins suggested the presence of two canonical adenosine binding sites in a CBS module (Scott et al. 2004). In most structurally analyzed CBS modules only one binding site is occupied by a ligand which is explained by the amino acid composition.

In all ligand bound DarB structures each monomer had one nucleotide bound in one of the two canonical nucleotide binding sites which are chemically not identical. A DarB dimer has two cattycorner binding sites due to its head-to-head assembly, while in the OpuC dimer these binding sites are parallel to each other. This could explain why in case of DarB, only one adenine base (Ade1) of c-di-AMP is directly bound by the protein in each monomer, while the second adenine (Ade2) protrudes from the protein. However, in OpuC the parallel positioning of the binding sites might favor the binding of only one c-di-AMP molecule in an elongated manner in which both adenine base, Ade1 and Ade2 are bound.

In order to get further insights on the function of proteins that are structurally very similar to DarB and to find structural homologous a DALI search was performed (Holm and Rosenström 2010). The DALI search using only one monomer of DarB unveiled a plethora of different

proteins. 25 Protein structures were chosen with a Z-score above 13.5. All structures superimpose with an r.m.s.d between 1.3 and 2.9 Å. Seven of the 25 structures show an adenine derivative in the nucleotide binding site and these structures were used for further structural analysis (Tab. 2).

Structural comparison of the c-di-AMP binding site in DarB with the nucleotide binding sites of the seven CBS domain containing proteins unveiled high overall 3D similarity but also very conserved surrounding of bound ligand molecules. As pointed out previously CBS modules consist of two putative nucleotide binding sites which despite their structural similarity differ significantly in composition of amino acids and hence are chemically not equivalent (reviewed in (Ereño-Orbea et al. 2013)). This is the most plausible explanation why a DarB dimer binds only two nucleotides.

A structural comparison of the binding sites revealed that two amino acids: leucin 23 and alanine 25, which are positioned in the loop region (pink) proceeding the canonical CBS fold of CBS1, are crucial for ligand binding. These residues favor adenine over guanine derivatives as described for different CBS domain containing proteins (Rudolph et al. 2007; Ereño-Orbea et al. 2013). The results of the structural analysis are consistent with the biochemical and structural data. The binding pocket of DarB is specific for adenine binding, which is supported by the fact, that only the adenine base of the hetero di- nucleotide 3'3'cGAMP is bound deep in the binding pocket while the guanine base protrudes out of the protein.

We suggested that the binding is specific to c-di-AMP although also AMP binds to DarB, yet with low affinity. Probably the existence of 3'3' phosphate-sugar ring, present in both c-di-AMP and 3'3'cGAMP, is responsible for higher specificity of DarB to dinucleotides.

However, the question to answer is why 3'3'cGAMP binds with a lower affinity than c-di-AMP even though both molecules are coordinated by the same amino acids and also interatomic interactions are of similar lengths. Structural analysis exhibit that the outpointing guanine base is rotated towards the protein core. A closer look to the structure unveiled the presence of a conserved water molecule in all available DarB structures (apo_DarB, DarB_cdiAMP, DarB_AMP, DarB_3'3'cGAMP). This water molecule causes a steric clash with N2 amine group of the guanine base and is most likely responsible for the observed change in orientation of the guanine base when compared to Ade2 of c-di-AMP. In addition, the outpointing purine base is indirectly coordinated through water molecules. Therefore, we suggest that the decreased binding affinity of hetero dinucleotide is due to the approximately 41-degree rotation of the purine base leading to a conformation which is most likely energetically less optimal. Surprisingly in the other nucleotide binding site the outpointing base of the 3'3'cGAMP is oriented in a similar way as the adenine base (Ade2) in the c-di-AMP-DarB structure and unveils the positioning of two further dinucleotides in a coplanar assembly to the guanine base. These additional 3'3'cGAMP molecules are bound in a positively charge patch

on the protein surface (Fig. 4). Interestingly, cyclic dinucleotides have been described previously to form dimeric assemblies. While c-di-GMP was reported to form dimers in order to bind to the I-site of its synthesizing enzyme (diguanylate cyclases) to inhibit its activity, so far, no biological relevance has been described for c-di-AMP dimers (Blommers et al. 1988; Manikandan et al. 2014). This assembly is not a crystal lattice artefact, since it is not stabilized by crystal contacts. Hence, we wondered whether DarB might also be able to bind RNA as described in other studies for CBS domain proteins (McLean et al. 2004). The relative orientation of the nucleotide bases resembles the classical orientation of the nucleotide bases in DNA or RNA what strongly argues towards the ability of RNA binding (Fig. 4 and S4). It is commonly known that RNA molecules prefer to bind to positively charged amino acids (Ellis et al. 2007; Chen and Lim 2008).

The physiological function of DarB is still unclear as well as its putative interaction partner/partners.

In a plethora of different studies, it was argued that c-di-AMP is an essential nucleotide for bacteria that carry a c-di-AMP synthesizing enzyme (diadenylate cyclase). Therefore, diadenylate cyclases seem to be an attractive target for the development of new antibiotic drugs (Corrigan R. M. and Gründling 2013; Rosenberg et al. 2015; Commichau et al. 2019; Heidemann et al. 2019). The identification of c-di-AMP interaction partners might help to understand why c-di-AMP is essential and where potential resistances might develop.

Acknowledgments

We thank the EMBL-OutstationHamburg (DESY PETRAIII beamlines P13 and P14, Germany) for the allocation of beam time and the beamline staff for their support. Furthermore, we are grateful for Liza Vinhoven for her contribution in crystallization.

Funding information

This work was supported by grants of the Deutsche Forschungsgemeinschaft within the Priority Program SPP1879 (to R.F. and J.S.) and INST186/1117 (to R.F.).

Conflict of interest statement

The authors declare that they have no conflicts of interest with the contents of this article.

References

1. Bateman A. The structure of a domain dommon to archeabacteria and the homocystinuria disease protein. Trends Biochem Sci. 1997;(22):12–3.

2. Baykov AA, Tuominen HK, Lahti R. The CBS domain: A protein module with an emerging prominent role in regulation. ACS Chem Biol. 2011;6(11):1156–63.

3. Ereño-Orbea J, Oyenarte I, Martínez-Cruz LA. CBS domains: Ligand binding sites and conformational variability. Archives of Biochemistry and Biophysics. 2013.

4. Anashkin VA, Baykov AA, Lahti R. Enzymes regulated via cystathionine β-synthase domains. Biochem. 2017;82(10):1079–87.

5. Huynh TN, Choi PH, Sureka K, Ledvina HE, Tong L, Woodward JJ. Cyclic di-AMP targets the cystathionine beta-synthase domain of the osmolyte transporter OpuC. Mol Microbiol. 2017;102(2):233–43.

6. Schuster CF, Bellows LE, Tosi T, Campeotto I, Corrigan RM, Freemont P, et al. The second messenger c-di-AMP inhibits the osmolyte uptake system OpuC in Staphylococcus aureus. Sci Signal. 2016;9(441):1–31.

7. Corrigan RM, Gründling A. Cyclic di-AMP: Another second messenger enters the fray. Nat Rev Microbiol. 2013;11(8):513–24.

8. Commichau FM, Dickmanns A, Gundlach J, Ficner R, St??lke J. A jack of all trades: the multiple roles of the unique essential second messenger cyclic di-AMP. Mol Microbiol. 2015;97(May):189–204.

9. Commichau FM, Gibhardt J, Halbedel S, Gundlach J, Stülke J. A Delicate Connection: c-di-AMP Affects Cell Integrity by Controlling Osmolyte Transport. Trends Microbiol [Internet]. 2017;26(3):175–85.
Available from: http://dx.doi.org/10.1016/j.tim.2017.09.003

10. Corrigan RM, Campeotto I, Jeganathan T, Roelofs KG, Lee VT, Gründling A. Systematic identification of conserved bacterial c-di-AMP receptor proteins. PNAS. 2013;110(22):9084–9.

11. Bai Y, Yang J, Zarrella TM, Zhang Y, Metzger DW, Bai G. Cyclic Di-AMP Impairs Potassium Uptake Mediated by a Cyclic Di-AMP Binding Protein in Streptococcus pneumoniae. J Bacteriol [Internet]. 2014 Feb 1 [cited 2016 Sep 6];196(3):614–23. Available from: http://jb.asm.org/cgi/doi/10.1128/JB.01041-13

12. Kim H, Youn SJ, Kim SO, Ko J, Lee JO, Choi BS. Structural studies of potassium transport protein KtrA regulator of conductance of K+ (RCK) C domain in complex with cyclic diadenosine monophosphate (c-di-AMP). J Biol Chem. 2015;290(26):16393–402.

13. Gundlach J, Dickmanns A, Schröder-Tittmann K, Neumann P, Kaesler J, Kampf J, et al. Identification, characterization and structure analysis of the c-di-AMP binding PII-like signal transduction protein DarA. J Biol Chem [Internet]. 2015;290(5):3069–80. Available from: http://www.ncbi.nlm.nih.gov/pubmed/25433025

14. Quintana IM, Gibhardt J, Turdiev A, Hammer E, Commichau FM, Lee VT, et al. The KupA and KupB Proteins of Lactococcus lactis IL1403 Are Novel c-di-AMP Receptor Proteins Responsible for Potassium Uptake. J Bacteriol. 2019;201(10):1–13.

15. Moscoso JA, Schramke H, Zhang Y, Tosi T, Dehbi A, Jung K, et al. Binding of cyclic di-AMP to the Staphylococcus aureus sensor kinase KdpD occurs via the universal stress protein domain and downregulates the expression of the Kdp potassium transporter. J Bacteriol. 2016;198(1):98–110.

16. Sureka K, Choi PH, Precit M, Delince M, Pensinger DA, Huynh TN, et al. The Cyclic Dinucleotide c-di-AMP Is an Allosteric Regulator of Metabolic Enzyme Function. Cell [Internet]. 2014;158(6):1389–401.
Available from: http://www.ncbi.nlm.nih.gov/pubmed/25215494

17. Gundlach J, Krüger L, Herzberg C, Turdiev A, Poehlein A, Tascón I, et al. Sustained sensing in potassium homeostasis: Cyclic di-AMP controls potassium uptake by KimA at the levels of expression and activity. J Biol Chem. 2019;294(24):9605–14.

18. Bradford MM. Revisiting a dogma: The effect of volume exclusion in molecular crowding. Anal Biochem. 1976;72:248–54.

19. Kabsch W. Integration, scaling, space-group assignment and post-refinement. Acta Crystallogr Sect D Biol Crystallogr. 2010;66(2):133–44.

20. Kabsch W. XDS. Acta Crystallogr Sect D Biol Crystallogr [Internet]. 2010;66(2):125–32. Available from: http://scripts.iucr.org/cgi-bin/paper?S0907444909047337

21. McCoy AJ, Grosse-Kunstleve RW, Adams PD, Winn MD, Storoni LC, Read RJ. Phaser crystallographic software. J Appl Crystallogr. 2007;40(4):658–74.

22. Emsley P, Lohkamp B, Scott WG, Cowtan K. Features and development of Coot. Acta Crystallogr Sect D Biol Crystallogr. 2010;66(4):486–501.

23. Winn MD, Ballard CC, Cowtan KD, Dodson EJ, Emsley P, Evans PR, et al. Overview of the CCP 4 suite and current developments. Acta Crystallogr Sect D Biol Crystallogr [Internet]. 2011 Apr 1 [cited 2017 Mar 23];67(4):235–42. Available from: http://scripts.iucr.org/cgi-bin/paper?S0907444910045749

24. Liebschner D, Afonine P V., Moriarty NW, Poon BK, Sobolev O V., Terwilliger TC, et al. Polder maps: Improving OMIT maps by excluding bulk solvent. Acta Crystallogr Sect D Struct Biol. 2017;73(2):148–57.

25. Schrödinger LLC. The PyMOL Molecular Graphic SystemNo Title. 2010.

26. Woodward JJ, Lavarone AT, Portnoy DA. C-di-AMP secreted by intracellular Listeria monocytogenes activates a host type I interferon response. Science (80-). 2010;328(5986):1703–5.

27. Gundlach J, Herzberg C, Hertel D, Thürmer A, Daniel R, Link H, et al. Adaptation of Bacillus subtilis to Life at Extreme Potassium Limitation. Vol. 8, mBio. 2017. e00861-17 p.

28. Gundlach J, Mehne FMP, Herzberg C, Kampf J, Valerius O, Kaever V, et al. An essential poison: Synthesis and degradation of cyclic Di-AMP in Bacillus subtilis. J Bacteriol. 2015;197(20):3265–74.

29. Mehne FMP, Gunka K, Eilers H, Herzberg C, Kaever V, Stülke J. Cyclic Di-AMP homeostasis in bacillus subtilis: Both lack and high level accumulation of the nucleotide are detrimental for cell growth. J Biol Chem. 2013;288(3):2004–17.

30. Commichau FM, Heidemann JL, Ficner R, Stülke J. Making and breaking of an essential poison: The cyclases and phosphodiesterases that produce and degrade the essential second messenger cyclic di-AMP in bacteria. J Bacteriol. 2019;201(1):1–14.

31. Luo Y, Helmann JD. Analysis of the role of Bacillus subtilis sigma(M) in beta-lactam resistance reveals an essential role for c-di-AMP in peptidoglycan homeostasis. Mol Microbiol [Internet]. 2012;83(3):623–39.

32. Gundlach J, Herzberg C, Kaever V, Gunka K, Hoffmann T, Weiß M, et al. Control of potassium homeostasis is an essential function of the second messenger cyclic di-AMP in Bacillus subtilis. Sci Signal. 2017;10(475).

33. Scott JW, Hawley SA, Green KA, Anis M, Stewart G, Scullion GA, et al. CBS domains form energy-sensing modules whose binding of adenosine ligands is disrupted by disease mutations. J Clin Invest. 2004;113(2):274–84.

34. Holm L, Rosenström P. Dali server: Conservation mapping in 3D. Nucleic Acids Res. 2010;38:545–9.

35. Rudolph MJ, Amodeo GA, Iram SH, Hong SP, Pirino G, Carlson M, et al. Structure of the Bateman2 Domain of Yeast Snf4: Dimeric Association and Relevance for AMP Binding. Structure. 2007;15(1):65–74.

36. Blommers MJJ, Haasnoot CAG, I. WJAL, Van der Marel GA, Van Boom JH, Hilbers CW. Solution Structure of the 3'-5' cyclic Dinucleotide pApA. A combined NMR, UV melting and Molecular Mechanics study. Biochemistry. 1988;27(22):8361–9.

37. Manikandan K, Sabareesh V, Singh N, Saigal K, Mechold U, Sinha KM. Two-step synthesis and hydrolysis of cyclic di-AMP in Mycobacterium tuberculosis. PLoS One. 2014;9(1).

38. McLean JE, Hamaguchi N, Belenky P, Mortimer SE, Stanton M, Hedstrom L. Inosine 5′-monophosphate dehydrogenase binds nucleic acids in vitro and in vivo. Biochem J. 2004;379(2):243–51.

39. Ellis JJ, Broom M, Jones S. Protein-RNA interactions: Structural analysis and functional classes. Proteins Struct Funct Genet. 2007;

40. Chen YC, Lim C. Predicting RNA-binding sites from the protein structure based on electrostatics, evolution and geometry. Nucleic Acids Res. 2008;36(5).

41. Rosenberg J, Dickmanns A, Neumann P, Gunka K, Arens J, Kaever V, et al. Structural and biochemical analysis of the essential diadenylate cyclase CdaA from Listeria monocytogenes. J Biol Chem. 2015;290(10):6596–606.

42. Heidemann JL, Neumann P, Dickmanns A, Ficner R. Crystal structures of the c-di-AMP-synthesizing enzyme CdaA. J Biol Chem. 2019;294(27):10463–70.

Table and Figures

Table 1: Crystallographic data collection and refinement statistics

	DarB-APO	DarB-c-di-AMP	DarB-AMP	DarB-3‘3‘-cGAMP
Crystallographic data				
Beamline	Petra III-P13, EMBL, Hamburg	Petra III-P13, EMBL, Hamburg	Petra III-P14, EMBL, Hamburg	Petra III-P14, EMBL, Hamburg
Wavelength (Å)	0.97625	0.97625	0.97625	0.97625
Resolution range (Å)[a]	41.24-1.84 (1.88-1.84)	40.91-1.70 (1.76-1.70)	41.94-1.64 (1.71-1.64)	35.68-1.5 (1.52-1.50)
Unique reflections	24397	32669	37896	50229
Redundancy	5.1(5.3)	7.0(7.3)	13.25(13.52)	12.95 (13.34)
Completeness (%)	99.1 (99.7)	99.8 (99.8)	99.8(99.8)	99.9 (100)
Space group	$P2_12_12_1$	$P2_12_12_1$	$P2_12_12_1$	$P2_12_12_1$
a (Å)	38.67	42.15	41.31	41.49
b (Å)	67.76	65.41	69.26	69.92
c (Å)	103.96	104.85	105.42	105.78
R_{merge} (%)	5.8 (64.0)	5.2 (92.0)	2.9 (68.0)	3.9 (63.2)
I/σ (I)	16.81 (2.51)	24.45 (2.41)	40.44 (4.12)	31.06 (4.2)
$CC_{1/2}$	99.8 (87.3)	99.9 (88.6)	100 (97.4)	100 (94.2)
Refinement statistics				
R_{work}/R_{free}	0.2023/0.2509	0.1828/0.2105	0.1885/0.2204	0.1532/0.1907
No. of atoms	2418	2586	2488	2780
Average B factor (Å^2)	36.53	30.90	44.34	31.42
Root mean square deviation				
Bonds Å	0.005	0.007	0.011	0.009
Angles (degree)	0.775	1.062	1.138	1.145
Ramachandran plot				
Favoured (%)	98.15	99.26	98.51	98.18
Allowed (%)	1.85	0.74	1.49	1.82
Outliers (%)	0.00	0.00	0.00	0.00
PDB codes	6YJ8	6YJA	6YJ7	6YJ9

Tabelle 2: DALI search for structural homologs with bound ligand

PDB code	Protein	Ligand	Organism	Function	%id	Z-score
1YAV	DarB/YkuL	c-di-AMP	*Bacillus subtilis*	Unknown	100	A 22.8/ B 22.4
2YZQ	PH1780	SAM	*Pyrococcus horikoshii*	Unknown	19	14.5
2RC3	NE2398	NAD	*Nitrosomonas europaea*	Unknown	14	14.6
3FHM	ATU1752	AMP, NAI	*Agrobacterium tumefaciens*	Osmolyte transporter	19	14.1
5YZ2	CorC	AMP	*Geobacillus Kaustophilus*	Mg^{2+} and Co^{2+} efflux protein	13	A 14.9/ B 14.2
4FRY	BamMC406_4587	AMP, NAD	*Burkholderia ambifaria*	unknown	14	14.1
3FNA	yrbH	AMP	*Escherichia coli*	Possible Arabinose 5-phosphate Isomerase	15	13.5
5KS7	OpuCA	C-di-AMP	*Listeria monocytogenes*	Carnitine transporter	16	16.2

Tabelle 3: Parameters used for the ITC titration series

Injection no.	Injection Volume [µl]	Injection duration [sec.]	Spacing [sec.]	Filter period [sec.]
1	5	10	360	2
2-19	15	30	360	2

Figure 1

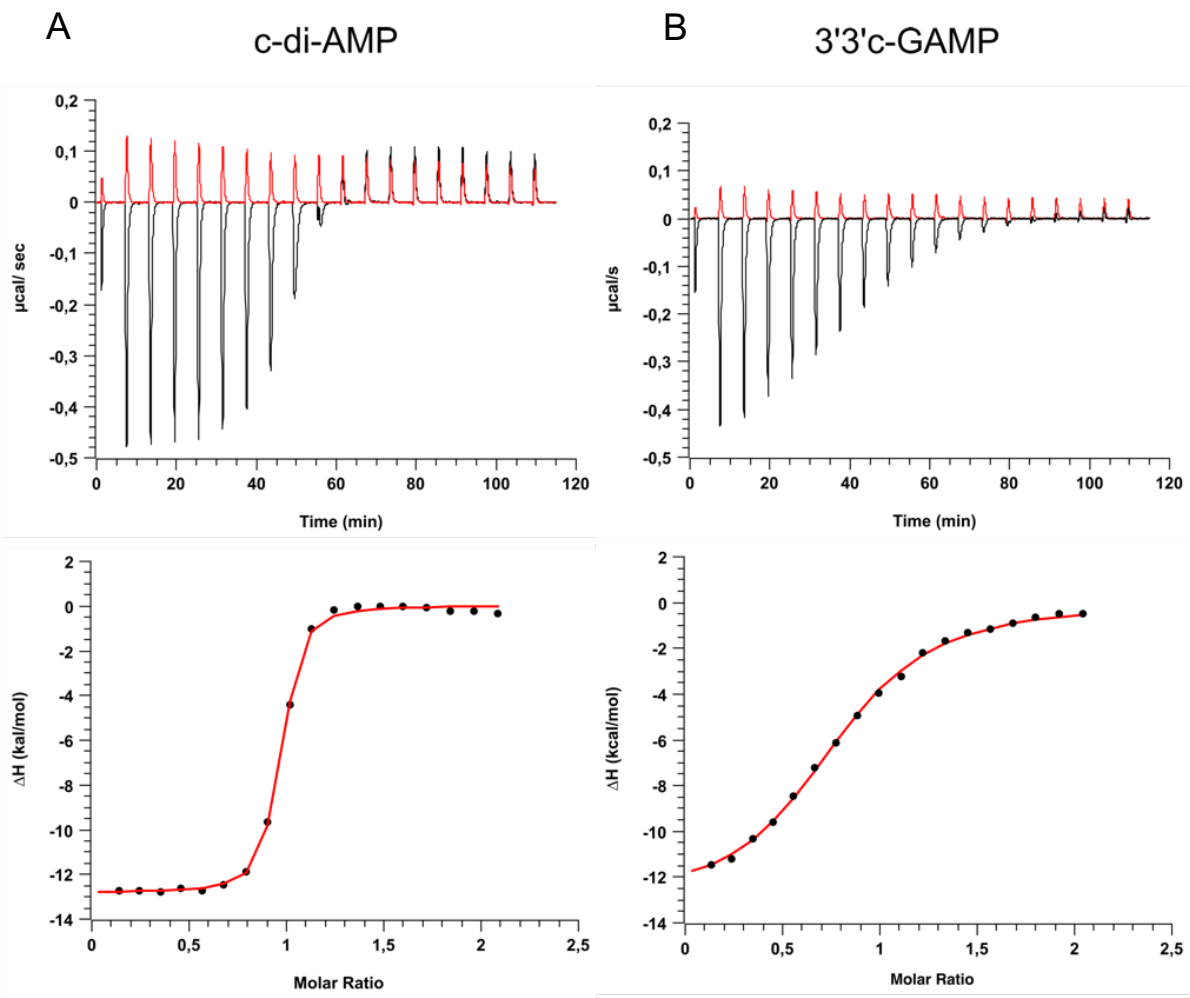

Figure 1: Nucleotide binding measured by means of ITC. A) The nucleotide-based second messenger c-di-AMP specifically binds to DarB with a K_D of 27.0 nM ± 1.98 nM. **B)** The hetero di-nucleotide 3'3' cGAMP binds to DarB with an approximately 40-fold lower affinity in comparison to c-di-AMP.

Figure 2

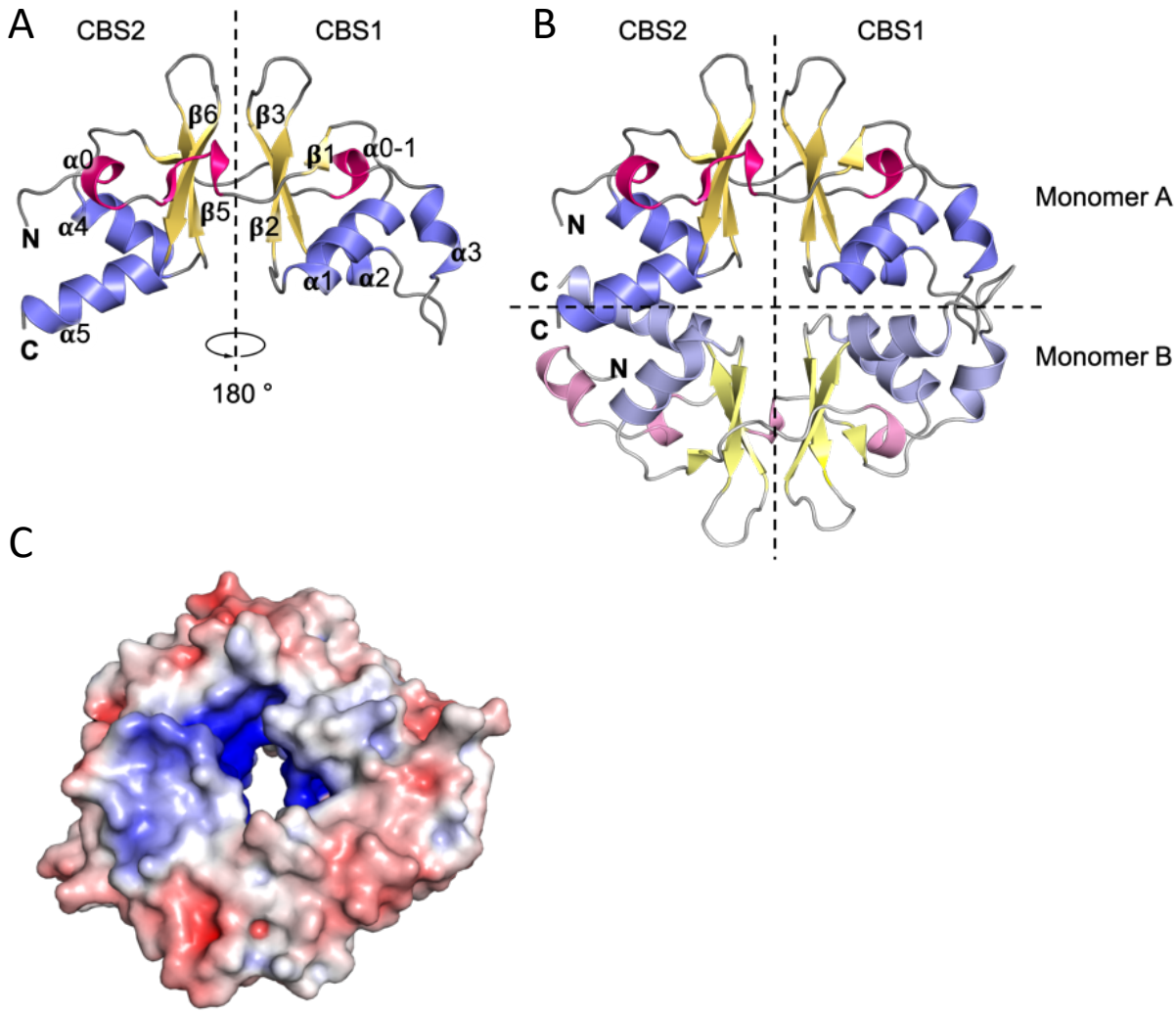

Figure 2: Crystal structure of DarB. A) The monomer structure of DarB is depicted in cartoon mode (helices: blue, β-strands: yellow, linker region: red, loop region: gray). Each DarB monomer occurs as a tandem repeat which is composed of two CBS domains (CBS1 and CBS2), possessing canonical βαββα fold. **B)** DarB forms a donut-shaped dimer with the N- and C-termini close to each other which is according to the CBS protein classification a parallel head-to-head assembly. **C)** The electrostatic surface potential of DarB exhibits that the outer surface is mainly negatively charged with a prominent positive patch connected to the highly positively charged central pore.

Figure 3

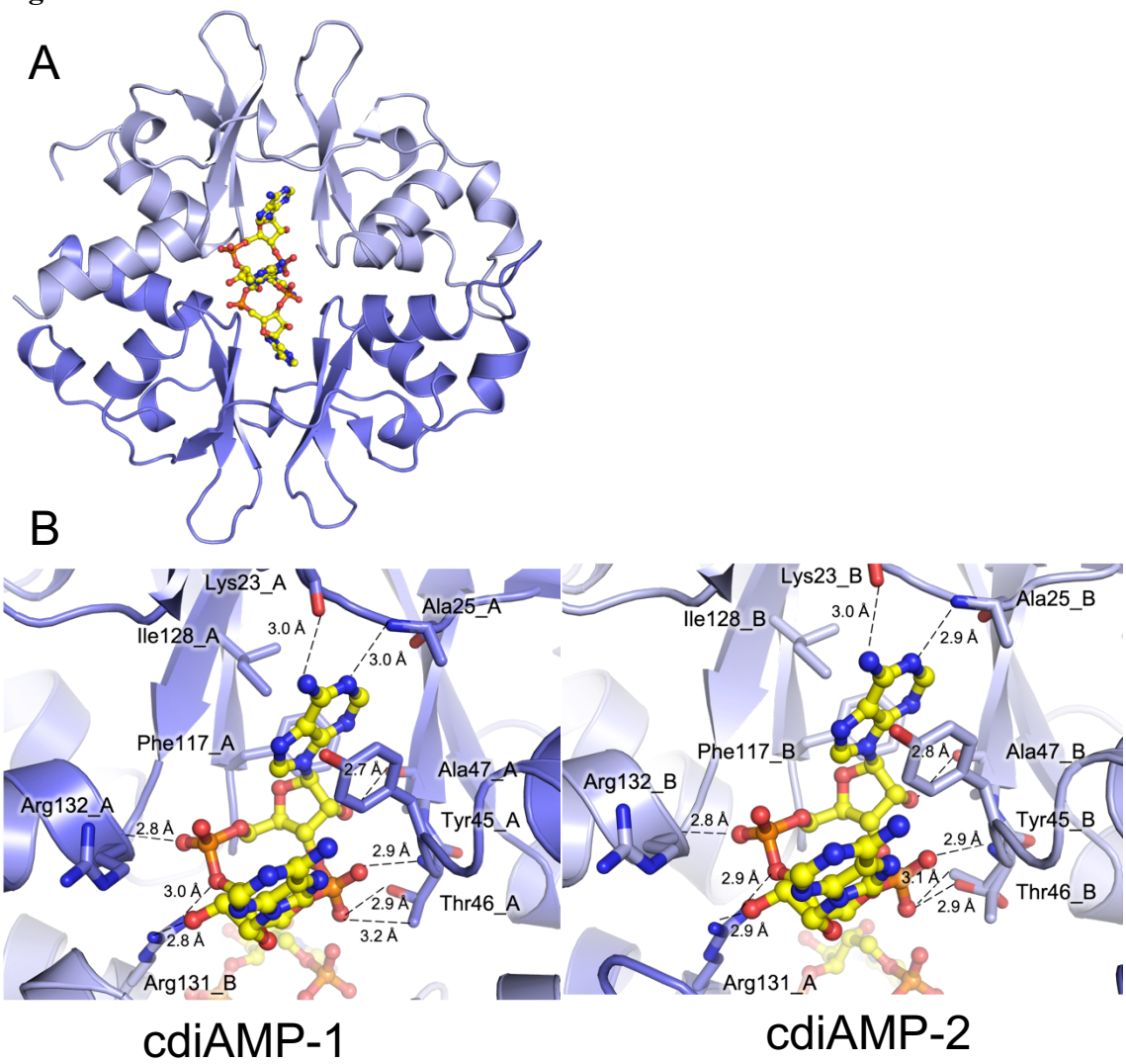

Figure 3: **Crystal structure of DarB with two nucleotide binding sites. A)** Cartoon representation of the donut-shaped homo-dimeric DarB with two bound c-di-AMPs. Monomer A is colored in dark blue; Monomer B is colored in light blue. The two c-di-AMP molecules are depicted in ball and stick mode (carbon: yellow, phosphate: orange, nitrogen: blue, oxygen: red). **B)** A detailed view of the nucleotide binding site in monomer A and B, showing amino acids involved in the c-di-AMP binding. Only one adenine base is coordinated by amino acids, while the other protrudes out of the protein core and coordinated through water molecules. The dashed lines indicate distances between the protein and the ligand up to 3.2 Å.

Figure 4

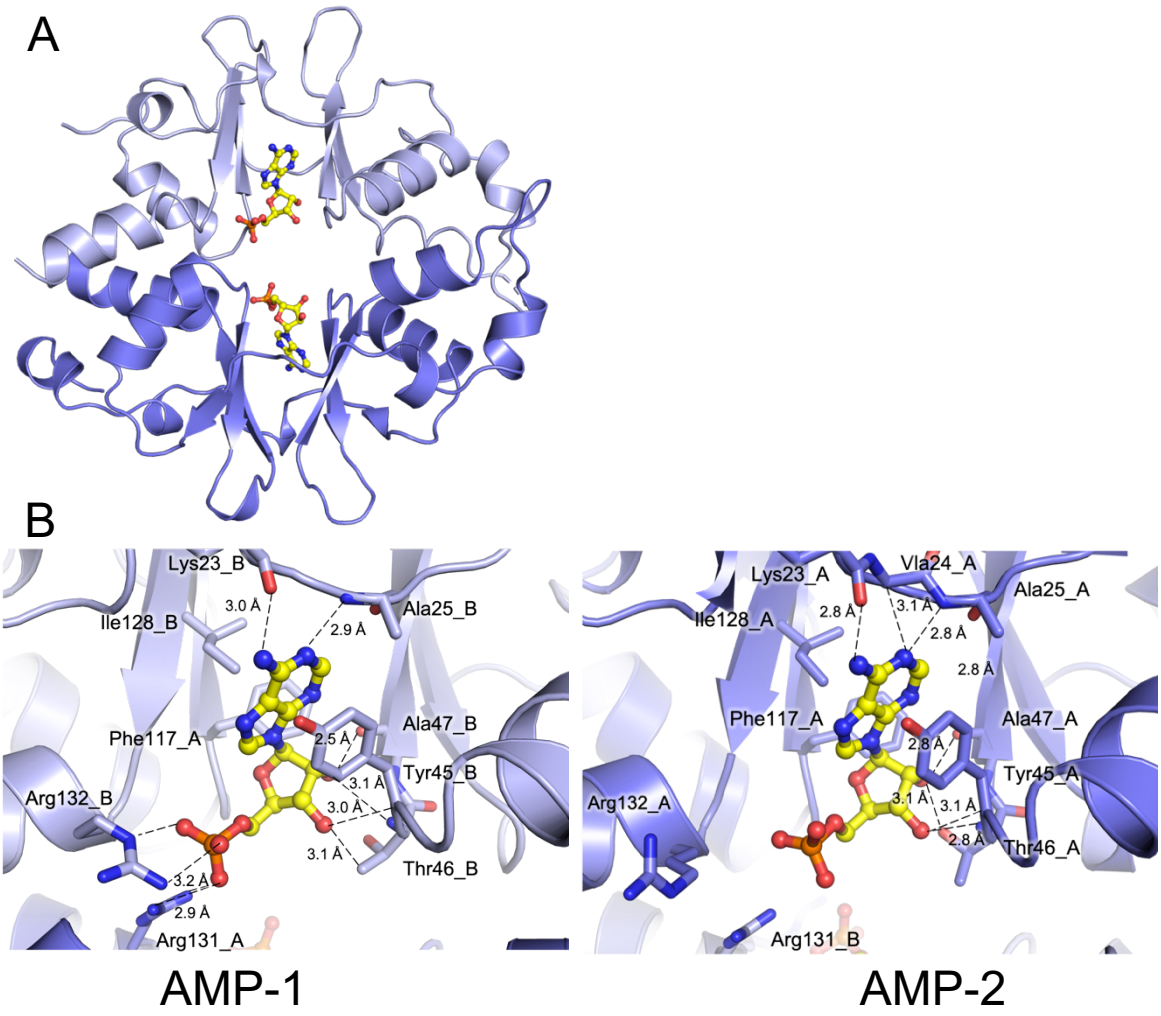

Figure 4 Crystal structure of DarB in complex with AMP. A) Cartoon representation of the DarB with two bound AMPs. Monomer A is colored in dark blue; Monomer B is colored in light blue. The two AMP molecules are depicted in ball and stick mode (carbon: yellow, phosphate: orange, nitrogen: blue, oxygen: red). **B)** A detailed view of the nucleotide binding in molecule A and B. The dashed lines indicate distances between the protein and the ligand up to 3.2 Å.

Figure 5

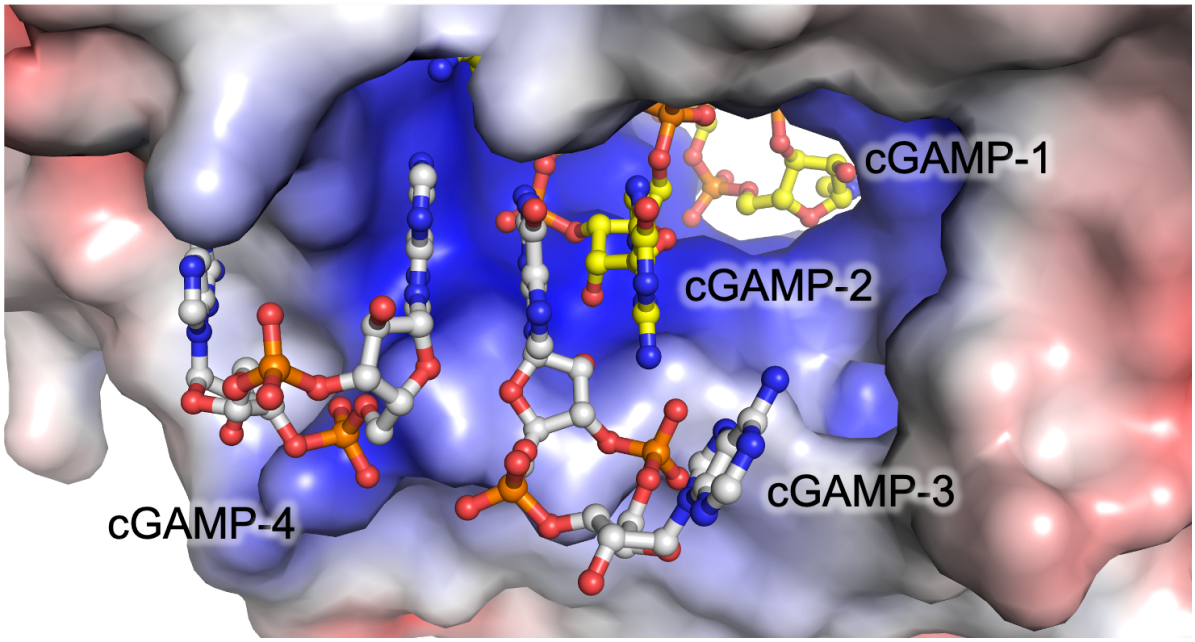

Figure 5: Crystal structure of DarB in complex with 3'3'cGAMP. In this structure two additional 3′3′cGAMP molecules are bound to DarB adjacent to one of the two canonically bound 3′3′cGAMP. The additional 3'3'cGAMP molecules are bound along the positive patch one the protein surface and interact via π-π stacking with the protruding guanine of the 3'3'cGAMP located in the c-di-AMP binding site. The nucleotides are depicted in ball and stick mode (phosphate: orange, nitrogen: blue, oxygen: red, canonical 3'3'cGAMP: carbon: yellow; non-canonical 3'3'cGAMP: carbon: grey)

Crystal structures of DarB reveal a novel c-di-AMP binding mode of CBS domains

Jana L. Heidemann[1], Piotr Neumann[1], Larissa Krüger[2], Achim Dickmanns[1], Jörg Stülke[2], Ralf Ficner[1*]

Supporting Information

Figure S1

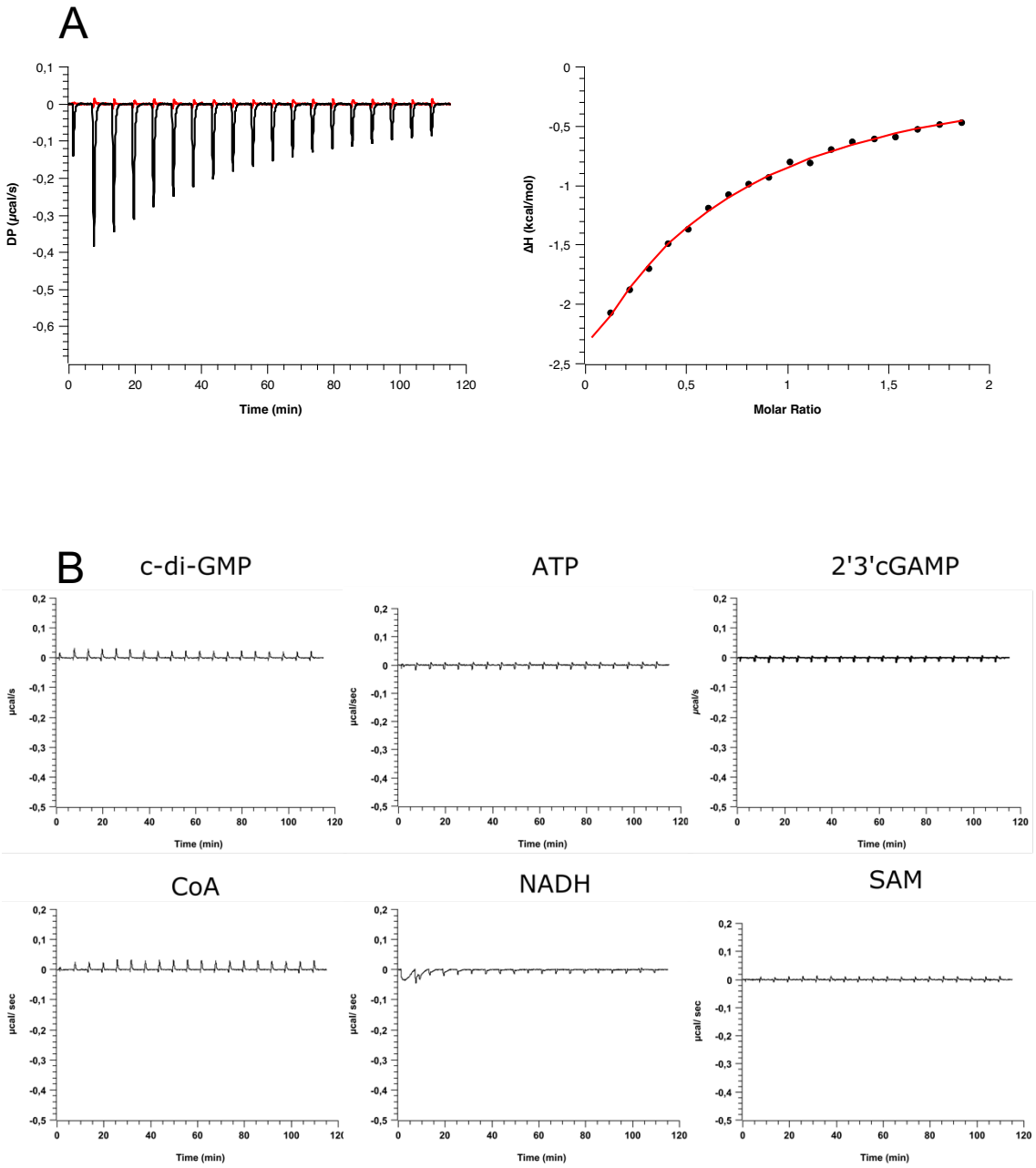

Supporting Figure S1: Nucleotide binding studies. A) CBS domain containing proteins are known to bind a diversity of adenine derivatives like, ATP, NADH or AMP. The binding of various nucleotides was measured by means of ITC. The nucleotide AMP binds with a very low affinity to DarB. **B)** No other nucleotide binding than to c-di-AMP, 3'3'cGAMP or AMP was detected.

Figure S2

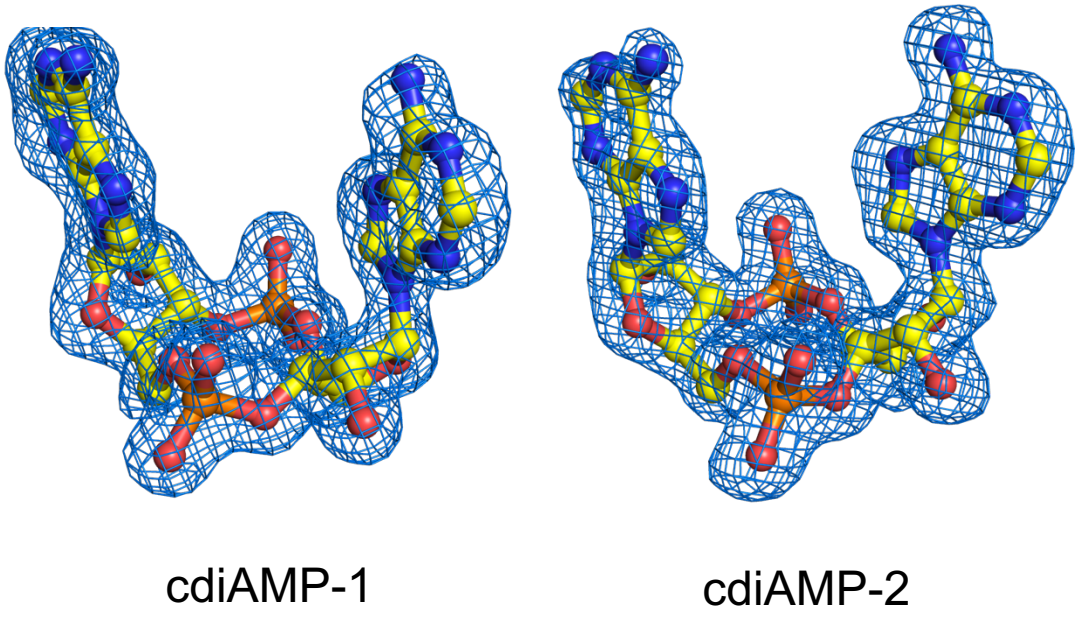

Supporting Figure S2: Fo-Fc omit electron density maps of the two c-di-AMP molecules bound to DarB. C-di-AMP is depicted in ball-stick mode. The mFo-DFc omit electron density map (blue mesh) is contoured at a sigma level of 3.0.

Figure S3

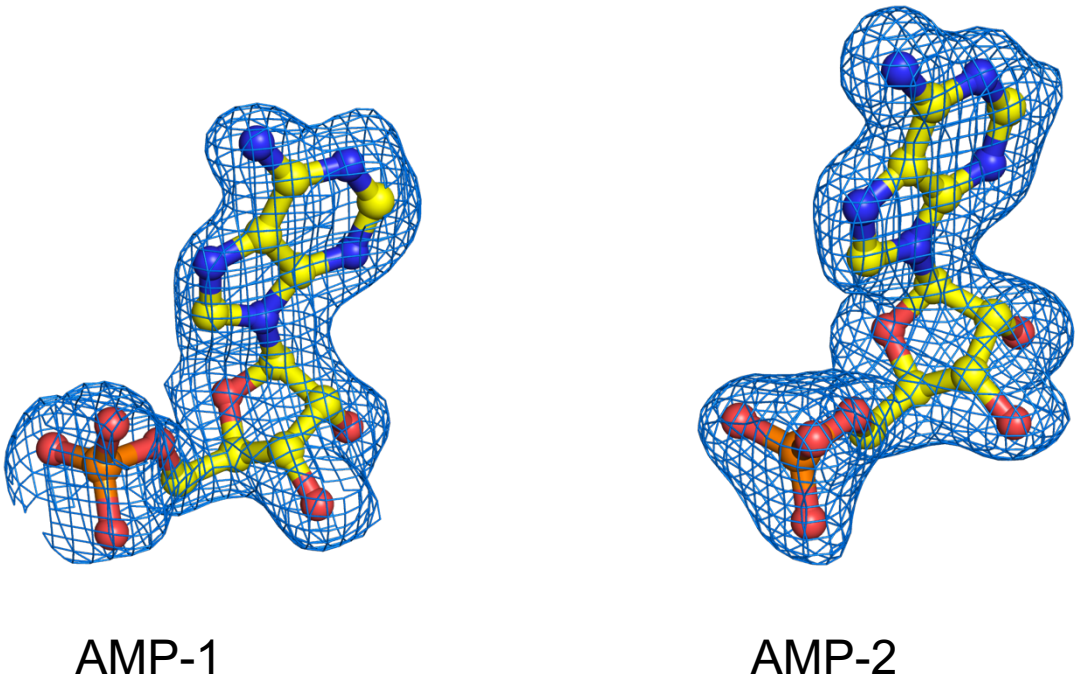

Supporting Figure S3: Fo-Fc omit electron density maps of the two AMP molecules bound to DarB. AMP is depicted in ball-stick mode (carbon: yellow, phosphate: orange, nitrogen: blue, oxygen: red). The mFo-DFc omit electron density map (blue mesh) is contoured at a sigma level of 3.0.

Figure S4

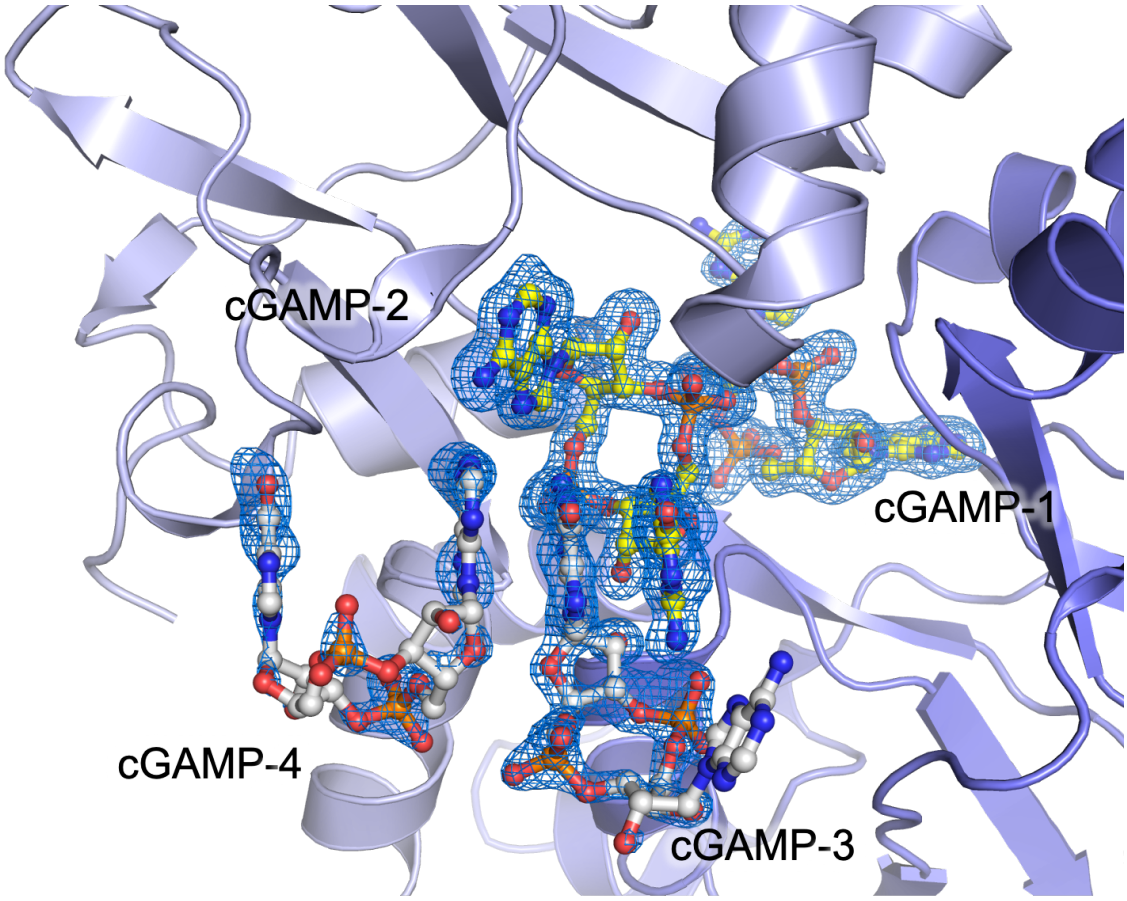

Supporting Figure S4: Crystal structure of DarB with bound 3'3'cGAMP at 1.64 Å resolution. Cartoon representation of the homo-dimeric DarB with two bound 3'3'cGAMP in the c-di-AMP binding site. Adjacent to one of the two canonical 3'3'cGAMP molecules, two additional 3'3'cGAMP molecules (cGAMP-3 and cGAMP-4) are present. The nucleotides are depicted in ball and stick mode (phosphate: orange, nitrogen: blue, oxygen: red, canonical 3'3'cGAMP: carbon: yellow; non-canonical 3'3'cGAMP: carbon: grey). The mFo-DFc omit electron density map (blue mesh) is contoured at a sigma level of 3.0.

Figure S5

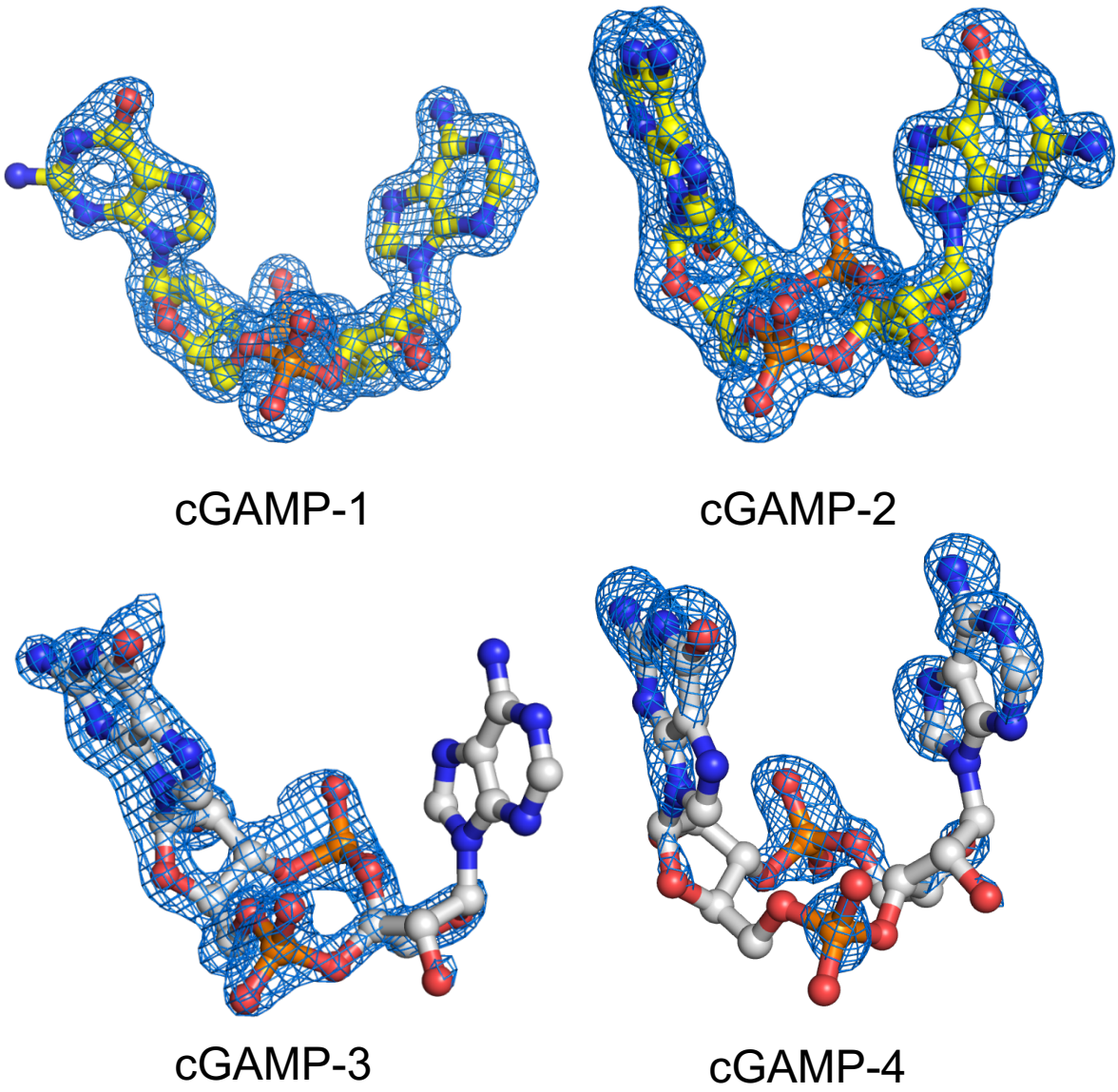

Supporting Figure S5: Fo-Fc omit electron density maps of the four 3‘3‘cAMP molecules bound to DarB. AMP is depicted in ball-stick mode (phosphate: orange, nitrogen: blue, oxygen: red, canonical 3’3’cGAMP: carbon: yellow; non-canonical 3’3’cGAMP: carbon: grey). The mFo-DFc omit electron density map (blue mesh) is contoured at a sigma level of 3.0.

Chapter 5: A crystallographic Fragment Screen unveils three different binding sites on the c-di-AMP synthesizing Enzyme CdaA

This manuscript has not been published

A crystallographic Fragment Screen unveils three different binding sites on the c-di-AMP synthesizing Enzyme CdaA

Jana L. Heidemann[1], Jan Wollenhaupt[2], Piotr Neumann[1], Manfred Weiss[2] and Ralf Ficner[1*]

[1]Department of Molecular Structural Biology, Institute for Microbiology and Genetics, GZMB, Georg-August-University Goettingen, 37077 Goettingen, Germany
[2] Research Group Macromolecular Crystallography, Helmholtz-Zentrum Berlin für Materialien Und Energie, HZB, 12109 Berlin, Germany

* To whom correspondence should be addressed: Ralf Ficner, Department of Molecular Structural Biology, Institute for Microbiology and Genetics, Georg-August-University Göttingen, 37077 Göttingen, rficner@uni-goettingen.de; Tel. +49 551 3914072

Authors contribution

J.L.H.: data curation; formal analysis; validation; writing-original draft;

J.W.: data analysis with PanDDA, PanDDA data validation

R.F.: conceptualization; funding acquisition

A crystallographic Fragment Screen unveils three different binding sites on the c-di-AMP synthesizing Enzyme CdaA

Jana L. Heidemann[1], Jan Wollenhaupt[2], Piotr Neumann[1], Manfred Weiss[2] and Ralf Ficner[1*]

From the [1]Department of Molecular Structural Biology, Institute for Microbiology and Genetics, GZMB, Georg-August-University Goettingen, 37077 Goettingen, Germany

From the [2] Research Group Macromolecular Crystallography, Helmholtz-Zentrum Berlin für Materialien Und Energie, HZB, 12109 Berlin, Germany

* To whom correspondence should be addressed: Ralf Ficner, Department of Molecular Structural Biology, Institute for Microbiology and Genetics, Georg-August-University Göttingen, 37077 Göttingen, rficner@uni-goettingen.de; Tel. +49 551 3914072

5.1 Introduction

In the recent years the importance of developing new antibiotic drugs has increased due to the rising number of multidrug resistant bacterial species. Bacteria are getting less susceptible or completely resistant to antibiotics what reduces the repertoire of available drugs used to control bacterial infections (WHO 2017). According to the German federal government every year 400,000 to 600,000 people become severe bacterial infections in Germany that need to be treated in hospitals. Statistics show that already 10,000 to 15,000 patients die annually due to the lack of effective antibiotics (German Federal Government 2020). One major challenge of antibiotic research is the identification of new targets. A pivotal aspect of a promising target is its conservation and essentiality for the survival of a wide range of bacterial species. Its inhibition should hamper bacterial growth. Furthermore, the lack of structural and functional homology of identified target proteins to proteins of the mammalian host is of great importance in order to avoid side effects as well as to ensure the "drugability" of the chosen target (Silver 2011).

In 2008 the bacterial second messenger cyclic di-AMP (c-di-AMP) was discovered which opened new perspectives in antibiotic research as it fulfills these requirements (Witte et al. 2008). It quickly became clear that c-di-AMP is rather unique compared to other known secondary metabolites. Several studies reported the presence of c-di-AMP in a wide range of different bacterial species, mainly in Gram-positive but in part also Gram-negative bacteria and archaea (Romling 2008; Corrigan R. M. and Gründling 2013). Many of these bacteria are

known to be human pathogens e.g. *Listeria monocytogenes*, *Staphylococcus aureus* or *Mycobacterium tuberculosis* (Woodward et al. 2010; Corrigan et al. 2011; Bai et al. 2012). c-di-AMP is described as the only known essential second messenger in bacteria so far, since it is involved in regulating the bacterial osmolyte and potassium ion homeostasis (Bai et al. 2013; Blötz et al. 2017; Gundlach et al. 2017b; Gundlach et al. 2019). Loss of function mutation in the genes of the c-di-AMP synthesizing enzymes, the diadenylate cyclases (DACs) is lethal to the bacterial cell. Interestingly, DACs are absent in mammalian cells and therefore c-di-AMP cannot be detected in humans (Rosenberg et al. 2015).

DACs catalyze the cyclisation of two ATP molecules into c-di-AMP in a metal ion dependent manner (Witte et al. 2008; Müller et al. 2015). Up to now five different classes of DACs are known, named DisA, CdaA, CdaS, CdaM, and CdaZ (Romling 2008; Corrigan R. M. and Gründling 2013; Blötz et al. 2017; Commichau et al. 2019). All of them share the highly conserved diadenylate cyclase domain (DAC domain) accompanied by different types of regulatory domains (Commichau et al. 2019). Some bacteria like *Bacillus subtilis* carry more than one class of DACs while most bacteria that are known to synthesize c-di-AMP possess only one, either the DAC class DisA or CdaA. The latter is described as the most prevailing DAC domain containing protein among different bacterial species (Commichau et al. 2019).

Three DACs have been structurally characterized, the DNA scanning protein DisA, the membrane bound protein CdaA which is expressed at high extracellular K^+ ion concentration and CdaS which is known to be exclusively expressed during spore germation in the order *Bacillales* (Witte et al. 2008; Corrigan Rebecca M and Gründling 2013; Mehne et al. 2013; Mehne et al. 2014; Rosenberg et al. 2015; Heidemann et al. 2019). Since CdaA is the prevailing DAC it provides a promising starting model for antibiotic research.

CdaA is a membrane bound protein consisting of an N-terminal three α-helical transmembrane domain followed by a linker region connecting the membrane domain and the active cyclase domain. The DAC domain shows an overall globular fold with a central β-sheet of seven parallel and antiparallel β-strands (β1-β7) which is flanked by five α-helices. The active site is formed by α-helix 4, the β-strands 1 and 5 as well as several loops connecting α1 and β1, α3 and β3, α4 and β4, and β5 and β6 (Fig. 1A). In order to form c-di-AMP the two ATP molecules need to be in close vicinity. This is ensured by two with ATP loaded CdaA monomers facing each other (Fig.1B) (Rosenberg et al. 2015; Heidemann et al. 2019). A comparison of DisA and CdaA unveiled differences concerning the accessibility of the active site (Witte et al. 2008; Heidemann et al. 2019). While DisA contains stably associated catalytically active dimers, it was suggested that the active dimer of a CdaA exists only transiently which makes its nucleotide binding site easier accessible to potential inhibiting substances and thus promising target for drug discovery (Heidemann et al. 2019).

A common approach and a powerful tool of drug development is the fragment-based drug discovery which was firstly applied in 1996 (Shuker et al. 1997; Congreve et al. 2008; Schulz et

al. 2011). Those fragments are usually small molecules typically with a molecular mass under 300 Da which allows to cover a broader range of chemical space (Murray and Rees 2009; Barelier et al. 2014; Lamoree and Hubbard 2017).

This is a major difference compared to the approach of high throughput screening where a library is composed of millions of different compounds. In fact, these fragments provide a good starting point for building target specific drug-like compounds. However, since fragments are rather small, they only provide a small attack surface to the protein which leads to weak interactions that are difficult to obtain with conventional crystallographic analysis methods. X-ray crystallography has been used intensively as a sensitive detection method for fragment screening in order to identify weak binders (Congreve et al. 2008; Schiebel et al. 2016). Crystallographic fragment screening copes with the limitation of the weak binding affinities of fragments as high concentrations can be employed during the experiment. As a drawback of crystal lattice averaging, an electron density map of a partially occupied binding sites reveals features corresponding to bound and unbound state. In fact, this may completely obscure the evidence for the ligand bound state or at least makes a distinct identification difficult, if relying on conventional identification methods (Pearce et al. 2017b). In order to overcome the problem of uninterpretable density and to increase the contrast of the signal to noise ratio corresponding to the weakly bound ligand the Pan-Density Dataset Analysis (PanDDA) method was employed. This method is based on the voxel analysis approach requiring multiple crystallographic data sets (Ashburner and Friston 2000; Pearce et al. 2017b). It allows the contrasting of bound and unbound state against each other and enables unveiling of weakly bound ligands or other structural differences. After the identification of a dataset with significant differences, i.e. a potential bound ligand, the superimposed non-bound (ground) state density maps are subtracted from the bound electron density map revealing the partially occupied ligand state. The resulting density map is called event map. The event map represents only the bound state in the crystal which can be used for ligand modeling (Pearce et al. 2017b; Pearce et al. 2017c; Pearce et al. 2017a).

Luckily, in our first study we were able to obtain a new crystal form of apo-CdaA which diffracted to a reasonable resolution and more important the crystal packing seemed suitable for a fragment screening campaign (Heidemann et al. 2019). Two Δ100CdaA molecules are present in the asymmetric unit forming a non-catalytic dimer with outwards facing active sites (Fig. 1C). According to the crystal packing at least the active sites of one CdaA monomer seems to be accessible.

Our crystallographic fragment screening analysis using the PanDDA method unveiled three different ligand binding sites on CdaA which can be used as a starting point for drug design of a novel antibiotic.

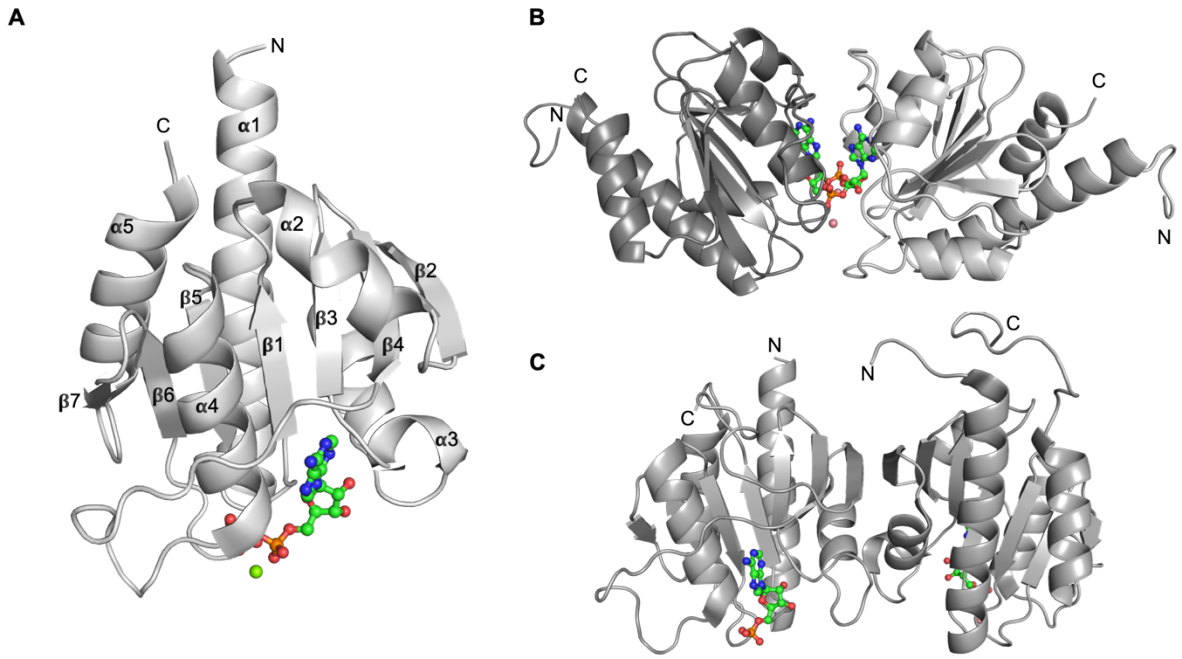

Figure 1: Crystal structure of Δ100CdaA. (A) Overall structure of the truncated Δ100CdaA. CdaA shows an overall globular fold with a slightly twisted β-sheet which is surrounded by 5 α–helices. The protein structure is depicted in cartoon mode in light grey. The bound ATP in the active site is depicted in ball and sticks mode (carbon in green, phosphates in orange, oxygens in red, and nitrogen in blue) (PDB: 4RV7; Rosenberg et al. 2015). **(B)** Representation of a Δ100CdaA dimer in its post-catalytic state with a c-di-AMP bound in the active site. Two face-to-face orientate CdaA nucleotide binding sites are forming the catalytic active dimer. The protein structure is depicted in cartoon mode in light and dark grey. The atoms in c-di-AMP are colour-coded as described for ATP bound structure (PDB: 6HVL; Heidemann et al. 2019). **(C)** Representation of the Δ100CdaA dimer formation in the asymmetric unit. Δ100CdaA shows a non-catalytic dimer with two outwards facing nucleotide binding sites which are antiparallel oriented to each other. The positioning of the active site is marked by two bound AMP molecules. The atoms in AMP are colour-coded as described for ATP (PDB: 6HVM; Heidemann et al. 2019).

5.2 Experimental procedures

5.2.1 Bacterial strains and Growth Conditions

For overexpression of the protein *Escherichia coli* BL21 (DE3) was used. The *E. coli* strain was cultivated in 2 YT medium.

5.2.2 Protein expression and purification

The protein expression and purification were performed according to the published procedure by Heidemann et al. 2019. The construct Δ100CdaA used is equipped with an N-terminal GST-tag and was generated as described before.
The pGEX-6P-1-Δ100CdaA plasmid was transformed into *E. coli* BL21 (DE3) and grown in 1 L 2YT medium at 37 °C. after the cell culture reached an optical density (OD_{600}) of ~ 0.6 the protein expression was induced by adding 1 mM IPTG and incubated over night at 16 °C. The harvested cells were disrupted with a microfluidizer (M-110S Microfluidizer, Microfluidics) and centrifugation at 15.600 xg for 30 min. Subsequent to centrifugation the lysate was loaded onto a Glutathione Sepharose column (GE Healthcare) in 1 M NaCl, 20 mM Tris/HCl pH 7.5, 10 mM EDTA. The GST-tagged target protein was eluted from the column with the addition of 40 mM reduced glutathione. The eluate was incubated over night with PreScission protease (ration 1:100 (w/w)) in a cellulose tubing during dialysis (buffer: 300 mM NaCl, 20 mM Tris/HCl pH 7.5) at 4 °C. In order to sperate the cleaved-off GST-tag from the protein a second glutathione sepharose purification step was included.

5.2.3 Crystallization

The sitting-drop vapour-diffusion method was applied for crystallization. The original published crystallization condition of the apo CdaA form was optimized in order to be more suited for fragment screening (Heidemann et al. 2019). The crystallization trails were performed at 20 °C at a protein concentration of 6 mg/ml Δ*100CdaA* in 2 µl droplets and 1:1 protein-to-reservoir ratio. In order to facilitate crystal growth, micro seeding has been performed. Thin crystal plates were obtained overnight in 3.7 M NaCl, 0.1M Na-HEPES pH 8.5 and 3 % DMSO. The ideal DMSO concentration was determined by preceding stability tests.

5.2.4 Fragment soaking, data collection and structure determination

For fragment screening the two following fragment libraries were used: HZB 96 fragment screen (Helmholz Zentrum Berlin) (Huschmann et al. 2016) and the commercially available Frag Xtal Screen (Jena BioScience). Each fragment screen plate provides 96 different fragments that are spotted in the two protein wells of a crystallization plate. In order to solubilize the dried fragments 0.5 µl crystallization reservoir was pipetted to one of the two wells for each fragment, resulting in nominal fragment concentrations of 100 mM. The second well was supplemented with the saturated sucrose cryo-buffer (Heidemann et al. 2019). The crystallization

plates were sealed with crystallization foil and stored at 20 °C overnight, allowing the fragments to solubilize. Subsequently, two crystals were transferred to each well with solubilized fragment. All crystals were soaked overnight in fragment solution and cryo-protected in the second drop prior to plunging them into liquid nitrogen.
Diffraction images were collected at PETRA III EMBL beamlines P13 and P14 (DESY, Hamburg, Germany) as well as at MASSIF-3 beamline (ESRF, Grenoble, France). All images were automatically processed with the XDS package (Kabsch 2010b; Kabsch 2010a). The processed data were automatically refined by using their customized refinement pipeline (fspipeline, Helmholtz-Zentrum Berlin) (Schiebel et al. 2016). The refined structural models were than used as input for PanDDA (Pearce et al. 2017c). Identified ligands or conformational changes triggered by ligand binding were modeled in an event map and merged with the unbound protein state of the crystal.

5.3 Results and Discussion

A bottle neck of antibiotic research is the identification of new drug targets specific for the causative organism and not for the host. Recent discovery of c-di-AMP opened the field to a potential new class of antibiotics, targeting c-di-AMP synthesizing enzymes which are absent in humans but present in a variety of pathogenic bacteria (Song et al. 2005; Woodward et al. 2010; Corrigan et al. 2011; Bai et al. 2012).
In order to identify molecules that bind to a new potential drug target the approach of fragment screening in combination with X-ray crystallography as a sensitive detection tool is often used. Fragments provide a good starting point to build a target specific drug.
In a previous study we presented a stable crystallization system of apo-Δ100CdaA with reasonable diffracting crystals at around 1.7 Å – 2.2 Å resolution, respectively (Heidemann et al. 2019). In the asymmetric unit two Δ100CdaA monomers are present forming a non-catalytic dimer with two outwards facing active sites. The two active sites are exposed to the solvent making them accessible for fragment binding. However, in one of the two active sites the Tyr^{187} which is known to lock ATP in the binding pocket is blocked by the N-terminus of α-helix 1 of a symmetry mate which could hamper fragment binding.
Two 96-fragment libraries were used for initial screening and around 200 datasets were collected subsequently for 91 individual fragments (Tab. S3). Around 50 % of soaked crystals did not diffract or dissolved during soaking. Two crystals were soaked for each fragment condition. In order to perform a successful fragment screening, it is of great importance to work with high resolution datasets. The distribution of the resolutions of all collected datasets is represented in Figure S1.

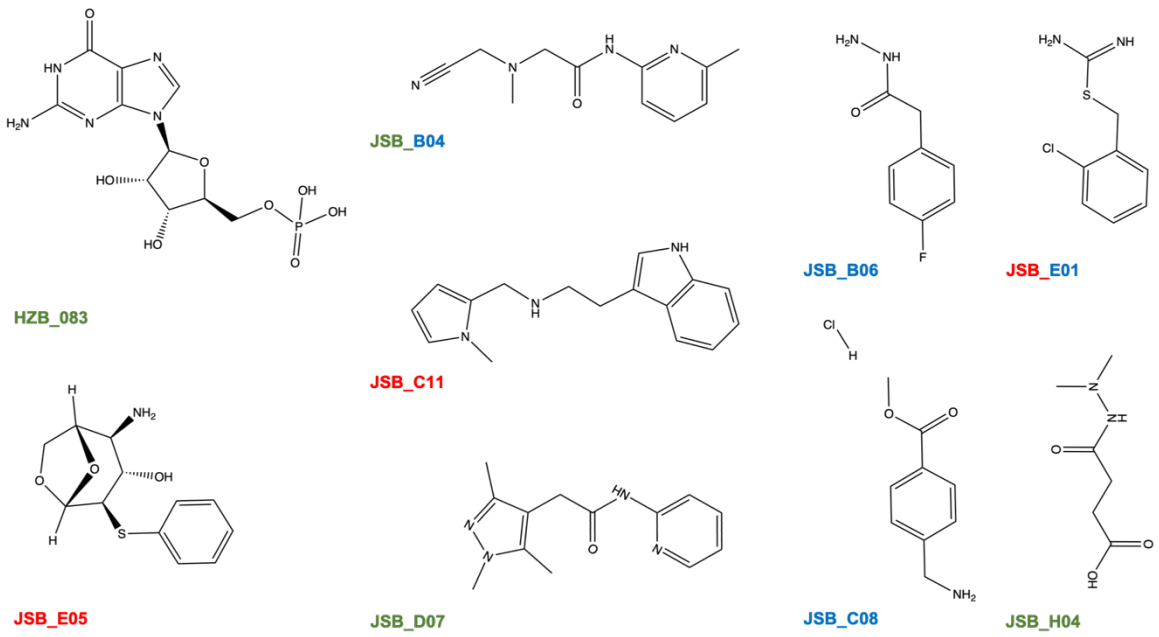

Figure 2: Chemical structures of all fragments. Representation of all fragments that gave a positive signal by data analysis**.** The colours show the positioning of the fragment in one of the 3 binding pockets as seen in figure 3.

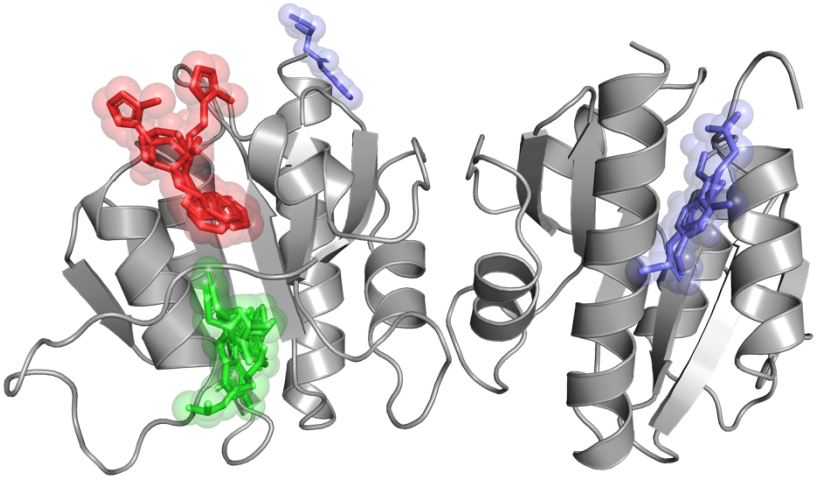

Figure 3: Fragment binding sites. Overall structure of CdaA with three different fragment binding sites highlighted different colours: The first set of fragments is positioned to the nucleotide binding site (green). In close vicinity to the ATP binding pocket the second set of fragments was observed (red). The third set of bound fragments was identified to be bound between the N-terminal α-helix 1 and the C-terminal α-helix 5 (blue).

Following automated refinement with the fspipeline (Schiebel et al. 2016), the output models and maps were submitted to PanDDA using by the PanDDA default settings. Initially only one fragment was identified by the conventional analysis (Fragment E05, Jena BioScience), resulting in a hit rate of about 1 %. By using the PanDDA method the hit rate could be increased by almost a tenfold. Eight additional fragments were identified, increasing the hit rate of unique fragment hits to 10 %. Fragments JBS_B04 and JBS_E01 could be detected at two different binding sites in the protein. The crystallographic data are summarized in table S 1 & 2) and each ligand hit is represented in its chemical structure in figure 3. In summery three different fragment binding site could be identified which are referred to as

binding site I (green), II (red) and III (blue) by using the PanDDA method. With respect to the three binding sites a clear preference is obtained in binding site I and II. Most of the ligands are bound to the upper part of the ATP binding pocket were the purine base is positioned (binding site I) or in the vicinity of the binding site between helix α2 and α4 as well as the loop region β4-α4 (binding site II) (Fig. 1A and 3). A third set of fragments is positioned between the N-terminal α-helix 1 and C-terminal α-helix5 (Fig. 3) which is referred to as binding site III.

In total four unique fragment hits were identified to be bound to the nucleotide binding pocket (binding site I) of CdaA. One of these hits is GMP (Fragment 83, HZB Screen) which is a rather impractical candidate for further drug design since GMP is an intermediate of guanine derived metabolites and thus highly abundant in the cell. However, in case of CdaA the ribose of the GMP molecule is bound at the adenine base binding site of the ATP. Through steric hinderance the purine base of the GMP is not able to bind at the same position as the adenine base of the ATP and protrudes out of the binding pocket (Fig. 4A). It might be worth to check data banks for GMP modifications to test in a subsequent step by *in silico* docking experiments to find binding positions of a modified GMP. Nevertheless, it is indispensable to consider early on that the altered GMP will not bind to GDP or GTP binding pockets of other proteins but specifically binds to CdaA. A higher affinity of a GMP modified follow-up to CdaA might hamper ATP binding as well as the formation of a dimer.

As mentioned previously three further fragments were detected to bind to the nucleotide binding site (B04, D07, H04; Jena Bioscience) (Fig 4 B-F).

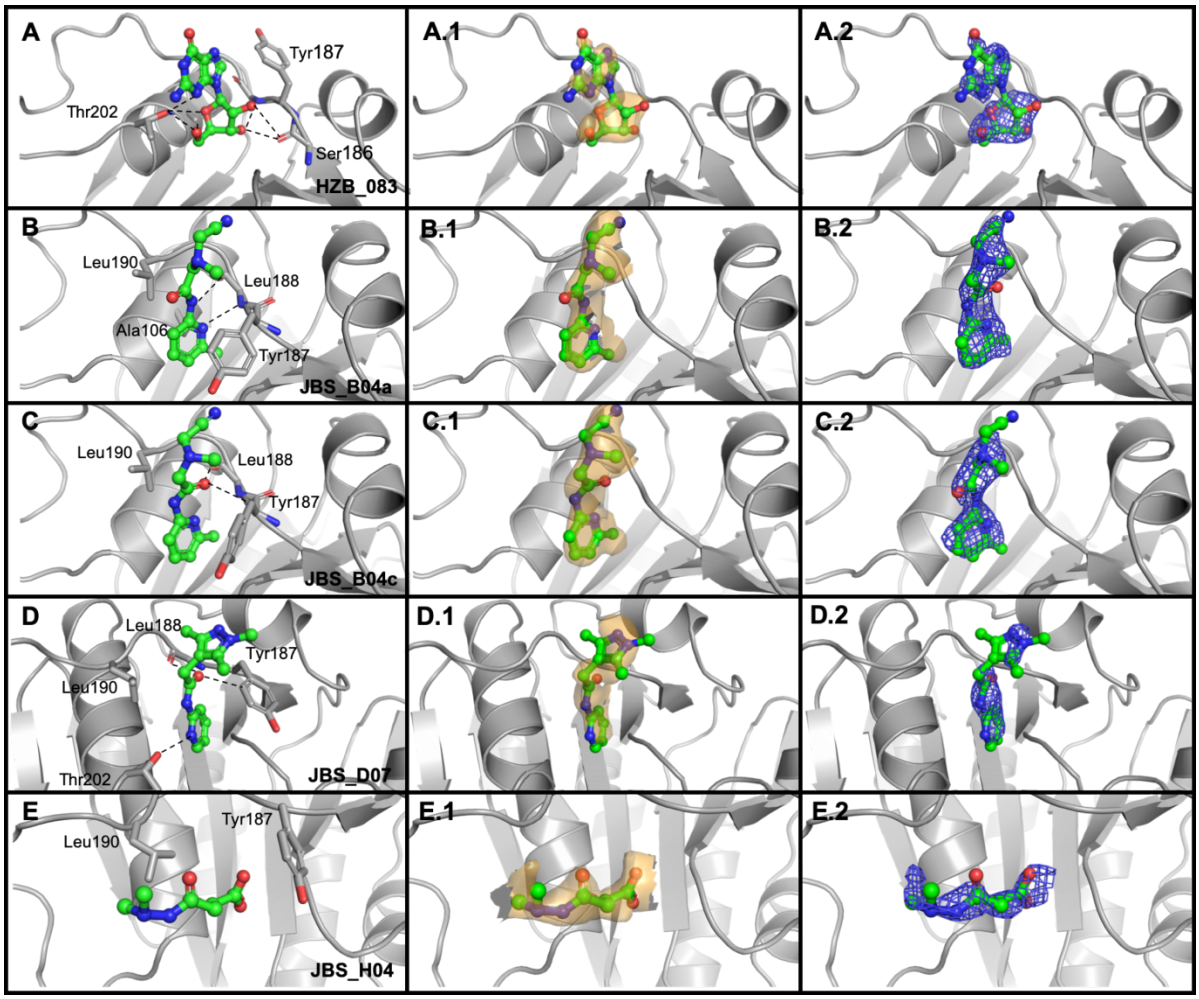

Figure 4: Representation of fragments bound to the nucleotide binding pocket in CdaA and their corresponding results of the Z-scoring approach shown as a map in column one and the PanDDA event map in column 2. The Δ100CdaA structure is depicted as ribbon cartoon (grey) and the bound ligands are represented in balls and sticks (carbon in green, oxygen in red and nitrogen in dark blue). The fragments (HZB_083, JBS_B04a/c, JBS_D07 and JBS_H04) and all amino acids involved in ligand binding are shown in column A-E. Polar interactions to 3.2 Å are marked by dashed lines. Binding of the fragments lead to a conformational change of Tyr^{187} side chain locking the fragment in the binding pocket. Differences to the ground state analysed by the voxel analysis approach are represented as a Z-map (transparent surface representation in light orange, Z=2). The PanDDA event map (blue 2 σ; A.1 BDC=0.14, B.1 BDC= 0.35, C.1 BDC= 0.29, D.1 BDC= 0.4, E.1 BDC= 0.54) shows clear evidence for a bound ligand in the upper part of the ATP binding pocket.

Interestingly two fragments embody an aromatic ring (B04 and D07). In each case this ring is bound to the coordination area of the six-ring of the ATP purine base (Fig. 4 B, C and D). All fragments bound to the nucleotide binding site, except the GMP, lead to a rotation of the tyrosine 187 side chain towards the fragment, locking it in the binding pocket by π–π stacking interaction (Fig. 4B-E). This movement of the tyrosine towards the active site of CdaA was described previously up on ATP binding (Heidemann et al. 2019). That means these fragments

are locked to the active site in the nucleotide binding pocket. All three fragments seem promising to be used for further follow-up compound studies as their binding introduces a conformational change of an essential amino acid for ATP binding. It should also not go unnoticed that this set of fragments do not bind along the ATP or c-di-AMP coordination site (for review ATP or c-di-AMP coordination (Rosenberg et al. 2015; Heidemann et al. 2019)) and are rather pointing out of the binding pocket and thus might block the ability of forming catalytic dimers.

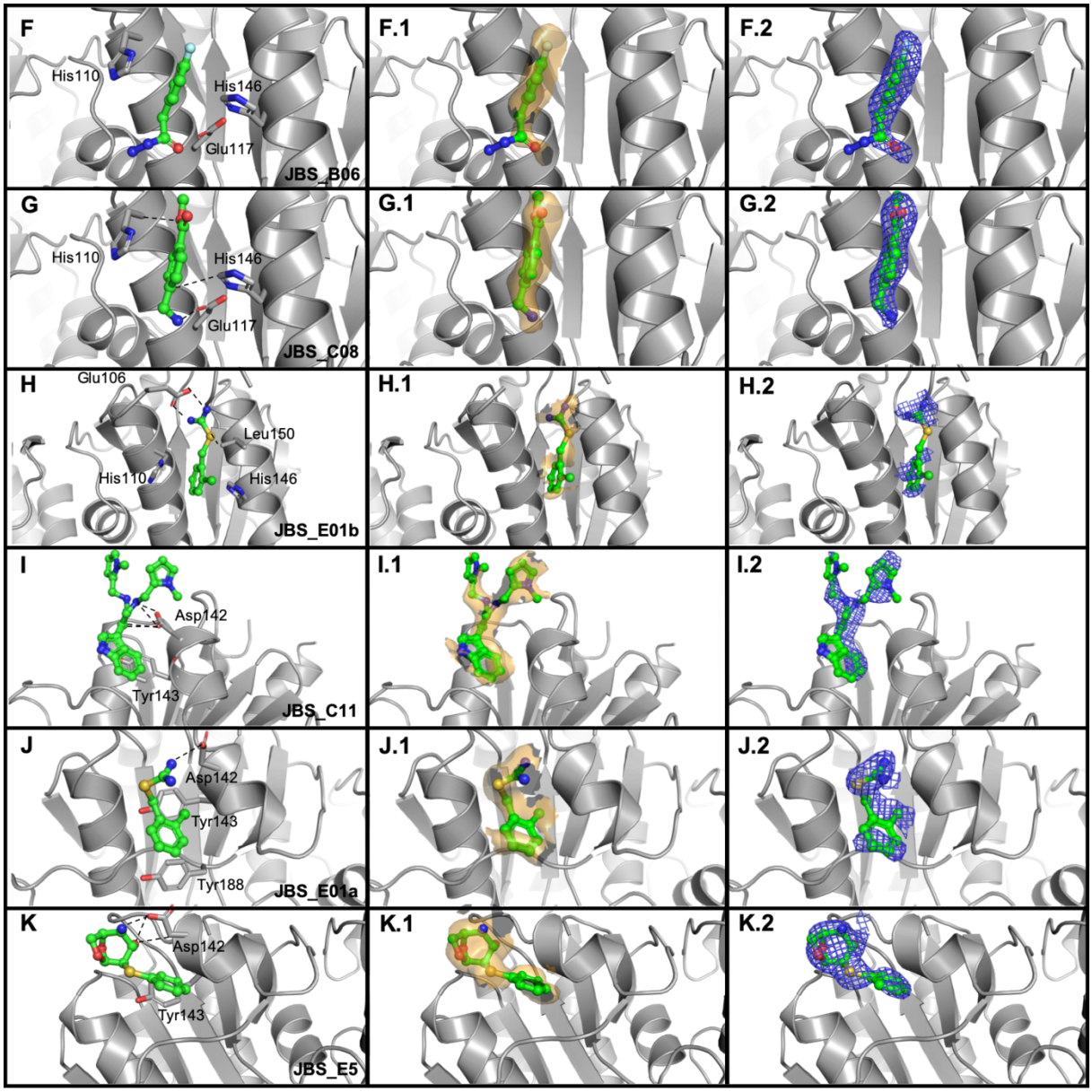

Figure 5: Representation of all Fragments not bound to the nucleotide binding pocket. I-K shows fragments bound in close vicinity to the ATP binding pocket. F-G shows fragments bound via π-stacking between N-terminal α-helix 1 and C-terminal α-helix 2. The corresponding results of the Z-scoring approach are shown as a map representation in column one and the PanDDA "event map" is illustrated in column 2. The Δ100CdaA structure is depicted as ribbon cartoon (grey) and the bound ligands are represented in balls and sticks (carbon in green, oxygen in red and nitrogen in dark blue). Polar interactions to 3.2 Å are marked by dashed lines. Binding of the

fragments lead to a conformational change of Tyr^{187} side chain locking the fragment in the binding pocket. Differences to the ground state analysed by the voxel analysis approach are represented as a Z-map (transparent surface representation in light orange, Z=2). The PanDDA event map (blue 2 σ; F.1 BDC= 0.35, G.1 BDC= 0.40, H.1 BDC= 0.43, I.1 BDC= 0.38, J.1 BDC= 0.50, JK1 BDC= 0.46) shows clear evidence for ligand binding.

In fact, further development could lead to a novel kind of inhibitor that are not based on ATP mimicry which could also help to create a very specific inhibitor with less side effects.
In the lead discovery of fragments there are several ways of proceeding with a hit: for instance, fragment growing, linking and merging. In case of binding site I fragment growth seems to be a suitable approach to follow (GMP, B04, D07, H04, Fig. 4) (Hubbard 2016).
Beside the first binding site, a second fragment binding spot, binding site II (C11, E01, E05; Jena Bioscience) was observed in close vicinity to the ATP binding pocket (Fig. 5 I-K). This binding site is formed by two α-helices, namely α2 and α4 as well as a loop region which embodies amino acids that contribute to nucleotide binding. All three compounds possess a ring structure which are interacting with a tyrosine (Tyr^{143} and Tyr^{187}) of the protein. The ring structure is forming the central scaffold of all three fragments and could form the basis for ligand growth into the active site of CdaA. As described for fragments in binding site I, lead compounds could be built in a way that they either hinder the protein to form active dimers or that they have a strong influence on the catalytic tyrosine which could prevent ATP binding. The ring substituents point towards the N-terminus, away from the active site. An alteration or further growth of the substituents along the protein surface could increase polar interactions which in fact might increase the binding affinity and additionally the target specificity. As already pointed out target specificity is an important aspect to consider in order to reduce the interaction with other human proteins. Inhibition of essential human proteins could result in severe, toxic side effects which should be kept rather small. Due to its positioning this second set of fragments might be suited for both, for individual fragment growth but also fragment linking to the first set of fragments. The ligand binding site I and II are in close vicinity to each other, therefore it might be worth to consider searching for linkers connecting these fragments.
The last set of fragments (binding site III) which were identified by fragment screening are located distant to the active site (B04, B06, C08, E01b) (Fig. 3A (red) and Fig. 5 F-H). While the fragment B04 was described above to be located in the active site of CdaA it was also detected at the N-terminal α-helix 1, entangled by the flexible region (Fig. 3A). It should be kept in mind that the working CdaA construct is a truncated version lacking the N-terminal membrane domain as well as an additional helix linking the membrane domain and the cyclase domain (predicted coiled-coil) (Rosenberg et al. 2015; Heidemann et al. 2019). If the additional helix is present and CdaA is located on the membrane this binding site might be shielded. It is not known what kind of influence the missing part has on the activity of the protein and whether

the fragment would still bind to the full-length CdaA. Therefore, this binding site is probably not the first choice for further optimization.

The additional three fragments (B06, C08, E01b) that are grouped as binding site III are positioned between the N-terminal α-helix 1 and the C-terminal α-helix 5 (Fig. 5 J & H and Fig. 1). The fragment was also described above to bind to binding site II, yet here we are concentrating on binding site III.

If either B06, C08 and E01 bind to the protein a histidine (His^{110}) changes the position of its site chain, interacting with the benzoic ring of the fragments via π–π stacking interaction. In these cases, it might also be difficult to predict the influence of the bound fragments on the protein activity because they are located distant from the active site and the dimeric interface.

A comparison of all bound fragments revealed a certain structural feature on how the fragments are bound to the macromolecule. A key interplay in all cases are π-π aromatic or cation-π interactions which geometrically arrange either in sandwich, T-shaped or parallel displacement formations (Sinnokrot et al. 2002). The availability of ring systems is a common characteristic of commercial drugs and also fragment libraries (Feher and Schmidt 2003; Ertl et al. 2006). Ring systems are often used as central scaffolds as they contribute to the basic shape, rigidity or flexibility of the molecule and keep substituents in their proper position and directly interact with the protein. They can be easily used for further development of lead compounds (Ertl et al. 2006). On the ground of similar scaffolds certain characteristic substituents of different overlaying fragment hits can be merged in order to form a more potent drug compound.

With the results of this first fragment screening with CdaA we are planning to proceed with a follow-up campaign. Subsequent identification of lead compounds a templet-based *in silico* docking experiment will be performed. That means, after selecting larger compounds that share the core structure of the respective fragment hit, these follow-up compounds will be filtered by a docking algorithm which takes the binding pose of the fragment hit as a starting restraint into account. The resulting binding poses will be computationally scored and manually chosen for the next round of crystallographic experiments.

We aim to modify the identified fragments in a way that they will bind with a higher affinity to CdaA and will in the long run influence c-di-AMP synthesis.

References

Ashburner J, Friston KJ (2000): Voxel-based morphometry - The methods. Neuroimage 11, 805–821

Bai Y, Yang J, Zhou X, Ding X, Eisele LE, Bai G (2012): Mycobacterium tuberculosis Rv3586 (DacA) is a diadenylate cyclase that converts ATP or ADP into c-di-amp. PLoS One 7

Bai Y, Yang J, Eisele LE, Underwood AJ, Koestler BJ, Waters CM, Metzger DW, Bai G (2013): Two DHH subfamily 1 proteins in Streptococcus pneumoniae possess cyclic Di-AMP phosphodiesterase activity and affect bacterial growth and virulence. J Bacteriol 195, 5123–5132

Barelier S, Eidam O, Fish I, Hollander J, Figaroa F, Nachane R, Irwin JJ, Shoichet BK, Siegal G (2014): Increasing chemical space coverage by combining empirical and computational fragment screens. ACS Chem Biol 9, 1528–1535

Blötz C, Treffon K, Kaever V, Schwede F, Hammer E, Stülke J (2017): Identification of the components involved in cyclic di-AMP signaling in Mycoplasma pneumoniae. Front Microbiol 8, 1–10

Commichau FM, Heidemann JL, Ficner R, Stülke J (2019): Making and breaking of an essential poison: The cyclases and phosphodiesterases that produce and degrade the essential second messenger cyclic di-AMP in bacteria. J Bacteriol 201, 1–14

Congreve M, Chessari G, Tisi D, Woodhead AJ (2008): Recent developments in fragment-based drug discovery. J Med Chem 51, 3661–3680

Corrigan Rebecca M, Gründling A (2013): Cyclic di-AMP: another second messenger enters the fray. Nat Rev Microbiol 11, 513–24

Corrigan R. M., Gründling A (2013): Cyclic di-AMP: Another second messenger enters the fray. Nat Rev Microbiol 11, 513–524

Corrigan RM, Abbott JC, Burhenne H, Kaever V, Gründling A (2011): C-di-amp is a new second messenger in staphylococcus aureus with a role in controlling cell size and envelope stress. PLoS Pathog 7

Ertl P, Jelfs S, Mühlbacher J, Schuffenhauer A, Selzer P (2006): Quest for the rings. In silico exploration of ring universe to identify novel bioactive heteroaromatic scaffolds. J Med Chem 49, 4568–4573

Feher M, Schmidt JM (2003): Property distributions: Differences between drugs, natural products, and molecules from combinatorial chemistry. J Chem Inf Comput Sci 43, 218–227

Gundlach J, Herzberg C, Kaever V, Gunka K, Hoffmann T, Weiß M, Gibhardt J, Thürmer A, Hertel D, Daniel R, et al. (2017): Control of potassium homeostasis is an essential function of the second messenger cyclic di-AMP in Bacillus subtilis. Sci Signal 10

Gundlach J, Krüger L, Herzberg C, Turdiev A, Poehlein A, Tascón I, Weiss M, Hertel D, Daniel R, Hänelt I, et al. (2019): Sustained sensing in potassium homeostasis: Cyclic di-AMP controls potassium uptake by KimA at the levels of expression and activity. J Biol Chem 294, 9605–9614

Heidemann JL, Neumann P, Dickmanns A, Ficner R (2019): Crystal structures of the c-di-AMP-synthesizing enzyme CdaA. J Biol Chem 294, 10463–10470

Hubbard R. E: Fragment-based Drug Discovery Lessons and Outlook. In: Fragment-based Drug Discovery Lessons and Outlook. Wiley-VCH Verlag GmbH & Co. KGaA, Weinheim 2016, 1–500

Huschmann FU, Linnik J, Sparta K, Ühlein M, Wang X, Metz A, Schiebel J, Heine A, Klebe G, Weiss MS, Mueller U (2016): Structures of endothiapepsin-fragment complexes from crystallographic fragment screening using a novel, diverse and affordable 96-compound fragment library. Acta Crystallogr Sect FStructural Biol Commun 72, 346–355

Kabsch W (2010a): Integration, scaling, space-group assignment and post-refinement. Acta Crystallogr Sect D Biol Crystallogr 66, 133–144
Kabsch W (2010b): XDS. Acta Crystallogr Sect D Biol Crystallogr 66, 125–132
Lamoree B, Hubbard RE (2017): Current perspectives in fragment-based lead discovery (FBLD). Essays Biochem 61, 453–464
Mehne FMP, Gunka K, Eilers H, Herzberg C, Kaever V, Stülke J (2013): Cyclic Di-AMP homeostasis in bacillus subtilis: Both lack and high level accumulation of the nucleotide are detrimental for cell growth. J Biol Chem 288, 2004–2017
Mehne FMP, Schröder-Tittmann K, Eijlander RT, Herzberg C, Hewitt L, Kaever V, Lewis RJ, Kuipers OP, Tittmann K, Stülke J (2014): Control of the diadenylate cyclase CdaS in Bacillus subtilis: An autoinhibitory domain limits cyclic di-AMP production. J Biol Chem 289, 21098–21107
Müller M, Deimling T, Hopfner K-P, Witte G (2015): Structural analysis of the diadenylate cyclase reaction of DNA-integrity scanning protein A (DisA) and its inhibition by 3'-dATP. Biochem J 469, 367–74
Murray CW, Rees DC (2009): The rise of fragment-based drug discovery. Nat Chem 1, 187–192
Pearce NM, Krojer T, Bradley AR, Collins P, Nowak RP, Talon R, Marsden BD, Kelm S, Shi J, Deane CM, Von Delft F (2017a): A multi-crystal method for extracting obscured crystallographic states from conventionally uninterpretable electron density. Nat Commun 8, 24–29
Pearce NM, Bradley AR, Krojer T, Marsden BD, Deane CM, Delft F Von (2017b): Partial-occupancy binders identified by the Pan-Dataset Density Analysis method offer new chemical opportunities and reveal cryptic binding sites. Struct Dyn 4, 1–9
Pearce NM, Krojer T, Von Delft F (2017c): Proper modelling of ligand binding requires an ensemble of bound and unbound states. Acta Crystallogr Sect D Struct Biol 73, 256–266
Romling U (2008): Great times for small molecules: c-di-AMP, a second messenger candidate in Bacteria and Archaea. Sci Signal 1, pe39
Rosenberg J, Dickmanns A, Neumann P, Gunka K, Arens J, Kaever V, Stülke J, Ficner R, Commichau FM (2015): Structural and biochemical analysis of the essential diadenylate cyclase CdaA from Listeria monocytogenes. J Biol Chem 290, 6596–6606
Schiebel J, Krimmer SG, Röwer K, Knörlein A, Wang X, Park AY, Stieler M, Ehrmann FR, Fu K, Radeva N, et al. (2016): High-Throughput Crystallography: Reliable and Efficient Identification of Fragment Hits. Structure 24, 1398–1409
Schulz MN, Fanghänel J, Schäfer M, Badock V, Briem H, Boemer U, Nguyen D, Husemann M, Hillig RC (2011): A crystallographic fragment screen identifies cinnamic acid derivatives as starting points for potent Pim-1 inhibitors. Acta Crystallogr Sect D Biol Crystallogr 67, 156–166
Shuker SB, Hajduk PJ, Meadows RP, Fesik SW (1997): Discovering high-affinity ligands for proteins: SAR by NMR. Science (80-) 274, 1531–1534
Silver LL (2011): Challenges of antibacterial discovery. Clin Microbiol Rev 24, 71–109
Sinnokrot MO, Valeev EF, Sherrill CD (2002): Estimates of the Ab Initio limit for π-π Interactions: The Benzene Dimer. J Am Chem Soc 124, 10887–10893
Song JH, Ko KS, Lee JY, Baek JY, Oh WS, Yoon HS, Jeong JY, Chun J (2005): Identification of essential genes in Streptococcus pneumoniae by allelic replacement mutagenesis. Mol Cells 19, 365–374
Witte G, Hartung S, Büttner K, Hopfner KP (2008): Structural Biochemistry of a Bacterial Checkpoint Protein Reveals Diadenylate Cyclase Activity Regulated by DNA Recombination Intermediates. Mol Cell 30, 167–178
Woodward JJ, Lavarone AT, Portnoy DA (2010): C-di-AMP secreted by intracellular Listeria monocytogenes activates a host type I interferon response. Science (80-) 328, 1703–

A crystallographic Fragment Screen unveils three fragment binding sites for the c-di-AMP synthesizing Enzyme CdaA

Jana L. Heidemann[1], Jan Wollenhaupt[2], Piotr Neumann[1], Manfred Weiss[2] and Ralf Ficner[1*]

Supporting Information

Table S1: Crystallographic data collection and refinement statistics

	Δ100CdaA-GMP	**Δ100CdaA-B04a**	**Δ100CdaA-B04c**	**Δ100CdaA-B06**	**Δ100CdaA-C08**	**Δ100CdaA-C11**
Crystallographic data						
Beamline	Petra III-P13, EMBL, Hamburg	MASSIF-3, ESRF, Grenoble	MASSIF-3, ESRF, Grenoble	Petra III-P13, EMBL, Hamburg	Petra III-P13, EMBL, Hamburg	Petra III-P13, EMBL, Hamburg
Wavelength (Å)	0.97625	0.96770	0.96770	0.97625	0.97625	0.97625
Resolution range (Å)[a]	45.76-1.76 (1.86-1.76)	45.54-2.38 (2.48-2.38)	40.56-1.99 (2.09-1.99)	45.7-1.94 (2.04-1.94)	45.70-2.17 (2.27-2.17)	45.63-2.17 (2.27-2.17)
Unique reflections	35112	14055	25538	26642	19433	18986
Redundancy	6.5 (6.7)	7.4 (6.5)	8.2 (8.6)	7.9 (8.3)	8.0 (8.2)	12.9 (13.5)
Completeness (%)	98.1 (97.4)	96.2 (94.9)	99.6(99.9)	99.4 (99.0)	99.8 (99.8)	99.8 (99.6)
Space group	$P2_12_12_1$	$P2_12_12_1$	$P2_12_12_1$	$P2_12_12_1$	$P2_12_12_1$	$P2_12_12_1$
a (Å)	41.970	41.700	42.690	41.660	42.250	41.130
b (Å)	64.680	64.460	64.850	64.750	64.920	64.710
c (Å)	129.520	128.690	129.980	129.060	128.700	128.710
R_{merge} (%)	3.7 (94.1)	13.0 (120.8)	10.4 (140.2)	5.3 (56.1)	6.2 (71.1)	4.7 (30.3)
I/σ (I)	2.4 (25.3)	1.9 (12.9)	1.8 (16.0)	4.94 (20.09)	3.6 (19.87)	9.52 (30.85)
$CC_{1/2}$	99.9 (87.3)	99.7 (64.3)	99.9 (73.9)	99.9 (96.5)	100.0 (95.0)	99.9 (99.5)
Refinement statistics						
R_{work}/R_{free}	0.1920 /0.2290	0.2188/ 0.2885	0.1951/ 0.2609	0.2432/ 0.2863	0.2032/ 0.2611	0.1942/ 0.2686
Root mean square deviation						
Bonds Å	0.010	0.014	0.011	0.012	0.012	0.011
Angles (degree)	1.047	1.473	1.104	1.281	1.184	1.189

Table S2: Crystallographic data collection and refinement statistics

	Δ100CdaA-D07	Δ100CdaA-E01a	Δ100CdaA-E01b	Δ100CdaA-E05	Δ100CdaA-H04
Crystallographic data					
Beamline	Petra III-P13, EMBL, Hamburg	MASSIF-3, ESRF, Grenoble	MASSIF-3, ESRF, Grenoble	MASSIF-3, ESRF, Grenoble	MASSIF-3, ESRF, Grenoble
Wavelength (Å)	0.97625	0.96770	0.96770	0.96770	0.96770
Resolution range (Å)[a]	46.045-2.393(-2.393)	38.50-2.076(2.18-2.08)	45.84-1.99(2.09-1.99)	39.72-1.73 (1.83-1.73)	45.61-1.83(1.93-1.83)
Unique reflections	15518	21084	23622	37303	32944
Redundancy	13.0 (13.4)	8.1 (8.5)	8.2 (8.6)	8.3 (8.6)	8.3 (8.7)
Completeness (%)	99.9 (100.0)	98.68 (98.7)	99.7 (99.8)	99.5 (99.1)	99.9 (99.9)
Space group	$P2_12_12_1$	$P2_12_12_1$	$P2_12_12_1$	$P2_12_12_1$	$P2_12_12_1$
a (Å)	44.220	40.320	39.79	41.750	43.740
b (Å)	65.070	64.810	64.65	64.710	64.110
c (Å)	130.330	129.580	130.02	129.040	129.790
R_{merge} (%)	8.9(89.9)	8.2 (199.1)	8.6(281.1)	5.5 (183.2)	5.5 (165.0)
I/σ (I)	3.73 (19.70)	1.4 (17.6)	1.02 (15.8)	1.5 (19.0)	1.4 (18.9)
$CC_{1/2}$	99.9 (95.3)	100.0 (69.7)	100.0 (61.1)	99.9 (78.5)	99.8 (75.4)
Refinement statistics					
R_{work}/R_{free}	0.2302/0.2985	0.2635/0.3340	0.3143/0.3473	0.2184/0.2670	0.2157/0.2616
Root mean square deviation					
Bonds Å	0.014	0.014	0.014	0.010	0.010
Angles (degree)	1.456	1.438	1.613	1.119	1.141

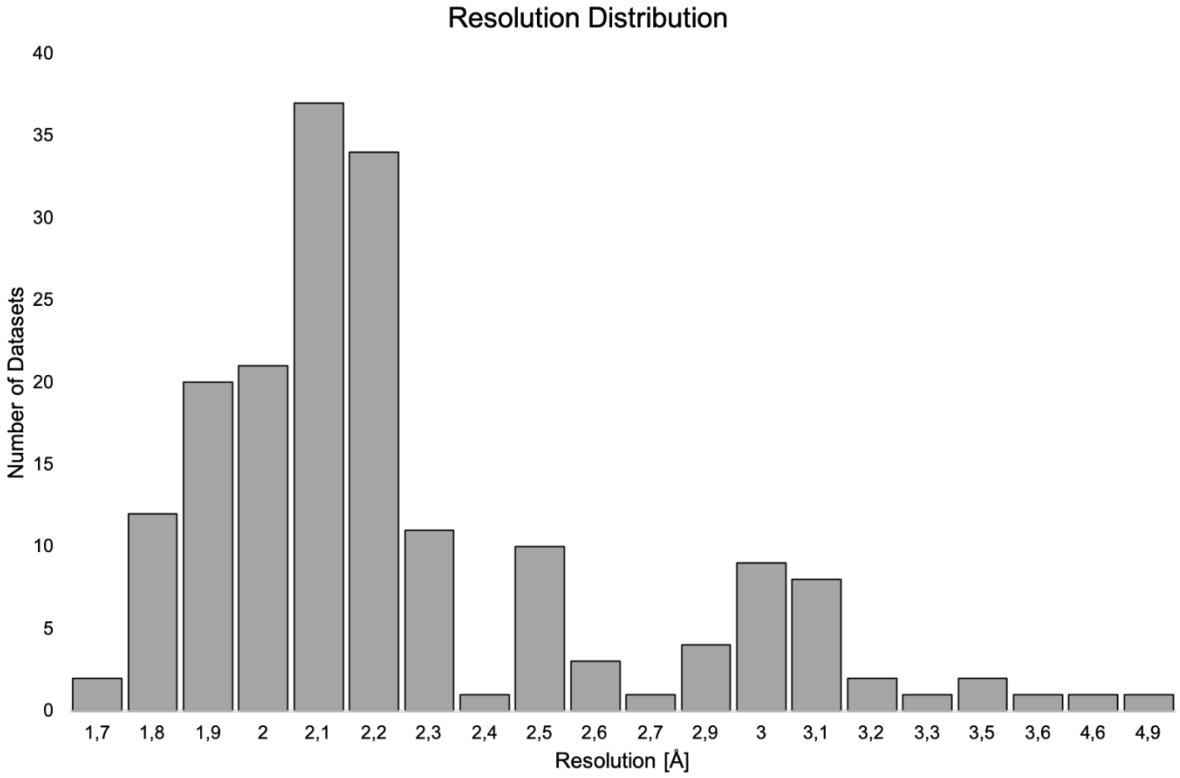

Supporting Figure S1: Histogram showing resolution distribution of all dataset. 69.6 % of all collected datasets show reasonable diffraction between 1.7 and 2.2 Å resolution.

Table S3: Overview of all collected data sets.

1	Fragment #	Name	X-ray data resolution	Complet-ness X-ray data R-sym (Rmerge)	Structure Rwork / Rfree	Directory final pdb & mtz
2	B01 1H-Pyrazole- 5-methanamine, 1,3-dimethyl	cdaA-Y009_B01_2_1_076.pdb	2.072 [A]	99.3% 9.8%	0.2143 0.2421	/people/jana/LIGANDS_IX-2018 /people/jana/LIGANDS-ESRF_XI-2018-NEU_REFINEMENT /people/jana/LIGANDS-HAMBURG-07-12-2018
3	F03 1H-Purine-2,6-dione, 3,7-dihydro-3,7-dimethyl-	cdaA-Y036_F03_w1_1_1_064.pdb	3.121 [A]	99.7% 31.4%	0.2261 0.2571	
4	E01 Carbamimidothioic acid, (2-chlorophenyl) methyl ester	cdaA-Y017_E01_1_1_712.pdb	2.076 [A]	98.8% 7.7%	0.2235 0.2454	
5	H03 Methionine, N-(aminocarbonyl)	cdaA-Y025_H03_1_1_052.pdb	2.388 [A]	99.9% 9.4%	0.2248 0.2442	
6	C01	cdaA-Y013_C01_	1.978 [A]	99.9% 7.3%	0.2138 0.2375	

	3- Pyridinecarbonitrile , 4, 6- dimethyl- 2- [[3- (4- morpholinyl) propyl] amino]	2_1_711.pdb				
7	G01 1H- Thieno[3, 4- d] imidazole- 6- pentanoic acid, 2- amino 3a, 4, 6, 6a- tetrahydro- , (3a R, 6S, 6aS)	cdaA-Y021_G01_1_1_712.pdb	1.877 [A]	95.5% 9.0%	0.2296 0.2600	
8	C03 1, 3, 5- Triazine- 2, 4- diamine, 6- [1- (hexahydro- 1H- azepin- 1-yl) ethyl] - N2, N2- dimethyl-	cdaA-Y031_C03_1_1_061.pdb	1.914 [A]	99.5% 7.9%	0.2184 0.2429	
9	D01 1H- Imidazole- 2- methanamine, N, 1- dimethyl	cdaA-Y014_D01_2_1_072.pdb	3.538 [A]	90.3% 15.0%	0.3428 0.3892	
10	E04 1H-Imidazole-1- acetamide, N-(4- methylcyclohexyl)	cdaA-Y045_E04_1_1_512.pdb	1.835 [A]	99.9% 8.1%	0.2242 0.2520	

11	A05 4- Morpholine-ethanamine , β-ethyl- β-methyl	cdaA-Y052_A05_1_1_065.pdb	1.669 [A]	99.3% 5.7%	0.2388 0.2613	
12	E05 INDEX NAME NOT YET ASSIGNED	cdaA-Y059_E05_1_1_065.pdb	1.818 [A]	98.9% 6.0%	0.2092 0.2442	
13	B04 Acetamide, 2-[(cyanomethyl) methylamino]- N- (6- methyl- 2-pyridinyl)	cdaA-Y027_B04_2_1_042.pdb	2.381 [A]	97.2% 31.4%	0.2469 0.2913	
14	B01 1H-Pyrazole- 5-methanamine, 1,3-dimethyl	cdaA-Y010_B01_w1_1_1_065.pdb	1.880 [A]	99.4% 7.8%	0.2315 0.2650	
15	E01 Carbamimidothioic acid, (2-chlorophenyl)methyl ester	cdaA-Y018_E01_1_1_065.pdb	1.994 [A]	99.7% 8.1%	0.2348 0.2579	
16	C05 3-Thiophenecarboximidamide, hydrochloride (1:1)	cdaA-Y055_C05_w1_2_1_065.pdb	2.233 [A]	99.1% 12.9%	0.3732 0.4138	
17	G04 L-Proline, 5-oxo-	cdaA-Y038_G04_	1.949 [A]	99.3% 6.3%	0.2055 0.2243	

		_00_065.pdb				
18	C04 3-Pyridineethanamine	cdaA-Y042_C04_1_1_512.pdb	2.377 [A]	91.3% 12.5%	0.2091 0.2505	
19	F05 Benzoic acid, 4-nitro-	cdaA-Y061_F05_2_1_025.pdb	2.972 [A]	99.9% 21.7%	0.2453 0.2695	
20	D03 Cyclohexanecarboxamide, N-[(tetrahydro-2-furanyl)methyl]	cdaA-Y035_D03_1_1_064.pdb	2.010 [A]	99.3% 9.4%	0.2264 0.2507	
21	F04 6H-Purin-6-one, 2-amino-1,9-dihydro	cdaA-Y046_F04_1_1_711.pdb	1.892 [A]	99.7% 7.0%	0.2242 0.2541	
22	A03 Thiourea, N- (4-bromo- 2-chloro-phenyl) - N'- methyl	cdaA-Y006_A03_w1_1_1_043.pdb	2.170 [A]	98.9% 18.1%	0.2412 0.2756	
23	F01 L-Histidine, 1-methyl	cdaA-Y011_F01_2_1_064.pdb	2.078 [A]	98.4% 6.2%	0.2193 0.2415	
24	D05 3-Pyridinecarboxylic acid, 6-(dimethylamino)	cdaA-Y057_D05_1_1_066.pdb	2.012 [A]	99.0% 5.7%	0.2102 0.2384	
25	E03 Furo[2,3-d]pyrimidine-3(4H)-	cdaA-Y024_E03_1_1_712.pdb	1.830 [A]	99.3% 7.8%	0.1971 0.2288	

	propana-mine, 4-imino-N,N,5,6-tetrame-thyl					
26	C01 3- Pyri-dinecar-bonitrile , 4, 6-dimethyl-2-[[3- (4-mor-pholinyl) propyl] amino]	cdaA-Y012_C01_2_1_042.pdb	2.078 [A]	99.7% 10.9%	0.2121 0.2538	
27	E05 INDEX NAME NOT YET AS-SIGNED	cdaA-Y059_E05_2_1_041.pdb	1.727 [A]	99.1% 5.2%	0.2218 0.2451	
28	B03 Benzoic acid, 2-hydroxy-, compd. with N, N –diethyl-ethanimid-amide (1:1)	cdaA-Y004_B03_1_1_043.pdb	2.100 [A]	99.3% 9.2%	0.2684 0.3145	
29	B04 Acetam-ide, 2-[(cy-anome-thyl) me-thylamino] - N- (6- me-thyl- 2-pyridinyl)	cdaA-Y027_B04_1_1_045.pdb	2.379 [A]	96.2% 12.0%	0.2133 0.2364	
30	B01 1H-Pyra-zole- 5-	cdaA-Y009_B01_1_1_041.pdb	2.077 [A]	99.2% 12.6%	0.2643 0.3142	

	methana-mine, 1, 3- dime-thyl					
31	C01 3- Pyri-dinecar-bonitrile , 4, 6-dimethyl-2- [[3- (4-mor-pholinyl) propyl] amino]	cdaA-Y012_C01_1_1_712.pdb	2.095 [A]	99.7% 11.0%	0.2217 0.2372	
32	A05 4- Mor-pholine-ethana-mine , β-ethyl- β-methyl	cdaA-Y051_A05_w1_1_1_065.pdb	1.788 [A]	93.9% 7.1%	0.2637 0.2739	
33	D04 4(3H)-Quinazoli-none, 2-[[(1-cyclopro-pylethyl)methylamino]methyl]	cdaA-Y044_D04_w1_1_1_043.pdb	1.992 [A]	99.1% 11.2%	0.2167 0.2458	
34	G04 L-Proline, 5-oxo-	cdaA-Y023_G04_1_1_712.pdb	1.899 [A]	99.8% 6.8%	0.2185 0.2555	
35	D03 Cyclohex-anecar-boxamide, N-[(tetrahy-dro-2-furanyl)methyl]	cdaA-Y034_D03_w1_1_1_044.pdb	1.845 [A]	99.9% 6.5%	0.2164 0.2304	
36	C05 3-	cdaA-Y054_C05_1_1_025.pdb	3.298 [A]	99.8% 21.9%	0.3464 0.3810	

	Thiophenecarboximidamide, hydrochloride (1:1)					
37	C03 1, 3, 5-Triazine-2, 4- diamine, 6-[1- (hexahydro-1H- azepin- 1-yl) ethyl] -N2, N2-dimethyl	cdaA-Y030_C03_1_1_063.pdb	2.076 [A]	99.3% 10.8%	0.2211 0.2564	
38	F05 Benzoic acid, 4-nitro	cdaA-Y060_F05_w1_1_1_064.pdb	1.973 [A]	97.8% 7.7%	0.2522 0.2666	
39	C1 3- Pyridinecarbonitrile , 4, 6-dimethyl-2- [[3- (4-morpholinyl) propyl] amino]	cdaA-Y013_C01_1_1_042.pdb	2.526 [A]	99.7% 8.8%	0.2260 0.2612	
40	H03 Methionine, N-(aminocarbonyl)	cdaA-Y026_H03_2_1_044.pdb	2.376 [A]	99.5% 22.3%	0.3675 0.3834	
41	E05 INDEX NAME NOT YET ASSIGNED	cdaA-Y058_E05_w1_1_1_044.pdb	1.755 [A]	99.9% 5.6%	0.2274 0.2467	
42	G04 L-Proline, 5-oxo	cdaA-Y038_G04_w1_1_1_065.pdb	1.949 [A]	99.3% 6.3%	0.2055 0.2243	

43	H03 Furo[2,3-d]pyrimidine-3(4H)-propanamine, 4-imino-N,N,5,6-tetramethyl	cdaA-Y026_H03_1_1_034.pdb	2.102 [A]	99.8% 13.9%	0.2754 0.3062	
44	C03 1, 3, 5-Triazine-2, 4- diamine, 6-[1- (hexahydro-1H- azepin- 1-yl) ethyl] - N2, N2-dimethyl	cdaA-Y030_C03_2_1_065.pdb	2.096 [A]	98.6% 13.5%	0.3147 0.3383	
45	B01 1H-Pyrazole- 5-methanamine, 1, 3- dimethyl-	cdaA-Y010_B01_w1_2_1_044.pdb	2.183 [A]	99.2% 8.5%	0.2209 0.2529	
46	C04 3-Pyridineethanamine	cdaA-Y041_C04_w1_1_1_066.pdb	3.120 [A]	95.7% 16.7%	0.2448 0.2784	
47	H04 Butanedioic acid, 1-(2,2-dimethylhydrazide)	cdaA-Y050_H04_1_1_043.pdb	1.832 [A]	99.9% 5.1%	0.2222 0.2429	
48	B04 Acetamide, 2-[(cyanomethyl) methylamino] -	cdaA-Y028_B04_1_1_062.pdb	1.989 [A]	99.6% 9.7%	0.2136 0.2398	

	N- (6- methyl- 2-pyridinyl)					
49	G5 D-Arginine	cdaA-Y062_G05_1_1_512.pdb	2.080 [A]	96.4% 5.5%	0.2233 0.2594	
50	A03 Thiourea, N- (4-bromo- 2-chloro-phenyl) - N'- methyl	cdaA-Y006_A03_w1_2_1_046.pdb	2.088 [A]	99.1% 11.5%	0.2220 0.2476	
51	H01 Benzamide, 3-amino	cdaA-Y020_H01_1_1_064.pdb	2.496 [A]	99.0% 9.0%	0.2339 0.2655	
52	E03 Furo[2,3d] pyrimidine-3(4H)-propanamine, 4-imino-N,N,5,6-tetramethyl	cdaA-Y024_E03_2_1_066.pdb	1.769 [A]	99.3% 7.9%	0.2151 0.2258	
53	H04 Butanedioic acid, 1-(2,2-dimethylhydrazide)	cdaA-Y049_H04_1_1_512.pdb	2.421 [A]	99.0% 10.4%	0.2258 0.2459	
54	E04 1H-Imidazole-1-acetamide, N-(4-methylcyclohexyl)	cdaA-Y043_E04_w1_1_1_064.pdb	1.986 [A]	95.4% 8.8%	0.2097 0.2510	
55	D01 1H- Imidazole- 2-	cdaA-Y016_D01_1_1_064.pdb	2.467 [A]	98.6% 9.2%	0.2220 0.2543	

	methana-mine, N, 1- di-methyl					
56	G01 1H-Thieno[3, 4- d]imid-azole- 6-pentanoic acid, 2-amino-3a, 4, 6, 6a-tetrahy-dro-, (3aR, 6S, 6aS)	cdaA-Y022_G01_1_1_065.pdb	2.399 [A]	98.3% 12.0%	0.2452 0.2920	
57	F05 Benzoic acid, 4-ni-tro	cdaA-Y061_F05_1_1_112.pdb	2.974 [A]	99.5% 22.7%	0.2515 0.2871	
58	G01 1H-Thieno[3, 4- d]imid-azole- 6-pentanoic acid, 2-amino-3a, 4, 6, 6a-tetrahy-dro- , (3aR, 6S, 6aS)	cdaA-Y021_G01_2_1_075.pdb	1.913 [A]	95.0% 7.3%	0.2563 0.2807	
59	G04 L-Proline, 5-oxo	cdaA-Y029_G04_1_1_064.pdb	2.071 [A]	95.9% 17.8%	0.2959 0.3074	
60	D01 1H- Imid-azole- 2-methana-mine, N, 1- di-methyl	cdaA-Y014_D01_1_1_062.pdb	2.713 [A]	97.4% 31.5%	0.3228 0.3440	
61	D01 1H-Imidazole-2-meth-anamine,	cdaA-Y015_D01_2_1_042.pdb	2.385 [A]	99.6% 24.1%	0.2805 0.3266	

	N, 1- di-methyl					
62	B12 2- Thio-phenebu-tanamide, γ-oxo- N-[1- (3- pyr-idinyl) ethyl]	CdaA-Y053_B12_w1_1_0a_022.pdb	2.193 [A]	99.8% 5.4%	0.2237 0.2811	
63		CdaA-Y042_w1_1_0a_512.pdb	2.195 [A]	99.7% 5.4%	0.2028 0.2309	
64	A11 Imidazo[2, 1- c] [1, 2, 4] triazine, 3- (3, 4-difluoro-phenyl) - 1, 4, 6, 7-tetrahydro	CdaA-0085_A11_w1_1_0b_043.pdb	3.123 [A]	90.5% 16.7%	0.2921 0.3494	
65	G06 Glycine, glycyl-glycyl	CdaA-Y091_G06_w1_1_0a_033.pdb	2.413 [A]	99.9% 7.2%	0.2013 0.2370	
67	Suramin	CdaA-Y065_SU-RAMIN_w1_1_0a_042.pdb	2.496 [A]	99.7% 8.3%	0.2491 0.2810	
68	A02 1H-Isoin-dol-3-amine	CdaA-Y068_A02_w1_1_0a_023.pdb	4.622 [A]	94.0% 10.8%	0.2924 0.3169	
69	D02 Imid-azo[1,2-a]pyri-dine-2-acetamide, N-phenyl	CdaA-Y071_D02_w1_1_0a_044.pdb	2.371 [A]	98.5% 5.2%	0.1897 0.2355	
70	H02 Cyclohex-anecar-boxylic acid,	CdaA-G002_H02_1_0b_021.pdb	4.876 [A]	99.5% 8.3%	0.1920 0.2440	

	4-(aminomethyl)-, trans					
71	F08 Imidazo[4,5-d]imidazole-2,5(1H,3H)-dione, tetrahydro	CdaA-Y011_F08_w1_1_0a_511.pdb	2.190 [A]	99.8% 6.6%	0.2334 0.2760	
72	H11 3- Furancarboxamide, tetrahydro	CdaA-Y049_H11_w1_1_0a_044.pdb	2.168 [A]	99.9% 5.8%	0.2166 0.2562	
73	F02 L-Phenylalanine, methyl ester, hydrochloride (1:1)	CdaA-Y076_F02_1_0b_063.pdb	2.946 [A]	99.0% 24.5%	0.3730 0.4251	
74	E02 6H-Purin-6-one, 1,9-dihydro-8-(1-piperidinyl)	CdaA-Y074_E02_1_0b_062.pdb	2.374 [A]	98.4% 5.7%	0.2206 0.2566	
75	F07 Pentanoic acid, 5-amino	CdaA-Y101_F07_w1_1_0a_064.pdb	3.019 [A]	99.6% 5.6%	0.2079 0.2360	
76	E02 6H-Purin-6-one, 1,9-dihydro-8-(1-piperidinyl)	CdaA-Y073_E02_1_0b_065.pdb	2.135 [A]	99.4% 5.3%	0.2023 0.2246	
77	C10 Guanidine, N- (4- ethoxy- 8-methyl- 2-quinazolinyl)	CdaA-Y032_C10_w1_1_0a_063.pdb	2.273 [A]	99.8% 4.3%	0.2024 0.2307	

78	C11 1H-Indole-3-ethanamine, N-[(1-methyl-1H-pyrrol-2-yl)methyl]-	CdaA-Y045_C11_w1_1_0a_512.pdb	2.167 [A]	99.8% 4.5%	0.2062 0.2427	
79	A02 1H-Isoindol-3-amine	CdaA-Y065_A02_1_0b_511.pdb	2.951 [A]	99.9% 6.1%	0.1978 0.2427	
80	B11 1-Piperidineacetamide, 4-methyl-N-[3-(1-methylethyl)-5-isoxazolyl]	CdaA-0087_B11_w1_1_0b_073.pdb	2.383 [A]	99.8% 8.9%	0.2226 0.2704	
81	H02 Cyclohexanecarboxylic acid, 4-(aminomethyl)-, trans	CdaA-Y078_H02_1_0b_042.pdb	2.375 [A]	99.4% 4.8%	0.1976 0.2272	
82	C09 Benzenecarboximidamide, 4-(trifluoromethyl)	CdaA-Y017_C09_w1_2_0a_045.pdb	2.188 [A]	99.8% 5.6%	0.2179 0.2454	
83	E10 1, 2, 4-Oxadiazole, 3-(1-methylethyl)-5-(2-pyrrolidinyl)	CdaA-Y036_E10_w1_2_0a_711.pdb	3.553 [A]	98.5% 9.2%	0.2305 0.2744	

84	B11 1- Piperi-dine-acet-amide, 4-methyl- N-[3- (1-meth-ylethyl)-5- isoxa-zolyl]	CdaA-Y043_B11_1_0b_312.pdb	1.957 [A]	99.7% 3.7%	0.2097 0.2397	
85	B10 3- Isoxa-zole-car-boxamide , 5-methyl-N- (2, 2, 2-trifluoro-ethyl)	CdaA-Y031_B10_w1_1_0a_064.pdb	2.522 [A]	99.1% 6.9%	0.2542 0.2836	
86	G02 1,2-Ben-zenediol, 4-[(1R)-2-amino-1-hydroxy-ethyl]	CdaA-Y077_G02_1_0b_112.pdb	2.941 [A]	98.8% 6.1%	0.2034 0.2389	
87	G07 3H-1,2,3-Tria-zolo[4,5-d]pyrimi-dine-5,7(4H,6H)-dione	CdaA-Y103_G07_1_0a_045.pdb	2.217 [A]	97.8% 6.3%	0.2233 0.2544	
89	D07 1H-Pyra-zole-4-ac-etamide, 1,3,5-tri-methyl-N-2-pyridi-nyl	CdaA-Y097_D07_w1_1_0a_711.pdb	2.393 [A]	99.9% 8.5%	0.2141 0.2329	
90	H12 Bicy-clo[2.2.1] heptane-1-carbox-amide,	CdaA-00812_H12_w1_1_0b_061.pdb	2.216 [A]	99.5% 7.4%	0.2216 0.2400	

	N- hydroxy					
91	D10 Acetamide, N-[3-(aminomethyl)phenyl]	CdaA-Y034_D10_w1_1_0a_311.pdb	2.167 [A]	99.8% 5.0%	0.2240 0.2361	
92	F07 Pentanoic acid, 5-amino	CdaA-Y100_F07_w1_1_0b_065.pdb	2.100 [A]	98.1% 5.9%	0.2094 0.2289	
93	C07 Methanone, 1-piperidinyl- 3-piperidinyl	CdaA-Y096_C07_w1_1_0b_046.pdb	2.591 [A]	96.9% 5.6%	0.1943 0.2372	
94	C08 Benzoic acid, 4-(aminomethyl)-, methyl ester, hydrochloride (1:1)	CdaA-Y007_C08_w1_1_0a_065.pdb	2.171 [A]	99.8% 5.8%	0.2015 0.2162	
95	A07 1- Piperidine-acetamide, N-1, 3-benzodioxol-5-yl	CdaA-Y094_A07_1_0b_031.pdb	3.030 [A]	99.8% 10.3%	0.2313 0.2758	
96	A06 1, 3- Benzodioxole-5-methanamine, N-cyclopentyl	CdaA-Y080_A06_w1_2_0a_022.pdb	2.947 [A]	92.6% 9.8%	0.2282 0.2685	
97	F10 L-Histidine, 1-methyl	CdaA-Y038_F10_w1_1_0a_063.pdb	2.522 [A]	94.6% 7.5%	0.2858 0.3010	
98	E09 NO NAME	CdaA-Y021_E09_w1_1_0a_712.pdb	3.136 [A]	99.6% 7.8%	0.2665 0.3128	

	AS-SIGNED IN SCIFIND ER					
99	G09 1-Pro-panamin-ium, 3-car-boxy-2-hy-droxy-N,N,N-tri-methyl-, inner salt, (2R)	CdaA-Y025_G09_w1_1_0a_061.pdb	2.176 [A]	99.1% 7.4%	0.2253 0.2588	
100	H12 Bicy-clo[2.2.1] heptane-1-carbox-amide, N- hy-droxy	CdaA-Y064_H12_w1_2_0a_019.pdb	3.121 [A]	99.6% 8.4%	0.2183 0.2419	
101	A06 1, 3- Ben-zodioxole-5-methana-mine, N-cyclo-pentyl	CdaA-Y079_A06_w1_1_0a_065.pdb	2.065 [A]	99.4% 4.4%	0.2103 0.2373	
102	C02 2- Thia-zolamine, 4- methyl-5-(1- me-thyl- 1H-imidazol-2- yl)	CdaA-Y069_C02_1_0b_024.pdb	2.617 [A]	99.8% 5.4%	0.2266 0.2546	
103	A11 Imidazo[2, 1- c] [1, 2, 4]triazine,	CdaA-Y015_A11_1_0b_063.pdb	2.063 [A]	99.8% 5.5%	0.2119 0.2399	

	3- (3, 4-difluoro-phenyl) - 1, 4, 6, 7-tetrahydro					
104	G07 3H-1,2,3-Tria-zolo[4,5-d] pyrimi-dine 5,7 (4H,6H)-dione	CdaA-Y102_G07_1_0b_065.pdb	2.451 [A]	98.6% 6.5%	0.2492 0.2575	
105	C07 Meth-anone, 1-piperidi-nyl- 3-piperidinyl	CdaA-Y095_C07_1_0b_023.pdb	2.371 [A]	98.2% 4.6%	0.2229 0.2386	
106	A08 1,3,5-Cy-clohepta-trien-1-amine, N-(1-meth-ylethyl)-7-[(1-meth-ylethyl) imino]	CdaA-Y004_A08_w1_2_0a_112.pdb	3.103 [A]	95.7% 9.0%	0.2122 0.2713	
107	C03 1, 3, 5-Triazine-2, 4- dia-mine, 6-[1- (hexa-hydro-1H- aze-pin- 1-yl) ethyl] - N2, N2-dimethyl	CdaA-Y083_C03_w1_1_0a_021.pdb	2.526 [A]	99.4% 5.9%	0.2241 0.2559	
108	G08 Benzene-sulfona-mide, 4-amino-N-(5-methyl-3-	CdaA-Y013_G08_w1_1_0a_712.pdb	2.002 [A]	99.8% 4.5%	0.2222 0.2480	

	isoxa-zolyl)					
109	H06 8-Quino-linol, 5-ni-tro	CdaA-Y092_H06_1_0b_044.pdb	2.446 [A]	99.6% 4.9%	0.2060 0.2473	
110	F04 6H-Purin-6-one, 2-amino-1,9-dihydro	CdaA-Y047_F04_w1_2_0a_066.pdb	1.978 [A]	98.6% 5.5%	0.1995 0.2246	
111	F02 L-Phenyl-alanine, methyl es-ter, hydro-chloride (1:1)	CdaA-Y075_F02_1_0b_052.pdb	2.110 [A]	99.4% 3.1%	0.2071 0.2480	
112	B06 Ben-zeneacetic acid, 4-fluoro-, hydrazid	CdaA-Y082_B06_1_0b_051.pdb	1.938 [A]	99.4% 5.0%	0.2116 0.2298	
113	G11 Benzena-mine, 3-(5- oxa-zolyl)	CdaA-Y046_G11_w1_1_0a_711.pdb	2.193 [A]	99.3% 5.9%	0.2521 0.2732	
114	E11 3H- Oxa-zolo[3, 4-a] pyrazin-3-one, hexa-hydro	CdaA-00810_E11_w1_1_0a_051.pdb	3.483 [A]	92.0% 11.3%	0.1947 0.2506	
115	E10 1, 2, 4-Oxadia-zole, 3- (1-meth-ylethyl) -5- (2-pyr-rolidinyl)	CdaA-Y036_E10_w1_1_0a_512.pdb	3.214 [A]	97.1% 6.9%	0.1963 0.2431	

116	A10 Ethanone, 2-amino-1-(4-bromo-phenyl)-, hydrochloride (1:1)	CdaA-Y028_A10_w1_1_0a_042.pdb	1.959 [A]	99.1% 6.1%	0.2262 0.2387	
117	C02 2- Thiazolamine, 4- methyl-5-(1- methyl- 1H-imidazol-2- yl)	CdaA-Y070_C02_1_0b_062.pdb	3.082 [A]	98.8% 7.2%	0.2189 0.2566	
118	D11 Phenol, 5-(aminomethyl)-2-methoxy-, hydrochloride (1:1)	CdaA-0089_D11_w1_1_0b_044.pdb	2.414 [A]	99.8% 9.0%	0.2485 0.2799	
119	E06 3-Oxetanamine, 3-[[5-(1,1-dimethylethyl)-3-isoxazolyl] methyl]	CdaA-Y85_E06_w1_1_0a_711.pdb	2.952 [A]	99.3% 6.9%	0.2662 0.3207	
120	D06 3-Furancarboxamide, 2,5-dimethyl-N-4-pyridinyl	CdaA-Y084_D06_1_0b_063.pdb	2.378 [A]	98.3% 8.0%	0.2327 0.2670	
121	Myo-Inositol PDB: INS	CdaA-INS18h_G2_1_0_044.pdb	2.129 [A]	98.7% 4.3%	0.2156 0.2481	
122	Xylitol PDB: XYL	CdaA-XYL30min_Y23_1_0_711.pdb	2.112 [A]	99.8% 6.1%	0.2244 0.2353	

123	Salicylic acid PDB: SAL	CdaA-SAL2h_Y49_2_0_711.pdb	2.179 [A]	99.8% 9.1%	0.2159 0.2417	
124	Salicylic acid PDB: SAL	CdaA-SAL2h_Y49_2_0-dmso_001.pdb	2.179 [A]	99.8% 9.1%	0.2115 0.2620	
125	Biotin PDb: BTN	CdaA-BTN18h_Y61_1_0_041.pdb	2.072 [A]	99.9% 6.3%	0.2210 0.2353	
126	Aspartame PDB: PME	CdaA-PME1_30h_Y37_w1_3_0_065.pdb	1.838 [A]	96.6% 19.3%	0.5189 0.5087	
127	Myo-Inositol PDB: INS	CdaA-INS18h_G3_2_0_061.pdb	3.126 [A]	99.0% 26.2%	0.3288 0.3397	
128	N-Cyclohexyl-2-aminoethanesulfonic acid (CHES)	CdaA-CHES18h_Y57_1_0_311.pdb	2.305 [A]	97.5% 7.6%	0.2238 0.2547	
129	2-(*N*-morpholino)ethanesulfonic acid (MES)	CdaA-MES18h_Y47_1_0_712.pdb	2.109 [A]	99.9% 5.7%	0.2137 0.2329	
130	Biotin PDB: BTN	CdaA-BTN18h_Y61_2_0_024.pdb	2.906 [A]	99.8% 9.3%	0.2120 0.2333	
131	3-Nitropropanoic acid PDB: 3NP	CdaA-3NP20min_0084_w1_2_0_063.pdb	2.324 [A]	99.4% 4.9%	0.2022 0.2263	
132	Nitroxolin PDB: HNQ	CdaA-Nitroxolynie18h_Y40_1_0_052.pdb	2.223 [A]	97.9% 4.7%	0.2058 0.2341	

133	Noradrenaline PDB: LNR	CdaA-LNR18h_Y42_1_0_042.pdb	2.205 [A]	99.9% 6.6%	0.2188 0.2561	
134	S-(-) Carbidopa PDB: 142	CdaA-1421h_Y31_2_0_064.pdb	1.995 [A]	99.9% 4.8%	0.2031 0.2429	
135	Trans-4-Aminomethylcyclohexane-1-Carboxylic acid PDB: AMH	CdaA-AMH1_30h_00814_w1_2_0_026.pdb	2.855 [A]	97.3% 15.9%	0.2279 0.2631	
136	8-Azaxanthine PDB: AZA	CdaA-AZA2h_Y51_1_0_045.pdb	2.079 [A]	99.9% 5.7%	0.2191 0.2460	
137	L-Carnitine PDB: 152	CdaA-15218h_Y8_1_0_511.pdb	2.050 [A]	99.9% 5.8%	0.2040 0.2291	
138	O-Diazoacetyl-L-Serine Azaserine PDB: AZS	CdaA-AZS24h_Y66_2_0_511.pdb	2.437 [A]	100.0% 7.7%	0.2122 0.2316	
139	(4R)-4-hydroxy-L-proline PRB: 0AZ	CdaA-OAZ1_30h_Y40_1_0_043.pdb	2.058 [A]	99.9% 5.5%	0.2043 0.2239	
140	Barbituricacid	CdaA-Barbituricacid_18h_Y65_2_0_064.pdb	2.169 [A]	99.9% 6.9%	0.2242 0.2546	
141	HEPES	CdaA-HEPES30min_Y22_1_0_062.pdb	2.377 [A]	99.3% 10.4%	0.2184 0.2437	
142	S-(-) Carbidopa	CdaA-1421h_0081	2.060 [A]	99.7% 5.2%	0.2024 0.2276	

	PDB: 142	2_2_0_712.pdb				
143	Noradrenaline PDB: LNR	CdaA-LNR18h_Y42_2_0_712.pdb	2.292 [A]	99.8% 7.0%	0.2119 0.2485	
144	Trans-4-Aminomethylcyclohexane-1-Carboxylic acid PDB: AMH	CdaA-AMH1_30h_00814_w1_1_0_011.pdb	3.028 [A]	99.8% 13.8%	0.2300 0.2627	
145	L-Phenylalanine methyl ester hydrochloride PDB: 0A9	CdaA-0A920min_Y11_2_0_062.pdb	1.944 [A]	97.0% 6.7%	0.2279 0.2383	
146	Theobromine PDB: 37T	CdaA-3FT20min_Y12_3_0_712.pdb	1.831 [A]	99.9% 4.0%	0.2082 0.2262	
147	Guanosine PDB: GMP	CdaA-GMP1_30h_Y35_1_0_062.pdb	1.762 [A]	98.1% 3.4%	0.2188 0.2245	
148	Noradrenaline PDB: LNR	CdaA-LNR40min_Y16_w1_1_0_044.pdb	2.181 [A]	99.9% 7.8%	0.2246 0.2650	
149	N-acetylmethionine PDB: AME	CdaA-AME-FewSec_Y33_1_0_042.pdb	2.233 [A]	97.6% 9.0%	0.2777 0.3012	
150	N-acetylmethionine PDB: AME	CdaA-AME-FewSec_Y33_2_0_312.pdb	2.225 [A]	96.7% 5.3%	0.2335 0.2664	
151	N-acetyl-D-Glucosamine PDB: NAG	CdaA-NAG20min_Y2_1_0_065.pdb	2.075 [A]	99.8% 6.4%	0.2399 0.2790	

152	1-Methyl-L-histidine PDB: HIC	CdaA-HIC2h_Y28_2_0_035.pdb	2.032 [A]	95.1% 5.1%	0.2192 0.2477	
153	L-Phenylalanine methyl ester hydrochloride PDB: 0A9	CdaA-0A920min_Y11_1_0_312.pdb	1.945 [A]	97.5% 4.2%	0.2030 0.2289	
154	3-Nitropropanoic acid PDB: 3NP	CdaA-3NP20min_0086_w1_1_0_046.pdb	2.327 [A]	98.9% 8.3%	0.2098 0.2441	
155	Biotin PDB: BNT	CdaA-BNT2h_Y53_2_0_062.pdb	1.943 [A]	99.2% 4.2%	0.2039 0.2414	
156	Xylitol PDB: XYL	CdaA-XYL-40minY26_1_0_062.pdb	1.943 [A]	98.4% 4.0%	0.2266 0.2392	
157	N-Alpha-Acetyl-L-Arginine Dihydrate	CdaA-N-Alpha1h_Y29_1_0_063.pdb	2.163 [A]	99.4% 53.9%	0.4380 0.4574	
158	Glycoluril PDB: GLL	CdaA-GLL20min_0089_w1_1_0_042.pdb	2.236 [A]	98.9% 5.7%	0.2198 0.2547	
159	1-methyl-d-tryptophane	CdaA-Methyltrypto_18h_Y59_1_0_064.pdb	1.974 [A]	99.4% 5.7%	0.2092 0.2343	
160	Barbituric acid	CdaA-Barbituricacid_18h_Y65_1_0_062.pdb	2.561 [A]	99.9% 9.3%	0.2349 0.2440	
161	Xylitol PDB: XLY	CdaA-XLY30min_Y24_1_0_064.pdb	1.946 [A]	99.9% 5.6%	0.2156 0.2249	
162	Glycoluril PDB: GLL	CdaA-GLL20min_	2.118 [A]	98.6% 7.5%	0.2885 0.3056	

		Y20_1_0_021.pdb				
163	Noradrenaline PDB: LNR	CdaA-LNR40min_Y16_w1_2_0_043.pdb	2.202 [A]	99.9% 8.3%	0.2271 0.2485	
164	S-(-) Carbidopa PDB: 142	CdaA-1421h_00812_1_0_046.pdb	1.907 [A]	99.7% 4.7%	0.2143 0.2337	
165	Theobromine PDB: 37T	CdaA-3FT20min_Y12_2_0_042.pdb	1.862 [A]	99.9% 4.2%	0.2130 0.2192	
166	Sulfamethoxazole PDB: 08D	CdaA-08D20min_Y14_2_0_024.pdb	2.439 [A]	99.7% 11.5%	0.2403 0.2690	
167	N-acetyl-D-Glucosamine PDB: NAG	CdaA-NAG20min_Y1_2_0_063.pdb	2.114 [A]	99.4% 6.6%	0.2560 0.2599	
168	Noradrenaline PDB: LNR	CdaA-LNR40min_Y16_w1_4_0_064.pdb	2.404 [A]	99.9% 8.8%	0.2145 0.2566	
169	N-acetyl-D-Glucosamine PDB: NAG	CdaA-NAG20min_Y1_1_0_045.pdb	1.981 [A]	99.5% 5.0%	0.2014 0.2242	
170	Aspartame PDB: PME	CdaA-PME1_30h_Y37_w1_1_0_056.pdb	1.841 [A]	97.0% 3.4%	0.1971 0.2314	
171	Aspartame PDB: PME	CdaA-PME1_30h_Y37_w1_2_0_512.pdb	1.879 [A]	98.5% 3.3%	0.2125 0.2293	
172	(4R)-4-hydroxy-L-proline PDB: 0AZ	CdaA-OAZ1_30h_Y40_2_0_512.pdb	2.057 [A]	99.8% 6.4%	0.2386 0.2852	
173	N-acetylmethionine	CdaA-AMEFew-Min_Y32_	2.264 [A]	99.7% 7.7%	0.2561 0.3021	

	PDB: AME	w1_4_0_063.pdb				
174	Riboflavin PDB: RBF	CdaA-RBF24h_Y67_1_0_078.pdb	1.923 [A]	20.4% 91.3%	0.3657 0.3847	
175	L-Carnitine PDB: 152	CdaA-1521_30h_Y41_3_0_042.pdb	2.224 [A]	98.8% 5.0%	0.2081 0.2490	
176	S-(-) Carbidopa PDB: 142	CdaA-1421h_Y31_1_0_712.pdb	2.218 [A]	99.6% 9.0%	0.2558 0.2744	
177	Salicylic acid PDB: SAL	CdaA-SAL2h_Y49_1_0_711.pdb	2.327 [A]	98.1% 4.5%	0.1994 0.2307	
178	Aspartame PDB: PME	CdaA-PME18h_Y46_2_0_046.pdb	2.174 [A]	98.5% 31.4%	0.4540 0.4518	
179	Sulfamethoxazole PDB: 08D	CdaA-08D20min_Y14_1_0_045.pdb	2.236 [A]	99.7% 8.1%	0.2298 0.2497	
180	2-Nitrothiophene PDB 265	CdaA-26518h_Y60_1_0_062.pdb	2.312 [A]	99.2% 7.6%	0.2350 0.2706	
181	HEPES	CdaA-HEPES1h_Y21_1_0_063.pdb	2.256 [A]	99.6% 7.0%	0.2013 0.2319	
182	N-acetyl-D-Glucosamine PDB: NAG	CdaA-NAG20min_Y2_2_0_074.pdb	2.102 [A]	99.8% 7.7%	0.2016 0.2413	
183	D-(+)-Trehalose dihydrate PDB: TRE	CdaA-TRE1_30h_Y39_2_0_054.pdb	2.047 [A]	99.7% 6.5%	0.2054 0.2420	
184	Myo-Inositol PDB: INS	CdaA-INS18h_G2_2_0_042.pdb	2.131 [A]	98.8% 3.6%	0.1942 0.2359	

185	N-Alpha-Acetyl-L-Arginine Dihydrate	CdaA-N-Alpha1h_Y30_1_0_064.pdb	1.870 [A]	99.8% 5.3%	0.2151 0.2290	
186	4-Amino-6-Chloro-benzene-1,3-Disulfonamide PDB: I7B	CdaA-I7B24h_Y25_1_0_044.pdb	2.456 [A]	99.4% 9.6%	0.2187 0.2640	
187	L-Carnitine PDB: 152	CdaA-1521_30h_Y41_2_0_045.pdb	2.221 [A]	98.9% 3.8%	0.2123 0.2314	
188	D-(+)-Trehalose dihydrate PDB: TRE	CdaA-TRE1_30h_Y39_3_0_062.pdb	2.045 [A]	99.9% 5.1%	0.2078 0.2302	
189	L-Carnitine PDB: 152	CdaA-15218h_Y8_2_0_065.pdb	2.144 [A]	99.9% 7.9%	0.2268 0.2457	
190	Riboflavin PDB: RBF	CdaA-RBF24h_Y67_4_0_076.pdb	2.060 [A]	99.6% 5.4%	0.1964 0.2284	
191	PDB: AZS	CdaA-HZS24h_Y66_1_0_712.pdb	2.321 [A]	99.2% 6.2%	0.2001 0.2454	
192	Nitroxolin PDB: HNQ	CdaA-Nitroxolynie18h_Y40_2_0_045.pdb	2.295 [A]	99.7% 6.6%	0.2142 0.2476	
193	N-acetyl-methionine PDB: AME	CdaA-AMEFewMin_Y32_w1_1_0_712.pdb	2.376 [A]	93.8% 8.3%	0.2689 0.2883	
194	1-Methyl-L-histidine PDB: HIC	CdaA-HIC2h_Y28_1_0_063.pdb	1.935 [A]	97.0% 5.7%	0.2002 0.2379	
195	Biopertin PDB: BIO	CdaA-BIO18h_Y7	1.986 [A]	99.8% 4.6%	0.2033 0.2319	

		_1_0_044.pdb				
196	N-acetyl-D-Glucosamine PDB: NAG	CdaA-NAG20min_Y5_1_0_064.pdb	2.184 [A]	99.9% 9.5%	0.2189 0.2475	
197	MES	CdaA-MES18h_Y47_2_0_062.pdb	2.160 [A]	99.8% 4.8%	0.1974 0.2389	
198	Riboflavin PDB: RBF	CdaA-RBF24h_Y67_2_0_711.pdb	1.894 [A]	96.8% 22.7%	0.5027 0.5295	
199	Nitroxolin PDB: HNQ	CdaA-NItroxolyine18h_Y62_1_0_042.pdb	2.287 [A]	98.8% 7.2%	0.2339 0.2534	
200	Aspartame PDB: PME	CdaA-PME18h_Y46_1_0_017.pdb	2.099 [A]	98.8% 6.2%	0.2446 0.2987	
201	N-acetyl-D-Glucosamine PDB: NAG	CdaA-NAG20min_Y5_2_0_064.pdb	1.906 [A]	99.8% 6.3%	0.2125 0.2372	
202	Guanosine PDB: GMP	CdaA-GMP18h_Y45_1_0_712.pdb	2.187 [A]	99.1% 10.2%	0.3152 0.3546	
203	Theobromine PDB: 37T	CdaA-37T20min_Y13_1_0_062.pdb	1.983 [A]	99.9% 4.2%	0.2115 0.2313	
204	Theobromine PDB: 37T	CdaA-3FT20min_Y12_1_0_046.pdb	1.905 [A]	99.9% 5.3%	0.2003 0.2177	

Chapter 6: Discussion

The ability of bacteria to cope with environmental changes is an essential selective advantage. Bacteria possess a plethora of transduction pathways in order to adapt rapidly to changes in nature (Goudreau and Stock 1998). In all kingdoms of live these intracellular signaling molecules are often nucleotide-based second messengers. In bacteria c-AMP, (p)ppGpp and c-di-GMP are the most comprehensively studied among the long list of known nucleotide-based signaling molecules (Pesavento and Hengge 2009).

In 2008 the bacterial second messenger c-di-AMP "entered the fray" (Witte et al. 2008; Corrigan Rebecca M and Gründling 2013). Henceforth, the research interest on the c-di-AMP synthesis, degradation and function increased rapidly giving more remarkable insights into its importance for bacteria (Corrigan R. M. and Gründling 2013; Commichau et al. 2015a; Commichau et al. 2019). c-di-AMP is synthesized out of two ATP molecules by the so called diadenylate cyclases in a metal ion-dependent manner. The first discovered DAC is the DNA scanning protein DisA. DisA forms a stable associated homo octamer *in vivo* and *in vitro* composed of two N-terminal "head-to-head" tetrameric rings which are accompanied by a C-terminal signaling domain. The nucleotide binding site was identified directly between the interface of these two N-terminal domains forming dimeric "head-to-head" assemblies which are characterized as the catalytic units. Each monomer of the four dimers is described as a DAC domain. (Witte et al. 2008; Müller et al. 2015). Five classes of c-di-AMP synthases with different regulatory domains have been identified so far (Romling 2008; Corrigan Rebecca M and Gründling 2013; Blötz et al. 2017; Commichau et al. 2019). However, most bacteria possess only one diadenylate cyclase either of the class DisA or CdaA, while the latter is the most prevailing DAC among all bacteria that synthesize c-di-AMP (Corrigan et al. 2013; Commichau et al. 2019). In several studies it was shown that the presence of c-di-AMP is essential for some bacteria under standard laboratory conditions (Gundlach et al. 2015a; Commichau et al. 2017; Gundlach et al. 2017a). Nonetheless, an extensive excess of c-di-AMP is equally harmful to the cell and therefore the level of c-di-AMP needs to be tightly regulated (Woodward et al. 2010; Luo Y and Helmann 2012; Mehne et al. 2013; Gundlach et al. 2015a; Commichau et al. 2017; Gundlach et al. 2017a; Gundlach et al. 2017b; Commichau et al. 2019). In comparison to other nucleotide-based second messengers, c-di-AMP is rather unique and opens new perspectives in antibiotic research (Corrigan R. M. and Gründling 2013; Rosenberg et al. 2015; Commichau et al. 2019; Heidemann et al. 2019). This work mainly focuses on the diadenylate cyclase class CdaA from the human pathogen *L. monocytogenes* which is the sole DAC in this organism. In this Chapter the CdaA functionality as well as a CdaA regulation model and the oligomerization state in the cell are discussed. Furthermore, a comparison of c-di-AMP to the well-studied bacterial second messenger c-di-GMP will be presented. Finally,

the importance of new antibiotics development is discussed with the focus on diadenylate cyclases as promising targets for new antibiotic substances. The structural and biochemical characterization of the c-di-AMP binding protein DarB/YkuL from *B. subtilis* was also part of this work. However, it is not discussed in the following as it is a non-essential protein and is not part of the drug discovery campaign.

6.1 CdaA Structure and function

The structure of the DAC class CdaA from *L. monocytogenes* (Δ100CdaA) was already published in the beginning of 2015 (Rosenberg et al. 2015). Based on the structural comparison of DisA and CdaA it was assumed that CdaA is able to synthetize c-di-AMP upon dimerization. Even though the crystal structure represented only an inactive monomer of CdaA which is incompatible with the formation of c-di-AMP, biochemical data confirmed the formation of a dimer in solution. The dimeric assembly has been observed also for truncated constructs Δ80CdaA and Δ100CdaA *in vivo* and *in vitro* (Fig. 6). The same study suggested that the CdaA activity is, as described for DisA, Mg^{2+} ion dependent. However, CdaA is only active in presence of Mn^{2+} or Co^{2+} ions and not active in presence of Mg^{2+} ions. Further experiments confirmed Mn^{2+} as the main CdaA cofactor by a coralyne-based assay (Heidemann et al. 2019). In addition, a significantly lower activity has been observed in presence of Co^{2+} ions but no activity in presence of Mg^{2+} ions. This is consistent with the previous results (Rosenberg et al. 2015). Utilizing this knowledge, we succeeded in crystalizing CdaA in its post-catalytic state with its product c-di-AMP bound. In addition, apo CdaA has been also crystallized. The ligand-free crystals were used for fragment screening (Heidemann et al. 2019) (Chapter 5).

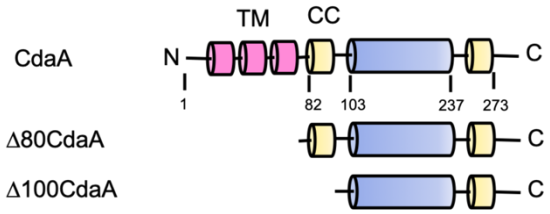

Figure 6: Schematic illustration of the domain organization of the different available CdaA *L. monocytogenes* constructs. CdaA consists of transmembrane (TM) domain made of three α-helices, 2 coiled-coil domains and the active cyclase domain. The construct Δ80CdaA lacks the TM domain while the construct Δ100CdaA additionally lacks the following coiled-coil domain (modified from Rosenberg et al. 2015).

Interestingly, the asymmetric unit of both crystal forms contained two CdaA monomers forming a non-catalytic dimer with outwards facing active sites. This assembly has also been observed in different crystal forms under different crystallization conditions and for CdaA from different organisms (Heidemann et al. 2019; Tosi et al. 2019) (Fig. 7).

In addition to structural data Tosi *et al.* reported that *S. aureus* DacA (described as CdaA in *L. monocytogenes* and *B. subtilis*) exhibits cyclase activity mainly in presence of Mn^{2+}, Co^{2+} but also Mg^{2+} ions. This is surprising as the structural comparison of the active sites (*lmo*CdaA-

*sau*DacA) unveiled an identical positioning of the amino acids involved in binding of both c-di-AMP and the metal ion (Heidemann et al. 2019) (Chapter 2).

The unexpected catalytic activity of Mg^{2+} ions could result from different experimental approaches which were used to determine the conversion of two ATP molecules into c-di-AMP. While Tosi *et al.* used a radio-thin-layer chromatography (radio-TLC) approach with labeled ATP (α–P^{32}), we used the c-di-AMP-specific coralyne-based assay (Zhou et al. 2014). In order to investigate potential differences between CdaA of these two organisms, a GST-tagged, codon optimized CdaA from *S. aureus* was tested using the coralyne-based assay. The results suggested a similar metal dependence of CdaA/DacA from *S. aureus* and *L. monocytogenes*. However, an activity in presence of Mg^{2+} as shown by the radio-TLC method could not be confirmed (Chapter 8, Fig. 11). The observed discrepancy could result from differences in the purification protocol as well as the used construct (Tosi et al. 2019 = His-Δ100CdaA). The ultimate prove would require the measurement of the GST-CdaA construct of *S. aureus* and *L. monocytogenes* with the sensitive radio-TLC method.

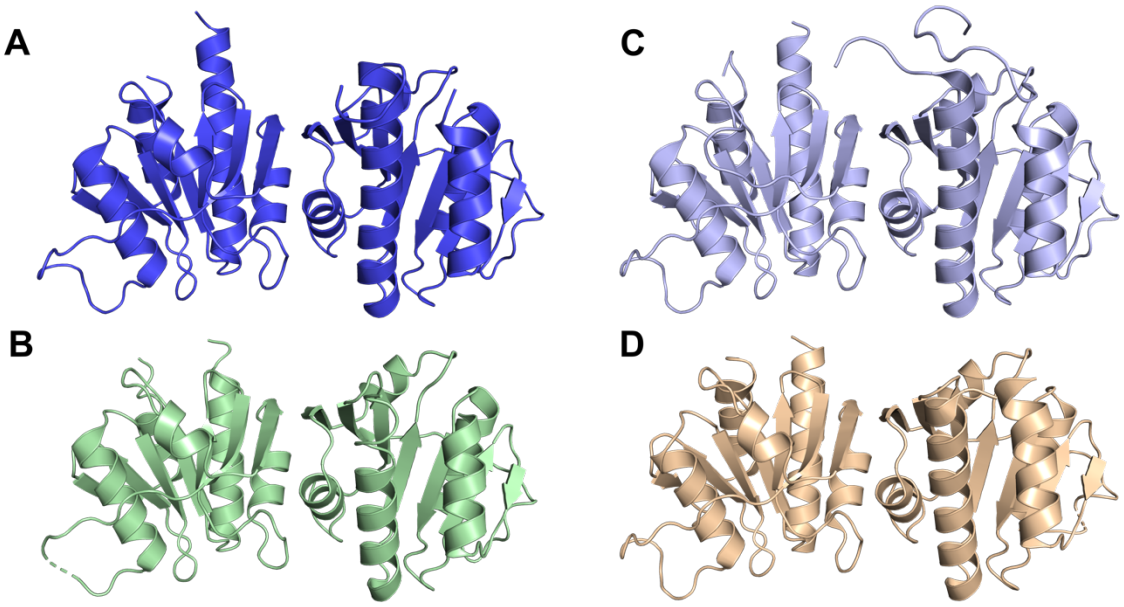

Figure 7: Crystal structures of Δ100CdaA from different organisms and in different space groups. (A) Crystal structure of CdaA from *L. monocytogenes* (Space group: $H3_2$) (PDB code: 6HVL). **(B)** Crystal structure of CdaA from *B. subtilis* (Space group: $P4_32_12$) (PDB code: 6HUW). **(C)** Crystal structure of CdaA from *L. monocytogenes* (Space group: $P2_12_12_1$) (PDB code: 6HVM). **(D)** Crystal structure of CdaA from *S. aureus* (Space group: $P2_12_12_1$) (PDB code: 6GYW). The asymmetric unit of all crystal forms contains two CdaA monomers forming a non-catalytic dimer with an interface between α-helix 3 (Fig. 4/ Introduction). A superposition of all CdaA structures available in the protein data bank (PDB) is represented in figure 13 (Chapter 8). All protein structures are depicted in cartoon mode, *L. monocytogenes* CdaA structures are colored light and dark blue, the CdaA structure from *B. subtilis* is colored light green and the one from *S. aureus* is colored in light brown.

6.2 Oligomerization state of CdaA in solution and its biological relevance

The synthesis of c-di-AMP requires the formation of DAC dimers with face-to-face oriented active sites. This is known from structural analysis of DisA, which forms stable associated DAC dimers in solution. Comparison of the active sites of CdaA and DisA reveals a more crowded active site in CdaA which explains why the active CdaA dimer is only transiently formed (Heidemann et al. 2019) (Chapter 2). Therefore, unlike DisA, the catalytic CdaA dimer needs to disassemble in order to release c-di-AMP (Heidemann et al. 2019) (Chapter 2).
In 2015 Rosenberg and colleagues published *in vitro* experiments (SEC-MALS data) that demonstrated the formation of CdaA dimers in solution. Yet this dimer formation was described as the ability of CdaA to form catalytic active dimers, although it could not be experimentally proven (Rosenberg et al. 2015). The formation of a CdaA dimer in solution was confirmed by us (Chapter 3, Fig. 4 and 5) and by Tosi *et al.* 2019. Therefore, the question was asked whether CdaA forms under non-catalytic conditions a catalytic dimer in solution or a non-catalytic dimer?
The dimer in solution seems rather stable which is non-corresponded to the assumption that CdaA forms transient catalytic dimers (Heidemann et al. 2019). Previously the DAC class CdaS was proposed to form hexamers in solution. In this hexamer model the DAC domains form non-head-to-head dimer assemblies, similar to these described for CdaA/DacA (Mehne et al. 2014; Tosi et al. 2019). However, no further experiments were performed in order to confirm that the hexamer assembly is the active form of CdaS and whether additional oligomerization is required to synthesize c-di-AMP (Mehne et al. 2014). In contrast, the DAC class DisA was shown to form octamer assemblies in *in vivo* and *in vitro* in order to form c-di-AMP. Therefore, Tosi *et al.* suggested that a non-catalytic CdaA/DacA dimer is present in solution (Witte et al. 2008; Mehne et al. 2014; Müller et al. 2015).
Our structural data and the crystal structures obtained by Tosi *et al.* suggested the formation of a CdaA dimer. This dimer in the crystal structures is non-catalytic with outwards facing active sites forming a dimeric interface between the two α-helices 3 and β-strand 2 which results in an extended twisted β-sheet (Fig. 4 and 8). This specific assembly of CdaA is not only obtained in crystals with different space groups but also by the crystallographic analysis of CdaA from different organisms like *L. monocytogenes* (6HVM, 6HVL, Heidemann J. et al. 2019), *B. subtilis* (6HUW; Tosi T. et al. 2019) and *S. aureus* (6GYW; Tosi T. et al. 2019) (Fig. 7).
Based on this prominent non-catalytic assembly seen in different crystal structures and the fact that other crystallographic characterized DACs were described to form higher oligomeric complexes Tosi *et al.* suggested that this non-catalytic dimer formation has a biological relevance (Witte et al. 2008; Mehne et al. 2014; Müller et al. 2015). In order to address this question, mutations were introduced into the *S. aureus* interface of the non-catalytic dimer showing a negative effect on the CdaA activity (Tosi et al. 2019). All these biochemical and crystallographic data suggest that CdaA forms a non-catalytic dimer in solution.

The next question which needs to be considered is whether the assembly of a non-catalytic CdaA dimer can be present in the cell and whether CdaA is still able to form catalytic dimers. The structural analysis of the non-catalytic dimer clearly shows that the N-terminal part of each of the two α-helices 1, which are connected to the membrane domain by a 20 amino acid linker region, point in the same direction (Fig. 8). This is consistent with the fact that CdaA is bound to the membrane. As described in Chapter 2 CdaA from *L. monocytogenes* was successfully crystallized in its post-catalytic state with bound c-di-AMP. In the asymmetric unit a non-catalytic dimer is present of which each monomer represents a different catalytic state. While monomer one forms a transiently existing catalytic dimer (2-fold axis, crystallographic assembly), the second forms a non-catalytic dimer with the first one and in addition reveals an AMP molecule bound in the active site (Heidemann et al. 2019). Comparing the orientation of four monomers forming an active dimer reveals that the N-terminal helices of all DAC domains are pointing in the same direction (Fig. 8). This indicates that based on crystal structure two non-catalytic dimers are needed to form one catalytic CdaA dimer. It might be an interesting aspect to think of, that the formation of catalytic CdaA dimers might be directly regulated by the cellular turgor which was described to be controlled through the presence and absence of c-di-AMP (Commichau et al. 2017).

It should be kept in mind that all crystallization experiments were performed with a truncated construct. Although further biochemical data suggested that the additional N-terminal α-helix (Δ80CdaA) has no influence on the CdaA activity compared to Δ100CdaA the influence on the full-length CdaA has not been biochemically and structurally studied so far (Chapter 8, Fig. 12). Structural and biochemical data on the full-length CdaA could help to better understand what CdaA full-length looks like and how it is functioning in the cell.

One can only speculate of the biological relevance and whether CdaA is present as a non-catalytic dimer in the cell and only forms catalytic dimers under c-di-AMP synthesizing conditions. The formation of higher oligomers is well known for soluble and membrane bound proteins in living cells (Goodsell and Olson 2000). As well as the communication between active sites in oligomers through hydrogen bonds or allosteric effects could result for example in negative or positive cooperativity (Ferrell 2009). Whether this is also true for CdaA needs to be elucidated in future experiments.

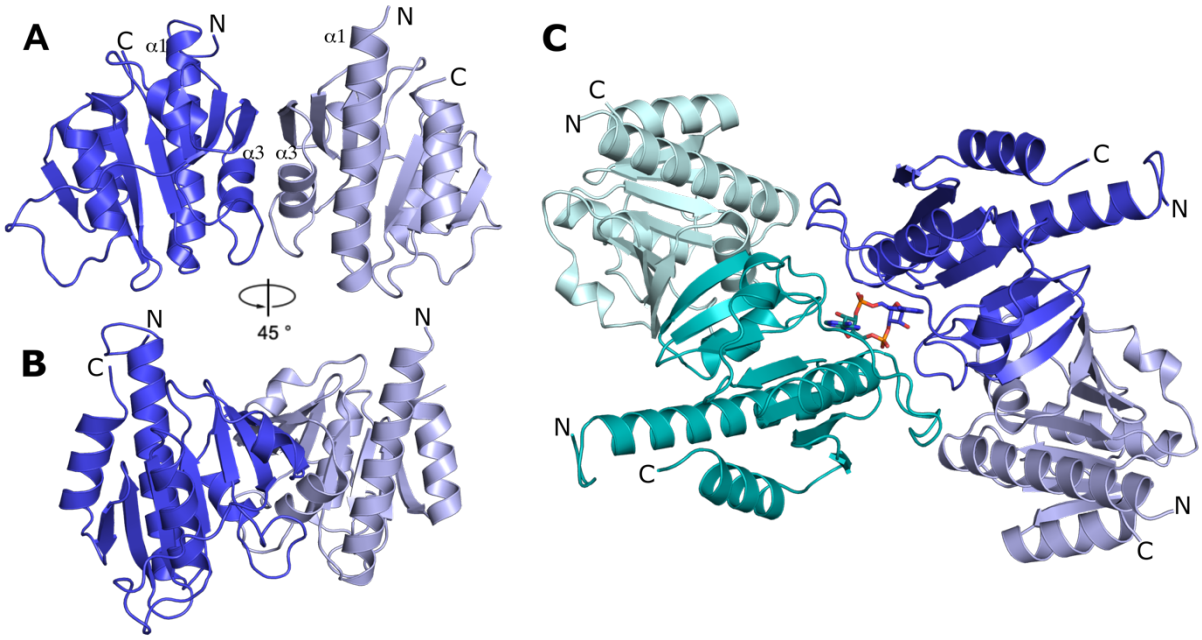

Figure 8: Suggested oligomerization state model of CdaA from *L. monocytogenes*. (A) Non-catalytic CdaA dimer of two CdaA monomers with an interface between α-helix 3 (monomer A: dark blue, monomer B: light blue). The N-terminal part of the two α-helices 1 of both CdaA monomers are pointing in the same direction which is consistent with the fact that the cyclase domain is linked by a 20 amino acid linker to a membrane. **(B)** Non-catalytic CdaA dimer which is rotated by 45 degree in comparison to (A). **(C)** A tetramer of CdaA molecules formed by two non-catalytic dimers exhibiting a catalytic dimer with bound c-di-AMP (non-catalytic dimer 1 is depicted in dark and light blue, non-catalytic dimer 2 is depicted in dark and light cyan). The catalytic dimer is formed by monomer A (dark blue) of the non-catalytic dimer 1 and monomer A (dark cyan) of the non-catalytic dimer 2. The N-terminal part of all four α-helices 1 point in the same direction. The protein structures are depicted in cartoon mode in light and dark blue as well as in light and dark cyan. c-di-AMP is depicted in stick mode (carbon in dark blue and cyan, phosphate in orange, oxygen in red, and nitrogen in blue) (PDB: 6HVL).

6.3 CdaA regulation

Even though the presence of c-di-AMP has been described to be essential for some bacteria, an overproduction of c-di-AMP was demonstrated to be harmful for the cell. Hence, c-di-AMP was named the “essential poison” which requires a tight control of its synthesis (Gundlach et al. 2015a; Huynh and Woodward 2016; Blötz et al. 2017).

CdaA is present in a conserved gene cluster which encodes besides *cdaA* the regulatory protein CdaR and the glucosamine mutase GlmM (Mehne et al. 2013; Rismondo et al. 2016; Zhu et al. 2016). Therefore, a functional relation between these three proteins was suggested. Indeed, a direct interaction between CdaA and CdaR as well as modulation of the CdaA activity were reported previously (Mehne et al. 2013; Gundlach et al. 2015a; Rismondo et al. 2016). *In silico* experiments suggested a positioning of CdaR extracellular (Corrigan Rebecca M and

Gründling 2013). This was confirmed in Chapter 3. Here it was also shown that CdaR interacts through the transmembrane domain with CdaA suggesting that the CdaA TM importantly contributes to the activity of the DAC domain and also the transfer of a sensed signal by CdaR. The importance of the membrane domain was also demonstrated by mutations resulting in a decrease of CdaA activity (Zhu et al. 2016). It is suggested that CdaR is a signal receptor sensing an external signal. So far, a signal sensed by CdaR and the signal transduction through the interacting TM domains of CdaR and CdaA is not known. In order to shed light on this unsolved problem it is of great interest to identify the signal which is transduced to the DAC domain. Crystallographic and biochemical experiments might also help to further understand the mode of interaction between CdaR and CdaA and how the activity of DAC domain is modulated.

The second protein encoded in the conserved gene cluster is GlmM. A direct interaction between CdaA and GlmM has been reported in *B. subtilis*, *L. lactis* and *S. aureus* (Gundlach et al. 2015a; Zhu et al. 2016; Tosi et al. 2019). In Chapter 3 an interaction between GlmM and CdaA was also confirmed *in vivo* and *in vitro* for *L. monocytogenes*. Furthermore, it was demonstrated that GlmM inhibits the c-di-AMP synthesis of CdaA under hyperosmotic stress preventing the cell from uncontrolled water loss through e.g. carnitine and betaine uptake (Zhu et al. 2016, Chapter 3). Zhu and colleagues discovered in *L. lactis* under hyperosmotic stress conditions a point mutation in GlmM at position 154 (I^{154} to F) leading to an osmoresistent strain. This strain showed a reduced c-di-AMP level in comparison to the wild type GlmM strain, suggesting an interaction between CdaA and GlmM. Sequence alignments of GlmM from related bacteria unveiled a phenylalanine in *S. aureus*, *L. monocytogenes* and *B. subtilis* at the position of an isoleucine (I^{154}) in *L. lactis* wild type. As the *L. lactis* mutant strain carries also a Phe, it was suggested that this amino acid might play an important role in modulating CdaA and therefore might be involved in CdaA and GlmM interaction. Indeed, mutations of the phenylalanine to an isoleucine showed a similar effect in *L. monocytogenes* as the wildtype GlmM in *L. lactis*. Interestingly, the phenylalanine (Phe^{155}) in the available *S. aureus* GlmM (PDB: 6GYZ) structure is exposed on the protein surface and could indeed be crucial for protein-protein interactions (Tosi et al. 2019).

How could an interaction of GlmM with CdaA result in altering cyclase activity?

The crystal structure of GlmM reveals, as suggested from biochemical data, a homodimer as a biologically active form. This oligomerization of two GlmM monomers results in a V-shaped structure, right above the dimeric interface is the previously discussed Phe^{155} exposed to the surface (Fig. 9). So far, no crystallographic data of a CdaA and GlmM complex are available. However, Tosi *et al.* performed SAXS experiments in which the *ab initio* SAXS molecular envelope suggested that, at least in solution, CdaA sits on top of the GlmM homodimer interface. It was suggested that GlmM blocks the formation of higher CdaA oligomers which might be important for activity (described in 6.2). Nonetheless, these results seem to be inconsistent with the fact that only a single mutation (in *L. monocytogenes* Phe^{154} to Ile) leads to an increase

in the intracellular c-di-AMP level. The question to address is whether a single amino acid mutation in GlmM could have such a strong impact on the GlmM-CdaA complex formation and is able to perturbate the inhibition of the suggested higher CdaA oligomers. So far, no data are available describing the influence of the single mutation on the GlmM-CdaA binding affinity. In order to argue about the mode of GlmM-CdaA interaction additional experimental data would be required. Even though we know that GlmM inhibits CdaA as a reaction of hyperosmotic stress, the signal leading to a complex formation and thereby inhibition of c-di-AMP synthesis still needs to be elucidated.

Structural characterization of the GlmM-CdaA complex would be of great interest in order to understand CdaA inhibition on a structural level which in turn could be useful for a CdaA drug discovery campaign.

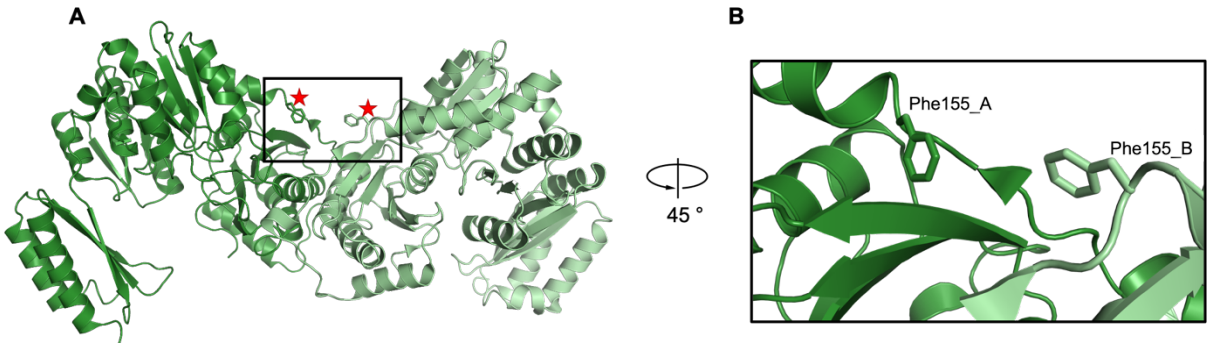

Figure 9: Crystal structure of the Glucosamine mutase GlmM from *S. aureus*. (A) GlmM homodimer (monomer 1: dark green, monomer 2: light green) with a V-shaped dimeric interface in which the two Phe^{155} are exposed on the protein interface. The protein is depicted in a cartoon mode in light and dark green. The two phenylalanine are shown in stick mode (carbon in light and dark green, oxygen in red and nitrogen in blue). These two Phe^{155} were shown to negatively influence CdaA activity and its position is indicated by the two red stars. **(B)** A detailed view of the two Phe^{155} exposed on the protein surface (PDB code: 6GYZ) (Tosi et al. 2019).

6.4 DAC and DGC comparison

Besides the bacterial second messenger c-di-AMP diverse cyclic nucleotides are known, like the closely related c-di-GMP. c-di-GMP was already discovered in 1987 by Benziman and coworkers which is together with c-AMP and (p)ppGpp probably the most comprehensively studied nucleotide-based second messenger (Ross et al. 1990; Pesavento and Hengge 2009).

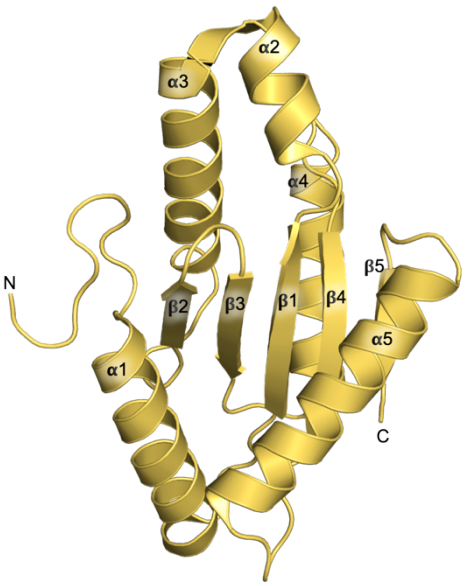

Figure 10: Crystal structure of a GGDEF domain of a diguanylate cyclase from *Xanthomonas campestris*. The protein is composed of a β-sheet formed by five β-strands which are surrounded by five α-helices. The overall fold is different to the DAC domain fold. The protein structure is depicted in cartoon mode in yellow (PDB code: 3QYY) (Yang et al. 2011).

The synthesis of c-di-GMP requires two GTP molecules positioned in close proximity in order to facilitate a nucleophilic attack of the 3'OH group of one GTP on the α-phosphate of the other GTP molecule, leading to their cyclization and the release of two pyrophosphates. This reaction is ensured by dimerization of two GGDEF domains of the so called diguanylate cyclases (DGC) that is metal ion-dependent, as it is known for the diadenylate cyclases (Romling et al. 2013). However, not all GGDEF domain-containing proteins necessarily possess DGC activity (Suzuki et al. 2006; Bordeleau et al. 2011). It was mentioned above that only five classes of DACs are known of which most have been identified in Gram-positive and only some in Gram-negative bacteria and archaea. Furthermore, it is known that most bacteria possess only one DAC class which is different to c-di-GMP synthesizing enzymes (Galperin et al. 2001; Corrigan et al. 2013; Commichau et al. 2019). DGCs are ubiquitously distributed in bacteria, in addition many bacteria are known to synthesize more than one DGC (e.g. *Escherichia coli* (*E. coli*) (Pfiffer et al. 2019) or *Bdellovibrio Bacteriovorus* (Meek et al. 2019)). Even though both Gram-positive and Gram-negative bacteria are known to carry c-di-GMP synthesizing enzymes. It has been also shown that Gram-positive bacteria possess fewer DGCs in comparison to Gram-negative bacteria (Galperin et al., 2001; Pei & Grishin, 2001). DGCs often exhibit a modular domain architecture (Jenal 2004; Pfiffer et al. 2019). They are either present as standalone proteins or in multidomain proteins accompanied by specific c-di-GMP degrading phosphodiesterases namely EAL and HD-GYP domains (Pesavento and Hengge 2009; Romling et al. 2013; Opoku-Temeng et al. 2016). In many cases an N-terminal domain is linked to the membrane where it can function as a signaling receptor for external stimuli. This is similar to the DAC domains that were described to be accompanied by different regulatory domains (Witte et al. 2008; Corrigan Rebecca M and Gründling 2013; Commichau et al. 2015b;

Rosenberg et al. 2015). Even though it seems to be likely that the DGCs and DACs share structural and sequence similarities, both protein groups are rather different.

The active DGC domain consists, as described for DACs, of a central β-sheet yet it is composed of usually five β-strands instead of seven (DACs) which are surrounded by five α-helices. Compared to the overall fold of the DAC domain, the DGC domains are elongated and not globular (Fig. 4/Introduction and Fig. 10) (Yang et al. 2011). Amino acids in the active site that contribute to the cyclase activity are also different. DACs most commonly use the conserved DGA and RHR motif for cyclase activity while DGC activity is dependent on the GGDEF motif (Witte et al. 2008; Pesavento and Hengge 2009; Romling et al. 2013; Müller et al. 2015; Rosenberg et al. 2015; Römling et al. 2017). Due to the sequence and structural differences it is assumed that the c-di-AMP and c-di-GMP signaling pathways evolved differently during evolution (Fahmi et al. 2017). Furthermore, some DGC were described to get allosterically inhibited by its product c-di-GMP. This inhibition requires formation of c-di-GMP dimeric assembly which subsequently binds to the so called I-site (inhibitory-site) (Christen et al. 2006; Gentner et al. 2012; Dahlstrom et al. 2016). Such a behavior of forming dimeric assemblies has also been reported for c-di-AMP, although in contrast to c-di-GMP its biological relevance has not been discovered so far (Blommers et al. 1988; Manikandan et al. 2014).

These two secondary metabolites differ not only in their synthesizing enzymes, but they also show differences in their biological role in bacteria. The major difference between these two molecules is their essentiality. c-di-AMP was reported to be essential for the survival of the bacteria since osmolyte control is indispensable. An osmolyte imbalance e.g. for K^+ ions can be toxic to the cell and needs to be tightly controlled (Epstein 2003). Based on these findings it was suggested that DACs seem to be an interesting target for novel antibiotic substances.

Even though c-di-GMP was shown to be ubiquitously distributed in bacteria it has not been reported to be essential for the bacterial survival. c-di-GMP is mainly involved in the molecular decision between the motile-to-sessile transition and therefore biofilm formation. Interestingly, biofilm formation in pathogenic bacteria leads to an increase in their resistance to antibiotics. An increase in the intracellular c-di-GMP level triggers the formation of biofilms, while its reduction was observed in biofilm dispersal (Roy and Sauer 2015). Therefore, it was suggested to develop DGCs inhibitor in order to support the efficacy of applied antibiotics by increase the bacterial susceptibility. Lowering of the intracellular c-di-GMP pool might be much more difficult as it is possible for c-di-AMP since there is a much higher number of different DGCs compared to the known number DAC classes (see the c-di-GMP census [http://ncbi.nlm.nih.gov/Complete_Genomes/c-di-GMP.html]) (Chou and Galperin 2016). Furthermore, not all DGCs contribute to the global c-di-GMP level, some are known to increase concentration of c-di-GMP in a specific region (Kader et al. 2006; Opoku-Temeng et al. 2016).

6.6 DACs as a new drug target

The discovery of antibacterial substances in 1928 by Alexander Fleming revolutionized modern medicine (Fleming 1945). However, due to the rapid adaptability to environmental changes bacteria developed resistances to the pool of available antibiotics. Hence, it is of great importance to develop new ones. Many bacteria gained resistances to several antibiotics, resulting in multi-drug resistant bacteria not only due to an extensive misuse in e.g. agriculture and also healthcare systems (Phillips et al. 2004; Hume 2011; Michael et al. 2014; Woolhouse et al. 2016). One major challenge of antibiotic development is the identification of new suitable targets. Such a target needs to be absent in humans and at its best essential in a wide range of bacteria (Silver 2011). The discovery of c-di-AMP and its functional diversity opened new perspectives in antibiotic research.

This work is mainly focused on the understanding of how the most distributed c-di-AMP synthesizing enzyme CdaA is functioning and regulated in order to lay a foundation for drug development. However, the question whether DACs are a good drug target based on the scientific knowledge has not been discussed so far. Indeed, many facts seem to render DACs as a good drug target. DACs are widely distributed in a great diversity of different bacteria including bacteria that are on the "priority pathogen" list of the WHO (*S. aureus*, *S. pneumonia*, *M tuberculosis*) and most importantly they are not present in humans (Song et al. 2005; Woodward et al. 2010; Corrigan et al. 2011; Luo Yun and Helmann 2012; Andrade et al. 2016; Devaux et al. 2018). Its product c-di-AMP is involved in a plethora of different cellular functions and in some bacteria its absence has been lethal (Corrigan et al. 2011; Bai et al. 2012; Luo Y and Helmann 2012; Bai et al. 2013; Gundlach et al. 2017b). Therefore, diadenylate cyclases seem to be a very promising new drug target in the fight against bacterial infections.

In *L. monocytogenes* c-di-AMP controls the accumulation of the second messenger ppGpp to toxic levels (Whiteley et al. 2015). Therefore, its absence triggers the accumulation of ppGpp in *L. monocytogenes* leading to cell death. As c-di-AMP controls the K^+ ion influx under hyperosmotic stress conditions in *B. subtilis* here a deletion of all DACs leads to an uncontrolled K^+ influx and therefore cell lysis (Gundlach et al. 2017b). Yet it has been reported that *B. subtilis* is able to form suppressor mutants under high external potassium concentrations in a Na^+ K^+ ion efflux transporter NahK, suggesting an increased K^+ ion efflux activity restoring the ion balance (Gundlach et al. 2017b). This leads to the conclusion that bacteria may have the ability to compensate an inhibition of DACs in order to survive.

Bacteria are equipped with the selective advantage of fast adaption to environmental changes. This includes not only the adaptation to environmental stress like changes in the temperature, pH or osmolyte availability but also to antibiotics that are given to cure infections (Hawkey 1998; Casadesús 2012). Bacteria evolved different mechanisms to make antibiotics ineffective like enzymatic degradation, alteration of the antimicrobial target or permeability reduction of

the cell membrane (Dever and Dermody 1991; Zaman et al. 2017). The development of antibiotics and as a result the adaptation of the bacterium is a very dynamic process which should be considered in antibiotic drug discovery.

In addition to its essential role in bacterial survival, c-di-AMP has also been reported to be involved in cell wall homeostasis for example by modulating the cell turgor e.g. in *S. aureus* (Corrigan et al. 2011; Commichau et al. 2017; Commichau and Stülke 2018). The cell wall is an essential organ and forms a bacterial weak point. Therefore, inhibition of cell wall enzymes is in many cases lethal or leads to virulence defects (for review (Schneider and Sahl 2010)). Research on cell wall maintenance upon different intracellular c-di-AMP concentrations showed that an up-regulated c-di-AMP level significantly increases the number of cross-linked peptidoglycans. This in turn increases resistance to cell wall targeting enzymes (Corrigan et al. 2011). Hence, a reduced intracellular c-di-AMP level leads to weakened cell wall and therefore a higher susceptibility (Dengler et al. 2013; Witte et al. 2013; Cheng et al. 2016; Rismondo et al. 2016).

Bacteria with an inhered sessile lifestyle are highly tolerant to antibiotics. Infections of biofilm forming bacteria usually need higher antibiotic doses over a longer time (reviewed in (Gebreyohannes et al. 2019)). As it has been reported for c-di-GMP, in a plethora of different bacterial species also c-di-AMP influences the biofilm formation in e.g. *S. aureus* and *Streptococcus mutans* (Corrigan et al. 2011; Peng et al. 2016; Valentini and Filloux 2016).

It has been proposed previously that single enzymes might not be a good antibiotic drug target as they are prone to develop resistances very rapid (Silver 2011).

A leverage point in the future could be a combined antibiotic therapy of a DAC inhibitor and antibiotics that are already on the marked as it is already described for M. tuberculosis infections (Silver 2011). A reduction of the c-di-AMP level has been shown to increase bacterial susceptibility to already existing antibiotics and for some bacteria the absence of c-di-AMP is lethal. However, it should always be considered that identification of new antibiotics and the development of resistances is a very dynamic process and resistances will probably occur soon after the first treatment (Ventola 2015). In order to combat antibiotic resistance, research should additionally focus on understanding how adaptation and therefore resistances develop.

In addition to what has been reported on c-di-AMP in literature, our structural and biochemical characterization of CdaA unveiled important information that can be used for inhibitor development. As discussed previously it is assumed that in contrast to DisA, the active CdaA dimer is only transiently existing and is formed upon ATP binding. Therefore, it seems to be expected that CdaA comprises an amino acid which is able to lock ATP in the active site until dimerization will take place. Indeed, a tyrosine (187 in *L. monocytogenes*) has been shown to importantly contribute to the cyclase activity. Structural analysis unveiled that this tyrosine is positioned in the active site and is able to lock an ATP molecule by π-π stacking interactions. Upon dimerization this tyrosine is displaced by a threonine of the second CdaA monomer form-

ing the active dimeric assembly. These biochemical and structural data help to interpret fragment hits that were identified by using the fragment screen approach. Three binding pockets were identified on the surface of a CdaA monomer. The first fragment binding site (binding site I) is positioned in the upper part of the ATP/c-di-AMP binding pocket (Chapter 5) and involves π-π stacking with the tyrosine 187. This leads to the assumption that a potential inhibitor should be large enough to span between binding sites I and II (Chapter 5) and gain binding specificity by forming additional interactions outside the ATP binding site. Some of the fragments positioned in the first and second binding pocket are either protruding out or into the ATP binding site. Further fragment development might result in a specific inhibitor which hampers dimer formation as it is assumed that a catalytic CdaA dimer is only transient. In order to make potential CdaA inhibitors into a real future drug, physicochemical properties need to be considered like molecule permeability and accumulation in the bacterial cell (Jones 2017). Sintim and colleagues have been successful in identifying four DisA inhibitors. However, further optimization has been difficult and failed due to permeability issues, easy metabolization or low bioavailability *in vivo* (Spencer 2003; Opoku-Temeng et al. 2017).

Chapter 7: Summary and Outlook

7.1 Summary

One major concern of today's life is the increase of antimicrobial resistance and the rising number of multi drug resistant bacterial species. There is an urgent need of identifying new antibiotic drug targets since resistances threaten the repertoire of available antibiotics.
Cyclic di-AMP (c-di-AMP) is the only known essential second messenger mainly found in Gram-positive bacteria of which several are known as human pathogens (Woodward et al. 2010; Luo Y and Helmann 2012; Mehne et al. 2013; Gundlach et al. 2015a; Commichau et al. 2017; Gundlach et al. 2017a; Gundlach et al. 2017b; Commichau et al. 2019). It is involved in many cellular processes like cell wall metabolism and DNA integrity scanning (Corrigan Rebecca M and Gründling 2013; Commichau et al. 2019). c-di-AMP is synthesised by proteins containing diadenylate cyclase domains (DAC) (Romling 2008; Corrigan Rebecca M and Gründling 2013; Blötz et al. 2017; Commichau et al. 2019). CdaA is the sole DAC in the human pathogen *Listeria monocytogenes,* which is also conserved in many other human pathogenic bacteria (Rosenberg et al. 2015; Heidemann et al. 2019; Tosi et al. 2019). Since c-di-AMP is also essential for the growth of these pathogenic bacteria, CdaA seems to be an attractive target for the development of novel antibiotic compounds (Corrigan R. M. and Gründling 2013; Zheng et al. 2014; Rosenberg et al. 2015; Opoku-Temeng and Sintim 2016a; Commichau et al. 2019).
This work is focused on functionality and regulation of the most prevailing DAC class CdaA from *L. monocytogenes* and the c-di-AMP receptor DarB/YkuL from *B. subtilis*.
Here we report new crystal forms of CdaA from *Listeria monocytogenes* in its apo-state, post-catalytic state with bound c-di-AMP and two catalytic Co^{2+} ions as well as in complex with AMP. The comparison of the determined crystal structures revealed a tyrosine side chain (Tyr^{187}) positioned in different orientations but locking the adenine ring after ATP binding. A mutation of Tyr^{187} to Ala unveiled its essential role during catalysis. This data enables the suggestion of a slightly different mechanism compared to its homolog DisA which is also known to synthesize c-di-AMP. Each monomer of CdaA needs to bind an ATP molecule, subsequently a dimer is formed in order to perform catalysis. We suggest that this dimer formation is only transiently existing which is different to the stable associated DisA dimer comprising DAC domains positioned in a head to head assembly. This is an interesting and important assumption and helps to develop CdaA specific inhibitors that prevent dimerization. In order to identify potential compounds that reduce the CdaA activity we used crystallographic fragment screening. This approach requires well diffracting (~ 2.0 Å) crystals of CdaA in its apo-state. Obtained apo CdaA crystals belong to the space group $P2_12_12_1$ and diffracted up to 1.7 Å resolution. Furthermore, the active site of apo CdaA in the crystal is exposed to solvent channels

making it suitable for fragment screening. The results of our first crystallographic fragment screen unveiled three fragment binding sites in CdaA. Some fragments could be used to design inhibitors capable of preventing CdaA dimerisation and ATP binding due to π-π stacking interactions with the side chain of the Tyr^{187}. Additional *in vitro* and *in silico* experiments are needed to come up with a potential CdaA inhibitor.
Furthermore, we showed that the phosphoglucosamine mutase GlmM inhibits CdaA under hyperosmotic conditions. A phenylalanine 155 which is exposed on the surface of GlmM importantly contributes to the CdaA regulation. Further biochemical and structural experiments on how GlmM inhibits CdaA might also help to develop CdaA inhibitor which is based on the inhibitory mechanism of GlmM.
Beside studying the regulation and inhibition of CdaA it is not less interesting to understand more abound the function of c-di-AMP. Up to the present time a plethora of c-di-AMP binding proteins have been discovered. Many of these proteins are involved in potassium or osmolyte uptake (Gundlach et al. 2019). c-di-AMP was identified to bind to conserved domains like the RCK_C domain or the CBS domain.
It has been reported that *B. subtilis* carries 16 CBS domain containing proteins. c-di-AMP binding assays resulted in the identification of the CBS domain protein DarB/YkuL as a c-di-AMP receptor (Gundlach et al. 2019). Homologs have been identified in different Gram-positive bacteria like *L. monocytogenes* (CbpB) (Sureka et al. 2014). In order to get further insights into its function we crystallized DarB from *B. subtilis* in presence of c-di-AMP. Here we report new crystal forms of DarB in its apo-state and in complex with either c-di-AMP, 3'3'cGAMP or AMP. All determined crystals diffracted to a resolution of 1.5 - 1.8.4 Å and exhibit the same crystal packing ($P2_12_12_1$). The crystal structures revealed two DarB monomers in the asymmetric unit forming a disk-like dimer. Surprisingly, the difference electron density map of each complex crystal suggested one of the described ligands in each of the supposed nucleotide binding site. This is different to the CBS domain containing protein OpuCA which is known to bind only one c-di-AMP in an extended conformation (Schuster et al. 2016).

7.2 Outlook

In this work we succeeded in crystallizing CdaA from the human pathogen *L. monocytogenes* in its catalytic active dimeric form and also in its inactive apo form. The reproducibility of well diffracting crystals of apo CdaA provided the opportunity to perform a crystallographic fragment screen. This resulted in the identification of eight unique fragment hits. A next step will be a follow-up campaign in order to identify lead compounds. The resulting compounds will be used for *in silico* docking experiments which will be computationally scored. We aim to

come up with a compound which has an increased binding affinity to CdaA and inhibits its c-di-AMP synthesis.

Since c-di-AMP covers important regulatory functions in e.g. osmolyte homeostasis yet an excess of c-di-AMP is toxic to the cell its synthesis needs to be regulated. Here we succeeded in identifying the regulation of CdaA by GlmM in *L. monocytogenes*. We were able to show that CdaA and GlmM form a complex under hyperosmotic stress. So far, no crystallographic data on the GlmM-CdaA complex are available, therefore we aim to crystallize the GlmM-CdaA complex in order to get further insights into the inhibition mechanism.

c-di-AMP has been shown in several studies to bind to diverse binding partners. During this work we were able to crystallize DarB/YkuL from *B. subtilis* with bound c-di-AMP. Our collaboration partners were able to identify its interaction partner and putative function (Krüger et al. 2020, manuscript submitted). These results form the basis for further experimental work like crystallization and biochemical characterization.

Chapter 8: Supporting Information

8.1 In vitro diadenylate cyclase assay

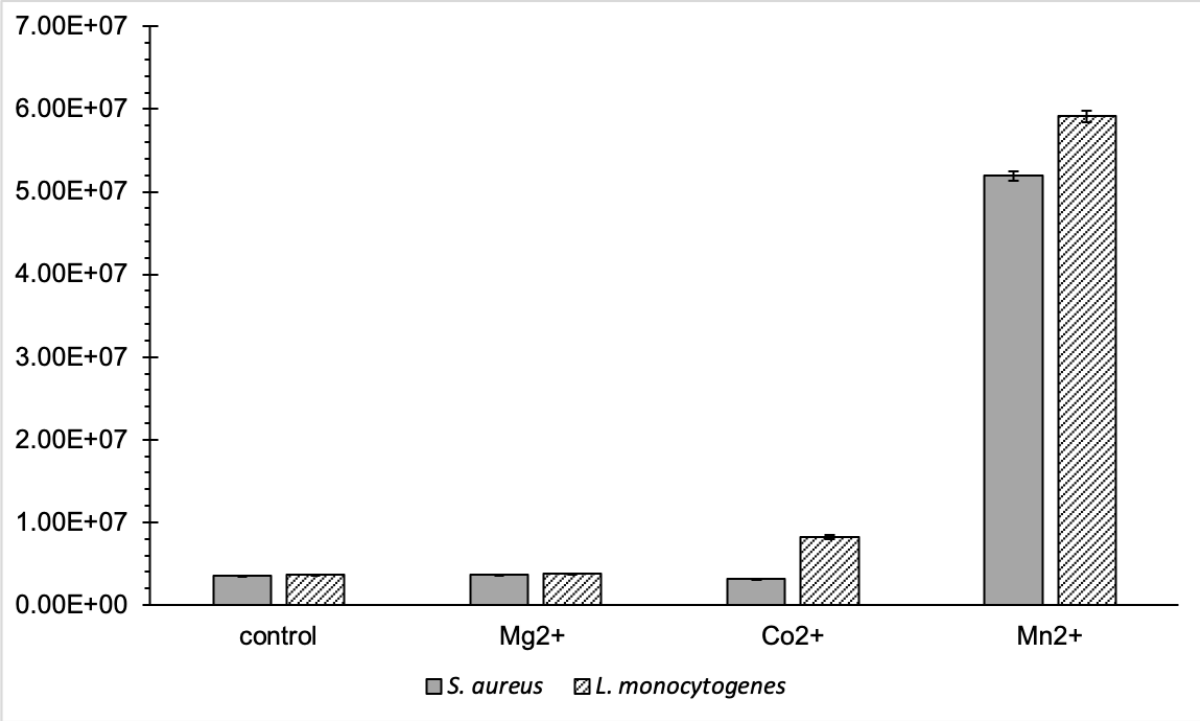

Figure 6: In vitro diadenylate cyclase activity of Δ100CdaA from *S. aureus* and *L. monocytogenes*. *L. monocytogenes* Δ100CdaA was cloned as described in Chapter 2. The *S. aureus* Δ100CdaA plasmid purification system was generated synthetically using the BioCat gene synthesis supply service (BioCat GmbH, used vector: pGEX-6P-1). Purification was performed as previously described for Δ100CdaA in Chapter 2 (Buffer: 300 mM NaCl, 20 mM Tris/HCl pH 7.5). The tag-less proteins were used for measuring the conversion of two ATPs to c-di-AMP. The cyclase activity was measured with the quantitative coralyne fluorescence assay (Zhou et al. 2014) as described in Chapter 2 (Heidemann et al. 2019). Three independent measurements were performed for each sample. 10 µM Δ100CdaA was incubated for around 1 h at 30 °C with 100 µM ATP and either 10 mM $MnCl_2$, $CoCl_2$ or $MgCl_2$. The control measurements were performed using Δ100CdaA constructs without addition of any metal ion. The results suggested a similar metal dependence of CdaA from *S. aureus* and *L. monocytogenes*. According to our results Mn^{2+} is the main cofactor for CdaA from both organisms. However, activity in presence of Mg^{2+} was neither observed for *L. monocytogenes* CdaA nor *S. aureus* CdaA.

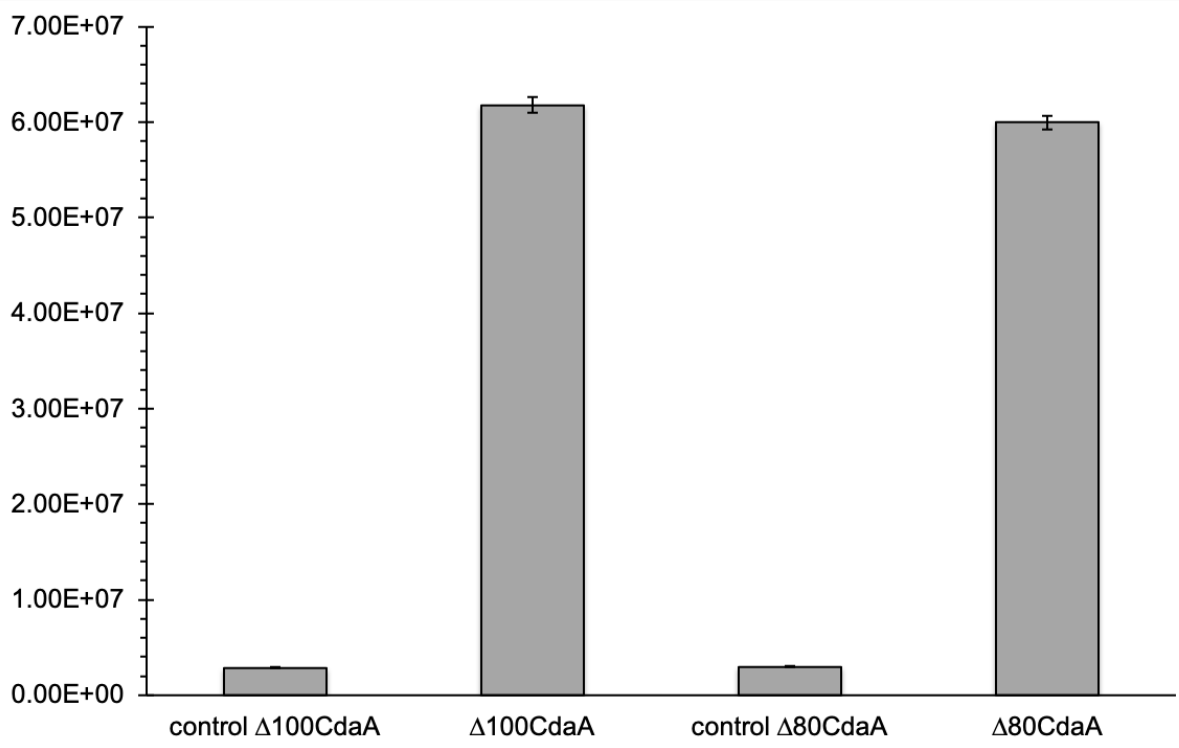

Figure 7: In vitro diadenylate cyclase activity of Δ80CdaA and Δ100CdaA. Construct Δ100CdaA was cloned and purified as described in Chapter 2 (Heidemann et al. 2019). For the purification procedure the longer construct Δ80CdaA was, as previously reported for the Δ100CdaA construct, equipped with a GST-tag. The Δ*240cdaA* allele was amplified using the primer pair (JH003 forward 5'-CCGGATCCTTCCAACCGGAATTACGCCG-3')/JH005 reverse (5'-GGCTCGAGTCATTCGCTTTTGCCTCCTTTCC-3'). As a template the plasmid pBP119 was used (Rosenberg et al. 2015). Subsequently the PCR product was cloned into the pGEX-6P-1 expression vector with the restriction sites XhoI and BamHI. The resulting plasmid encodes the purification construct Δ80CdaA with an N-terminal GST-tag. Purification was performed as previously described for Δ100CdaA in Chapter 2 (Buffer: 300 mM NaCl, 20 mM Tris/HCl pH 7.5). The tag-less proteins were used for measuring the conversion of two ATPs to c-di-AMP. The cyclase activity was measured with the quantitative coralyne fluorescence assay (Zhou et al. 2014) as described in Chapter 2 (Heidemann et al. 2019). Three independent measurements were performed for each sample. 10 µM Δ100CdaA and Δ80CdaA were incubated for around 1 h at 30 °C with 100 µM ATP + 10 mM $MnCl_2$. The control measurements were performed using either the wt Δ80CdaA or the wt Δ100CdaA construct without addition of any metal ion.
No significant difference in activity was observed comparing the longer Δ80CdaA with the shorter Δ100CdaA construct.

8.2 Superposition of in the PDB available CdaA structures

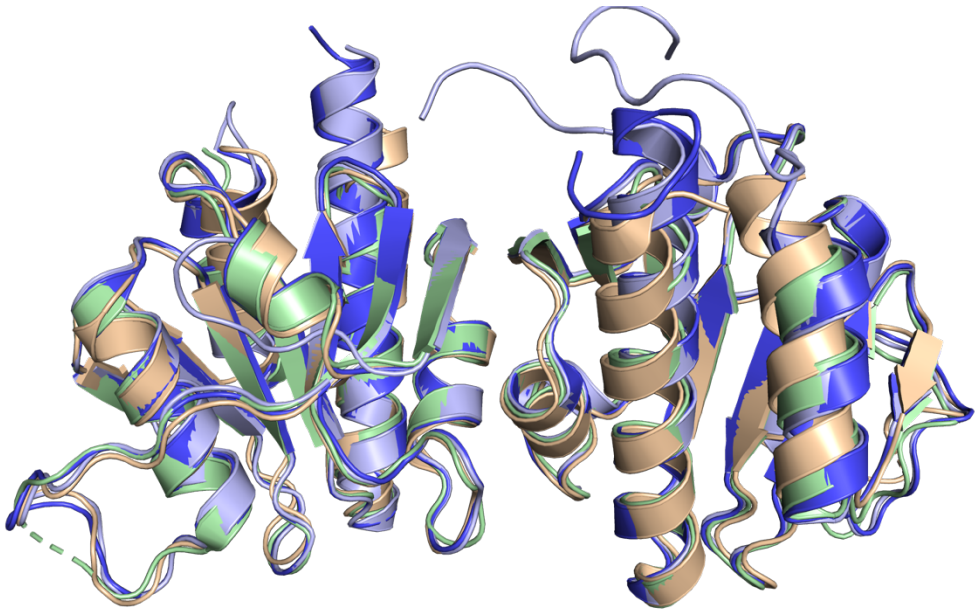

Figure 8: Superposition of in the PDB available CdaA structures from three different organisms. All structures show the same non-catalytic dimeric assembly in the asymmetric unit. *L. monocytogenes* Δ100CdaA (blue and light blue) was crystallised in two different space groups (dark blue, space group $H3_2$ (PDB code: 6HVL); light blue: space group $P2_12_12_1$ (PDB code: 6HVM)) (Heidemann et al. 2019); *S. aureus* (light brown, space group $P2_12_12_1$ (PDB code: 6GYW)); *B. subtilis* (light green, space group: $P4_32_12$ (PDB code: 6HUW)) (Tosi et al. 2019).

References

Ablasser A, Goldeck M, Cavlar T, Deimling T, Witte G, Röhl I, Hopfner K-P, Ludwig J, Hornung V (2013): cGAS produces a 2′-5′-linked cyclic dinucleotide second messenger that activates STING. Nature 498, 380–384

Anashkin VA, Baykov AA, Lahti R (2017): Enzymes regulated via cystathionine β-synthase domains. Biochem 82, 1079–1087

Andrade WA, Firon A, Schmidt T, Hornung V, Fitzgerald KA, Kurt-Jones EA, Trieu-Cuot P, Golenbock DT, Kaminski PA (2016): Group B Streptococcus Degrades Cyclic-di-AMP to Modulate STING-Dependent Type I Interferon Production. Cell Host Microbe 20, 49–59

Archer KA, Durack J, Portnoy DA (2014): STING-Dependent Type I IFN Production Inhibits Cell-Mediated Immunity to Listeria monocytogenes. PLoS Pathog 10, 1–14

Ashburner J, Friston KJ (2000): Voxel-based morphometry - The methods. Neuroimage 11, 805–821

Asokan G V., Ramadhan T, Ahmed E, Sanad H (2019): WHO global priority pathogens list: A bibliometric analysis of medline-pubmed for knowledge mobilization to infection prevention and control practices in Bahrain. Oman Med J 34, 184–193

Bai Y, Yang J, Zhou X, Ding X, Eisele LE, Bai G (2012): Mycobacterium tuberculosis Rv3586 (DacA) is a diadenylate cyclase that converts ATP or ADP into c-di-amp. PLoS One 7, 1–10

Bai Y, Yang J, Eisele LE, Underwood AJ, Koestler BJ, Waters CM, Metzger DW, Bai G (2013): Two DHH subfamily 1 proteins in Streptococcus pneumoniae possess cyclic Di-AMP phosphodiesterase activity and affect bacterial growth and virulence. J Bacteriol 195, 5123–5132

Bai Y, Yang J, Zarrella TM, Zhang Y, Metzger DW, Bai G (2014): Cyclic Di-AMP Impairs Potassium Uptake Mediated by a Cyclic Di-AMP Binding Protein in Streptococcus pneumoniae. J Bacteriol 196, 614–623

Barb AW, Cort JR, Seetharaman J, Lew S, Lee HW, Acton T, Xiao R, Kennedy MA, Tong L, Montelione GT, Prestegard JH (2010): Structures of domains I and IV from YbbR are representative of a widely distributed protein family. Protein Sci 20, 396–405

Barelier S, Eidam O, Fish I, Hollander J, Figaroa F, Nachane R, Irwin JJ, Shoichet BK, Siegal G (2014): Increasing chemical space coverage by combining empirical and computational fragment screens. ACS Chem Biol 9, 1528–1535

Barreteau H, Kovač A, Boniface A, Sova M, Gobec S, Blanot D (2008): Cytoplasmic steps of peptidoglycan biosynthesis. FEMS Microbiol Rev 32, 168–207

Bateman A (1997): The structure of a domain dommon to archeabacteria and the homocystinuria disease protein. Trends Biochem Sci 12–13

Baykov AA, Tuominen HK, Lahti R (2011): The CBS domain: A protein module with an emerging prominent role in regulation. ACS Chem Biol 6, 1156–1163

Bejerano-Sagie M, Oppenheimer-Shaanan Y, Berlatzky I, Rouvinski A, Meyerovich M, Ben-Yehuda S (2006): A Checkpoint Protein That Scans the Chromosome for Damage at the Start of Sporulation in Bacillus subtilis. Cell 125, 679–690

Blommers MJJ, Haasnoot CAG, I. WJAL, Van der Marel GA, Van Boom JH, Hilbers CW (1988): Solution Structure of the 3'-5' cyclic Dinucleotide pApA. A combined NMR, UV melting and Molecular Mechanics study. Biochemistry 27, 8361–8369

Blötz C, Treffon K, Kaever V, Schwede F, Hammer E, Stülke J (2017): Identification of the

components involved in cyclic di-AMP signaling in Mycoplasma pneumoniae. Front Microbiol 8, 1–10

Bordeleau E, Fortier LC, Malouin F, Burrus V (2011): c-di-GMP turn-over in Clostridium difficile is controlled by a plethora of diguanylate cyclases and phosphodiesterases. PLoS Genet 7, 1–12

Bowman L, Zeden MS, Schuster CF, Kaever V, Gründling A (2016): New insights into the cyclic di-adenosine monophosphate (c-di-AMP) degradation pathway and the requirement of the cyclic dinucleotide for acid stress resistance in Staphylococcus aureu. J Biol Chem 291, 26970–26986

Bradford MM (1976): Revisiting a dogma: The effect of volume exclusion in molecular crowding. Anal Biochem 72, 248–254

Brückner R, Titgemeyer F (2002): Carbon catabolite repression in bacteria: Choice of the carbon source and autoregulatory limitation of sugar utilization. FEMS Microbiol Lett 209, 141–148

Casadesús J: Bacterial Adaptation. In: Kolter R, Maloy S (Eds.): Microbes and Evolution. American Society for Microbiology (ASM) Press, Washington, DC 2012, 99–107

Cashel M, Gallant J (1969): Two Compounds implicated in the Function of RC gene. Nature 221, 838–841

Chandrangsu P, Rensing C, Helmann JD (2017): Metal Homeostasis and Resistance in Bacteria. Nat Rev Microbiol 15, 338–350

Chen YC, Lim C (2008): Predicting RNA-binding sites from the protein structure based on electrostatics, evolution and geometry. Nucleic Acids Res 36

Cheng X, Zheng X, Zhou X, Zeng J, Ren Z, Xu X, Cheng L, Li M, Li J, Li Y (2016): Regulation of oxidative response and extracellular polysaccharide synthesis by a diadenylate cyclase in Streptococcus mutans. Environ Microbiol 18, 904–922

Chou SH, Galperin MY (2016): Diversity of cyclic di-GMP-binding proteins and mechanisms. J Bacteriol 198, 32–46

Christen B, Christen M, Paul R, Schmid F, Folcher M, Jenoe P, Meuwly M, Jenal U (2006): Allosteric control of cyclic di-GMP signaling. J Biol Chem 281, 32015–32024

Commichau FM, Stülke J (2018): Coping with an essential poison: A genetic suppressor analysis corroborates a key function of c-di-AMP in controlling potassium ion homeostasis in Gram-positive bacteria. J Bacteriol 200

Commichau FM, Dickmanns A, Gundlach J, Ficner R, St??lke J (2015a): A jack of all trades: the multiple roles of the unique essential second messenger cyclic di-AMP. Mol Microbiol 97, 189–204

Commichau FM, Dickmanns A, Gundlach J, Ficner R, Stülke J (2015b): A jack of all trades: the multiple roles of the unique essential second messenger cyclic di-AMP. Mol Microbiol 97, 189–204

Commichau FM, Gibhardt J, Halbedel S, Gundlach J, Stülke J (2017): A Delicate Connection: c-di-AMP Affects Cell Integrity by Controlling Osmolyte Transport. Trends Microbiol 26, 175–185

Commichau FM, Heidemann JL, Ficner R, Stülke J (2019): Making and breaking of an essential poison: The cyclases and phosphodiesterases that produce and degrade the essential second messenger cyclic di-AMP in bacteria. J Bacteriol 201, 1–14

Congreve M, Chessari G, Tisi D, Woodhead AJ (2008): Recent developments in fragment-based drug discovery. J Med Chem 51, 3661–3680

Corrigan Rebecca M, Gründling A (2013): Cyclic di-AMP: another second messenger enters the fray. Nat Rev Microbiol 11, 513–24

Corrigan R. M., Gründling A (2013): Cyclic di-AMP: Another second messenger enters the fray. Nat Rev Microbiol 11, 513–524

Corrigan RM, Abbott JC, Burhenne H, Kaever V, Gründling A (2011): C-di-amp is a new second messenger in staphylococcus aureus with a role in controlling cell size and envelope stress. PLoS Pathog 7

Corrigan RM, Campeotto I, Jeganathan T, Roelofs KG, Lee VT, Gründling A (2013): Systematic identification of conserved bacterial c-di-AMP receptor proteins. PNAS 110, 9084–9089

Cotter PA, Stibitz S (2007): c-di-GMP-mediated regulation of virulence and biofilm formation. Curr Opin Microbiol 10, 17–23

Crimmins GT, Herskovits AA, Rehder K, Sivick KE, Lauer P, Dubensky TW, Portnoy DA (2008): Listeria monocytogenes multidrug resistance transporters activate a cytosolic surveillance pathway of innate immunity. Proc Natl Acad Sci U S A 105, 10191–10196

Dahlstrom KM, Giglio KM, Sondermann H, O'Toolea GA (2016): The inhibitory site of a diguanylate cyclase is a necessary element for interaction and signaling with an effector protein. J Bacteriol 198, 1595–1603

Day P, Sharff A, Parra L, Cleasby A, Williams M, Hörer S, Nar H, Redemann N, Tickle I, Yon J (2007): Structure of a CBS-domain pair from the regulatory γ1 subunit of human AMPK in complex with AMP and ZMP. Acta Crystallogr Sect D Biol Crystallogr

Dengler V, McCallum N, Kiefer P, Christen P, Patrignani A, Vorholt JA, Berger-Bächi B, Senn MM (2013): Mutation in the C-Di-AMP Cyclase dacA Affects Fitness and Resistance of Methicillin Resistant Staphylococcus aureus. PLoS One 8

Devaux L, Sleiman D, Mazzuoli MV, Gominet M, Lanotte P, Trieu-Cuot P, Kaminski PA, Firon A (2018): Cyclic di-AMP regulation of osmotic homeostasis is essential in Group B Streptococcus. PLoS Genet 14, 1–23

Dever LA, Dermody TS (1991): Mechanisms of bacterial resistance to antibiotics. Arch Intern Med 151, 886–895

Dey B, Dey RJ, Cheung LS, Pokkali S, Guo H, Lee JH, Bishai WR (2015): A bacterial cyclic dinucleotide activates the cytosolic surveillance pathway and mediates innate resistance to tuberculosis. Nat Med 21, 401–408

Ellis JJ, Broom M, Jones S (2007): Protein-RNA interactions: Structural analysis and functional classes. Proteins Struct Funct Genet

Emsley P, Lohkamp B, Scott WG, Cowtan K (2010): Features and development of Coot. Acta Crystallogr Sect D Biol Crystallogr 66, 486–501

Epstein W (2003): The Roles and Regulation of Potassium in Bacteria. Prog Nucleic Acid Res Mol Biol 75, 293–320

Ereño-Orbea J, Oyenarte I, Martínez-Cruz LA (2013): CBS domains: Ligand binding sites and conformational variability. Arch Biochem Biophys

Ertl P, Jelfs S, Mühlbacher J, Schuffenhauer A, Selzer P (2006): Quest for the rings. In silico exploration of ring universe to identify novel bioactive heteroaromatic scaffolds. J Med Chem 49, 4568–4573

Fahmi T, Port GC, Cho KH (2017): C-di-AMP: An essential molecule in the signaling pathways that regulate the viability and virulence of gram-positive bacteria. Genes (Basel) 8, 1–17

Feher M, Schmidt JM (2003): Property distributions: Differences between drugs, natural products, and molecules from combinatorial chemistry. J Chem Inf Comput Sci 43, 218–227

Ferrell JE (2009): Q&A: Cooperativity. J Biol 8, 1–6

Fleming SA (1945): Nobel Lecture, December 11, 1945. Nobel Lect Physiol or Med 1942-1962 83–93

Fujisawa M, Ito M, Krulwich TA (2007): Three two-component transporters with channel-like properties have monovalent cation/proton antiport activity. Proc Natl Acad Sci U S A 104,

13289–13294
Galperin MY, Nikolskaya AN, Koonin E V. (2001): Novel domains of the prokaryotic two-component signal transduction systems. FEMS Microbiol Lett 203, 11–21
Gebreyohannes G, Nyerere A, Bii C, Sbhatu DB (2019): Challenges of intervention, treatment, and antibiotic resistance of biofilm-forming microorganisms. Heliyon 5, 1–7
Gentner M, Allan MG, Zaehringer F, Schirmer T, Grzesiek S (2012): Oligomer formation of the bacterial second messenger c-di-GMP: Reaction rates and equilibrium constants indicate a monomeric state at physiological concentrations. J Am Chem Soc 134, 1019–1029
German Federal GovernmentDart 2020-Fighting antibiotic resistance for the good of both humans and animals. 2020
Gibhardt J, Hoffmann G, Turdiev A, Wang M, Lee VT, Commichau FM (2019): C-di-AMP assists osmoadaptation by regulating the Listeria monocytogenes potassium transporters KimA and KtrCD. J Biol Chem 294, 16020–16033
Goodsell DS, Olson AJ (2000): Structural Symmetry and Protein Function. Biophys Biomol Struct 29, 105–153
Goudreau PN, Stock AM (1998): Signal transduction in bacteria: Molecular mechanisms of stimulus-response coupling. Curr Opin Microbiol 1, 160–169
Gundlach J, Mehne FMP, Herzberg C, Kampf J, Valerius O, Kaever V, Stülke J (2015a): An essential poison: Synthesis and degradation of cyclic Di-AMP in Bacillus subtilis. J Bacteriol 197, 3265–3274
Gundlach J, Dickmanns A, Schröder-Tittmann K, Neumann P, Kaesler J, Kampf J, Herzberg C, Hammer E, Schwede F, Kaever V, et al. (2015b): Identification, characterization and structure analysis of the c-di-AMP binding PII-like signal transduction protein DarA. J Biol Chem 290, 3069–3080
Gundlach J, Herzberg C, Hertel D, Thürmer A, Daniel R, Link H, Stülke J: Adaptation of Bacillus subtilis to Life at Extreme Potassium Limitation. volume 8; 2017a
Gundlach J, Herzberg C, Kaever V, Gunka K, Hoffmann T, Weiß M, Gibhardt J, Thürmer A, Hertel D, Daniel R, et al. (2017b): Control of potassium homeostasis is an essential function of the second messenger cyclic di-AMP in Bacillus subtilis. Sci Signal 10
Gundlach J, Krüger L, Herzberg C, Turdiev A, Poehlein A, Tascón I, Weiss M, Hertel D, Daniel R, Hänelt I, et al. (2019): Sustained sensing in potassium homeostasis: Cyclic di-AMP controls potassium uptake by KimA at the levels of expression and activity. J Biol Chem 294, 9605–9614
Hawkey PM (1998): The origins and molecular basis of antibiotic resistance. N Engl J Med 317, 657–660
He J, Galperin MY, Chou SH (2020): Cyclic di-AMP, a second messenger of primary importance: tertiary structures. Nucleic Acids Res
Heidemann JL, Neumann P, Dickmanns A, Ficner R (2019): Crystal structures of the c-di-AMP-synthesizing enzyme CdaA. J Biol Chem 294, 10463–10470
Hengge R (2009): Principles of c-di-GMP signalling in bacteria. Nat Rev Microbiol 7, 263–273
Holm L, Rosenström P (2010): Dali server: Conservation mapping in 3D. Nucleic Acids Res 38, 545–549
Hubbard R. E: Fragment-based Drug Discovery Lessons and Outlook. In: Fragment-based Drug Discovery Lessons and Outlook. Wiley-VCH Verlag GmbH & Co. KGaA, Weinheim 2016, 1–500
Hume ME (2011): Food Safety Symposium: Potential Impact of Reduced Antibiotic Use and the Roles of Prebiotics, Probiotics, and Other Alternatives in Antibiotic-Free Broiler Production. Poult Sci 90, 2663–2669

Huschmann FU, Linnik J, Sparta K, Ühlein M, Wang X, Metz A, Schiebel J, Heine A, Klebe G, Weiss MS, Mueller U (2016): Structures of endothiapepsin-fragment complexes from crystallographic fragment screening using a novel, diverse and affordable 96-compound fragment library. Acta Crystallogr Sect FStructural Biol Commun 72, 346–355

Huynh TAN, Woodward JJ (2016): Too much of a good thing: Regulated depletion of c-di-AMP in the bacterial cytoplasm. Curr Opin Microbiol 30, 22–29

Huynh TAN, Luo S, Pensinger D, Sauer JD, Tong L, Woodward JJ (2015): An HD-domain phosphodiesterase mediates cooperative hydrolysis of c-di-AMP to affect bacterial growth and virulence. Proc Natl Acad Sci U S A 112, E747–E756

Huynh TN, Choi PH, Sureka K, Ledvina HE, Tong L, Woodward JJ (2017): Cyclic di-AMP targets the cystathionine beta-synthase domain of the osmolyte transporter OpuC. Mol Microbiol 102, 233–243

Jenal U (2004): Cyclic di-guanosine-monophosphate comes of age: A novel secondary messenger involved in modulating cell surface structures in bacteria? Curr Opin Microbiol 7, 185–191

Jones S (2017): Permeability rules for antibiotic design. Nat Biotechnol 35, 639

Kabsch W (2010a): Integration, scaling, space-group assignment and post-refinement. Acta Crystallogr Sect D Biol Crystallogr 66, 133–144

Kabsch W (2010b): XDS. Acta Crystallogr Sect D Biol Crystallogr 66, 125–132

Kader A, Simm R, Gerstel U, Morr M, Römling U (2006): Hierarchical involvement of various GGDEF domain proteins in rdar morphotype development of Salmonella enterica serovar Typhimurium. Mol Microbiol 60, 602–616

Kim H, Youn SJ, Kim SO, Ko J, Lee JO, Choi BS (2015): Structural studies of potassium transport protein KtrA regulator of conductance of K+ (RCK) C domain in complex with cyclic diadenosine monophosphate (c-di-AMP). J Biol Chem 290, 16393–16402

Kranzusch PJ (2019): cGAS and CD-NTase enzymes: structure, mechanism, and evolution. Curr Opin Struct Biol 59, 178–187

Lamoree B, Hubbard RE (2017): Current perspectives in fragment-based lead discovery (FBLD). Essays Biochem 61, 453–464

Liebschner D, Afonine P V., Moriarty NW, Poon BK, Sobolev O V., Terwilliger TC, Adams PD (2017): Polder maps: Improving OMIT maps by excluding bulk solvent. Acta Crystallogr Sect D Struct Biol 73, 148–157

Luo Y, Helmann JD (2012): Analysis of the role of Bacillus subtilis sigma(M) in beta-lactam resistance reveals an essential role for c-di-AMP in peptidoglycan homeostasis. Mol Microbiol 83, 623–639

Luo Yun, Helmann JD (2012): Analysis of the role of Bacillus subtilis σM in β-lactam resistance reveals an essential role for c-di-AMP in peptidoglycan homeostasis. Mol Microbiol 83, 623–639

Makman RS, Sutherland EW (1964): Adenosine 3', 5'-Phosphate in Escherichia. J Biol Chem 240, 1309–1314

Manikandan K, Sabareesh V, Singh N, Saigal K, Mechold U, Sinha KM (2014): Two-step synthesis and hydrolysis of cyclic di-AMP in Mycobacterium tuberculosis. PLoS One 9

McCoy AJ, Grosse-Kunstleve RW, Adams PD, Winn MD, Storoni LC, Read RJ (2007): Phaser crystallographic software. J Appl Crystallogr 40, 658–674

McFarland AP, Luo S, Ahmed-Qadri F, Zuck M, Thayer EF, Hybiske K, Tong L, Woodward JJ (2017): Sensing of bacterial cyclic dinucleotides by the oxidoreductase RECON promotes NF-κB activation and shapes a proinflammatory antibacterial state. Immunity 46, 433–445

McFarland AP, Burke TP, Carletti AA, Glover RC, Tabakh H, Welch MD, Woodward JJ (2018): RECON-dependent inflammation in hepatocytes enhances listeria

monocytogenes cell-to-cell spread. MBio 9, 1–15
McLean JE, Hamaguchi N, Belenky P, Mortimer SE, Stanton M, Hedstrom L (2004): Inosine 5′-monophosphate dehydrogenase binds nucleic acids in vitro and in vivo. Biochem J 379, 243–251
Meek RW, Cadby IT, Moynihan PJ, Lovering AL (2019): Structural basis for activation of a diguanylate cyclase required for bacterial predation in Bdellovibrio. Nat Commun 10
Mehne FMP, Gunka K, Eilers H, Herzberg C, Kaever V, Stülke J (2013): Cyclic Di-AMP homeostasis in bacillus subtilis: Both lack and high level accumulation of the nucleotide are detrimental for cell growth. J Biol Chem 288, 2004–2017
Mehne FMP, Schröder-Tittmann K, Eijlander RT, Herzberg C, Hewitt L, Kaever V, Lewis RJ, Kuipers OP, Tittmann K, Stülke J (2014): Control of the diadenylate cyclase CdaS in Bacillus subtilis: An autoinhibitory domain limits cyclic di-AMP production. J Biol Chem 289, 21098–21107
Mengin-Lecreulx D, Van Heijenoort J (1996): Characterization of the essential gene glmM encoding phosphoglucosamine mutase in Escherichia coli. J Biol Chem 271, 32–39
Michael CA, Dominey-Howes D, Labbate M (2014): The antimicrobial resistance crisis: causes, consequences, and management. Front public Heal 2, 145
Moscoso JA, Schramke H, Zhang Y, Tosi T, Dehbi A, Jung K, Gründling A (2016): Binding of cyclic di-AMP to the Staphylococcus aureus sensor kinase KdpD occurs via the universal stress protein domain and downregulates the expression of the Kdp potassium transporter. J Bacteriol 198, 98–110
Müller M, Deimling T, Hopfner K-P, Witte G (2015): Structural analysis of the diadenylate cyclase reaction of DNA-integrity scanning protein A (DisA) and its inhibition by 3'-dATP. Biochem J 469, 367–74
Murray CW, Rees DC (2009): The rise of fragment-based drug discovery. Nat Chem 1, 187–192
Nelson JW, Sudarsan N, Furukawa K, Weinberg Z, Wang JX, Breaker RR (2013): Riboswitches in eubacteria sense the second messenger c-di-AMP. Nat Chem Biol 9, 834–839
Opoku-Temeng C, Sintim HO (2016a): Inhibition of cyclic diadenylate cyclase, DisA, by polyphenols. Nat Sci REPORTS 52, 3754–3757
Opoku-Temeng C, Sintim HO (2016b): Potent inhibition of cyclic diadenylate monophosphate cyclase by the antiparasitic drug, suramin. Chem Commun 52, 3754–3757
Opoku-Temeng C, Zhou J, Zheng Y, Su J, Sintim HO (2016): Cyclic dinucleotide (c-di-GMP, c-di-AMP, and cGAMP) signalings have come of age to be inhibited by small molecules. Chem Commun 52, 9327–9342
Opoku-Temeng C, Dayal N, Miller J, Sintim HO (2017): Hydroxybenzylidene-indolinones, c-di-AMP synthase inhibitors, have antibacterial and anti-biofilm activities and also re-sensitize resistant bacteria to methicillin and vancomycin. RSC Adv 7, 8288–8294
Oppenheimer-Shaanan Y, Wexselblatt E, Katzhendler J, Yavin E, Ben-Yehuda S (2011): c-di-AMP reports DNA integrity during sporulation in Bacillus subtilis. EMBO Rep 12, 594–601
Pearce NM, Krojer T, Bradley AR, Collins P, Nowak RP, Talon R, Marsden BD, Kelm S, Shi J, Deane CM, Von Delft F (2017a): A multi-crystal method for extracting obscured crystallographic states from conventionally uninterpretable electron density. Nat Commun 8, 24–29
Pearce NM, Bradley AR, Krojer T, Marsden BD, Deane CM, Delft F Von (2017b): Partial-occupancy binders identified by the Pan-Dataset Density Analysis method offer new chemical opportunities and reveal cryptic binding sites. Struct Dyn 4, 1–9
Pearce NM, Krojer T, Von Delft F (2017c): Proper modelling of ligand binding requires an

ensemble of bound and unbound states. Acta Crystallogr Sect D Struct Biol 73, 256–266
Peng X, Zhang Y, Bai G, Zhou X, Wu H (2016): Cyclic di-AMP mediates biofilm formation. Mol Microbiol 99, 945–959
Pesavento C, Hengge R (2009): Bacterial nucleotide-based second messengers. Curr Opin Microbiol 12, 170–176
Pfiffer V, Sarenko O, Possling A, Hengge R (2019): Genetic dissection of Escherichia coli's master diguanylate cyclase DgcE: Role of the N-terminal MASE1 domain and direct signal input from a GTPase partner system. PLoS Genet 15, 1–28
Pham HT, Nhiep NTH, Vu TNM, Huynh TAN, Zhu Y, Huynh ALD, Chakrabortti A, Marcellin E, Lo R, Howard CB, et al. (2018): Enhanced uptake of potassium or glycine betaine or export of cyclic-di-AMP restores osmoresistance in a high cyclic-di-AMP Lactococcus lactis mutant. PLoS Genet 14, 1–23
Phillips I, Casewell M, Cox T, De Groot B, Friis C, Jones R, Nightingale C, Preston R, Waddell J (2004): Does the use of antibiotics in food animals pose a risk to human health? A critical review of published data. J Antimicrob Chemother 53, 28–52
Quintana IM, Gibhardt J, Turdiev A, Hammer E, Commichau FM, Lee VT, Magni C, Stülke J (2019): The KupA and KupB Proteins of Lactococcus lactis IL1403 Are Novel c-di-AMP Receptor Proteins Responsible for Potassium Uptake. J Bacteriol 201, 1–13
Rall TW, Sutherland EW (1958): Formation of a cyclic by tissue. J Biol Chem Vol. 232, 1065-1076.
Rao F, See RY, Zhang D, Toh DC, Ji Q, Liang ZX (2010): YybT is a signaling protein that contains a cyclic dinucleotide phosphodiesterase domain and a GGDEF domain with ATPase activity. J Biol Chem 285, 473–482
Rao F, Ji Q, Soehano I, Liang ZX (2011): Unusual heme-binding PAS domain from YybT family proteins. J Bacteriol 193, 1543–1551
Rismondo J, Gibhardt J, Rosenberg J, Kaever V, Halbedel S, Commichau FM (2016): Phenotypes associated with the essential diadenylate cyclase CdaA and its potential regulator CdaR in the human pathogen Listeria monocytogenes. J Bacteriol 198, 416–426
Romling U (2008): Great times for small molecules: c-di-AMP, a second messenger candidate in Bacteria and Archaea. Sci Signal 1
Romling U, Galperin MY, Gomelsky M (2013): Cyclic di-GMP: the First 25 Years of a Universal Bacterial Second Messenger. Microbiol Mol Biol Rev 77, 1–52
Römling U, Liang ZX, Dow JM (2017): Progress in Understanding the Molecular Basis Underlying Functional Diversification of Cyclic Dinucleotide Turnover Proteins. J Bacteriol 199, 1–16
Rosenberg J, Dickmanns A, Neumann P, Gunka K, Arens J, Kaever V, Stülke J, Ficner R, Commichau FM (2015): Structural and biochemical analysis of the essential diadenylate cyclase CdaA from Listeria monocytogenes. J Biol Chem 290, 6596–6606
Ross P, Weinhouse H, Aloni Y, Michaeli D, Weinberger-Ohana P, Mayer R, Braun S, De Vroom E, Van Der Marel GA, Van Boom JH, Benziman M (1987): Regulation of cellulose synthesis in Acetobacter xylinum by cyclic diguanylic acid. Nature 325, 279–281
Ross P, Benziman M, Vroom E De, Fidder A, Boom JH Van (1990): The Cyclic Diguanylic Acid Regulatory in Acetobacter xylinum System of Cellulose Synthesis. Biochemistry 265, 18933–18943
Roy AB, Sauer K (2015): Diguanylate cyclase NicD based signaling mechanism of nutrient-induced dispersion by Pseudomonas aeruginosa Ankita. Mol Microbiol 94, 771–793
Rudolph MJ, Amodeo GA, Iram SH, Hong SP, Pirino G, Carlson M, Tong L (2007): Structure of the Bateman2 Domain of Yeast Snf4: Dimeric Association and Relevance for AMP Binding. Structure 15, 65–74

Schiebel J, Krimmer SG, Röwer K, Knörlein A, Wang X, Park AY, Stieler M, Ehrmann FR, Fu K, Radeva N, et al. (2016): High-Throughput Crystallography: Reliable and Efficient Identification of Fragment Hits. Structure 24, 1398–1409

Schneider T, Sahl HG (2010): An oldie but a goodie - cell wall biosynthesis as antibiotic target pathway. Int J Med Microbiol 300, 161–169

Schrödinger LLC (2010): The PyMOL Molecular Graphic SystemNo Title.

Schulz MN, Fanghänel J, Schäfer M, Badock V, Briem H, Boemer U, Nguyen D, Husemann M, Hillig RC (2011): A crystallographic fragment screen identifies cinnamic acid derivatives as starting points for potent Pim-1 inhibitors. Acta Crystallogr Sect D Biol Crystallogr 67, 156–166

Schuster CF, Bellows LE, Tosi T, Campeotto I, Corrigan RM, Freemont P, Gründling A (2016): The second messenger c-di-AMP inhibits the osmolyte uptake system OpuC in Staphylococcus aureus. Sci Signal 9, 1–31

Scott JW, Hawley SA, Green KA, Anis M, Stewart G, Scullion GA, Norman DG, Hardie DG (2004): CBS domains form energy-sensing modules whose binding of adenosine ligands is disrupted by disease mutations. J Clin Invest 113, 274–284

Severin GB, Waters CM (2019): Pyrimidines and Cyclic Trinucleotides Join the Second Messenger Symphony. Cell Host Microbe 25, 471–473

Shuker SB, Hajduk PJ, Meadows RP, Fesik SW (1997): Discovering high-affinity ligands for proteins: SAR by NMR. Science (80-) 274, 1531–1534

Silver LL (2011): Challenges of antibacterial discovery. Clin Microbiol Rev 24, 71–109

Sinnokrot MO, Valeev EF, Sherrill CD (2002): Estimates of the Ab Initio limit for π-π Interactions: The Benzene Dimer. J Am Chem Soc 124, 10887–10893

Song JH, Ko KS, Lee JY, Baek JY, Oh WS, Yoon HS, Jeong JY, Chun J (2005): Identification of essential genes in Streptococcus pneumoniae by allelic replacement mutagenesis. Mol Cells 19, 365–374

Spencer JPE (2003): Proceedings of the Third International Scientific Symposium on Tea and Human Health : Role of Flavonoids in the Diet Metabolism of Tea Flavonoids in the Gastrointestinal Tract 1 , 2. J Nutr 133, 3255–3261

Sureka K, Choi PH, Precit M, Delince M, Pensinger DA, Huynh TN, Jurado AR, Goo YA, Sadilek M, Iavarone AT, et al. (2014): The Cyclic Dinucleotide c-di-AMP Is an Allosteric Regulator of Metabolic Enzyme Function. Cell 158, 1389–1401

Sutherland EW, Rall TW (1957): Fractionation and Characterization of a cyclic adenine ribonucleotide formed by tissue particles. J Chem Inf Model 53, 1689–1699

Suzuki K, Babitzke P, Kushner SR, Romeo T (2006): Identification of a novel regulatory protein (CsrD) that targets the global regulatory RNAs CsrB and CsrC for degradation by RNase E. Genes Dev 20, 2605–2617

Tosi T, Hoshiga F, Millership C, Singh R, Eldrid C, Patin D, Mengin-Lecreulx D, Thalassinos K, Freemont P, Gründling A (2019): Inhibition of the Staphylococcus aureus c-di-AMP cyclase DacA by direct interaction with the phosphoglucosamine mutase GlmM. PLoS Pathog 15, 1–28

Ullmann A, Monod J (1968): Cyclic AMP as an antagonist of catabolite repression in Escherichia coli. FEBS Lett 2, 57–60

Valentini M, Filloux A (2016): Biofilms and Cyclic di-GMP (c-di-GMP) signaling: Lessons from Pseudomonas aeruginosa and other bacteria. J Biol Chem 291, 12547–12555

Ventola CL (2015): The antibiotic resistance crisis: part 1: causes and threats. P T A peer-reviewed J Formul Manag 40, 277–83

Wang W, Arshad MI, Khurshid M, Rasool MH, Nisar MA, Aslam MA, Qamar MU (2018): Antibiotic resistance : a rundown of a global crisis. Infect Drug Resist 1645–1658

Whiteley AT, Pollock AJ, Portnoy DA (2015): The PAMP c-di-AMP is essential for listeria

monocytogenes growth in rich but not minimal media due to a toxic increase in (p)ppGpp. Cell Host Microbe 17, 788–798

Whiteley AT, Garelis NE, Peterson BN, Choi PH, Tong L, Woodward JJ, Portnoy DA (2017): c-di-AMP modulates Listeria monocytogenes central metabolism to regulate growth, antibiotic resistance, and osmoregulation. Mol Microbiol 104, 212–233

Whiteley AT, Eaglesham JB, Mann CCDO, Benjamin R, Lowey B, Nieminen EA, Danilchanka O, King DS, Lee ASY, Mekalanos JJ, Kranzusch PJ (2019): Bacterial cGAS-like enzymes synthesize diverse nucleotide signals. Nature 567, 194–199

WHO_Global priority list of antibiotic-resistant batceria to guide research, discovery, and development of new antibiotics. 2017

WHO (2020): Lack of new antibiotics threatens global efforts to contain drug-resistant infections, World Health Organization (WHO). https://www.who.int/news-room/detail/17-01-2020-lack-of-new-antibiotics-threatens-global-efforts-to-contain-drug-resistant-infections, accessed 22nd January 2020

Winn MD, Ballard CC, Cowtan KD, Dodson EJ, Emsley P, Evans PR, Keegan RM, Krissinel EB, Leslie AGW, McCoy A, et al. (2011): Overview of the *CCP* 4 suite and current developments. Acta Crystallogr Sect D Biol Crystallogr 67, 235–242

Witte CE, Whiteley AT, Burke TP, Sauer JD, Portnoy DA, Woodward JJ (2013): Cyclic di-AMP is critical for Listeria monocytogenes growth, cell wall homeostasis, and establishment of infection. MBio 4

Witte G, Hartung S, Büttner K, Hopfner KP (2008): Structural Biochemistry of a Bacterial Checkpoint Protein Reveals Diadenylate Cyclase Activity Regulated by DNA Recombination Intermediates. Mol Cell 30, 167–178

Woodward JJ, Lavarone AT, Portnoy DA (2010): C-di-AMP secreted by intracellular Listeria monocytogenes activates a host type I interferon response. Science (80-) 328, 1703–1705

Woolhouse M, Waugh C, Perry MR, Nair H (2016): Global disease burden due to antibiotic resistance - State of the evidence. J Glob Health 6, 1–5

Yang CY, Chin KH, Chuah MLC, Liang ZX, Wang AHJ, Chou SH (2011): The structure and inhibition of a GGDEF diguanylate cyclase complexed with (c-di-GMP) 2 at the active site. Acta Crystallogr Sect D Biol Crystallogr 67, 997–1008

Zaman S Bin, Hussain MA, Nye R, Mehta V, Mamun KT, Hossain N (2017): A Review on Antibiotic Resistance: Alarm Bells are Ringing. Cureus 9, 2–9

Zhang L, Li W, He ZG (2013): DarR, a TetR-like transcriptional factor, is a cyclic di-AMP-responsive repressor in Mycobacterium smegmatis. J Biol Chem 288, 3085–3096

Zheng Y, Zhou J, Sayre D, Sintim HO (2014): Identification of bromophenol thiohydantoin as an inhibitor of DisA{,} a c-di-AMP synthase{,} from a 1000 compound library{,} using the coralyne assay. Chem Commun 50, 11234–11237

Zhou J, Sayre DA, Zheng Y, Szmacinski H, Sintim HO (2014): Unexpected complex formation between coralyne and cyclic diadenosine monophosphate providing a simple fluorescent turn-on assay to detect this bacterial second messenger. Anal Chem 86, 2412–2420

Zhu Y, Pham TH, Nhiep THN, Vu NMT, Marcellin E, Chakrabortti A, Wang Y, Waanders J, Lo R, Huston WM, et al. (2016): Cyclic-di-AMP synthesis by the diadenylate cyclase CdaA is modulated by the peptidoglycan biosynthesis enzyme GlmM in lactococcus lactis. Mol Microbiol 99, 1015–1027

Abbreviation

Δ80CdaA	cyclic di-AMP synthase A lacking the first 80 amino acids
Δ100CdaA	cyclic di-AMP synthase A lacking the first 100 amino acids
°C	Degree Celsius
2YT	2X YT medium (yeast tryptone)
3’ OH	3’ hydroxyl
3’3’ cGAMP	Adenosine-Guanosine-3',3'-cyclic monophosphate
3’dATP	3’ deoxy Adenosine triphosphate
5’pApA	5'- Phosphoadenylyl- adenosine
Å	Angstrom (1Å = 10^{-10} m)
Ala (A)	Alanine
AMP	Adenosine monophosphate
Asp (D)	Aspartic acid
ATP	adenosine triphosphate
Arg (R)	Arginine
B04	Acetamide, 2-[(cyanomethyl) methylamino] -N- (6- methyl- 2-pyridinyl)
B06	Benzeneacetic acid, 4- fluoro-, hydrazid
B2H	bacterial two-hybrid
BDC	Background Density Correction factor
BHI medium	Brain-heart-infusion medium
B. subtilis	*Bacillus subtilis*
Ca^{2+}	Calcium ion
$CaCl_2$	Calcium chloride
cAMP	Cyclic adenosine monophosphate
C08	Benzoic acid, 4-(amino methyl)-, methyl ester, hydrochloride (1:1)
C11	1H-Indole-3-ethanamine, N-[(1-methyl-1H-pyrrol-2-yl) methyl]
CBS	cystathionine-beta-synthase domain
CC	Coiled-coil
CdaA/DacA	cyclic di-AMP synthase A
CdaM	c-di-AMP synthase of Mycoplasma
CdaR	cyclic di-AMP synthase A regulator
CdaS	cyclic di-AMP synthase S, sporulation-specific

c-di-AMP	Bis-(3'-5')-cyclic dimeric adenosine monophosphate
c-di-GMP	bis-(3',5')-cyclic dimeric guanosine monophosphate
cGAS	cyclic GMP-AMP synthase
Co^{2+}	Cobalt ion
$CoCl_2$	Cobalt chlorid
C-terminal	Carboxy-terminal
D07	1H-Pyrazole-4-acetamide, 1,3,5-trimethyl-N-2-pyridinyl
DAC	Diadenylate cyclase
DarB/YkuL	c-di- AMP receptor protein B
DFG	Deutsche Forschungsgemeinschaft
DESY	Deutsches Elektronen-Synchrotron
DGC	diguanylate cyclase
DisA	DNA integrity scanning protein A
DMSO	Dimethylsulfoxid
DNA	deoxyribonucleic acid
E01	Carbamimidothioic acid, (2-chlorophenyl) methyl ester
E. coli	*Escherichia coli*
EDTA	ethylenediaminetetraacetic acid
EMBL	European Molecular Biology Laboratory
ESRF	European Synchrotron Radiation Facility
GDP	guanosine diphosphate
GGDEF domain	Gly-Gly-Asp-Glu- Phe domain
GlmM	phosphoglucoseamine mutase
Glu (E)	Glutamic acid
Gly (G)	Glycine
GMP	Guanosine monophosphate
GTP	guanosine triphosphate
GST	glutathione S transferase
H04	Butanedioic acid, 1-(2,2-dimethylhydrazide)
H1	inhibitory helix 1
H2	inhibitory helix 2
HhH	helix-hinge-helix domain
HZB	Helmholtz-Zentrum Berlin
HZB083	GMP, Guanosine monophosphate
His (H)	Histidine

IC_{50}	50 % inhibitor concentration
IPTG	isopropyl-β-D-thiogalactopyranosid
Ile (I)	Isoleucine
ITC	Isothermal titration calorimetry
I-site	Inhibitory site
K^+	Potassium ion
K_D	Dissociation constant
kDa	Kilodalton 1 kDa = 1.000 Dalton
LB medium	lysogeny broth medium
Leu (L)	Leucine
L. lactis	*Lactococcus lactis*
LSM	Listeria Synthetic Medium
lmo/L. monocytogenes	*Listeria monocytogenes*
MDR	multidrug efflux pumps
Mg^{2+}	Magnesium ion
$MgCl_2$	Magnesium chloride
min	minute
Mn^{2+}	Manganese ion
$MnCl_2$	Manganese chloride
mRNA	messenger RNA
M. smegmatis	*Mycobacterium smegmatis*
M. tuberculosis	*Mycobacterium tuberculosis*
NADH	Nicotinamide adenine dinucleotide
N-terminus	Amino terminal
OD	Optical density
ONPG	o-nitrophenyl-β-D-galactopyranoside
PanDDA	Pan-Density Dataset Analysis
PAS	Per-Arnt-Sim
PCR	polymerase chain reaction
PDB	Protein Data Bank
PDE	Phosphodiesterase
PEG	Polyethylene glycol
PETRA III	Positron-Elektron-Tandem-Ring-Anlage III
Phe (F)	phenylalanine
p(p)pGpp	guanosine-(penta)-tetraphosphate

PPi	Pyrophosphate
PYK	Pyruvate kinase-like domain
RCK_C	regulator of conductance of K^+
RNA	Ribonucleic acid
rpm	Revolutions per minute
SAM	S-Adenosylmethionine
SAXS	small-angle x-ray scattering
SDS	sodium dodecyl sulfate
SDS-PAGE	SDS polyacrylamide gel electrophoresis
sec/s	Second
SEC-MALS	size exclusion chromatography with multiangle light scattering
Ser (S)	Serine
S. aureus	*Staphylococcus aureus*
S. pneumonia	*Staphylococcus pneumonia*
SUMO	small ubiquitin-like modifier
T. maritima	*Thermotoga maritima*
tRNA	transfer RNA
Thr (T)	Threonine
TM	Transmembrane domain
wt	Wild type
WHO	World Healthcare organization

Acknowledgements

First and foremost, I am grateful to Prof. Dr. Ralf Ficner for the opportunity to work on this amazing project. His continuous support and encouragement over the past few years as well as his fruitful discussions and many ideas. Thank you!

Additionally, I would like to thank the members of my thesis committee, Prof. Dr. Kai Tittmann for his ideas and helpful advice and especially Prof. Dr. Fabian Commichau for his continuous support, many discussions and ideas as well as a rewarding collaboration. I would like to thank Prof. Dr. Rolf Daniel, Dr. Till Ischebeck and Prof. Dr. Carsten Lüder for willingly accept to be part of my extended examination board.

Furthermore, I would like to thank our collaboration partners from the microbiology department, Prof. Dr. Jörg Stülke, Dr. Johannes Gibhardt, Christina Herzberg, Larissa Krüger and Rica Bremenkamp for the excellent collaboration.
In addition, I would like to acknowledge the work of our collaboration partners from the Helmholz Zentrum Berlin Dr. Manfred Weiss and especially Dr. Jan Wollenhaupt for all the help and tips concerning fragment screening.

I am very grateful to all present and former members of the Department of Molecular and Structural Biology for the nice working atmosphere. In particular I would like to thank Dr. Achim Dickmanns for all his advice, answering all my questions and his constant efforts to keep the lab running. A special thanks goes to Dr. Piotr Neumann for never getting tired of answering all my questions concerning crystallography but also all the non-scientific discussions and amazing synchrotron trips.
Furthermore, I would like to thank Beate Heinze, for all the work she does for us so we can fully concentrate on our research and Anette Berndt, for being the best lab partner I can think of. Thank you two for all the nice and funny discussions but also your words of encouragement.

Thank you, Kathi, for the everyday coffee and the chitchat about life and work. Thank you, Alaa, for expressing your passion about food or your thesis project which makes us all smile. Thank you, guys, for all the exhausting but lovely synchrotron trips, for your help and patience during long nights were we all together measured hundreds of CdaA crystals. You guys are the best office partners. Thank you, Flo, for always offering your help, for your patience and for your comments on my thesis. Additionally, I am grateful for the valuable contribution of my master students Liza Vinhoven and Patrick Kloskowski.

Last but not least I am grateful to my parents, my little sister and Janek for their constant unconditional support and their encouragement. I would like to thank and all my friends who always had a sympathetic ear.

Thank you all!